APPLICATION OF INERTIAL SENSORS FOR PERFORMANCE AND SAFETY ANALYSIS IN ALPINE SKIING

Laureando: Quagliotto Omar

Relatore: Petrone Nicola, Dipartimento Ingegneria Meccanica

Corso di Laurea Magistrale in: Bioingegneria

21 Settembre 2014-2015

Dedico questo lavoro di tesi a tutte le persone che mi sono state vicine in questi anni di studio.

Alla mia famiglia, che mi ha supportato in tutti i miei 19 anni di carriera scolastica, permettendomi di raggiungere con successo questo traguardo.

A Francesca che mi ha regalato la sua presenza nei momenti peggiori e in quelli migliori, riuscendo ad offrirmi sempre il suo affetto, con gioia e serenità.

Ai tutti miei zii, in particolare Ivana e Roberto per aver sempre avuto parole di conforto e sostegno, nei momenti difficili, e a Mabel per avermi aiutato ad affrontare le prime difficoltà nel mio cammino scolastico ed avermi indirizzato a questa strada con il suo esempio.

A Nicola, che ha creduto in me, spronandomi a dare sempre di più, permettendomi così di portare a termine questo lavoro di tesi aiutandomi anche nella sua stesura e revisione, senza mai mancare negare un sorriso; per avermi inoltre permesso ottime esperienze, negli ambiti più disparati.

A Giulia, che in tutti questi anni si è confidata e confrontata con me, dando origine ad una grande amicizia.

A Mattia, che ha indirizzato la carriera universitaria; per la profonda amicizia e per essere stato sempre da riferimento.

A tutti coloro che, nel mio cammino, hanno creduto in me.

A tutti coloro che non hanno creduto in me, dandomi la possibilità di migliorare sempre di più.

Ai miei compagni di laboratori e di studi, per avermi regalato momenti felici.

A tutti i miei amici e coloro con cui ho condiviso tutti questi anni.

Sommario

Chapter 1: Introduction

1.1 General thesis introduction

Technology and equipment are two important elements in the suite of inventions available in sports. In the last decade, with the spread of always more compact devices, new fields have developed. Technology and equipment should be the end point of many research and translational activities, gaining knowledge from research and applying it to standards, designs and products.

The present work develops in three main areas:

- In the first sector, an investigation about the use of inertial measurement unit in skiing was carried out, together with the analysis of data in order to extrapolate parameters suitable for classify different skiing skill's level and turns type.
- Then, after a brief presentation of protective devices in sports like motorcycling recently developed, a study on an anthropomorphic dummy instrumented with IMUs is reported. This study aims to collect infield data to support certification of individual protective systems.
- The last part of the thesis paper, presents some ideas behind the investigation of simulated ski falls, in order to obtain some typical fall's values which would be used to activate a protective system.

1.2 Thesis objectives

The first aim of this work is to investigate on sensors and methods to analyse and improve both sport performance and safety.

The firsts factors considered were the cost of the overall technology adopted together with the complexity of the system. Expensive methods would fail in a consequent possible marketing. The reduction of cost and complexity of the equipment leads also to a more robust and extensive data collection. Considering those factors as fundamental, complex instrumentation has optical motion capture systems was not considered and the choice fell on Inertial Measurement Unit devices. The general low cost and dimension of those devices makes them suitable for outdoor infield tests.

Using such devices in motion tracking, however cannot lead to a fully understanding of the movements. In this thesis the first objective was to present a technique to analyse performance, in terms of skiing level, through inertial sensors, estimating significant parameters. In the second part of this thesis, focus will be on skiing safety problem. Our studies on this topic will be presented, considering fall's simulation methods and analysis technique to extrapolate parameters able to tune a protecting device.

In Figure 1-1:Thesis general diagram, an overall graph of the topic analysed in this thesis is presented.

Starting from the ski sport, two main areas can be distinguished:

- Performance analysis
- Safety analysis

The performance area can address both to racer skiers and recreational skiers. We decided to concentrate on recreational skiers, in terms of skiing level instead of turn type. Three different skiing level (Beginner, Intermediate and Expert) were analysed trying to estimate parameters able to distinguish between them.

The safety area instead, considered falls protection over skiers' collisions or impacts with obstacles. This in order to develop methods to develop airbag-based protective systems. Considering the informatics framework of Bioengineering, the focus was on electronically activated devices, were it is possible to set in software. To best collect signals without risk of severe injuries in testers, we decided consider:

- in-lab falls
- anthropomorphic dummy falls
- real falls while skiing

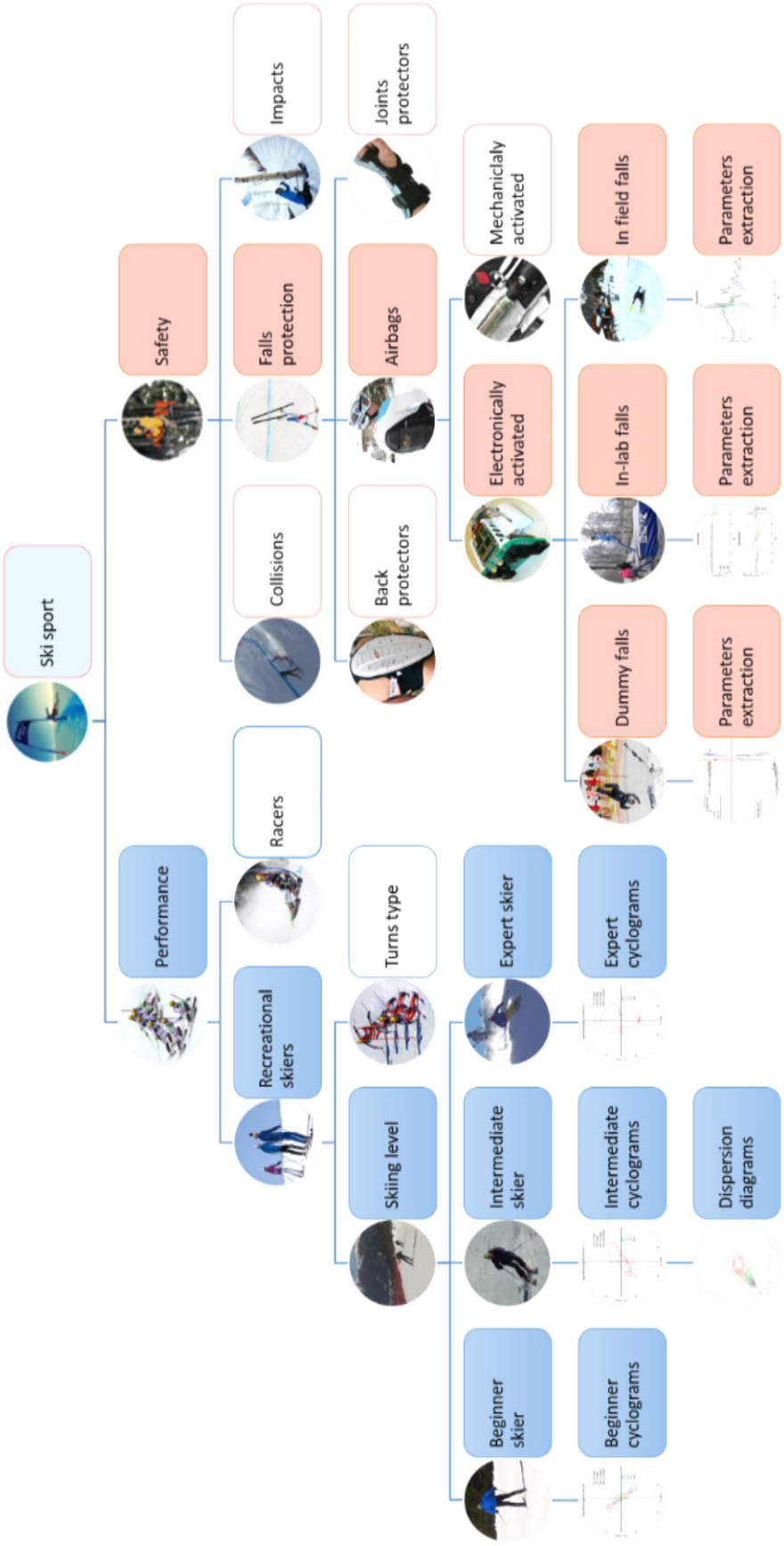

Figure 1-1:Thesis general diagram

Figure 1-1: General thesis' diagram

The analysis regarding performance of the present thesis can be considered as a 3x3 between-within research, with the comparison between three types of skiing styles and three different skiing levels:

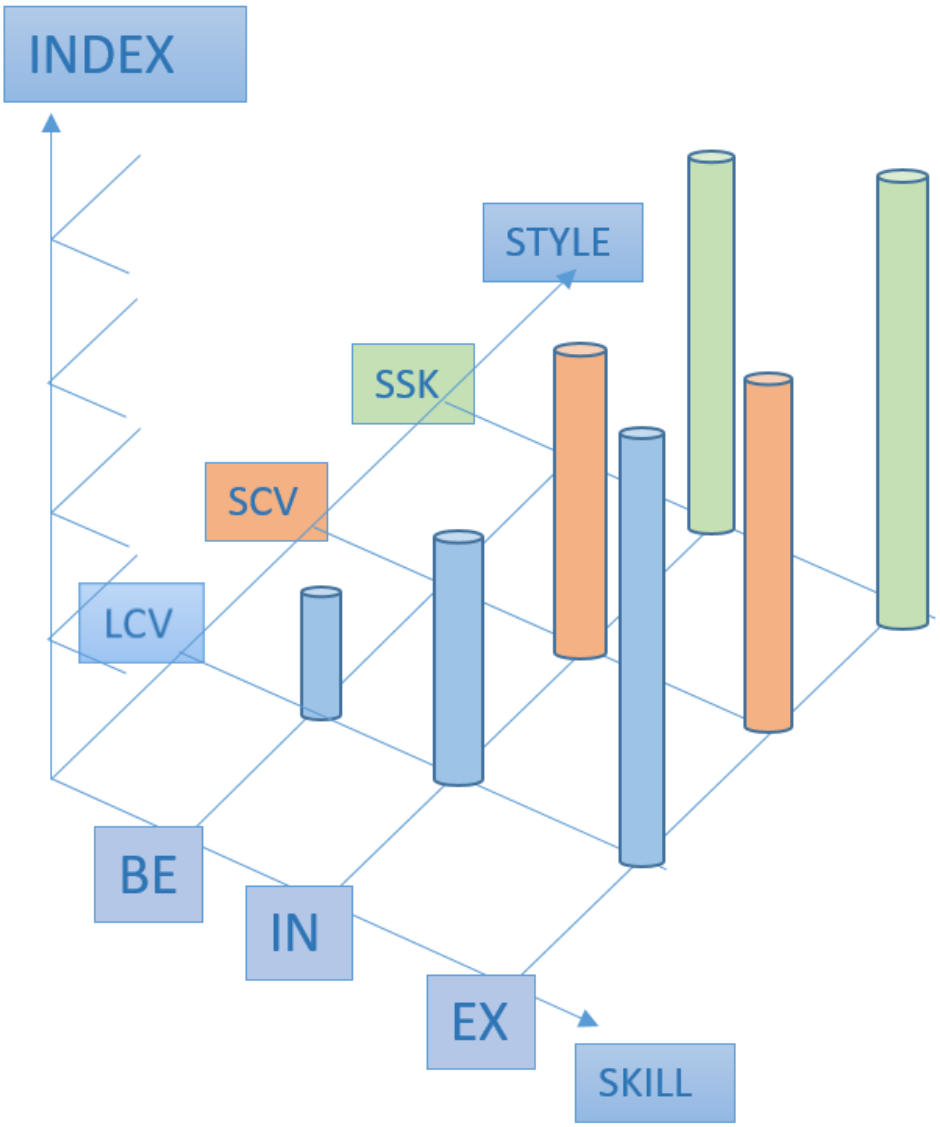

Figure 1-2: 3X3 study, considering skiing level and skiing style

In the Figure 1-2 in the skill axis are reported the three levels:

- Beginners (BE)
- Intermediate (IN)
- Expert (EX)

Instead in style-axis, the three different skiing styles are reported:

- LCV (Long Carved Turns)
- SCV (Short Carved Turns)
- SSK (Short Skidded Turns)

Then, the second type of analysis is still a 3x3 between-within analysis, but considers three different types of fall and three different tests. This in order to obtain peak values of both angular velocities and linear accelerations.

In Figure 1-3 is presented the diagram that refers to safety analysis.

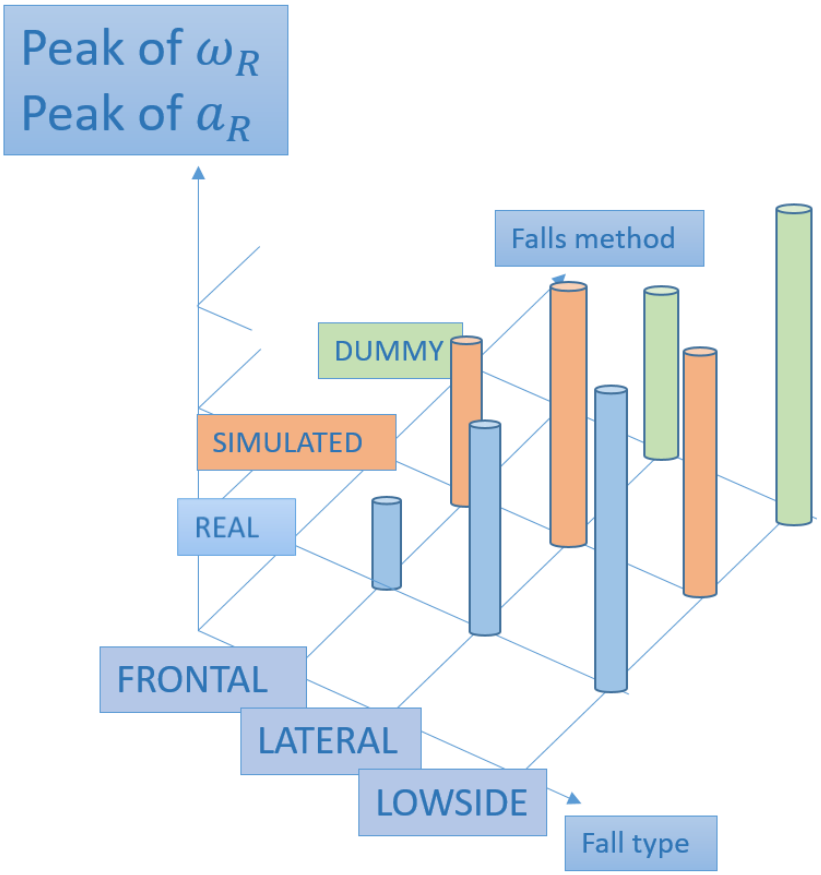

Figure 1-3: 3X3 analysis, with type of fall and type of test method.

The fall methods are divided into:

- Real falls – recorded on slopes during normal skiing
- Simulated falls – over a mattress
- Dummy falls- with an anthropomorphic dummy

In addition were considered different fall types:

- Frontal
- Lateral
- Low side

The frontal falls happens when a skiers impacts on an obstacle with the front part of its skies and tends to fall towards its moving direction. The Lateral fall occurs when the skiers hits an obstacle with the lateral part of the skies and the lowside falls consists in a sliding fall during a turn.

In addition the falls can be analysed in terms of obstacle type, as in the case of the dummy's falls. In this case it is possible to analyse the type of obstacle, for example a snow wall or a wooden tablet, in terms of impact's velocity.

The two main areas, performance and safety, discussed in this thesis work, were considered in the framework of Interreg IV project, 'Testing methods development and qualification of Airbag based systems applied to recreational skiers'. The project considered the collaboration with DolomitiCert, a testing laboratory located in Longarone (BL, Italy) and the University of Salzburg. The overall project was developed in a five years time frame, in which this thesis took about a year and an half, from March 2014 to September 2015.

Chapter 2: Inertial Measurement Units

2.1 Introduction to Inertial Measurement Units

Inertial Measurement Units (IMUs) are used worldwide in a huge number of application, from automotive to biomechanics. Their relatively low cost, together with small dimension make them suitable for most common applications. In addition, the possibility to combine them with a GPS system, in order to avoid drifts and error, makes the union very suitable for navigation systems.

An United states patent, dated December 8, 1987 by Melvin M. Morrison refers exactly to 'INERTIAL MEASUREMENT UNIT', which "provide three axis acceleration and angular turning rate detection with a cubical magnetically suspended sensor mass disposed within a cubical outer assembly" [Morrison, 1987].

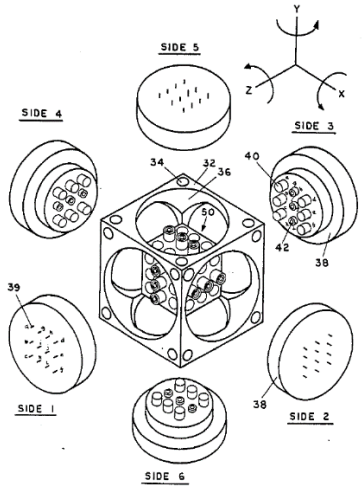

Figure 2-1: Figure 1: Inertial measurement units (US patent 4711125)

The sensor mass is free to move mechanically independently from the outer assembly; it has also a plurality of sensing and suspension elements of particular orientation on a selected plane for each axis of detection. The sensing elements are cross-coupled to minimize cross-axis sensitivity. To maintain the sensor mass in proper orientation, the device utilizes several servo-control loops of conventional design to process outputs from the pickoffs. Gyroscopes (gyros) are typically used to detect angular turning rates.

2.1.1 Gyroscope - definition

In its simplest form, a gyroscope is composed by a rapidly spinning rotor or flywheel supported on a mount which allows freedom of tit of the spin axis relative to the base. The rapid spinning of the flywheel gives the spin axis of the gyro a stubborn resistance to angular deflections. The gyro thus tends to preserve its original orientation which, with proper alignment, is also the desired platform frame of reference. Three degrees of freedom (DOF) are possible for gyroscope: a gyro with one DOF is one having a spin axis that is allowed to move in one direction and restrained on others. A two axis gyro has an axis of rotation capable of deflection in either of two planes or axes. Similarly, a three DOF gyro is one having an axis of rotation capable of deflection in either of three axis. Such two gyros are known as '*free gyros*'.

Since three axis of stabilization are required to stabilize a frame of reference, either three single axis, two two-axis or one three-axis gyros is required. The use of three single axis gyros was initially preferred, until techniques were developed to model and eliminate cross-coupling between axes in multiple axis gyros. U.S. Patent No. 3,823,990 [P.J. Gilinson Jr. 1974] discloses a three axis gyro. Gilinson typifies conventional gyros in that it operates on the principle of a spinning flywheel. In some applications such as space hover, the weight associated with the gyro flywheel is particularly undesirable. Thus, there is a need to reduce the weight and cost associated with conventional gyroscopes.

The accelerometer is the second typically essential component of conventional inertial measurement units.

2.1.2 Accelerometer - definition

An accelerometer is a device that measures the accelerations of a mass in one direction relative to the stabilized frame of reference. Conventional mechanical accelerometers include a spring or hinge adapted for deflection in response to acceleration. A mechanical, optical, inductive or capacitive pickoff is used to detect motion of the hinge. To meet manufacturing tolerances, the hinge or spring is biased. Factors like vibration, shock, temperature variations, and time dependent stress relief shift the bias and introduce errors in output calculation. Conventional mechanical accelerometers require frequent calibration and alignment relative to the gyros. In addition, these accelerometers are difficult to manufacture as the spring or hinge must typically be machined ground, or polished to exact specifications. The difficult in doing so, lowers the yield and raises the cost of producing such

instruments. A further disadvantage of these conventional mechanical accelerometers results from the need to mount physically the accelerometer on the frame of reference, typically either a stabilized platform or the vehicle itself. To protect the instrument from vibrations, rubber isolators are typically used. Over time, the isolators often lose resiliency and settle in a manner that causes misalignment of the accelerometer. This provide an additional source of error.

The degree of damping also imposes a limitation on gain. A high gain system requires a tight servo. That is, since a high gain system is quick to respond to vibration, inadequate damping may lead to a degradation in performance and/or undesired oscillation. Thus, it would be desirable to provide a system with high damping thereby permitting high servo gain with the associated improvement in system performance. Conventional mechanical accelerometers are also subject to resonance from the spring constant associated with the accelerometer on the restraint. Resonance is undesirable as an additional source of output error. It is desirable therefore to provide a single, suspended, integrated, accurate, inexpensive, lightweight instrument capable of providing a three axis angular turning rate detector and a self-damping nonmechanical three axis accelerometer with no mechanical supports or restraints. The utilization of embodied inertial measurement units, substantially overcomes many of the problems associated with prior art inertial measurement units, by providing a single, integrated, lightweight combination of three axis angular turning rate detector and three axis accelerometer with a mechanically independent fully suspended sensor mass.

Although being very useful in several analysis, conventional mechanical are not the only type of accelerometer available.

In the next few steps, several technologies regarding accelerations and angular velocities will be considered.

2.1.3 Different types of accelerometers

The first type of accelerometer, described in the patent above, is referred as “Force-balance (servo) Accelerometers. Even if they are heavy, combining a very high accuracy with a good complexity, they are a typical science instrument in aerospace engineering, especially in entry and descent of planetary probes.

The force balance sensor is intended for DC and low frequency acceleration measurements, such as those encountered in the motion of vehicles, aircrafts and ships. These sensors are capable of measuring levels from as low as 0.0001g up to 200g’s over a frequency range from DC to 1000Hz. In addition, due to their inherent sensitivity to gravity the force balance accelerometers with a certain modifications or special features become excellent instruments for measuring angles of inclination.

It is very useful in applications such as platform levelling, pipeline levelling, gun sight control, borecole mapping and other low level seismic measurement applications [www.crlsensors.com].

This kind of sensor has several advantages, which result in exceptional performance in the type of applications mentioned above. Internal displacements within any accelerometer lead to inaccuracies and errors usually in the form of excessive hysteresis, stickiness, non-linearity and non-repeatability. LVTD, potentiometric, variable reluctance and similar type sensors produce these errors because the sensing element must move over some distance in order to produce a measurable change in output.

In contrast, the output signal from a force balance accelerometer does not depend on the displacement of some internal element being a linear function of acceleration. Internal displacements are kept relatively small, typically less than one ten thousandth of an inch. In addition to minimizing static error, the minute displacements associated with the force balance sensor contribute to this type of sensor having a relatively high natural frequency. A strain gauge sensor does not require excessive internal displacements but does suffer from instability due to effects of temperature, creep and aging.

As example, the Honeywell QA 2000 (Used on Huygens HASI probe), has a total mass of 300g, and a servo sensor with a weight of 71g but provides resolutions up to 1/µg.

Figure 2-2: Honeywell QA2000 sensor

On the other hand, there are the piezoresistive accelerometers, which sacrifice accuracy in favour of the light weight. As example, the Endevco model 7264B [www.endevco.com] weighs only 1 gram. Those accelerometers have a scale varying from ±500g up to ±2000g depending on a sampling frequency up 0.5 MHz, but a sensitivity of 0.80 mV/g. Requiring low power, they are used in applications which require minimal mass loading and a broad frequency response. Used for shock testing of lightweight systems or structures, the 7264B meets SAE J211 [https://law.resource.org] specifications for instrumentation for impact testing and SAEJ2570 [http://standards.sae.org/] specification for anthropomorphic test device transducers.

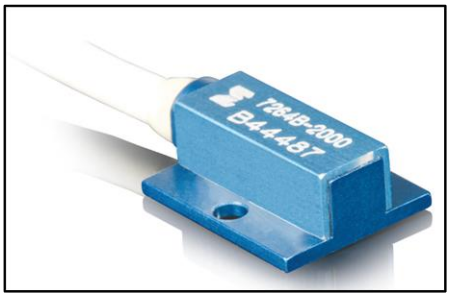

Figure 2-3: Endveco 7264B-2000

A further development of inertial measurement units has come with the spread of electronic and micro devices. MEMs can be defined as miniaturized mechanical and electro-mechanical elements that are made using the techniques of microfabrication.

Accelerometers based on Micro-ElectroMechanical Systems (MEMS), combine a good accuracy with light weightiness and robustness. Their accuracy goes from +-10g raises up to +-70g. Requiring low power (6.5 mW and +5V) and simple electronics, are very used on wearable sensors and in automotive applications, to detect collisions and to trigger air bag openings. The terms 'MEMs' defines the technology; not specific products. The common sensing principle of those type of accelerometers is capacitive. An acceleration in the lateral direction deflects the proof mass that is suspended by folded springs. One set of electrodes is attached to the proof mass and moves with acceleration. These movable electrodes form capacitors with two sets of fixed electrodes opposing them with a small air gap between. A change of the capacitances is detected and transformed into a corresponding analogy voltage by a capacitance/voltage converter [http://www.tf.uni-kiel.de/].

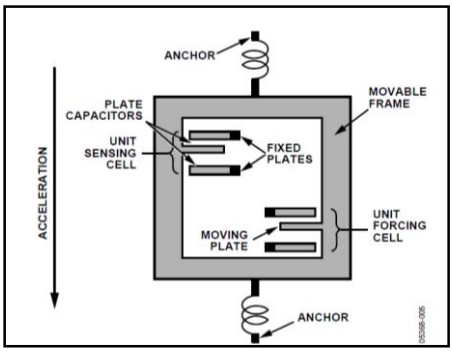

Figure 2-4: Simplified view of MEMS sensor under acceleration

2.1.4 Different types of gyroscopes

Three main different type of gyroscopes can be defined, at the state of art of actual technologies:

- Conventional mechanical gyroscopes
- Fibre optic gyroscopes
- Ring Laser gyroscopes
- MEMs based gyroscopes

A conventional gyroscope is a device for measuring or maintaining orientation, based on the principle of conservation of angular momentum.

The key component is a relatively heavy spinning rotor, mounted with nearly frictionless bearings inside two concentric lightweight rings (gimbals) each of which is also mounted with similar bearings inside the next outer ring, or the support frame in the case of the outer ring. The rotor and the two gimbals are mounted so the plane of rotation for each is perpendicular to the plane of rotation of the other two. The spinning rotor naturally resist changes to its orientation due to the angular momentum of the wheel. This phenomenon is known as gyroscopic inertia or rigidity in space. Thanks to its unique support in the nested gimbals, the rotor is able to hold a nearly constant orientation even as the support frame shifts its orientation.

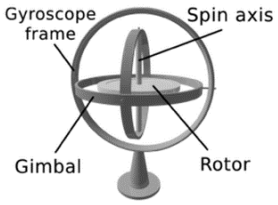

Figure 2-5: Mechanical gyroscope

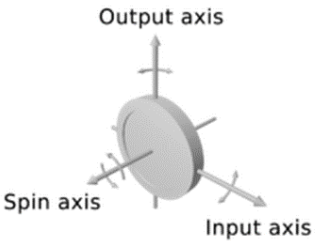

Figure 2-6: Diagram of a gyro wheel

The rotor wheel responds to a torque applied about the input axis (connected with the inner gimbal) by a reaction force about the output axis (connected with the outer gimbal). The three axis are perpendicular [http://www.newworldencyclopedia.org/].

Another type of gyroscopes are the Fibre Optic Gyroscope (FOG). It is a device that uses the interface light to detect mechanical rotation. The sensor is a coil of as much as five kilometres of optical fibre. Two light beams travel along the fibre in opposite direction. Due to the Sagnac effect, the beam traveling against the rotation experience a slightly shorter path than the other beam. The resulting phase shift affects how the beams interfere with each other when they are combined. The intensity of the combined beam then depends on the rotation rate of the device.

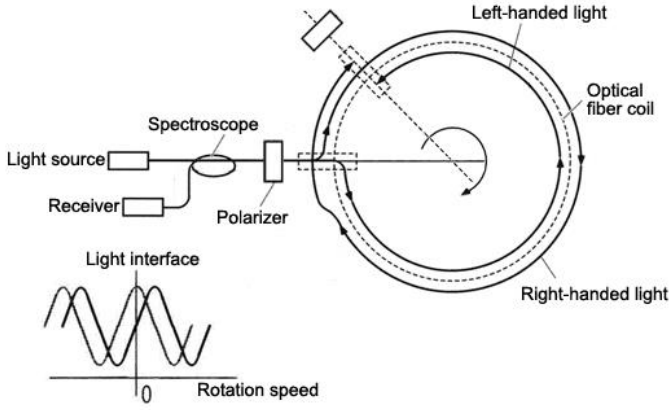

Figure 2-7: fibre optic gyroscope scheme

A FOG provides extremely precise rotational rate information, in part because of its lack of cross-axis sensitivity to vibration, acceleration, and shock. Unlike the classic spinning-mass gyroscope, the FOG has a virtually no moving parts and no inertial resistance to movement. FOG drift varies depending on production technology. They can be both digital and analog, with the same working principle. Usually analog FOG show a maximum input rate between ±100 deg/s and ±1000 deg/s in dependence to its cost. Bias instability also varies from a minimum of 0.05 °/h for digital FOG up tu 3 °/h for analog FOG [www.kvh.com]. Those type of gyroscope is typically used in surveying, stabilization, and inertial navigation tasks, thanks to its precision that can reach 1milliradiant [www.emcore.com]. Dimension are small, varying by producer; as example, DSP-1750 by KVH measures 45.7 mm in diameter x 22.9 mm with mass of 0.11kg.

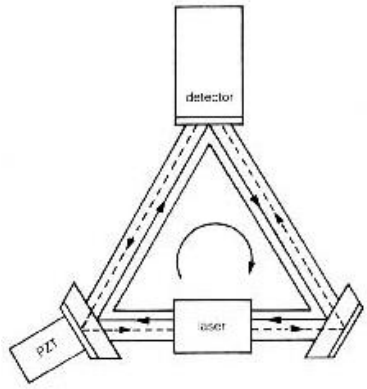

Figure 2-8: Ring Laser Gyroscope scheme

The Ring Laser Gyroscope (RLG), uses interference of a laser light within a bulk optic ring to detect changes in orientation and spin. It is an application of a Sagnac interferometer. Ring laser gyros (RLG) can be used as the stable elements (for one degree of freedom each) in an inertial reference system. The advantage of using a RLG is that there are no moving parts. Compared to conventional spinning gyro, this means there is no friction, which in turns means there will be no inherent drift terms. Additionally, the entire unit is compact, lightweight, and virtually indestructible, meaning it

can be used in aircrafts. Unlike mechanical gyroscope, the device does not resist changes to its orientation.

Physically, an RLG is composed of segments of transmission paths configured as either a square or a triangle and connected with mirrors. One of the mirrors will be partially silvered, allowing light through to the detectors. A laser beam is launched into the transmission path in both directions, establishing a standing wave resonant with the length of the path. As the apparatus rotates, light in one branch travels a different distance than the other branch, changing its phase and resonant frequency with respect to the light traveling in the other direction, resulting in the interference pattern beating at the detector. The angular position is measured by counting the interference fringes.

RLGs, while more accurate than mechanical gyros, suffer from an effect known as "lock in" at very slow rotation rates. When the ring laser is rotating very slowly, the frequencies of the counter rotating laser become very close (within the laser bandwidth). At this low rotation, the nulls in the standing wave tend to "get stuck" in the mirrors, locking the frequency of each beam to the same value, and the interference fringes no longer move relative to the detector; in this scenario, the device will not accurately track its angular position over time.

Dithering can compensate for lock-in. The entire apparatus is twisted and untwisted about its axis at a rate convenient to the mechanical resonance of the system, thus ensuring that the angular velocity of the system is usually far from the lock-in threshold. Typical rates are 400Hz, with a peak dither velocity of 1 arc-second per second. Primary applications include navigation systems on commercial airliners, ships and spacecraft, where RLGs are often referred to as Inertial Reference Systems. In these applications (airliners, ships and spacecrafts), it has replaced its mechanical counterpart, the Inertial guidance system. In addition, RLG shows a lower bias in respect to FOG, arriving to 0.0035°/h. The sampling frequency is high. GG1320AN digital laser gyro, by Honeywell [www.aerospace.honeywell.com] shows a 2000Hz sampling frequency at typical use that can grow up to 5000Hz at maximum. The accuracy can reach 0.003 deg [www.teledyne-cdl.com]. Dimension are comparable with FOG; for example GG1320 measures 87.8mm in diameter and is 45mm high, with a mass of 450 grams.

The last gyroscope technology presented is based on MEMs. Those use the Coriolis Effect to measure the angular rate. The Coriolis effects can be observe in a mass (m) moving in direction v, and with angular rotation velocity Ω_z. The mass will experience a force in the direction of the orange arrow as a result of the Coriolis force, that can be measured in $F_c = -2m\Omega \times \mathrm{v}$. The resulting physical displacement caused by the Coriolis force is read from a capacitive sensing structure.

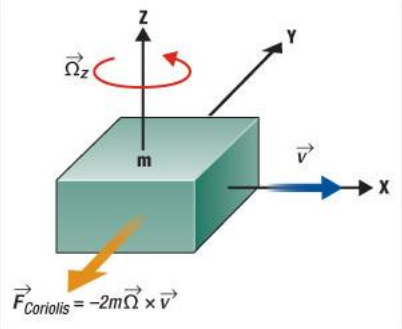

Figure 2-9: Principle of the Coriolis effect

Most available MEMs gyroscopes use a hybrid configuration. Two masses oscillate and move constantly in opposite directions (Figure 2-10). When angular velocity is applied, the Coriolis force on each mass acts in opposite direction, which results in a capacitance change. This differential value in capacitance is proportional to the angular velocity Ω_z and is then converted into output voltage (analog gyroscope) or into bit values (digital gyroscopes). When, instead, linear acceleration is applied to two masses, they move in the same direction. Therefore, there will be no capacitance difference detected. The gyroscope will output zero value [www.electroiq.com].

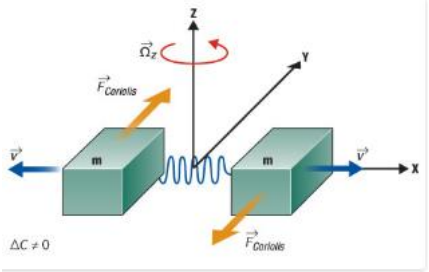

Figure 2-10: MEMs gyro when angular velocity is applied

2.2 Inertial measurement units in sports analysis

After a brief description of most common types of accelerometers and gyroscopes, will be explained the utilization of IMUs in sports and in sport engineering

2.2.1 Introduction

An IMU is a device which embodies both an accelerometer and a gyroscope, most usually on a three axis system, to detect as much information as possible in the most compact device. A calibrate IMU measures 3D angular velocity and 3D accelerations and gravity with respect to the sensor housing.

The utilization of MEMS in this applications is fundamental, in order to avoid to carry heavy and large instruments. In order to perform analysis as accurate as possible, the investigation of several technique of data collection has been done through years. Accurate systems, as Motion capture (MOCAP) have been developed and successfully used in a huge number of application, but its

mobility, cost and time limitations have been a severe obstacle on infield tests. It would be very difficult or expensive to set up a MOCAP system in ski or other outdoor sports, which requires wide open fields. To avoid such limitations, the IMUs have been considered with raising interest in the last decade.

The IMUs offer an alternative way to obtain kinematic data in a variety of environments. Commercially available systems (e.i. Xsens [www.xsens.com], Humotion [www.humotion.net], Exel [www.exelmicroel.com]), combine accelerometer, gyroscopes and magnetometers into an algorithm, and are able to transpose translator acceleration from the object system to the global system using a rotation matrix. Given an initial position and orientation, ideally the sensor's signals would contain sufficient information to derive the IMU kinematics completely. The orientation can be obtained using a known initial orientation and the change in orientation that can be obtained using gyroscopes. The resulting orientation can be used to subtract the gravity from the 3D accelerometer vector to yield an acceleration. Expressed in a nonrotating reference frame, double integration yields the position change. However, in the real world the sensor signals from micromachined gyroscope and accelerometers contain errors which makes it difficult to obtain orientation and position in the way described above, because of integration drift [www.xsens.com].

2.2.2 Sensor fusion and other IMU's data analysis methods

The orientation obtained from present day gyroscopes that can be worn shows an increasing error of a few degrees per second. This integration drift is mainly caused by fluctuations of the gyroscope offset and measurement noise. Obtaining a change in position using an IMU is even more difficult. In fact, the accelerometer registers not only the human movement but also the gravity acceleration. A small orientation error will yield to a large acceleration estimation error. Moreover, if double integration is carried out to derive position, integration drift may cause the error to increase rapidly in time. Because of these large errors, estimation of position using this method can not typically be performed with adequate accuracy for periods longer than a second.

Unfortunately, this method has a drawback, that is, the algorithms depend on assumption made about the movement to be measured. Therefore, the accuracy of the estimated kinematics depends on the particular movement to be performed. As example, a Kalman filter has been described by van der Kooij [Kooij, H.v.d, 1999] to investigate the human balancing system. This study showed that the Kalman filter, when assuming that the body uses a priori knowledge concerning its movements, could only explain actual body balancing.

Another study "A Bayesiian approach for pervasive estimation of breaststroke velocity using a wearable IMU", [F Dadashi et al, 2014] showed the possibility of using IMUs, together with a Bayesian framework to estimate breaststroke swimming velocity using a wearable IMU without a priori knowledge of pool length. They employed a Bayesian linear regression for that, mapping and

comparing the estimator result in terms of generalization and computational cost with a linear least-square estimator and Gaussian process regression (GPR). This work can be considered as in continuity with the previous work of Dadashi: "Gaussian process framework for pervasive estimation of swimming velocity with a body-worn IMU" [F.Dadashi et al, 2013]. The biggest drawback of this work can be considered in the large computational cost of the data analysis. In fact, the Gaussian process regression as a nonparametric approach is $O(N^3)$, where N is the number of training samples. Consequently, the direct application of Gaussian process for large training sets can be intractable.

The bayesan approach in the study, shows a complexity of $O(d^3)$ where d is the size of the square matrix that has to be inverted.

Further developments in using the IMUs in sports considered the utilization of a relatively large number of units to obtain body segments kinematics. In " fusion motion capture: the biomechanics of alpine ski racing" [Mathew Brodie et al, 2007], a member of New Zealand national team performed three runs through a ten-gate giant slalom training course of over 300 metres in length.

The athlete's body segment kinematics, angular velocity and local acceleration were obtained from 13 IMUs attached to the following body segments: Head, torso, pelvis, upper and lower arms, thighs, shanks and ski boots. The data were processed using Fusion integration algorithms and biomechanical man body model in MATLAB. The final result was an animation of the Biomechanical man negotiating the giant slalom course that can be used to present progression of lower limb dynamics through each turn.

If the utilization of a large number of IMUs is combined with a high-accuracy GPS system (GNSS RTK), the result can grant high precision in tracking the athlete's movement. In the study " 3D measurement of alpine skiing with an inertial sensor motion capture and GNSS RTK system" [M. Supej, 2010], it has been examined a novel system involving a GNSS RTK that returns a reference trajectory through the use of a suit, imbedded with inertial sensors, to reveal subject segments motion. The result shows high validity regarding the reference trajectory (0.008m) throughout an entire ski race. The system is capable of measuring an entire ski course with less manpower and therefore lower cost compared with camcorder-based techniques.

The high cost of this system, although, does not permit a commercial spread. The study presented in this thesis will present low-cost alternatives collect and analyse in field data.

In addition to performance research and analysis, IMUs have been used, together with high-speed accelerometers to develop methods to analyse safety issues in a large number of applications. Fields of applications of IMUs spreads from automotive to sports, passing through the analysis of several parameters in the rehabilitation framework.

For example, the Department of Mechanical Engineering of the University of Padua together with DolomitiCert's testing laboratories performed the study: "Development of an instrumented

anthropomorphic dummy for the study of impacts and falls in skiing" [Petrone N. et al., 2010]. The work was developed within the INTERREG project SkiProTech, in order to develop an instrumented anthropomorphic dummy suitable for simulated impacts against barriers or obstacles under controlled conditions. Later, this project turned and evolved in order to understand, with the utilization of IMUs and a more complex dummy, which parameters were more suitable to understand an incipient fall. This will be presented in the second part of this thesis.

Chapter 3: Performance in ski and training techniques

3.1 Research oriented to performance analysis

The development of new technologies is playing a significant role in enhancing performances of elite athletes in Olympic and world-class competition. An example can be seen prior to and during the 2008 Olympic games in Beijing, where swimmer set a large number of world records thanks to the introduction of the Speedo LZR racer swim suit. This was also observed in the 1998 Nagano Winter Olympic when Dutch scientists introduced 'clap skates' to speed skating. Those technologies played a significant role in lowering world record's times.

Also ski technology and materials have been significantly improved in the last few decades. In the early 90s, the introduction of carved ski has been the biggest development. The new curved-edge design replaced the straight-cut ski, meaning an improvement in skier's ability to turn and control the ski at high speeds, enhancing significantly the performance.

Such impressive developments cannot be found in other human-ski interface, such as ski boots and bindings where, after the initial growth of technology, we can now see not so great developments due to an adjustment of current technologies rather than a game-changer process.

For example, in the history of ski boots, the biggest development came in 1974 when Robert Lange adopted fiberglass reinforced epoxy resin for the outer shell of the boot.

The challenge of taking another significant step in ski technology for ski companies has been difficult, because of many factors influencing ski performance. Materials in general, ski and boots geometry, ski-snow interface and skier body dimensions are some of the parameters that should be strongly

considered. Also, new ski forced athletes to learn new skills. To observe how much is significant the ski development in ski races, we can report the 2012-2013 ski season where FIS introduced a controverted change in ski minimum turn radius of giant slalom (GS) ski to 35 meters as opposed to the 27 meter radius the skis were before required to have. This to quote racer safety as the reasoning for the change in turn radius. Most of the high level athletes argued this decision. Bode Miller said 'FIS should remove itself from the equipment issues'. To put the 35 meters radius skis into perspective it is needed to dive into the archives of ski museums. The last time GS skis were available with a turn radius this large was in the mid-1980. Considering that the distance between poles –set for 27 meters turns- didn't changed, even best athletes in the world can't afford the changes in skies. In addition, the US athlete Ted Ligety said, when asked about new skies: "This I fear will drive many young skiers out of racing at a greater rate" [www.tedligety.com]. This influenced not only young skiers, but also expert skiers. Many mid-range top athletes were pulled out from podium or winning ambitions after ski changes. We can remember Italian top racer Massimiliano Blardone, who take the podium in the season before the change of ski and, starting from the following season, hardly arrived in the top ten in a race.

Having understand how much a simple change in a parameter of skiing setup, the challenge is to determine where to focus to get the largest improvement.

The majority of the focus from commercial ski companies in recent years has been on improving ski surface preparation, including ski base grinding and waxing techniques. Looking for new hydrophobic coatings for the base of skis could be the next big step in improving ski-snow interface. Nano technologies have emerged on the commercial market that are claimed to have hydrophobic properties to reduce the surface friction of skis. Engineers have also manufactured this type of technology for other industries to create revolutionary, smart, hydrophobic surfaces with low surface tension.

In world elite level ski races, the difference between an Olympic medal and a simple placement con be addressed to the split time of only 10 hundredths of a second on a two minutes race time:

Sochi 2014 – Downhill man results

- Matthias Mayer [AUT] **2:06:23**
- Christof Innerhofer [ITA] **2:06:29**
- Kjetil Jansrud [NOR] **2:06:33**

Research for performance, in terms of new materials, design and training techniques is fundamental.

3.2 Research for the best training techniques

A significant challenge for coaches has been to accurately detect the speed and the trajectory of their skiers through train and race. A large number of studies have applied new technologies to study skier kinematic. The first studies using GPS techniques involved cross-country skiing during races. [Larsson P, Henriksson-Larse´n K. 2005].

However, little research have been published on the tracking of alpine skiers using GPS. Supej Matej [department of biomechanics, Faculty of sport, University of Ljubljana, Ljubljana, Slovenia] has made a big effort in this direction. In the past, camcorder-based three-dimensional (3D) measurements of whole body movement were used to study alpine skiing. Recently, a pan-tilt-zoom camcorder system eliminated the complexity of the multicamera solution by simultaneously covering the visual space and measuring the area with fewer cameras. Unfortunately, a complicated calibration process was still required, taking a lot of time and reducing the possibility to analyse a large number of testers. Locating joint positions manually from the video clips required anatomical expertise, was slow and labour intensive. Consequently there was a long delay between the measurements and the results. Another method considered the placement of reflective markers on the tester. Whereas the cameras were able to automatically recognize the points, the markers where not placed on the actual joint centre resulting in a systematic error. Additional markers to correct the error produced an increasing of the difficulty too set up the experiment. The low resolution and capture frequency of conventional and even more performing camcorders is also a problem when quantifying movements over large measurement volumes. Those deficiencies gave to researchers the idea to move towards new 3D measurement technology.

3.2.1 Matej Supej's study

Global positioning system (GPS) devices have been popular in sport measurements. Unfortunately, their accuracy in ski racing is problematic, even when describing the skier as a single point body. According to International Ski Association rules: (http://www.fisski.com/data/document/icr 2008.pdf) (15), the distance from turning pole to turning pole cannot be less than 6 meters. To limit the error to 1% would require a 6 cm accuracy. Only a few studies in human locomotion have used a high-end real-time kinematic GPS system that satisfies this level of accuracy. Brodie and al. [Brodie, Wakmsley, 2008) proposed a combination of sensors capable of recording whole-body 3D movement in alpine skiing based on inertial motion units, a GPS receiver and pressure insoles. This system used a GPS with an accuracy of 10m, which is not helpful in measuring differences between ski racers.

The study of Supej proposed the utilization of the *Moven motion capture suit* (Xsens Technologies, Enschede, Nederlands), which has 16 motion tracking sensors (MTx). Each sensor incorporates 3D acceleration, 3D rate of turn (gyroscopes), and 3D earth-magnetic field data. Together they are capable of tracking each body segment in real time. The system is not capable of measuring alpine

skiing autonomously, since it requires a flat surface and 'fixed contacts' with the ground (i.e. not sliding or rolling). However, using it in combination with an RTK (Real Time Kinematic) global navigation satellite system (GNSS) could result in a reliable system for 3D measurements in alpine skiing. As reported in Matej's experiment, four different experiment were performed:

- Force pendulum experiment
- Walking experiment
- Gate positions experiment
- Skiing experiment

The experimental setup is widely described in the paper. For the aim of the thesis, the final results are important, where the force pendulum experiment reported a drift between a simple MTx sensor and the camcorder were small: after 10s the drift was 0.8° (s=0.6°), while the mean drift at 35s was 2.1° (s=1.7°), 3.3° (s=2.2°), and 4.2° (s=2.9°) for 0.5, 1, and 2 Hz, respectively. Secondly they noted a systematic difference between the maximum swing angles about 2.1-2.7° lower with the MTx-based than camcorder-based measurements. Passing through the second (walking) and third (gate positions) experiments and moving to the final skiing experiment, this was set up and performed in 4h. The two skiers involved performed five runs, with the whole of each run being recorded. The data were available in one day. The participants wearing a motion capture suit under their normal racing suit, skied through the same gate set-up. The sensor were positioned according to the motion capture suit manufacturer's recommendations. The GNSS devices were carried in a small backpack (the rover) with the antenna positioned near his shoulder and posterior neckline. Data sampling rate was at 20 Hz with 5-7 mm horizontal and 12 – 15mm vertical standard error. GNSS data and from the motion capture suit were imported in Matlab, synchronized and then filtered with two unscented Kalman filters running forward and backward in time and performs fixed-interval offline smoothing of the estimated signals. Ski experts were unable to identify any segment between the animations from Moven studio (the software adopted to analyse xSens suit data) and the video clips. Since there is not an experimental setup to validate the reliability of the system in an entire run, camcorder-based 3D measurement validation is the only option. But the reference trajectory reliability was very high, together with a high absolute accuracy for the entire ski run. A potential limitation for such system is satellite visibility. The antenna with the in-built sensor that receives signals from the satellites is inclined in several directions in alpine skiing, or even hidden behind body parts. [M. Supej, 2010].

The motion capture suit and RTK (Real Time Kinematic) GNSS may be a great advantage in the study of alpine skiing, both from the research and the market point of view, since it allows motion capture over a large volume. Large capture volumes are especially important in alpine skiing, where the environment is constantly varying, resulting in a variety of skier movement strategy (For example, 2014 Winter Olympics downhill course was 3495 meters in length with a vertical drop of 1075 meters

[30.8 % average gradient] – information source: (https://en.wikipedia.org/wiki/Alpine_skiing_at_ the_2014_Winter_ Olympics) (17).

RTK GNSS systems, together with inertial sensors imbedded in a motion capture suit can improve human movement measurement. This reduces preparation time and operation that can be performed with limited manpower compared with camcorder-based systems. The short time needed for elaborate results give it more strength in develop technique or tactical analysis in elite racers.

Unfortunately, one disadvantage of the motion capture suit is that athletes could find it inhibiting. In elite skiing, each single particular of the racing equipment is strongly analysed and selected. A motion suit can be a real bother for such type of athletes. But if compared with the difficulties coming from the utilization of markers in camcorder-based applications, this can be marginal. Considering system's advantages, this can be suited also for the outdoor sport activities without fixed ground contact, like cross-country skiing, ice skating, inline skating, rowing, and cycling.

However, the advantages and disadvantage came to an end when the discussion leaves the research filed coming to the market sector. RTK GNSS system and the motion capture suit have a high cost. Considering that the basic setup of Xsens instrumentation starts by 40000€/US$, providing only sensors and basic software, it is clear that the price of the system presented in the work can raise up to hundreds of thousand dollars, making it unsustainable for most of ski teams.

Even biggest ski teams like USSA get no government funding, so athletes success is dependent on passionate of fans and private sponsorship [www.alpine.usskiteam.com]. Such system is, in this way, available only for a small part of elite racers.

In this thesis work, a method to obtain meaningful performance index is analysed, with the aim to strongly lower the correlated costs.

3.2.2 Airbag based protecting device in skiing

Ideas beyond the setup proposed in this work, start by considering a spreading protecting device in ski. In motorcycling, inflatable protectors are devices either embedded within or worn on top of other clothing, aiming to reduce severity of injuries in case of motorcycle accidents.

There are two categories of motorbike airbag: those activated by mechanic and those activated by electronics. The airbags mechanically activated are composed by a cylinder of gas for inflating it, connected with a cable to the motorbike. For skiing/snowboard, it will be necessary to connect the cable to the binding system.

Electronically activated airbags were initially only used for motorcycle races. Then spread towards tourist bikers and racing skiers. There are different types of such airbags. Some could protect the neck and the upper part of the back. Others protect the entire torso. The activation of the cylinder that inflates the airbag is controlled by an electro-device, which receives information from sensor and elaborate them with an embedded CPU. Those can be integrated on the airbag system or fixed in the motorbike. The absence of cables in the electronic airbag make them perfect for ski/snowboard applications. The only drawback is the high cost of such device. For mechanical airbag is between 200€ to 590€. Electronica airbag is between 1500€ to 4600€. [A.Marega, 2015].

An Air bag based protecting device has been developed by Dainese in racing framework, the D-Air Ski. The development started in 2011, with a collaboration with FIS. This gave Dainese the possibility to collect data from world cup racers like Werner Hell, Jan Hudec and Manuel Osborne Paradis. Unfortunately, the dynamics of a skier during a world cup competition is totally different from that of a recreational skier in a normal ski resort's slope. The D-air ski as it is cannot be addressed to any other skier than elite racers. The algorithms for falls recognising and to trigger air bag opening have to be developed. In this framework, this thesis' work aims firstly to analyse recreational skiers in terms skiing level to permit a future airbag device to be setup basing on the skier's skiing ability. Then the second part of this work, focused on safety in ski, aims to understand significant values during falls thanks to simulations with different methods.

The next part of this thesis will present the work done in this direction. In the next chapter, are reported firstly the in field tests session. Starting in April 2013, up to March 2015, several in field session were performed, in order to collect data aiming to skiers classification. Then the collected data were analysed and elaborated thanks to Matlab scripts.

The subsequent chapter (number 6), points towards skiing safety, presenting the different methods adopted to perform falls simulations. In addition, data analysis on those falls has been performed, obtaining significant values of angular velocities and accelerations that will be useful in the development of an Air bag protective system device for recreational skiers.

Chapter 4: In field Tests

4.1 Instrumentation

The first tests section presents materials and methodologies adopted in this study. Starting from the sensors and moving to softwares and Matlab analysis.

4.1.1 Sensors adopted

In this study, four different types of Inertial Measurement Units (IMUs) were considered:

- **2D-data collector**, from 2D Debus e Diebold Meßsysteme GmbH

  Measurement specs:

  - 3-axes Acceleration [±2, ±4, ±8, ±16 g]
  - 3-axes Angular velocity [±250, ±500, ±1000, ±2000 deg/s]
  - GPS

  Recording specs:

  - Battery not embedded
  - 30Mb internal capacity

  Other specs:

  - Sampling rate: user programmable from 25Hz to 800 HZ
  - Unit number:1

- Hard case
- Modular device

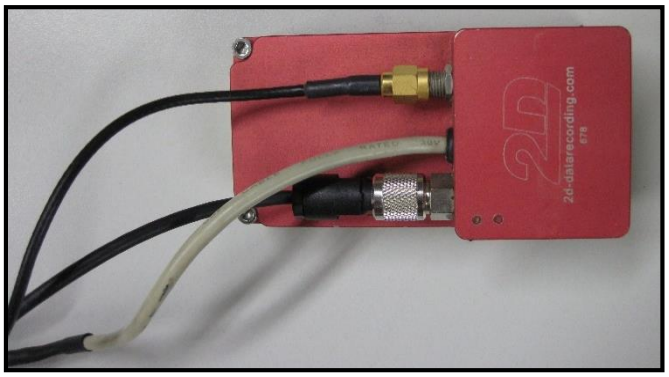

Figure 4-1: 2D data logger sensor

This sensor differs from the other three for embedded GPS that is very useful in order to track the skier's run. The GPS module had an update rate of 12.5 Hz. Technical specifications sheet of the GPS module reports in addition:

- Altitude sensibility: 0.01 m
- Course sensibility: 0.01 deg
- Speed sensibility: 0.01 km/h
- Latitude (decimal): 0.0000001 deg
- Longitude (decimal): 0.0000001 deg

The aluminium housing [44 x 34 x 15 mm] and the low weight (54g) make it suitable for a large applications, but the need of the external power supplier and of the laptop are an impediment on in field skiing tests.

- **MTw development kit**, from Xsens

The MTw development kit is a solution for applications where orientation is required via a wireless connection. It is highly suitable for markets like training and simulation, pedestrian navigation, test and measurement. The sensor are the same embedded in the Xsens motion suit adopted in Matej Supej's studies. The software (MT software suit) allows to configure Xsens' products and to wireless connect up to five sensors to a laptop. [www.xsens.com]

Measurement specs:

- 3-axes Acceleration [±16g]
- 3-axes Angular velocity [±1200 deg/s]

- Orientation data

Recording specs:

- Battery embedded [About 2.5h]
- Real-time saving on laptop

Other specs:

- Sampling rate depends of number of IMUs [Max 150Hz with one unit]
- Unit number:10
- Plastic case 34.5 x 57.8 x 145 mm

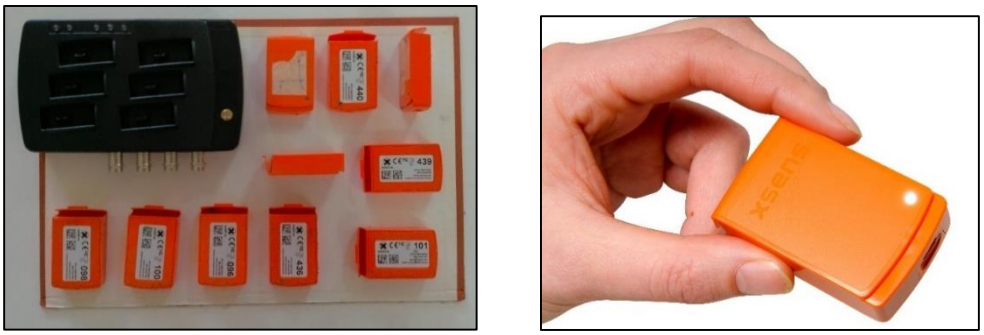

Figure 4-2: Xsens lite kit

Humotion, from Achillex GmbH

The Humotion IMUs provide great measurement specifications into a compact body frame. Their battery permits long outdoor test sessions. Easiness is a key factor for this sensor.

Measurement specs:

- 3-axes Acceleration [±16g]
- 3-axes Angular velocity [±2000 deg/s]
- Magnetic fields

Recording specs:

- Battery embedded [max 60h]
- Internal storage

Other specs:

- Sampling rate 400HZ
- Unit number:1
- Plastic
- Pressure sensor
- Temperature sensor

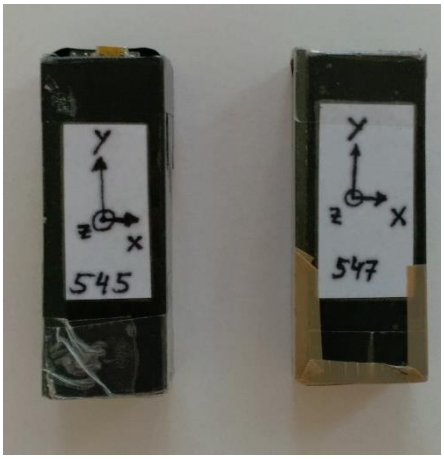

Figure 4-3: Two humotion sensors

- **EXLs3**, from EXEL s.r.l.

The EXLs3 is a miniaturized electronic device with the function of real-time Inertial Measurement Unit (IMU). It features a complete MEMS sensor set, which is composed of a tri-axial accelerometer, gyroscope and compass, a 32-bit Cortex microprocessor for data processing. The Bluetooth radio embedded, allows easy interfacing to a wide range of devices (PC, Tablet, Smartphone) without the need of additional hardware so that data can be transmitted wirelessly up to 10 meters.

The on-board CPU provides algorithms for orientation estimation with Kalman filtering in order to give positions measurements. [www.exelmicroel.com].

Measurement specs:

- 3-axes Acceleration [Selectable full range: ±2 / ±4 / ±8 / ±16g]
- 3-axes Angular velocity [Selectable full range: ±250 / ±500 / ±1000 / ± 2000deg/s]
- 3-axis magnetometer

Recording specs:

- Battery embedded [max 4h]
- Internal storage [1 GB]

Other specs:

- Sampling rate 200Hz for raw data, 100 Hz for orientation data
- Embedded CPU: S32-bit MCU, Cortex-M3 (low voltage) @72 MHz

- Plastic case 54 x 33 x 14 mm
- Bluetooth 2.1 class 1

Figure 4-4: Xsens kit and sensors

4.1.2 Sensors' software

The four sensors presented have different software and different data collection methods. We can associate Xsens and Exel sensors: both have the possibility to register real-time data and to register in the internal memory. In the first case, it is necessary to have a laptop near the sensor, as example in the backpack or carried by someone who follows the action. In the case of Xsens, the range of motion of the Wi-Fi transmission is a little bigger than the Bluetooth's one of the Exel. The 2D data recorder and the Humotion do not have the possibility to control the data collection, once started. They both need a physical connection to a laptop to start and stop the data collection.

1) **2D** software

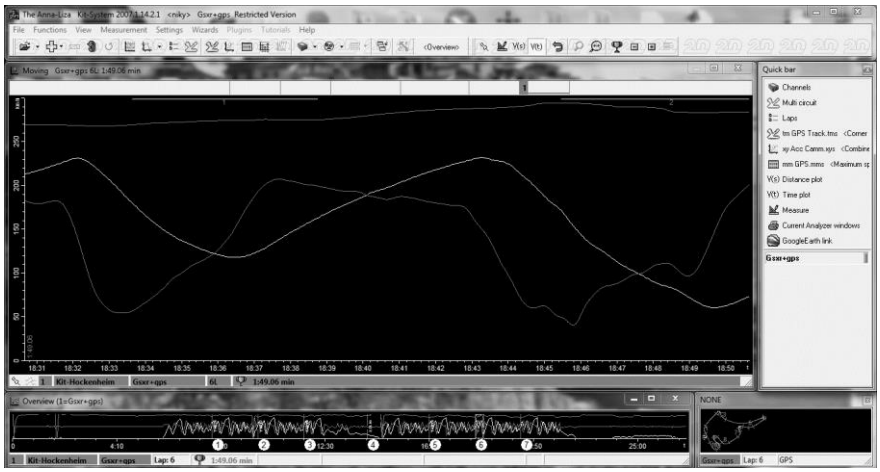

Figure 4-5: 2D software

2D software – vers 2007.1.14.2.1 is built for automotive and motorcycling but the software also suits for skiing tests. The sensor together with the software were chosen because are the base components of Dainese's D-Air system, both for motorcycling and skiing

2) **Xsens** software

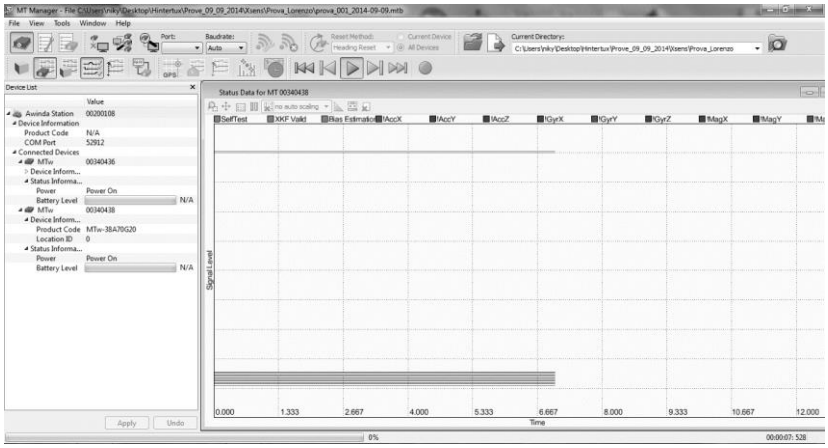

Figure 4-6: MT Manager

Xsens' software "MT manager" permits to control in real time the sensor. It is possible to observe their working status, and the orientation. There is a continuous data streaming towards the laptop, were the data are stored in specific folders.

3) **Humotion** software: " Humotion Data Collector - 3.1.553 "

Probably the easier software between the four presented in this thesis; "Humotion data logger", in its 3.1.553 version, present a user-friendly interface. The software automatically recognize the sensor, once connected via USB. Then it is possibly to set the pc folder were to extract data. To collect data, a simply start/stop button is available. Once pressed, is sufficiently to remove the USB cable to start the acquisition.

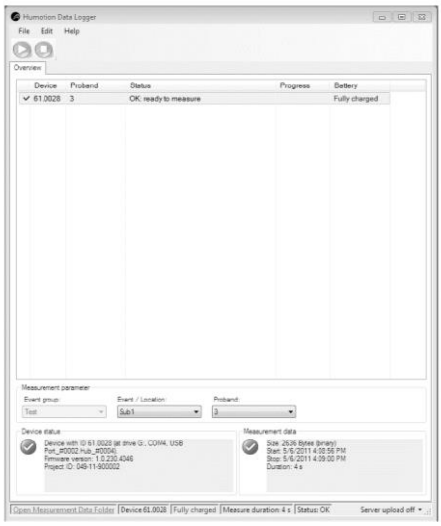

Figure 4-7: Humotion data logger start window

The sensor automatically saves uncalibrated data. When the humotion is reconnected to the pc, the acquisition can be stopped. Then, with the 'Export' function, it is possible to calibrate data thanks an internal file that contains calibration constants for the selected Humotion (are provided with the software in the purchase). The result is a .txt file that contains:

- Time stamps in milliseconds
- X axis acceleration [m/s^2]
- Y axis acceleration [m/s^2]
- Z axis acceleration [m/s^2]
- X axis gyroscope [rad/sec]
- Y axis gyroscope [rad/sec]
- Z axis gyroscope [rad/sec]
- X axis magnetometer [µTesla]
- Y axis magnetometer [µTesla]
- Z axis magnetometer [µTesla]
- Barometric pressure in hPA [not calibrated]
- Temperature of pressure sensor [not calibrated]
- Battery voltage [V]

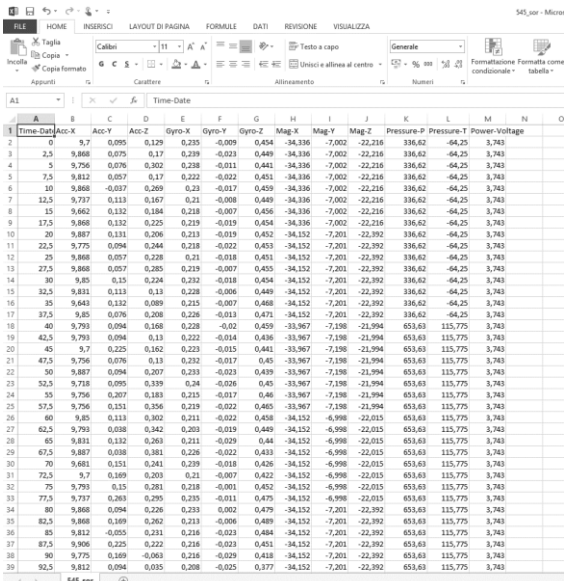

Time-Date	Acc-X	Acc-Y	Acc-Z	Gyro-X	Gyro-Y	Gyro-Z	Mag-X	Mag-Y	Mag-Z	Pressure-P	Pressure-T	Power-Voltage
0	9,7	0,095	0,129	0,235	-0,009	0,454	-34,336	-7,002	-22,216	336,62	-64,25	3,743
2,5	9,868	0,075	0,17	0,239	-0,023	0,449	-34,336	-7,002	-22,216	336,62	-64,25	3,743
5	9,756	0,076	0,302	0,238	-0,011	0,441	-34,336	-7,002	-22,216	336,62	-64,25	3,743
7,5	9,812	0,057	0,17	0,222	-0,022	0,451	-34,336	-7,002	-22,216	336,62	-64,25	3,743
10	9,868	-0,037	0,269	0,23	-0,017	0,459	-34,336	-7,002	-22,216	336,62	-64,25	3,743
12,5	9,737	0,113	0,167	0,21	-0,008	0,449	-34,336	-7,002	-22,216	336,62	-64,25	3,743
15	9,662	0,132	0,184	0,218	-0,007	0,456	-34,336	-7,002	-22,216	336,62	-64,25	3,743
17,5	9,868	0,132	0,225	0,219	-0,019	0,454	-34,336	-7,002	-22,216	336,62	-64,25	3,743
20	9,887	0,131	0,206	0,213	-0,019	0,452	-34,152	-7,201	-22,392	336,62	-64,25	3,743
22,5	9,775	0,094	0,244	0,218	-0,022	0,453	-34,152	-7,201	-22,392	336,62	-64,25	3,743
25	9,868	0,057	0,228	0,21	-0,018	0,451	-34,152	-7,201	-22,392	336,62	-64,25	3,743
27,5	9,868	0,057	0,285	0,219	-0,007	0,455	-34,152	-7,201	-22,392	336,62	-64,25	3,743
30	9,85	0,15	0,224	0,232	-0,018	0,454	-34,152	-7,201	-22,392	336,62	-64,25	3,743
32,5	9,831	0,113	0,13	0,228	-0,006	0,449	-34,152	-7,201	-22,392	336,62	-64,25	3,743
35	9,643	0,132	0,089	0,215	-0,007	0,468	-34,152	-7,201	-22,392	336,62	-64,25	3,743
37,5	9,85	0,076	0,208	0,226	-0,013	0,471	-34,152	-7,201	-22,392	336,62	-64,25	3,743
40	9,793	0,094	0,168	0,228	-0,02	0,459	-33,967	-7,198	-21,994	653,63	115,775	3,743
42,5	9,793	0,094	0,13	0,222	-0,014	0,436	-33,967	-7,198	-21,994	653,63	115,775	3,743
45	9,7	0,225	0,162	0,223	-0,015	0,441	-33,967	-7,198	-21,994	653,63	115,775	3,743
47,5	9,756	0,076	0,13	0,232	-0,017	0,45	-33,967	-7,198	-21,994	653,63	115,775	3,743
50	9,887	0,094	0,207	0,233	-0,023	0,439	-33,967	-7,198	-21,994	653,63	115,775	3,743
52,5	9,718	0,095	0,339	0,24	-0,026	0,45	-33,967	-7,198	-21,994	653,63	115,775	3,743
55	9,756	0,207	0,183	0,215	-0,017	0,46	-33,967	-7,198	-21,994	653,63	115,775	3,743
57,5	9,756	0,151	0,356	0,219	-0,022	0,465	-33,967	-7,198	-21,994	653,63	115,775	3,743
60	9,85	0,113	0,302	0,211	-0,022	0,458	-34,152	-6,998	-22,015	653,63	115,775	3,743
62,5	9,793	0,038	0,342	0,203	-0,019	0,449	-34,152	-6,998	-22,015	653,63	115,775	3,743
65	9,831	0,132	0,263	0,211	-0,029	0,44	-34,152	-6,998	-22,015	653,63	115,775	3,743
67,5	9,887	0,038	0,381	0,226	-0,022	0,433	-34,152	-6,998	-22,015	653,63	115,775	3,743
70	9,681	0,151	0,241	0,239	-0,018	0,426	-34,152	-6,998	-22,015	653,63	115,775	3,743
72,5	9,7	0,169	0,203	0,21	-0,007	0,422	-34,152	-6,998	-22,015	653,63	115,775	3,743
75	9,793	0,15	0,281	0,218	-0,001	0,452	-34,152	-6,998	-22,015	653,63	115,775	3,743
77,5	9,737	0,263	0,295	0,235	-0,011	0,475	-34,152	-6,998	-22,015	653,63	115,775	3,743
80	9,868	0,094	0,226	0,233	0,002	0,479	-34,152	-7,201	-22,392	653,63	115,775	3,743
82,5	9,868	0,169	0,262	0,213	-0,006	0,489	-34,152	-7,201	-22,392	653,63	115,775	3,743
85	9,812	-0,055	0,231	0,216	-0,023	0,484	-34,152	-7,201	-22,392	653,63	115,775	3,743
87,5	9,906	0,225	0,222	0,216	-0,023	0,451	-34,152	-7,201	-22,392	653,63	115,775	3,743
90	9,775	0,169	-0,063	0,216	-0,029	0,418	-34,152	-7,201	-22,392	653,63	115,775	3,743
92,5	9,812	0,094	0,035	0,208	-0,025	0,377	-34,152	-7,201	-22,392	653,63	115,775	3,743

Figure 4-8: Excel view of the sensor's output

The axes are written in the housing of the sensor. The x-axis is along small side of housing, right-handed coordinate system; the y-axis is along the long side of housing, positive on side of USB connector; z-axis is along the height of housing, positive on side of USB connector. Producer claims a 3° maximum deviation of sensor axis to housing.

4) **Exel** software: “EXEL IMU Controller - 1.4.0.3 ”

Figure 4-9: Exel Imu Controller

To connect the Exel sensor to the PC it is necessary a Bluetooth communication between them. Laptops have Bluetooth module integrated. Most desktop, need an additional receiver. It is important, after having installed the software and before starting first data collection, to take note about the number of the COM port (Communication port). After the connection, it is important to select in the software “EXEL IMU Controller 1.4.0.3”, the data collection mode:

- STREAM
- LOG

The Stream mode is available only if the laptop is near the sensor (within 10m). The data are stored in the internal storage of the laptop, in a user selectable folder. To start the acquisition is only need to press the “start” button in the software interface.

The Log mode stores data in the internal storage of the sensor. In this setup it is possible to select how the sensor will act once removed from it communication dock. It is possible to start the acquisition with the software start button, or when the sensor is removed from the dock. Once the sensor is collecting data, the led start blinking blue.

The stream modality is very important in the case of direct data streaming: it is possible to analyse visually the sensor’s position through the software interface. The user can define data’s collection structure. It is possible to select whereas to store magnetometer data, or quaternions obtained by magnetometer.

In addition, an Android application of the Exel software is available. Named “SkiloREC” is still (September 2015) available as private beta and still not published on Google Play Store. Thanks to an easy interface, it permits data collection via mobile phone. It automatically stores gyroscope, accelerometer and magnetometer data. In addition saves the same data obtained with the smartphone’s own sensors, together with the smartphone’s GPS signal. Easier to use, avoids the need to carry the laptop on test field.

However, the impossibility to have a full control in acquisition is its major drawback. To get a better understand the different specifications about the sensors, a comparative table is presented.

4.1.3 **Comparative table of the four sensors**

Sensor / Parameter	2D		Xsens		Humotion		Exel		
		Full scale		Full scale		Full scale		Full scale	Measurement unit
Time stamp	X				X		X		ms
X-axis acceleration	X	10	X	16	X	16	X	16	g
Y-axis acceleration	X	10	X	16	X	16	X	16	g
Z-axis acceleration	X	10	X	16	X	16	X	16	g
X-axis gyroscope	X	800	X	1200	X	2000	X	2000	Deg/s
Y-axis gyroscope	X	800	X	1200	X	2000	X	2000	Deg/s
Z-axis-gyroscope	X	800	X	1200	X	2000	X	2000	Deg/s
X-axis magnetometer			X		X		X		µT
Y-axis magnetometer			X		X		X		µT
Z-axis magnetometer			X		X		X		µT
Orientation q0							X		/
Orientation q1							X		/
Orientation q2							X		/
Orientation q3							X		/
Barometric pressure					X				hPa
Temperature of pressure sensor					X				/
Battery voltage					X		X		V
Altitude	X								/
Longitude	X								°
Latitude	X								°
GPS velocity	X								/
Satellite Velocity	X								/
Max Sampling rate		200		150		400		200	Hz
Battery life		/		2.5		8		4	hours

4.1.4 Other equipment

In addition to sensor's hardware and software, the study adopted also two different type of back-protectors, where to place the sensors:

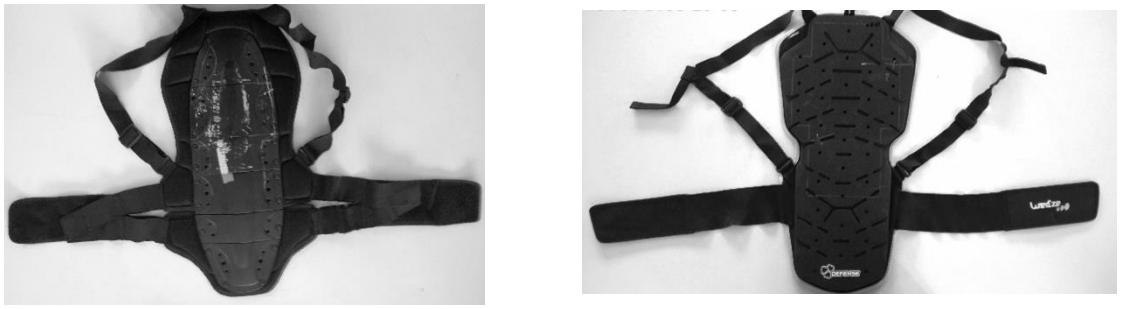

Figure 4-10: Dainese (left) and Wedze (right) back protectors

Left side photo: Dainese back protector, shock absorbing surface material, flexible and ergonomic. Right side photo: Wedze back protector, semi rigid material, with shock absorbing surface material, a little more uncomfortable to wear in respect to Dainese's one.

4.2 In field tests

Dainese D-air system is considered the status of art for what concern electronica activated airbags. The idea to apply the knowledge in the motorcycle field to alpine ski comes by considering the need of such a system both in competition and in recreational ski. The core of the D-air system is the embedded CPU that receives data from a 2D-datalogger sensor. In the first on-field test, this sensor was tested and compared with the others three.

The D-air system developed for alpine ski, is nowadays suitable only for elite ski racers. Those athletes are able to ski downhill to incredibly high speeds. In the Lauberhorn annually in mid-January take place world cup alpine ski races. The downhill course is the longest in the world with its 4480 meters. On its Haneggschuss was registered the highest speed ever measured in a FIS World cup race: in this section in 2013 the France athlete Johan Clarey was able to reach 161.9 Km/h. Recreational skiers cannot reach such speeds in any ski resort around the world.

Snow conditions, materials, other people and also speed limits are constraining factors for speed reduction. An average speed in ski resort for an expert skier is between 40 km/h and 70 km/h. Higher speeds are hardly reached and strictly not recommended. Generally, on ski resort the speed is lower than 40 km/h. But even if the speed is not very high, compared to that of ski racers, risk of severe injuries is high.

A research in the Parnassus ski resort found an overall rate of injury of 4.1 injuries per 1000 skiers. The injury rate for children and adolescent was 6.5 when for adult was 3.7 [Zacharopoulos A., Smyrnis A, Champipis A., 2015].

It is clear that an active protective device cannot generally suit ‘as it is’ for all the skiers. It is necessary to understand the skier’s skiing ability and to calibrate the system to the skier. A protecting device that works with an elite racing has to be calibrated differently from that applied to a beginner recreational skier.

With this idea, the first part of this work aim to find a setup and an algorithm able to differentiate between different skiers skiing levels. Once established the skier level it will be possible to setup the protective device.

With this aim, several on-field test were performed. This involved both the University of Padua, department of Industrial Engineering, and the University of Salzburg, Department of Sport Engineering. The University of Padua performed five on-field tests from April 2013 to March 2015. The University of Salzburg performed four on-field test in February 2014. The sensor adopted were the four presented above, in different setups.

The following tables summarize all the on-field tests:

Test session ID	Test session	Date	2D	Xsens	Humotion	Exel
I0	Cortina	25-26/04/2013	X	X	X	
A4, A6, A7, A9	St Christoph	06/02/2014			X	
I1	San Vito	05/02/2014			X	
I2	San Vito	10/03/2014			X	
I3	Folgaria	14/03/2014			X	
I4	Hintertux	08/09/2014		X	X	
I5	San Vito	07/03/2015				X

Figure 4-10: In field test session, reporting sensors adopted

- I0, Cortina.

  Test were performed in Ski Area Faloria, Cristallo, Mietres. With its 5 black slopes, 11 red slopes and 8 blue slopes, the ski area is suitable both for beginners and child and expert skiers. (http://cortina.dolomiti.org/index.cfm/Ski-Area/Ski-Area-Faloria-Cristallo-Mietres/) (23)

- A4, A6, A7, A9, St. Christoph.

  In the Arlberg ski area, St. Christoph best suits for beginners skiers with easy, snow-sure beginners slopes. Intermediate will be off and away to explore the huge Arlberg ski area. (https://www.inghams.co.uk/ski-holidays/ski-resorts/austria/arlberg-ski-area/st-christoph) (24). The number near the letter A is an ID that Austria research team established and it identifies the group of skiers: A4 are Beginner skiers, A6 are both beginner and intermediate, A7 are intermediate skier and A9 are expert skier.

- I1,I2,I5 San Vito.

  The San Vito ski area is a small ski resort in northern Italy. It doesn't have a large number of slopes but because of its wide tracks, it suits perfectly to families, child but also small ski teams. (www.skiareasanvito.com) (25). Most of the test were performed in Antelao and Serpentina slopes. Wide, straight, and with low steepness, are the optimal place to learn to ski but also to train self-performance.

- I3, Folgaria.

  In the Alpe Cimbara mountains, the ski area Folgaria Lavarone has 100km ski tracks which suit for almost every type of skiers, from beginners to racers. (http://www.folgariaski.com/it/neve/ski-area-folgaria-fiorentini) (26).

- I4, Hintertux.

The Hintertux Glacier is Austria's only year ski resort. Beginners as well as experienced skiers have over 60 km of slopes in all levels of difficulty. It is not difficult to meet several elite ski teams training in this ski area, especially during the summer-autumn (http://www.hintertuxergletscher.at/en/skiing/hintertux-glacier.html) (27).

The following table is a summary of the on-field test sessions performed.

In the first column there is a string that identifies the setup adopted in that session. Images are reported after the table. The second column "Sensors & Place" identifies which sensors were adopted. The column "Nr of testers" shows how many skiers took part of that skiing session and the next column shows how many Runs were recorded and analysed in the study.

Setup	Sensors & Place				Nr of testers	Nr of runs	Tester Level		
I0 Cortina 2b 26/04/2013									
Set_I0_1	10 Xsens	Various	1 Humotion	Pelvis	1	10	1 EX		
Set_I0_2	6 Xsens		Various		1	3	1 BE		
Set_I0_3	1 Humotion		Pelvis		2	6	2 EX		
Set_I0_4	1 2D		Pelvis		4	14	1 BE	3IN	
A1 St Christoph 06/02/2014									
Set_A4_1	1 Humotion		Pelvis		8	23	8 BE		
Set_A6_2	1 Humotion		Pelvis		8	24	2 BE	6 IN	
Set_A7_3	1 Humotion		Pelvis		8	33	8 IN		
Set_A9_4	1 Humotion		Pelvis		8	53	8 EX		
I1 San Vito 25/02/2014									
Set_I1_1	1 Humotion		C7		7	81	1 BE	2 IN	4 EX
I2 San Vito 10/03/2014									
Set_I2_1	1 Humotion		C7		7	84	2 BE	3 IN	2 EX
I3 Folgaria 14/03/2014									
Set_I3_1	1 Humotion		C7		1	15	1 EX		
I4 Hintertux 08/09/2014									
Set_I4_1	1 Humotion		Pelvis		1		1 EX		
Set_I_2	2 Xsens		C7, Pelvis		2		2 EX		

Figure 4-11: In field tests setups table

The right column of the table reports the skiing level of the testers in each session.

It is possible to split the skiers into four main classes:

- Beginners
- Intermediates
- Experts
- Racers

Beginners are those skiers at their first experience with skis: They are able to descend almost flat slopes, without maintain parallelism between skis. Beginner's skiing velocity is low and controlled. Skier is able to stay balanced and to change direction.

Figure 4-12: Example of beginner skier

Intermediate skiers are able to perform parallel skiing, in almost every slope. There is still a visible rigidity in the movement and a limited flexion-extension of the body. Their skiing speed is moderate and controlled; there is balance on slightly bumpy slopes

Figure 4-13: Example of intermediate skier

Expert skier can perform almost every skiing technique at high speed in every type of slopes with total control, and no fear of moguls, steeps or ice.

Figure 4-14: Example of expert skier

Racers are those skier who are able to compete at least in local FIS competitions. Those racers, together with high class materials got years of training in several techniques, performing them almost perfectly.

Figure 4-15: Example of racer skier

In our in field tests we collected data from Beginners, Intermediate and Expert skiers. Racers were not considered as the study presented in this thesis addresses to analyse recreational skiers.

The setups reported in the table in Figure 4-11, differs both for the type of sensor and for its position:

- Setup **I0_1**: Humotion placed on a belt over pelvis and 10 xsens placed in predefined body segments

- Trunk: Xsens
- Pelvis: Xsens + Humotion
- Right Ski: Xsens
- Right Wrist: Xsens
- Left Wrist: Xsens
- Right Thigh: Xsens
- Left Thigh: Xsens
- Right Calf: Xsens
- Left Calf: Xsens
- Left ski: Xsens

Setup **I0_2**: 6 xsens units placed in predefined body segments

- Pelvis: Xsens
- Rigth Thigh: Xsens
- Left Thigh: Xsens
- Rigth Calf: Xsens
- Left Calf: Xsens
- Trunk: Xsens

Setup **I0_3**: One Humotion unit placed on a belt over the pelvis

- Pelvis: Humotion

Setup **I0_4**: One 2D datalogger placed on a belt over the pelvis

- Pelvis: 2D datalogger

Setup **A4_1-A9_4**: One Humotion sensor placed over a rigid back protector, near to pelvis

- Pelvis: Humotion

Setup **I1-I4**: One Humotion sensor placed over a back protector, near C7-T12.

- C7: Humotion

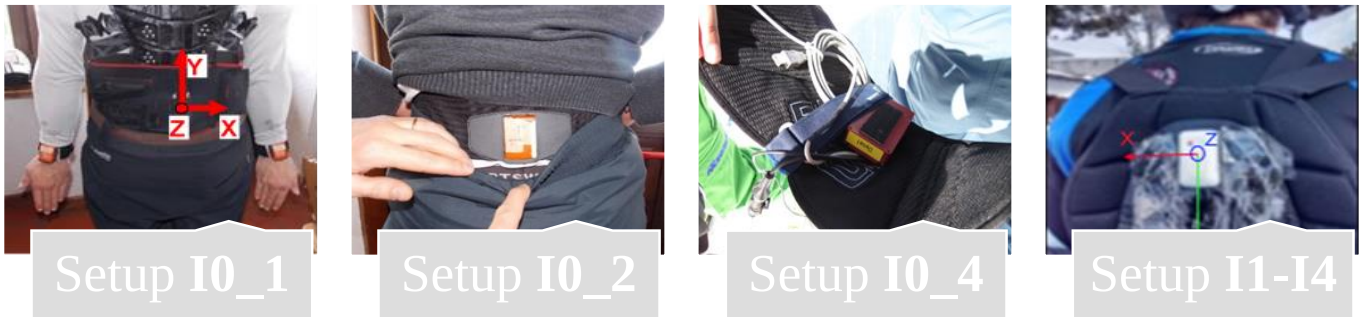

Figure 4-16: Different test setups

In the study we took care also at the skiing technique performed by the tester. Since it is not possible to remind what each skier performed, we distributed a diary sheet at the beginning of the test day. In this paper every tester had to write:

- The progressive number of the run
- the time of the end of the run
- the skiing technique
- The slope or the type of snow
- Any falls or almost fall event

In this way it was possible to associate the run to the skiing technique.

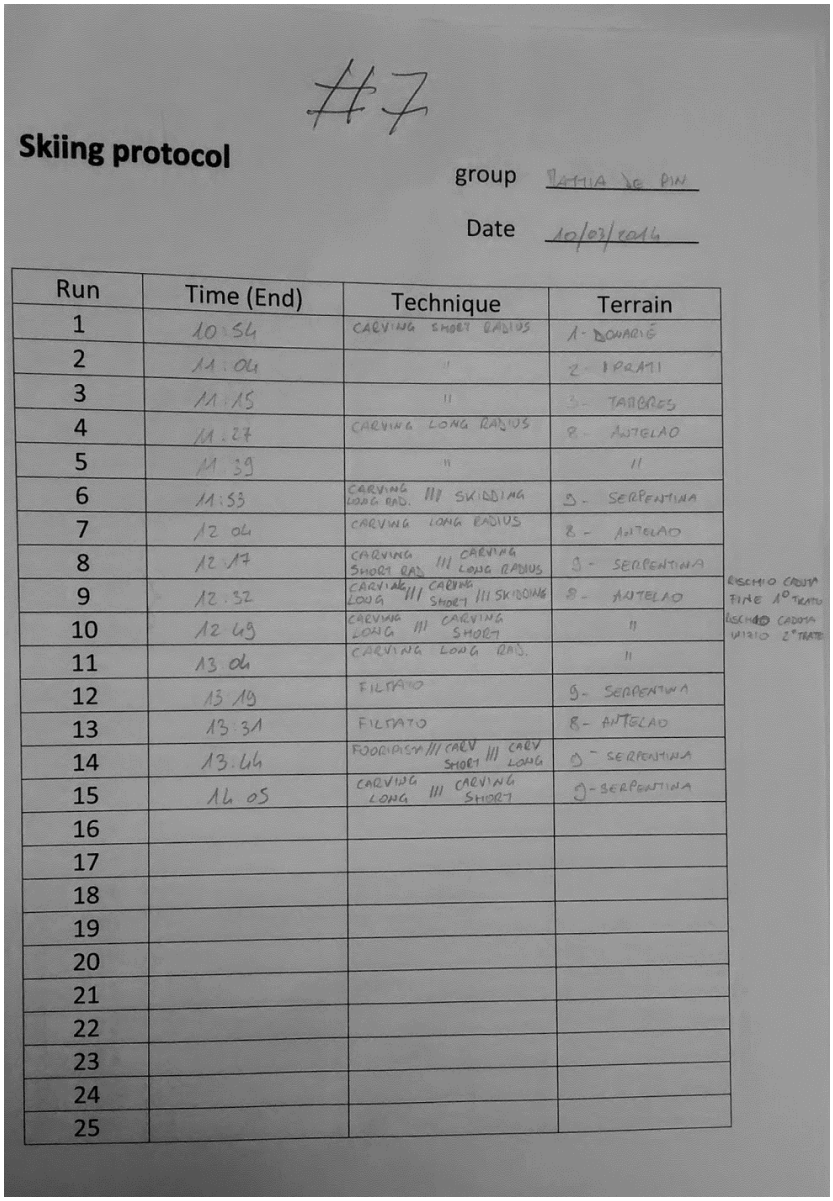

#7

Skiing protocol

group [illegible]

Date 10/03/2016

Run	Time (End)	Technique	Terrain
1	10:54	CARVING SHORT RADIUS	1- DOVARÈ
2	11:04	"	2- PRATI
3	11:15	"	3- TABBRES
4	11.27	CARVING LONG RADIUS	8- ANTELAO
5	11:39	"	"
6	11:53	CARVING LONG RAD. /// SKIDDING	5- SERPENTINA
7	12:04	CARVING LONG RADIUS	8- ANTELAO
8	12:17	CARVING SHORT RAD /// CARVING LONG RADIUS	5- SERPENTINA
9	12:32	CARVING LONG /// CARVING SHORT /// SKIDDING	8- ANTELAO
10	12:49	CARVING LONG /// CARVING SHORT	"
11	13:04	CARVING LONG RAD.	"
12	13:19	FILFATO	5- SERPENTINA
13	13:31	FILFATO	8- ANTELAO
14	13.44	FOORNISH /// CARV SHORT /// CARV LONG	5- SERPENTINA
15	14:05	CARVING LONG /// CARVING SHORT	5-SERPENTINA
16			
17			
18			
19			
20			
21			
22			
23			
24			
25			

RISCHIO CADUTA FINE 1° TRATTO
RISCHIO CADUTA INIZIO 2° TRATTO

Figure 4-17: Example of questionnaire

Chapter 5: Data analysis

5.1 Reference systems and preliminary raw data analysis

The four sensor have very different outboxes. It is impossible to place them with the same reference system. In each test field an accurate sensors placement was made, attempting to align with the most accuracy the housing to the tester's vertical axis. Due to the different conventions, this mean that the reference systems of the sensor were rotated depending on the sensor

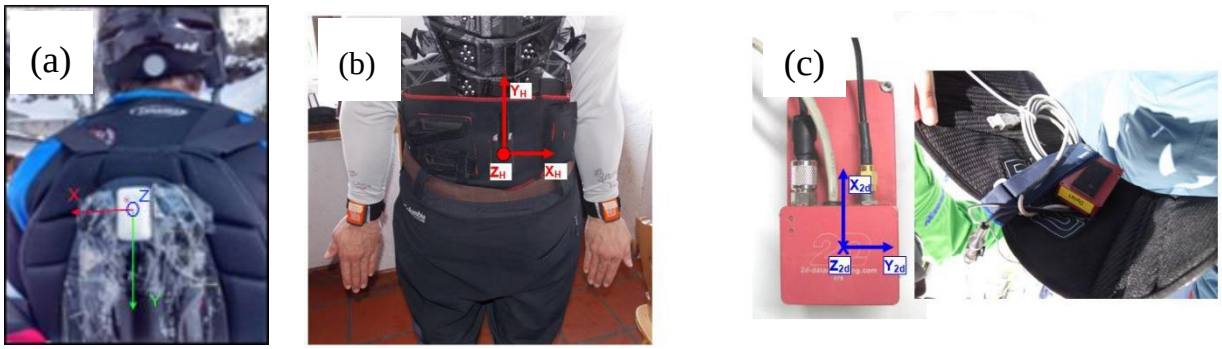

Figure 5-1: From left to right: (a) Exel,(b) Humotion and Xsens, (c) 2D datalogger

To analyse and compare the data, it was necessary to refer all the data to a common reference system. According to literature, it was chosen to refer the four systems to the ISB convention. The Standardization and Terminology Committee (STC) of the International Society of Biomechanics (ISB) proposes a general reporting standard for joint kinematics based on the Joint Coordinate Systme (JCS), first proposed by Grood and Suntay for the knee joint in 1983 [Grood and al, 1983]. STC proposes definition of JCS for the ankle, hip and spine. For each joint, a standard for the local axis system is generated. These axes then standardize the JCS.

In the study presented in this thesis, the most important articular joint is the hip, and it is necessary to refer to ISB convention to continue the analysis with a standardized method.

5.1.1 ISB convention

For most area of biomechanical research, the human hip joint is treated as a ball and socket joint. The centre of rotation is defined as the centre of hip joint, even if a measurable incongruity of ball and socket exist. [G. Wu et al, 2002]

The pelvic coordinate system (XYZ) - Figure 5-2:

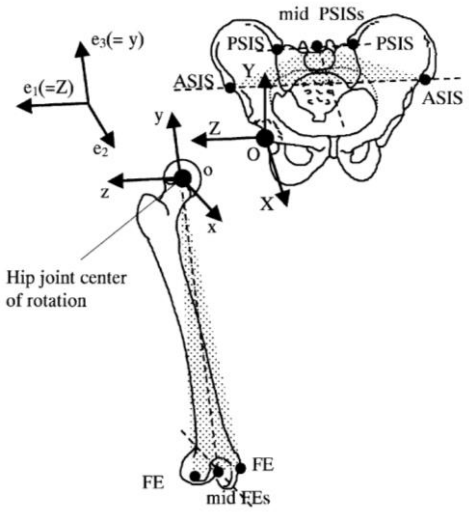

Figure 5-2: Illustration on the pelvic coordinate system (XYZ), femoral coordinate system (xyz), and the JCS for the right hip joint [G. WU et al, 2002]

O: The origin coincident with the right (or left) hip centre of rotation.

Z: The line parallel to a line connecting the right and left ASISs, and pointing to the right.

X: The line parallel to a line lying in the plane defined by the two ASISs and the midpoint of the two PSISs, orthogonal to the Z-axis, and pointing anteriorly.

Y: The line perpendicular to both X and Z, pointing Cranially [Cappozzo et al., 1995].

Femoral coordinate system (xyz) – Figure 5-2:

o: The origin coincident with the right (or left) hip centre of rotation, coincident with that of the pelvic coordinate system (O) in the neutral configuration.

y: The line joining the midpoint between the medial and lateral Fes and the origin, and pointing cranially.

z: The line perpendicular to the y-axis, lying in the plane defined by the origin and the two Fes, pointing to the right.

x: The line perpendicular to both y- and z-axis, pointing anteriorly [Cappozzo et al, 1995]

JCS and motion for the right (or left) hip joint:

e_1: The axis fixed to the pelvis and coincident with the Z-axis of the pelvic coordinate system. Rotation (α): flexion or extension. Displacement (q_1): mediolateral translation.

e_2: The axis fixed to the femur and coincident with the y-axis of the right (or left) femur coordinate system. Rotation (γ): internal or external rotation. Displacemente (q3): proximo-distal translation.

e_3: The floating axis, the common axis perpendicular to e_1 and e_3. Rotation (β): adduction or abduction. Displacement (q_2): antero-posterior translation.

The ISB convention uses landmark to define the systems. In the study presented in this thesis, the sensors were placed over rigid back protector at C7 level or at pelvis level, over a belt. It is not easly possible to exactly refer to the ISB convention. We decided to utilize the convention as definition of axes direction, but we referred to the local sensors' position as centre of the ISB system of reference.

In this way, placing a reference system on the tester's pelvis:

- the X-axis lays in the transverse plane, in posterior-anterior direction. ("ROLL")
- The Y-axis lays in the sagittal plane, in inferior-superior direction. ("YAW")
- The Z-axis lays in the transverse plane, in medial-lateral direction. ("PITCH")

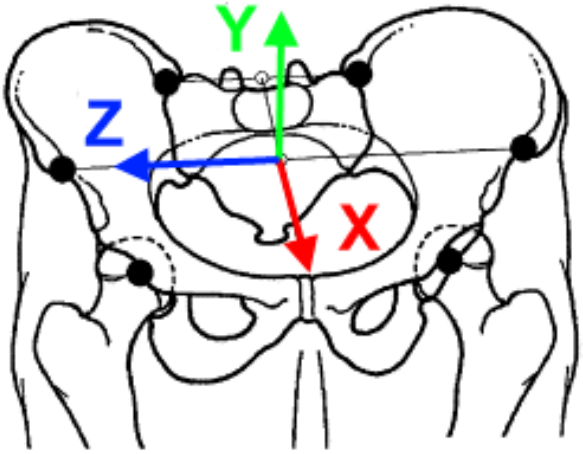

Figure 5-3: ISB convention

In the Figure 5-4 this system is applied to the skier, at pelvis level, on its back.

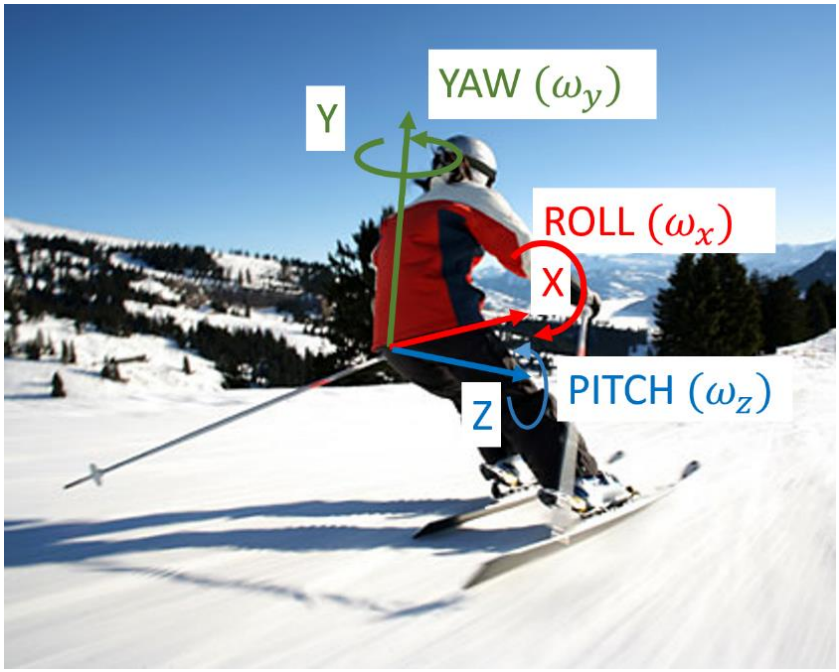

Figure 5-3: Roll, Pitch and Yaw angles and angular velocities

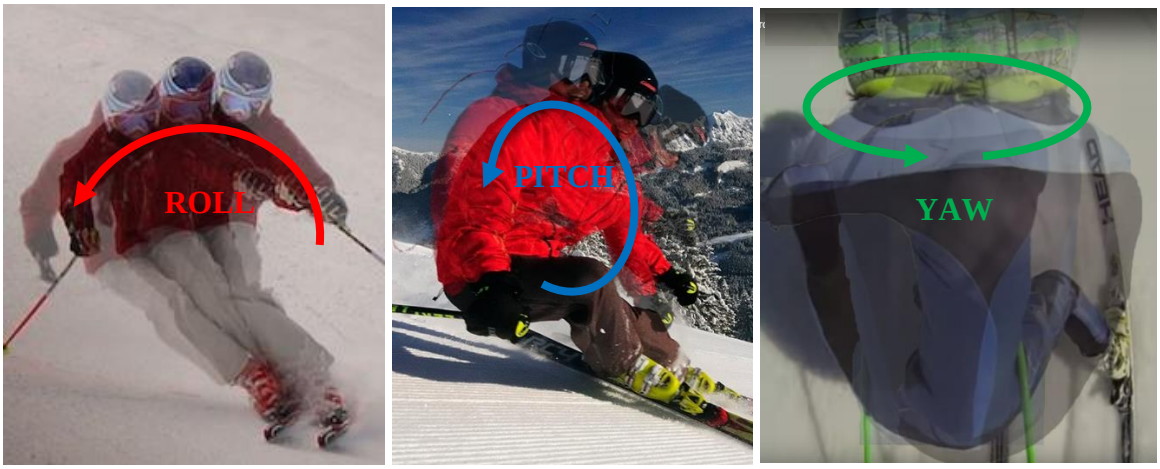

Figure 5-4: Roll, Pitch, Yaw detailed

Figure 5-4 reports a visual indication of "Roll, Pitch and Yaw" angles, applied to skier in different views.

5.1.2 Preliminary data processing

The sensors collect data into the embodied storage memory. After the tests, data have to be manipulated in order to obtain a processable data file. The passages, in the case of the Humotion sensors are reported in Figure 5-5:

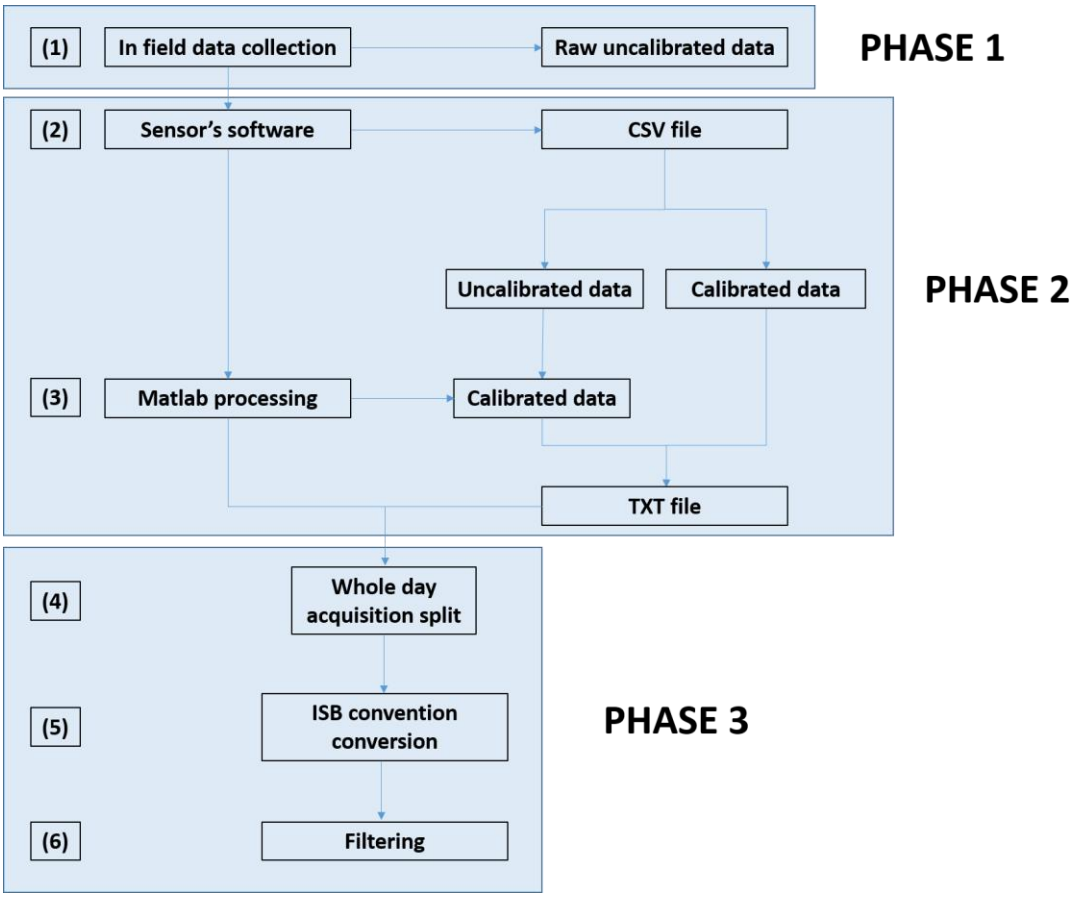

Figure 5-5: Passage to obtain a processable txt file

The data have to be processed through the sensors' software, in order to obtain standardized processable data for further Matlab reanalyses. The software's output are files with csv. With the older software releases (2014), it was not possible to obtain calibrated data from the software. It was needed a calibration procedure via Matlab software, having previously obtain the calibration constants. With later releases (September 2014), it was possible to export directly the CSV file into a txt calibrated file, because of with the sensors, Achillex Gmbh gave the calibration constants as a software's system file.

The calibrated data obtained were then processed via Matlab® in order to split the whole day acquisition file into single runs files. Then the axes of each sensor's data were aligned to the ISB convention, in order to start further data elaborations.

A first comparison of the collected data shows the strong difference between Xsens and Humotion data:

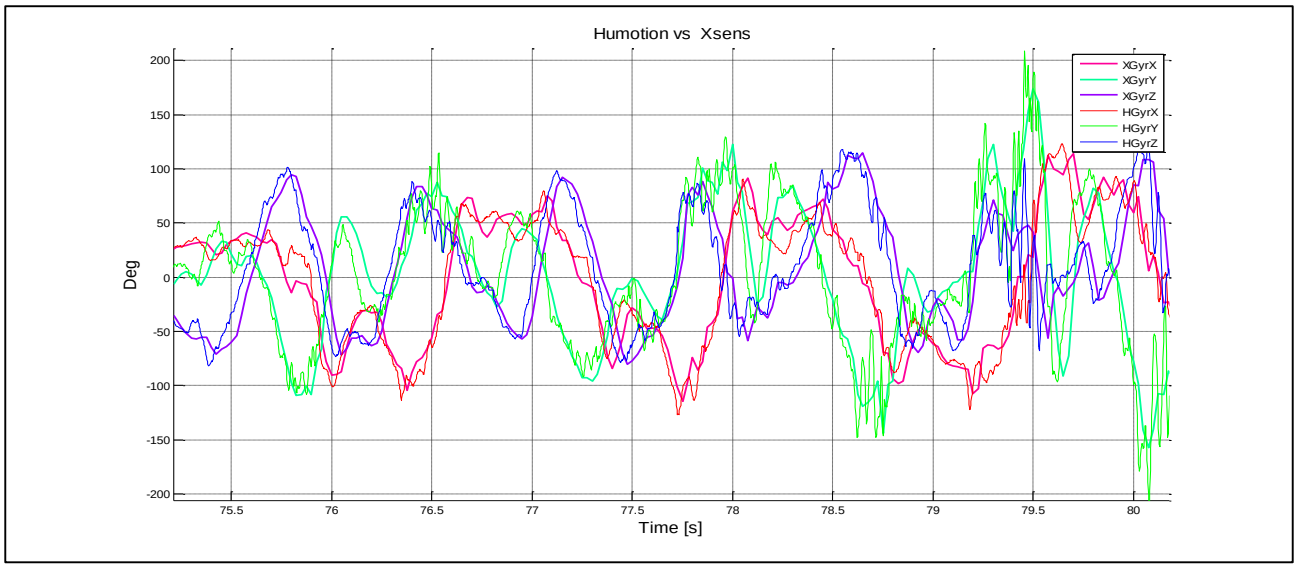

Figure 5-6: Humotion and Xsens signals overlapped

In the Figure 5-6 is reported a 5 seconds portion of a run, registred both with an Xsens and an Humotion sensors placed one on the top of the other. To differentiate the sensors, the Xsens signals are represented with a thicker line in respect the Humotion. The two sensors' signals have comparable trends, meaning that Xsens and Humotion have equivalent signals during skiing, but the Xsens has limited samping frequency if the picture is zoomed:

The second figure, 5-7, shows a zoom from the second 118.92 to 119.1. It is clear how the Xsens sampling frequency of 50Hz is critical in case of rapid signals. A quick action as a fall or a strong body displacement could not be observed. The Humotion with 400Hz of sampling frequency is good enough to register such fast actions.

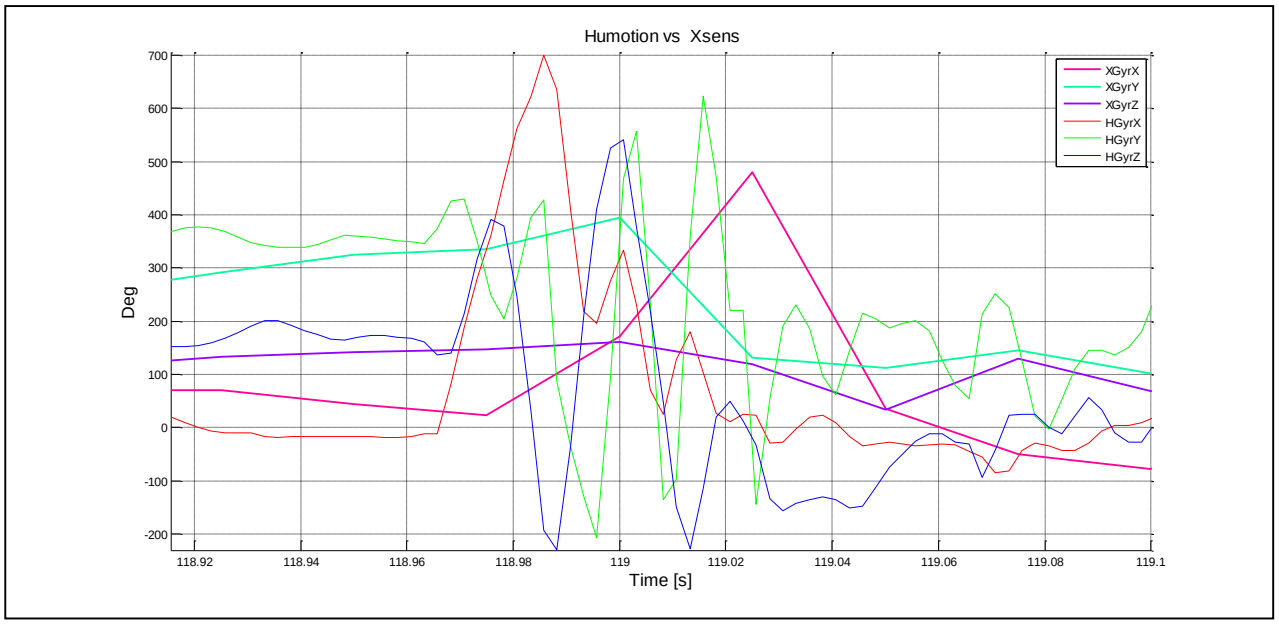

Figure 5-7: difference between Xsens and Humotion

The last step in data preparation is to filter the signals. Sensor have a great sensibility and skiing is a dynamic event. This leads to a strong amount of vibrations in the data. The data are filtered with a third order low pass Butterworth filter.

To have standardized signals, we decided to filter the data at the frequency of 2Hz. The result is a signal that contains the large part of the manoeuvre information, but removes all the unwanted due to vibrations.

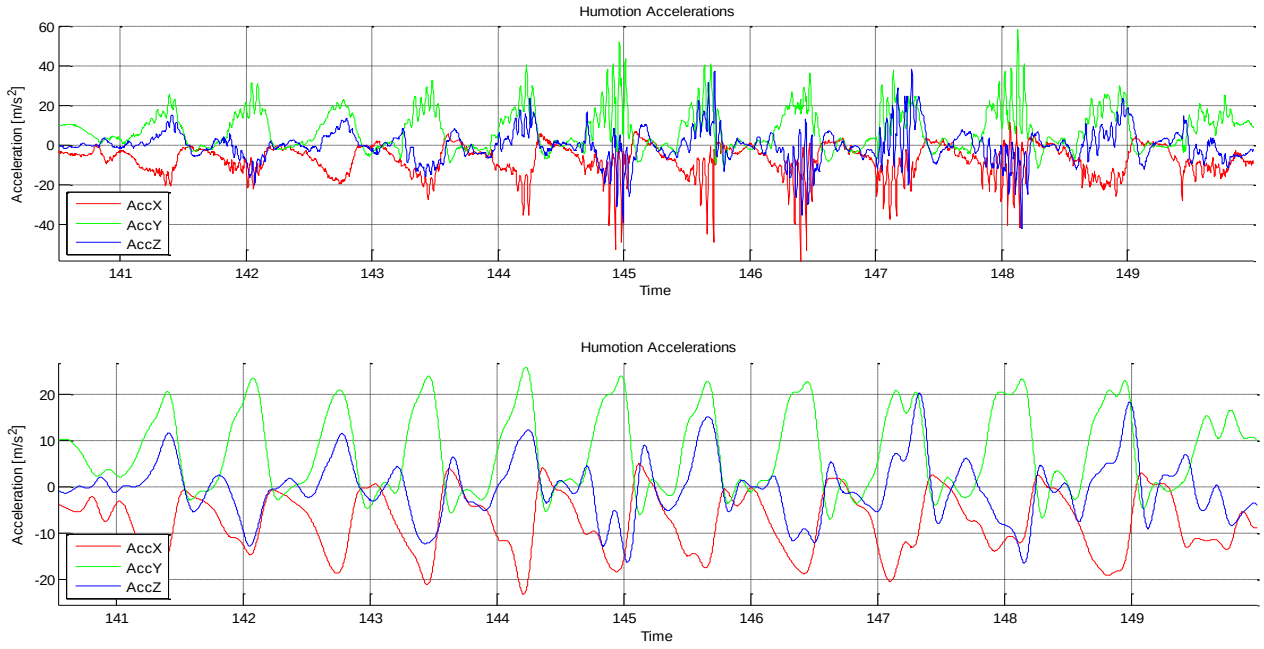

Figure 5-8: Unfiltered versus 2Hz filtered data

The result, shown in Figure 5-8 is a more regular signal, less influenced by the dynamic vibrations.

The biggest part of the analysis work was done by considering only acceleration and angular velocity, in different aspects. The magnetometer data are instead useful in case of sensor fusion algorithms. The low sampling frequency of the Xsens and the complex setup of the 2D datalogger, let us to concentrate on the Humotion sensor, considered the most pratical sensor due to its long lasting batteries, its small housing and the easiness to collect data.

5.2 Data analysis method

Having the output from the Humotion sensor software, stored as CSV format, the preliminary work that had to be done was to split the whole test session file into sub-files. For Example, in I1 test session Humotions recorded data for seven to eight hours. Elaborating almost a Gb of raw data for each sensor was not possible even for high end performance laptop, so it was necessary to find a way to split the day session. This was made through the Diadem® and Matlab® softwares.

Using the information carried by the barometric sensor, it was possible to identify the descending phase of the run and the ascending phase via cableway. An increment in the level of the atmospheric pressure meant a descending and skiing downhill phase. A reduction of such value triggered the ascending phase. In the case of absence of such a sensor, pre-defined triggers have to be made before the start and at the end of each run. Testers were asked to perform three consecutive wide trunk flexions. In this way, the skiing phase is clear enough to split the day-file. In addition, the cableway time is recognizable by a static position of the sensor in the space with only the noise given in input by the cableway acquired by the sensor.

Second step to proceed with the data analysis is to store all the splitted runs, in .txt format, in a well-known folders in order to get able to analyse all the runs together, if needed, via Matlab® software. To do this, we decided to insert in the run name, the following information:

- Session ID: I0-I5, A1.
- Humotion number: H1-H9.
- Tester level: BE (Beginner), IN (Intermediate), EX (Expert).
- Run number of the tester in the test day.
- The portion of the run, if needed, with a progressive enumeration.
- The style of skiing performed in that portion of run: SCV (Short carved turns), LCV (Long carve turns), SSK (Short skidded turns).

As an example, if an Intermediate tester wearing the Humotion number 4, in the second run of the first Italy test session performed a portion of run with short carved turns, the filename relative to that portion of run would be: I0_H4_IN_R02_SCV.

A clear and ordered file management gave us the possibility to create Matlab scripts that are able to take a large number of runs or run portions and to analyse them.

The first data analysis method came during the I0 test session. Considering the Humotion data, we decided to analyse firstly the angular velocities and linear accelerations.

The angular velocity is expressed as ω followed by a subscript letter indicating the axis considered:

The angular velocity about the X axis is ω_x, that about the Y axis is ω_y, and that about the Z axis is ω_z.

In the signals presented in this thesis, the red colour will be always referred to the X axis. The green will be referred to Y axis and blue colour will be referred to Z axis.

Having a large number of runs, is necessary to have a clear method to compare them. Using the velocities and acceleration "as they are" is difficult and messy, so it was considered to define a parameter called $\omega_R Sgn$, defined as:

$$\omega_R Sgn = \left(\sqrt{\omega_x^2 + \omega_y^2 + \omega_z^2}\right) Sgn(\omega_x)$$

Where the subscript R states that is the 'Resultant angular velocity' and is multiplied by the function $Sgn(\omega_x)$, having value +1 when the ω_x is positive and -1 when ω_x is negative:

$$Sgn(x) = \begin{cases} +1 & when\ \omega_x > 0 \\ -1 & when\ \omega_x < 0 \end{cases}$$

The resultant angular velocity gives a "summarizing graph", which is easier to be compared.

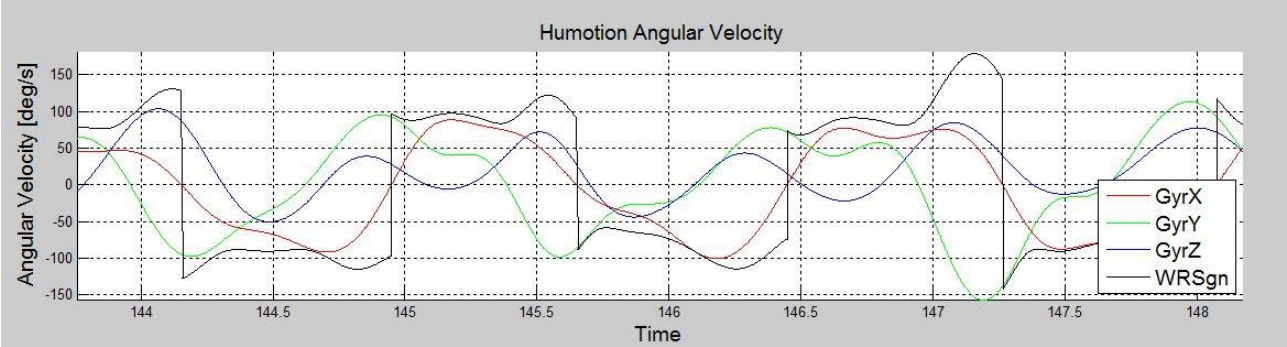

Figure 5-9: Example of Humotion signals

In the preliminary Cortina test, I0, a large effort was made trying to synchronize the sensor's output, with a video record. Only with a good synchronism, it is possible to understand what peaks and zeros of the sensor's signals mean.

Using Diadem software, the video/signal synchronization showed us three important points in the signals: considering a skier that is going downhill along the maximum slope line, we refer to “left turn” when he decides to move towards his right side and to perform a turn towards the left side of the slope; the edge changing moment occurs when the skier is in-between two turns, with the skies that changes the edge in contact with the snow, passing through a flat ski moment. The start of the right turn occurs after the edge changing, when the skier goes from the left side of the slope towards the right side performing a turn:

Figure 5-10: sequence from Cortina test with synchronization (Thanks to Matteo Cognolato))

5.2.1 Video-signal synchronization

The skiers in I2 test sessions were recorded with small action cameras. This in order to be able to synchronise the videos with the signals obtained by the sensors thanks to Matlab software.

After a visual analysis of those videos, the time stamps reported in Figure 5-11 were identified as significative:

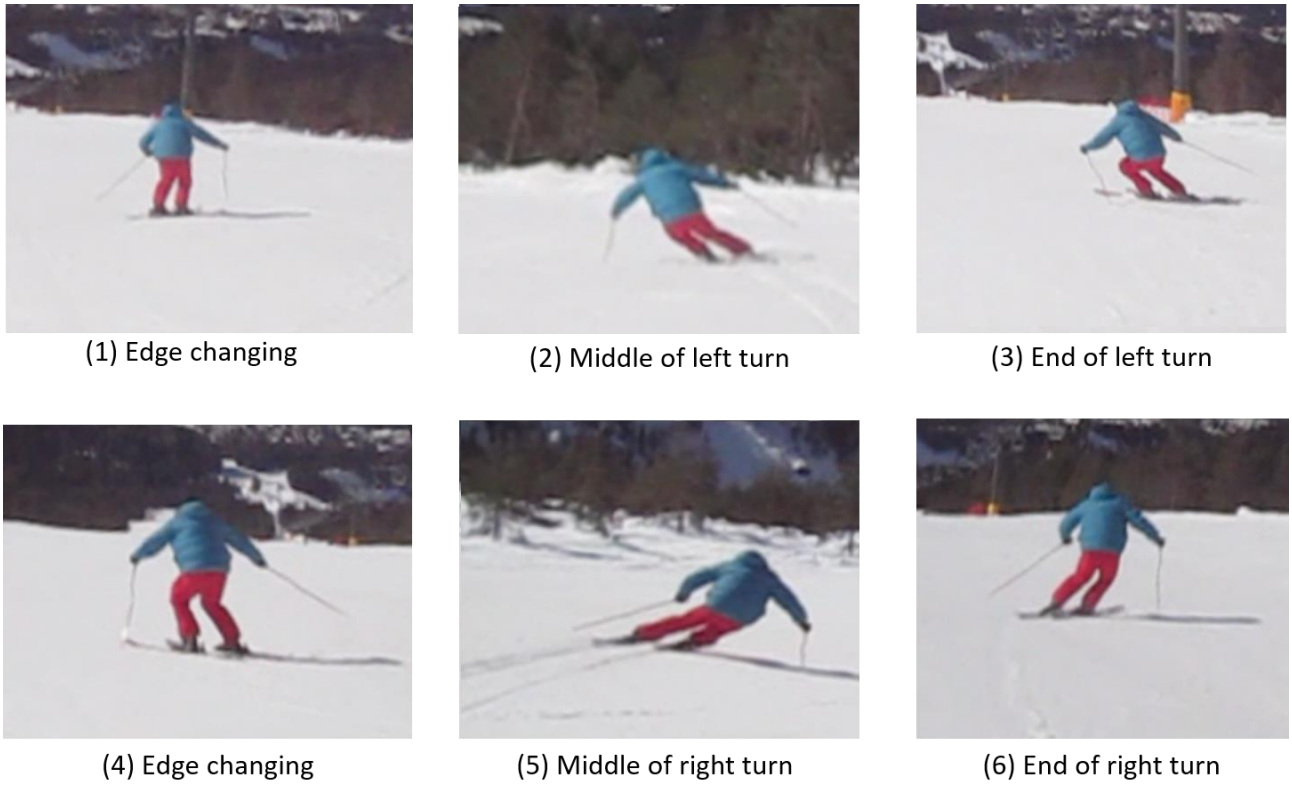

Figure 5-11: Expert skier performing LCV

Referring to the videoframes above, we can link the frame 1 to the first edge changing, figure (2) is the middle of the left turn, and figure (3) is the end of the first left turn. Then in figure (4) there is the edge changing between left and right turn. In figure (5) the skier is in the middle of the right turn and then comes (6), the edge changing that restart the cycle.

To have the highest repeatability, it was initially decided to adopt the ω_x zero value to trigger the start of the cycle. The first studies demonstrated that this zero value is in correspondence with the middle of the turn. The left turn then starts with a negative derivate and zero crossing. The minimum point marks the edge changing moment. Then the zero crossing with a positive derivate marks the right turn middle point, and the cycle ends in correspondence of peak of ω_x.

It was later observed that the Z axis linear accelerations presents instead peaks in the middle turn moment. Starting analysing the acceleration together with the videos synchronization, was established that Z axis linear acceleration crosses the zero value in the edge changing moment.

In the Figure 5-13 is reported an example of LCV synchronization. It is possible to observe that in correspondence of the ω_x zero value, the Z axis acceleration is in a local minimum point.

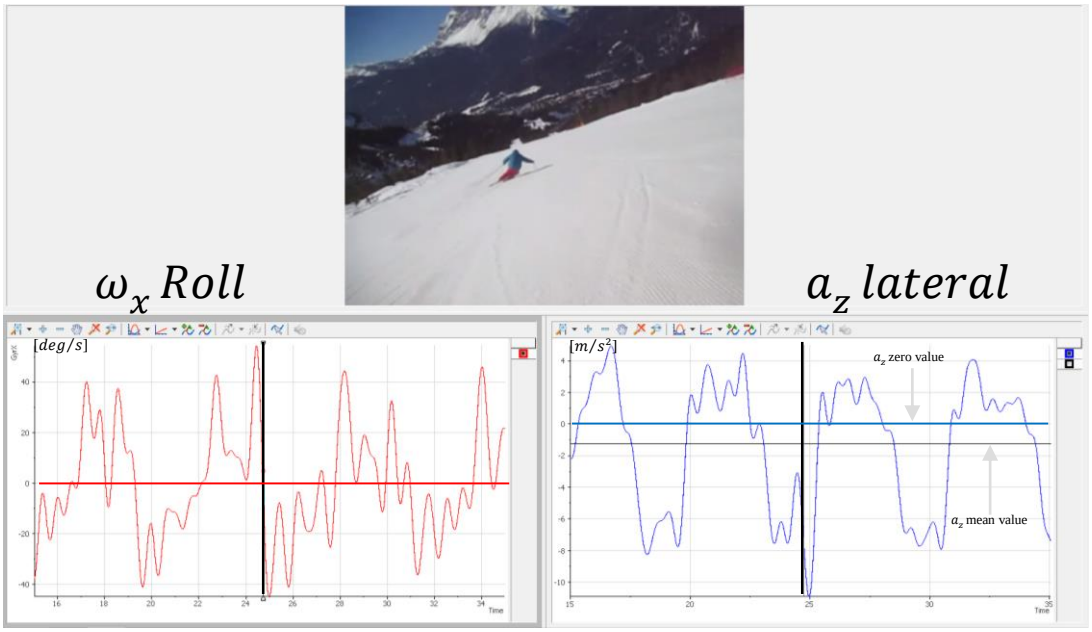

Figure 5-13: Diadem synchronization of a LCV, zero value of ω_x

In Figure 5.14 instead, is shown the moment when the acceleration along the Z axis crosses its mean point, that can be referred as a relative zero value for the acceleration. The ω_x signal is in a local minimum value.

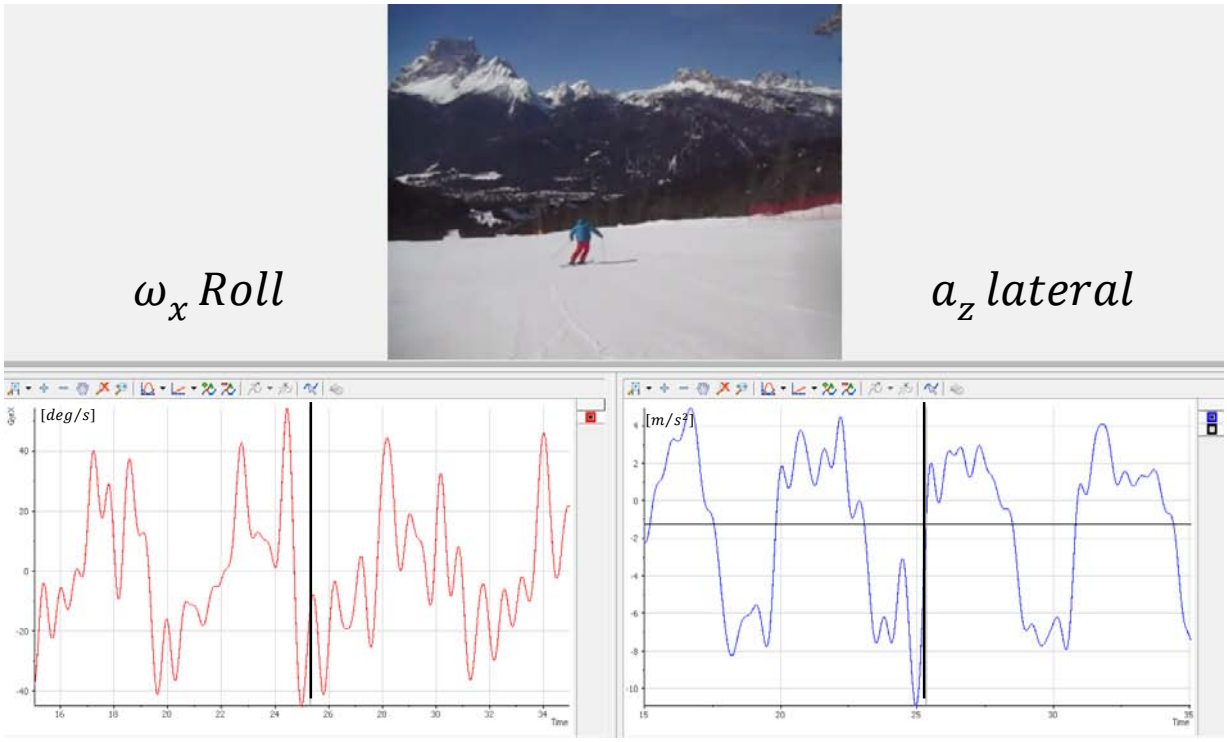

Figure 5-14: Example of LCV synchronization: zero value of Z axis acceleration

The Figure 5-15 summarizes those information in the LCV case:

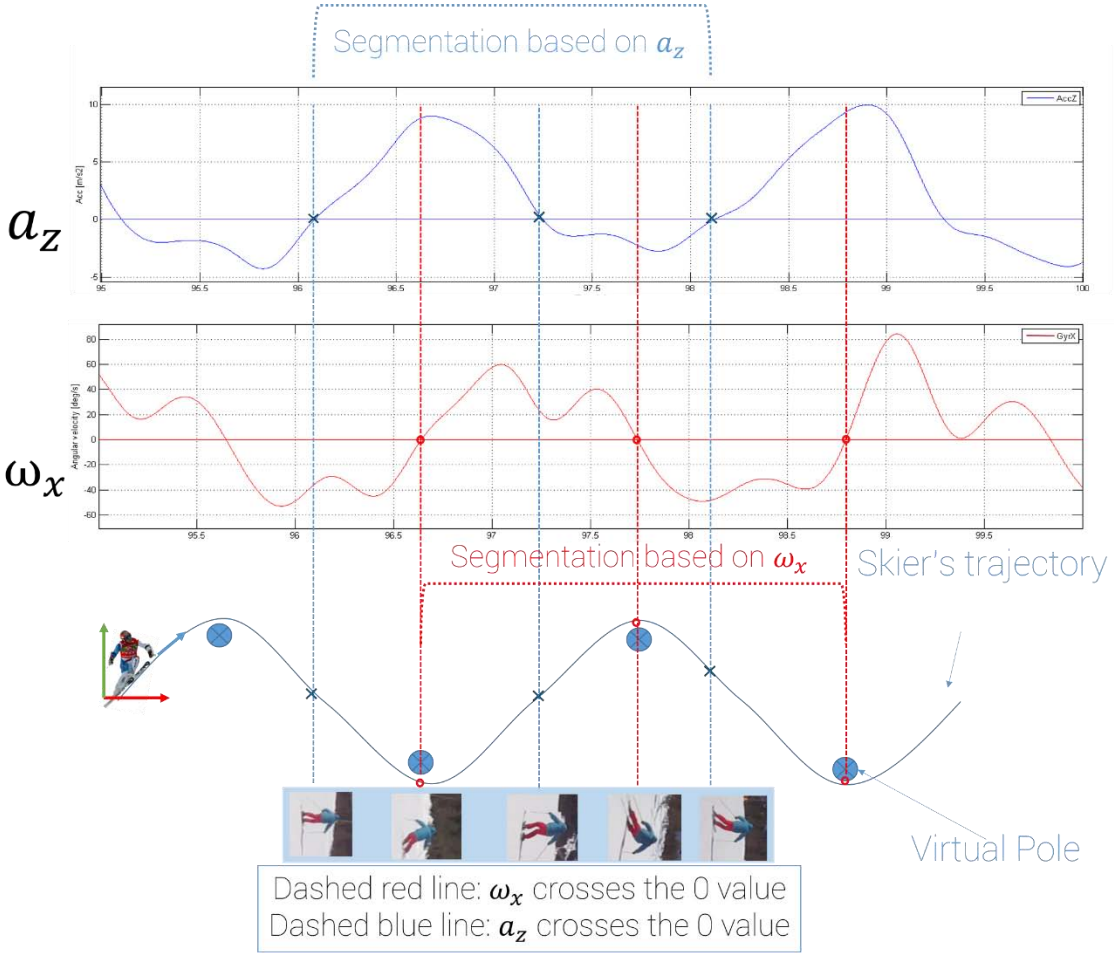

Figure 5-15: Schematic representation of LCV signals and turns, Expert skier

In the figure 5-15 it is important to notice that the a_z mean value differs from the zero value. The picture have been described without considering the mean value having the clarity of the picture.

The Diadem synchronization of videos and signals has been done also for the SSK style. In this case the results are different. The figures below report a sequence of synchronization focused on a couple of turns:

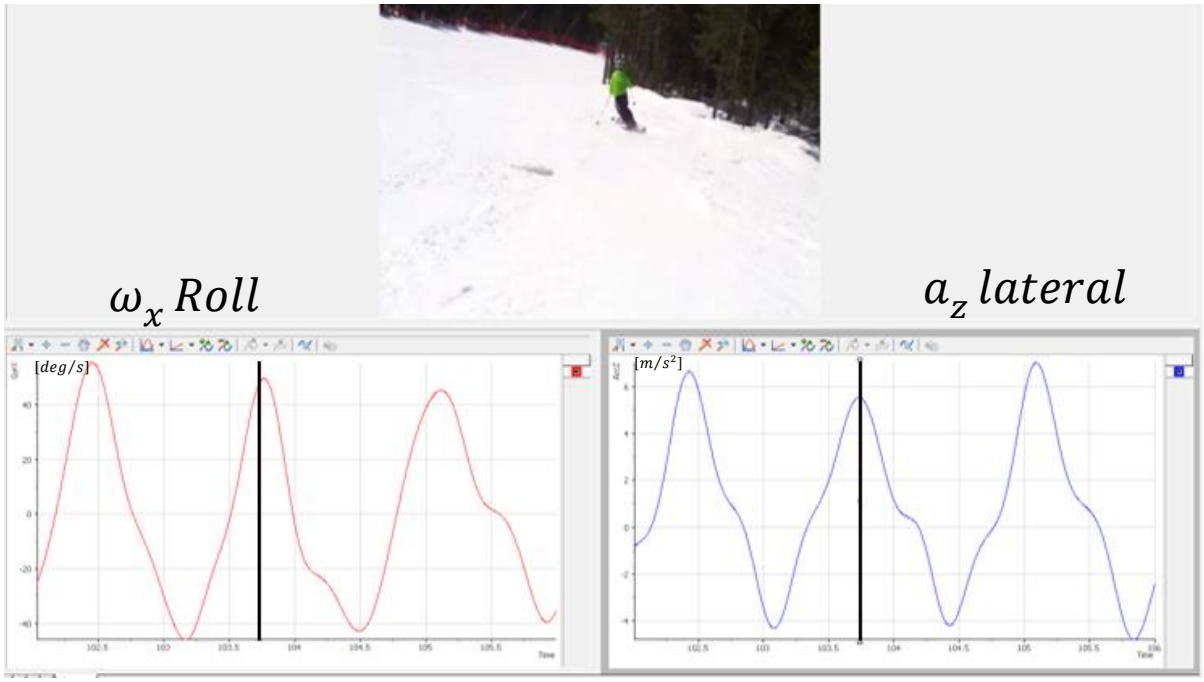

Figure 5-16: Diadem synchronization of an expert performing SSK, maximum value of acc_Z

In the Figure 5-16 it is possible to observe that the ω_x and the a_Z are in phase. There is no significant shift between the two signals. In this case a maximum value of the Z axis acceleration corresponds to a maximum value of ω_x and to the middle of the left turn.

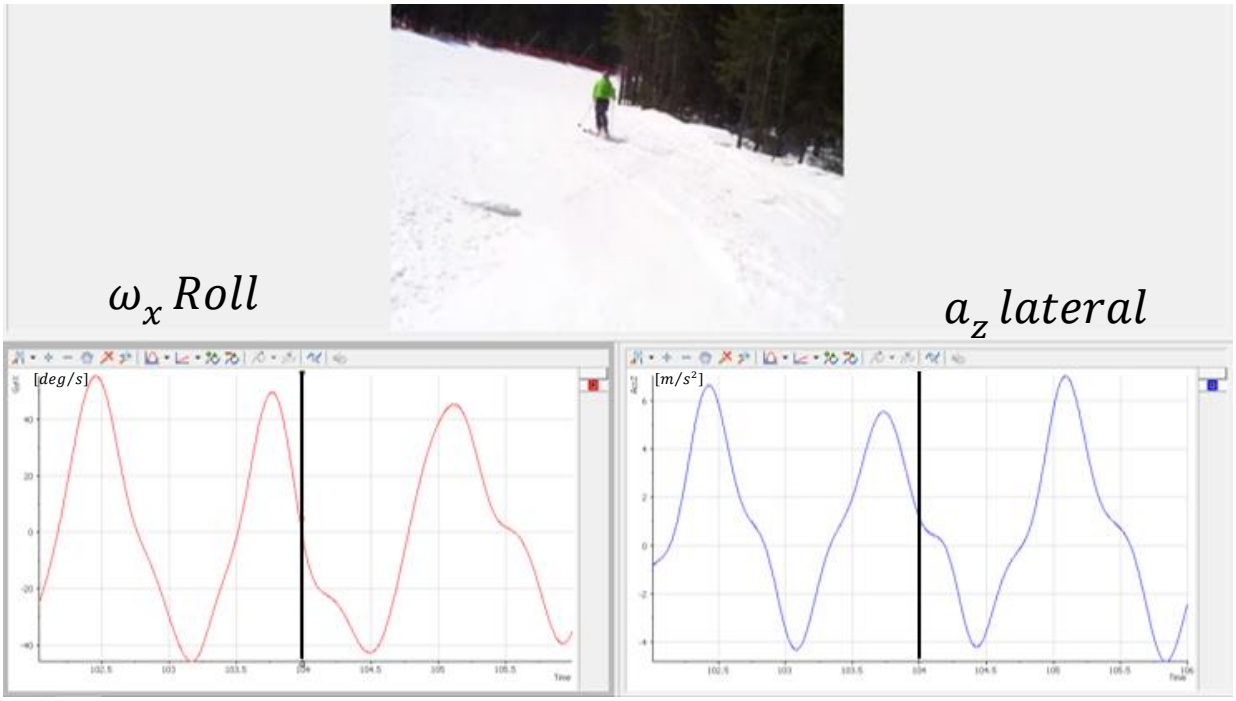

Figure 5-17:Diadem synchronization of an expert performing SSK, zero value of ωx

Moving forward in time, the zero crossing of ω_x shows the light shift in time of the zero crossing of the two signals. This is possible to observe in 5-17. The video shows clearly that this zero crossing corresponds to the edge changing moment. The following (5-18) shows again the synchronization of the two signals in the Z axis acceleration minimum point. The synchronization is noticeable and corresponds to the middle point in the right turn.

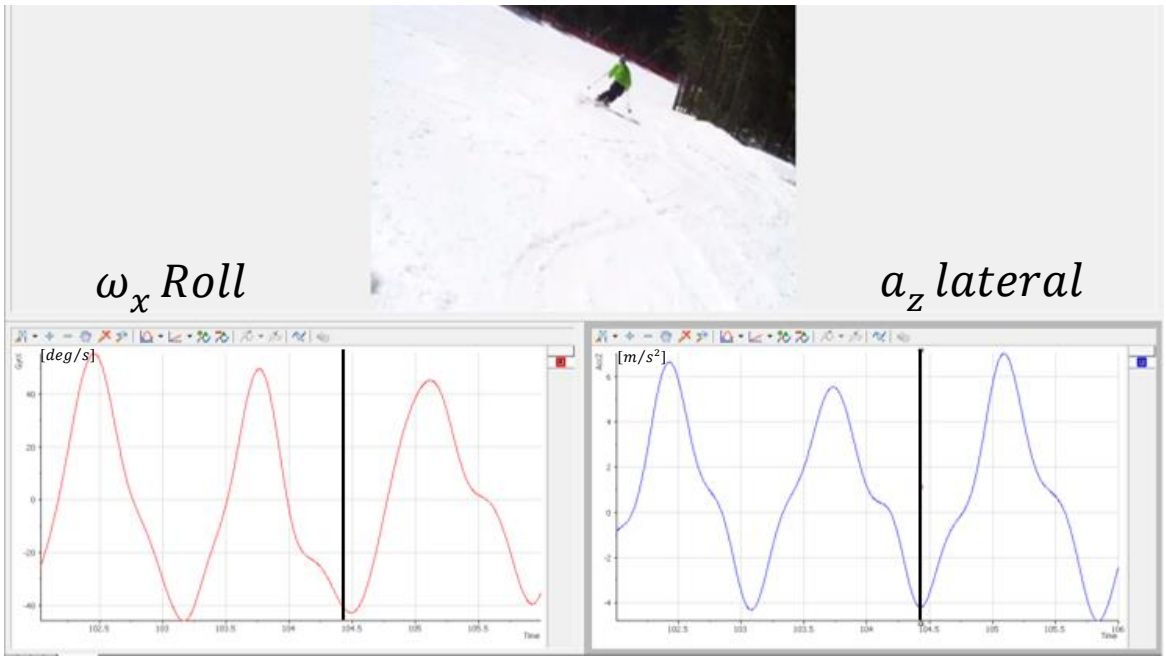

Figure 5-18: Diadem synchronization of an expert performing SSK, minimum value of a_z

To conclude the turns, the picture below show the contemporaneity of the zero crossing of the two signals, corresponding to the edge changing and the end of the two turns cycle.

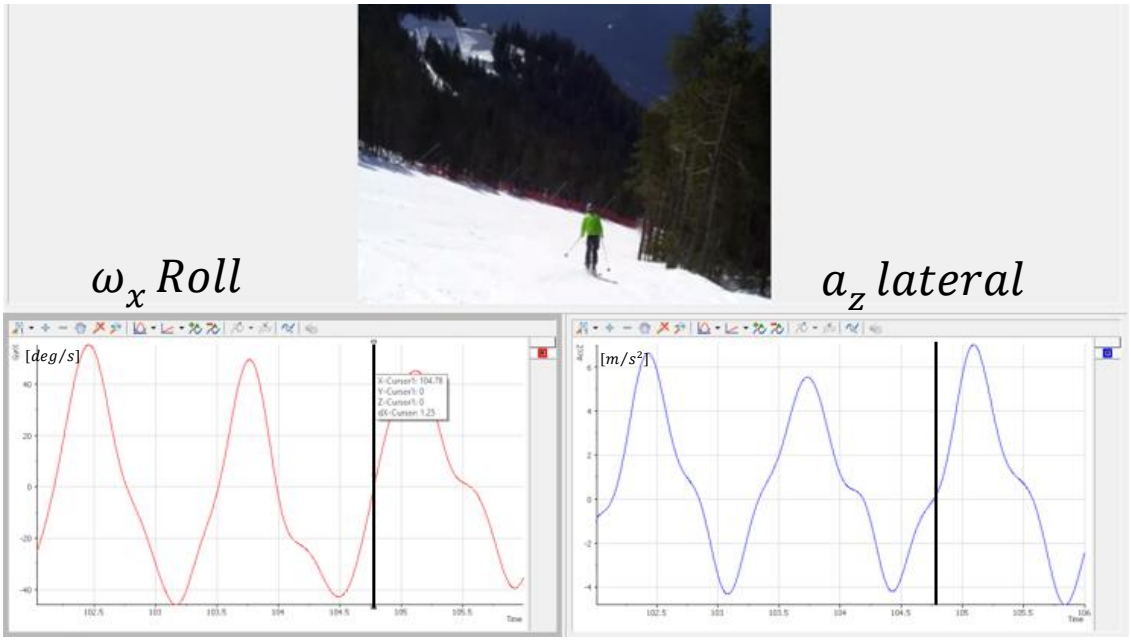

Figure 5-19: Diadem synchronization of an expert performing SSK, zero crossing of a_z

The SSK in this case can be summarized by the scheme below:

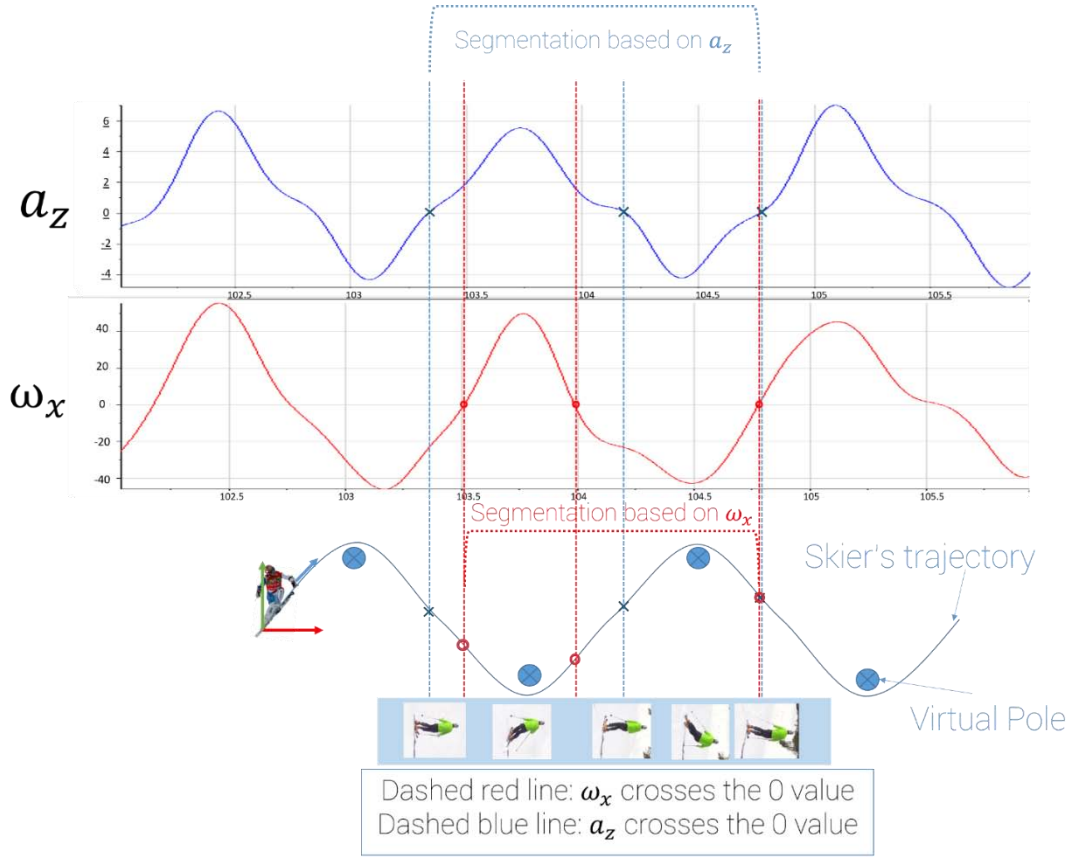

Figure 5-20: SSK turns scheme

The signals analysis in this thesis are done considering the ω_x zero crossing as reference for trigger the cycles as this was adopted since early stage. For a future work is strongly suggested to select the a_z zero passage as reference for select the turns. As reported in figure 5-4, this means that cycle starts in between the right and left turn, in the edge changing moment.

In the data analysis, to avoid measurement errors, we decided to study not only the single turn, but a set of at least five turns to reduce inter-turns variability.

5.2.2 Matlab scripts

To analyse the sensor's data, a Matlab script was developed. In the I0/I1 and I2 infield tests, were used uncalibrated Humotion sensors; calibration was performed afterwards. In the latest tests, was used a different version of the Humotion software: having an identifier of the Humotion serial number, it is possible to insert in the software's Pc folder, a fila containing the calibration constants. In the first tests, anyway, the calibration constants were calculated indoor. Having the angular velocity of the devices, it was possible to derive such constants. The analysis of the acceleration of gravity lead us to the determination of the constants for the accelerations. The numeric values were stored in a excel file, in order to be able to collect it in the Matlab script (Phase 1 and Phase 2).

The analysis followed the steps presented in the diagram in Figure 5-21:

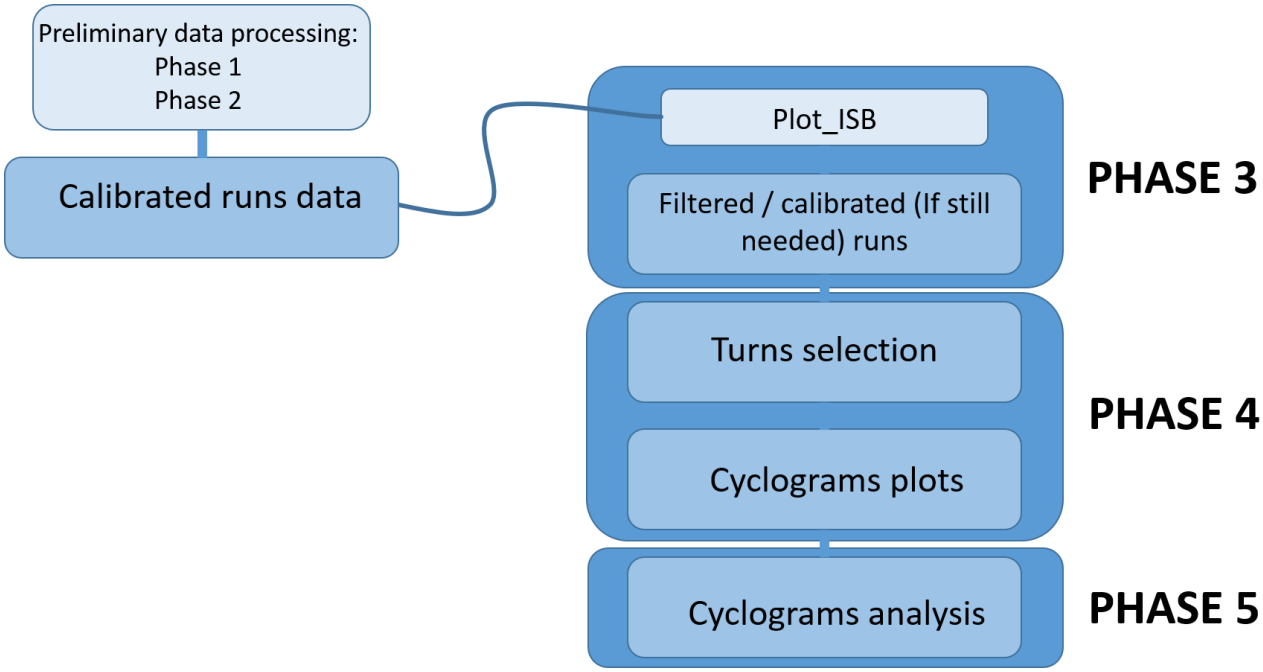

Figure 5-4: data analysis, from phase 2 to phase 5

The first data analysis main script, called "plot_ISB", permits to select manually a file to be analysed. Then the file is imported in Matlab; the sensor's data are stored in a structure in which the data are in a matrix, in which columns are reported the numerical values of the physical quantity under

observation. The first column reports time stamps expressed in milliseconds. The first raw contains header to identify which quantities are findable in the columns.

Then the script calls a function humotion_calibr which, given in input the sensor structure, and the number of the sensor, reported on the file name, applies the calibration constants to the data of the sensor. The function gives in output another structure, similar to the original one, with calibrated data. The second main operation of the script is a low-pass filtering of the signals at an input frequency. The software asks the user what is the desired cut off frequency. In our study we used a cut off frequency of 2Hz: as it can be seen in figure 5-3, the 2Hz frequency is sufficient to maintain all the desired information of the signal but also removes the dynamic vibrations.

The main script calls the function "filtr" which asks as "Nargin" the structure that contains the data to be filtered, the cut off frequency and the sampling frequency. Then calculates the optimal filter thanks the inbuilt Matlab function "butter", returning zeros and poles of the filter. Then it is used the "filtfilt" inbuilt function that performs a zero-phase filtering action on each signal. The filtered signals as a new structure are given in output. The main script then plots the filtered signals (Phase 3).

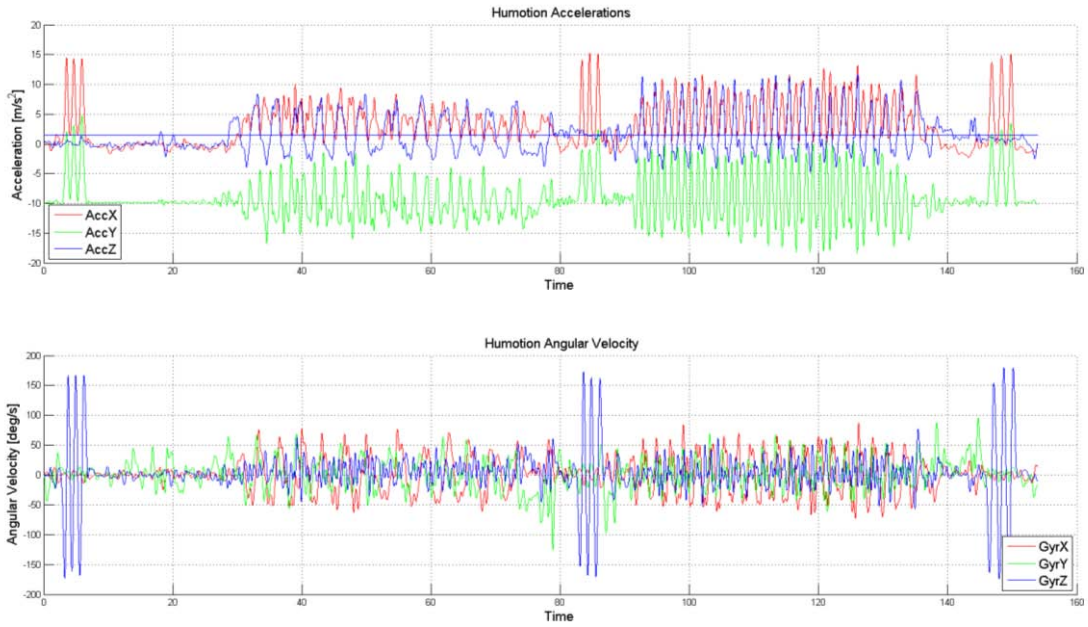

Figure 5-21: Full run filtered

In the Figure 5-5 it is possible to observe a full run as it appears after the operation mentioned above. The Humotion's output is calibrated, filtered and plotted. It is clear that the acceleration are expressed in $[m/s^2]$ and that the angular velocities are in $[deg/s]$

In the plot are very evident the event signals. The three consecutive peaks in three part of the run, at the start, in the middle and at the end are predefined movements the skier performed in order to understand the start and the finish of the run with a certain style. The middle ones are to indicate the change of skiing technique.

5.2.3 Cyclograms

Having observed the cyclical nature of the signals when skiing downhill, the first idea was to observe not only single signals, but also their crossplots [Petrone at al., 2013]. As it is possible to observe in Figure 5-22, the repeatability of the angular velocities about the X and Y axis, suggested to analyse them together. We decided to plot in the Cartesian plane the two quantities in a single couple of left-right turn, having the angular velocity about the X axis on the abscissa axis and the angular velocity about the Y axis on the ordinate axis. To have more significant plot, we decided to apply this study to five consecutive turns. In addition, the mean signals of the five turns were calculated, resulting in a 'Mean turn'. This was possible considering that the turns were selected considering as starting and ending point the ω_x zero value. The turns have different timestamps but, have the same Y-axis starting and ending points for each of the five turns. Using the Matlab function "resample", was possible to scale the turns length to the first turn of the group selected. The Matlab function "mean" performed a scalar mean for each channel of the five turns.

The script analyses the crossplots in the X-Y, Y-Z and X-Z axes but, as show in the picture below, only X-Y shows a clear shape.

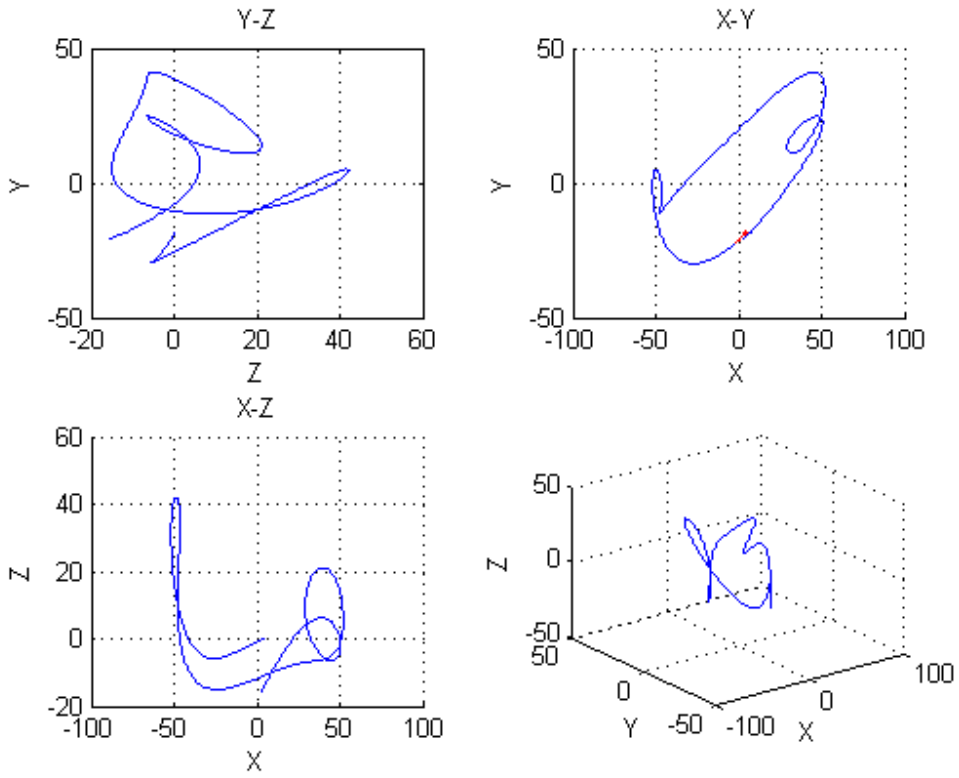

Figure 5-22: Cyclograms of an Intermediate skier

The Figure 5-22 shows the cyclograms obtained by analysing a single couple of left-right turns. In the top left the cyclograms obtained by crossplotting the angular velocities about the Y and Z axes, the top right the ones about X and Y axis and in bottom left there is the cyclogram obtained by the

X and Z axis angular velocities. The 3D plot in the bottom right represents the cyclogram obtained by crossplotting the three angular velocities on a 3-dimensions Cartesian plane.

After having analysed a large number of cyclograms, was evident that the repeatability of the Y-Z and X-Z crossplots was not assured. Instead, X-Y crossplots showed significant intra-subject repeatability and were further investigated.

This cyclograms extraction was made for every run that included at least five consecutive similar turns. Each set of five cyclograms and the mean cyclogram was stored in single folder containing:

- ID of the tester (initial letter of the Name and of the surname)
- Number of the run and the style performed.
- The number of the turns to which cyclogram refers.
- The mean cyclogram identified with the word "mean".

For example, to identify the third run of the skier MC, who performed long carved turns, the file name of the first turn of the set is 'MC_R2_LCV_1' and the mean turn is 'MC_R2_LCVmean'; For the Austria skiers, this was not possible because the name of the skier was not reported. We decided to store the turns extracted in a folder named with:

- The session ID
- The number of the sensor
- The run number
- The style performed
- The skier's level.

For example, an intermediate skier's set of turns in the run 5 is saved in the folder 'A7_H3_R5_LCV_IN'. Then the cyclograms followed the terminology decided, having a numerical index identifying the turn to which refers. For example, a cyclogram of the same subject would be: 'A7_H3_R5_LCV_IN_1'.

5.2.4 Results

In the preliminary field test in Cortina (I0), conformant result were obtained: comparing expert skiers with intermediate and beginners, performing the same technique, it was possible to observe clear differences in the cyclograms obtained by the angular velocities about the X and Y axis. In the figure 5-23 it is possible to observe the cyclogram obtained by the mean of the five couple of turns, in blue for the intermediate skier, green for the Beginner and red for the expert skier. In orange and with thicker line is indicated the cyclogram's starting section. We can immediately observe the difference between the cyclogram of the beginner skier in comparison to that of expert and intermediate: beginner skier has an 8-shape, thin and disposed on the second and fourth quadrant. The

intermediate's cyclogram is similar to an ellipsis with the main axis along the direction of the X axis. It is shorter but more open than the beginner's one. The expert, on the other hand, is very similar to the intermediate, but his cyclogram lays more on the first and third quadrant. The cycle starts at the zero value of ω_x (trunk lateral bending angular velocity) and moves towards negative values of trunk lateral bending angular velocity: this corresponds approximately from the maximum right leaning angle (about the apex of a right turn) towards the next left turn. In addition, was observed that expert cyclograms start in a clockwise direction, whereas Intermediate and Beginners presents counterclock wise directions.

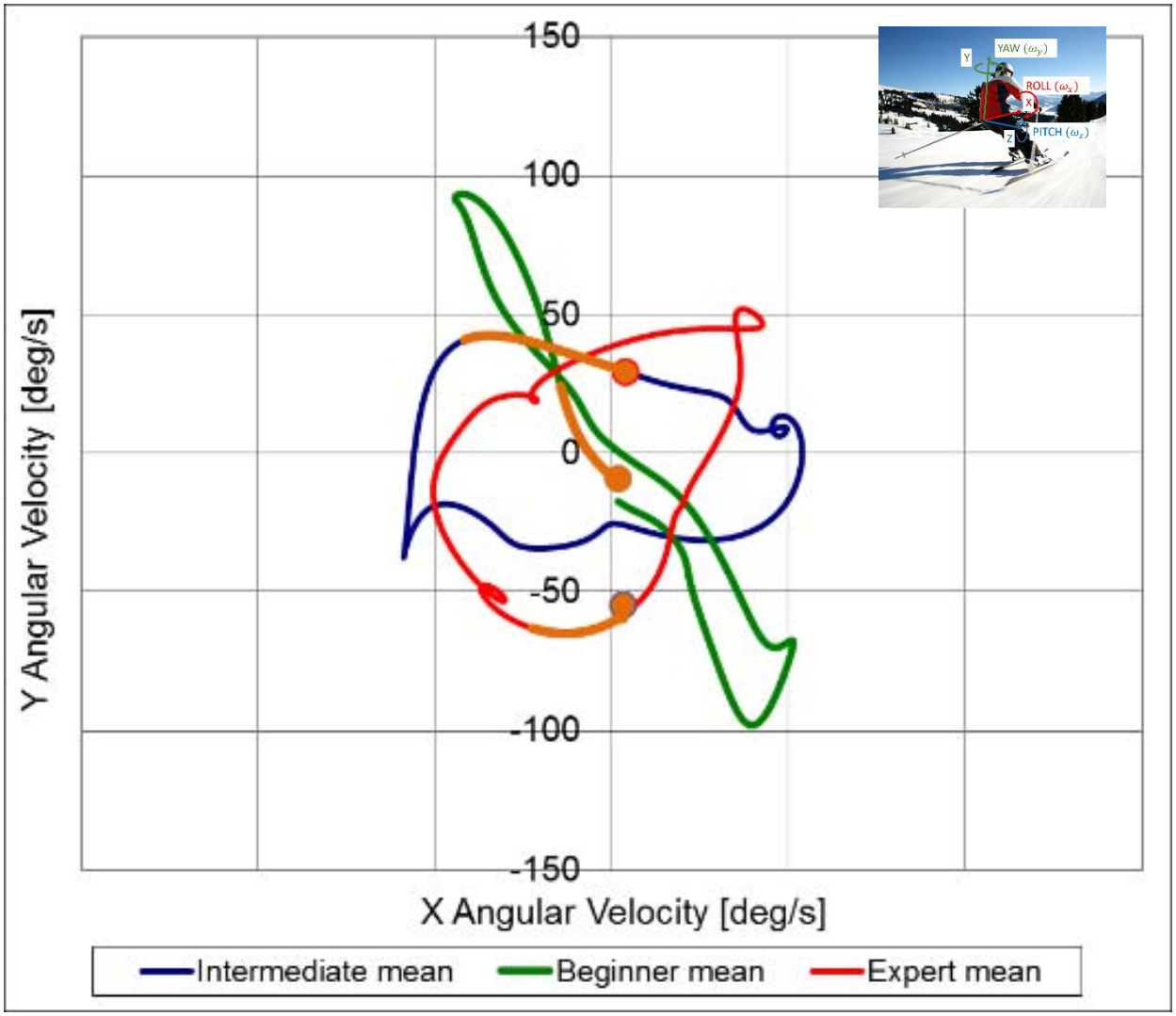

Figure 5-23: First comparison: BE, IN, EX

To get a clear comparison of the cyclograms associated with different ski levels and skiing techniques, another matlab script has been made. This took the files in user-selectable folders and let to compar the cyclogram by plotting them in the same graphic. The analysis of I2 test session, lead to the results presented in the following pages.

In addition to cyclograms, frameset of videos recorded by a skiers who followed the tester are reported.

Referring to Figure 5-24, we decided to capture the most significant event, considering:

1. Edge changing moment, at the beginning of the left turn. This is marked by a transition from interior to exterior edge of the skies;
2. The middle point of the left turn, characterized by the maximum “chrouching”;
3. The end of the left turn, marked by the ending of the carved part of the turn and the body extension start;
4. The edge changing towards the right turn;
5. The middle point of the right turn;
6. The edge changing towards the left turn and the next cycle.

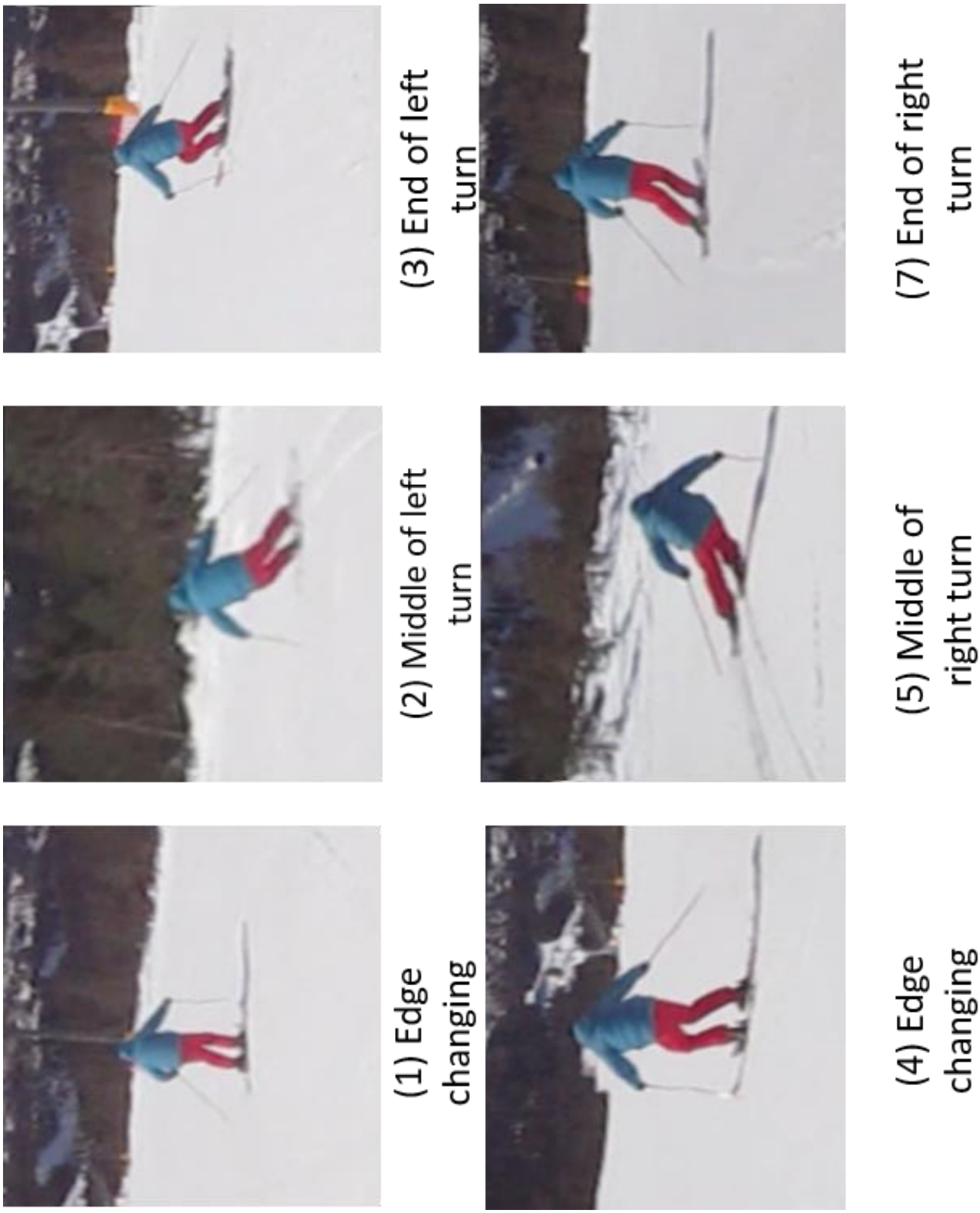

Figure 5-24: Expert performing long carved turns: framestamps of the selected turns events.

The frames in Figure 5-24 correspond to an expert skier performing a LCV single couple of turns. The signals of the sensor are plotted in Figure 5-25:

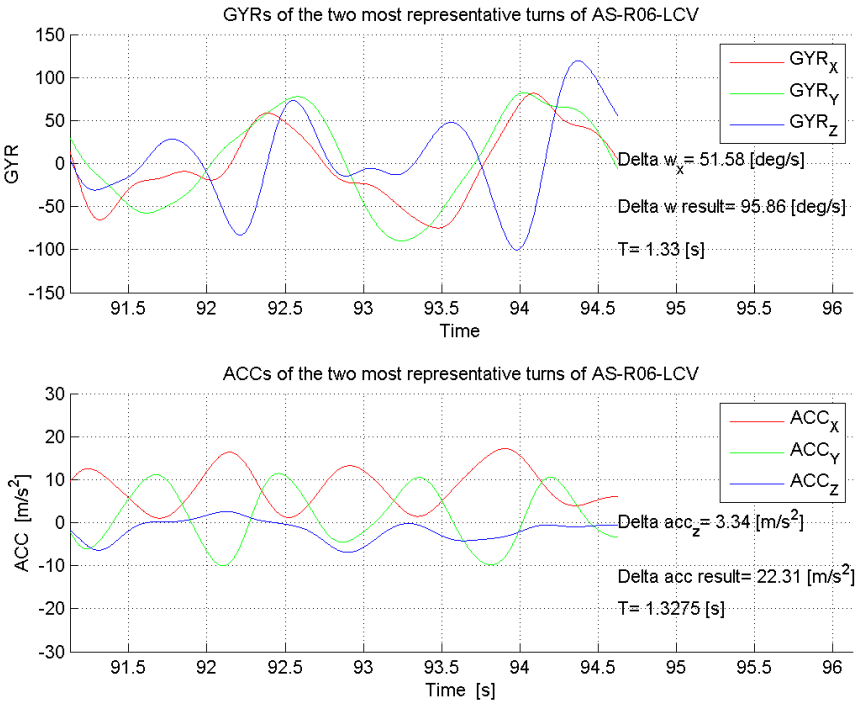

Figure 5-25: Signals of an expert performing LCV, two couples of turns

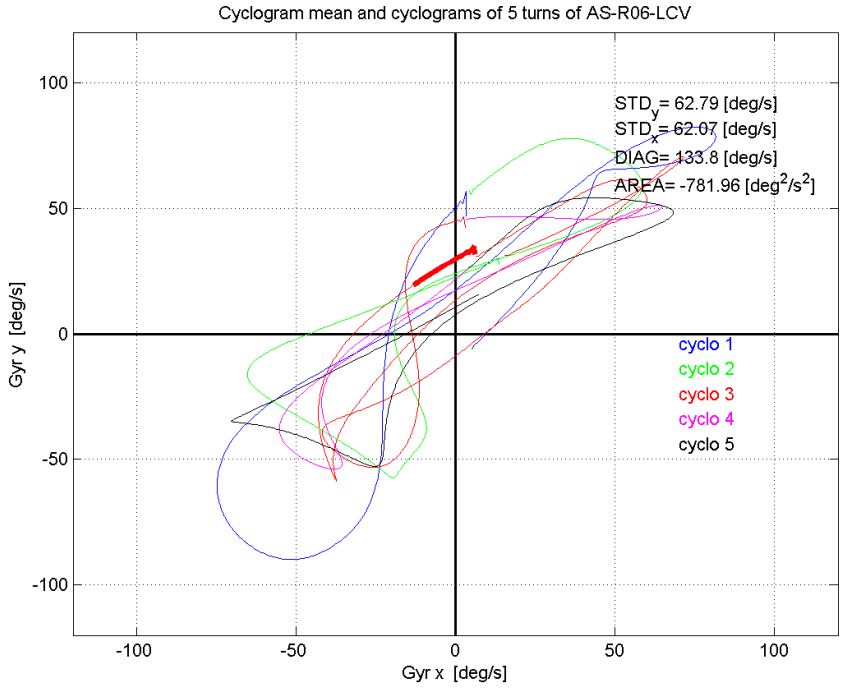

Figure 5-26: Cyclograms of five consecutive LCV turns and of the mean turn.

The Figure 5-26 the cyclograms, obtained by crossplotting the angular velocity about the X and Y axis are reported. The result are cyclograms stretched along the first and third sectors. The mean signals starts with a thicker red line.

5.2.5 Skiers cyclograms comparison

(a)

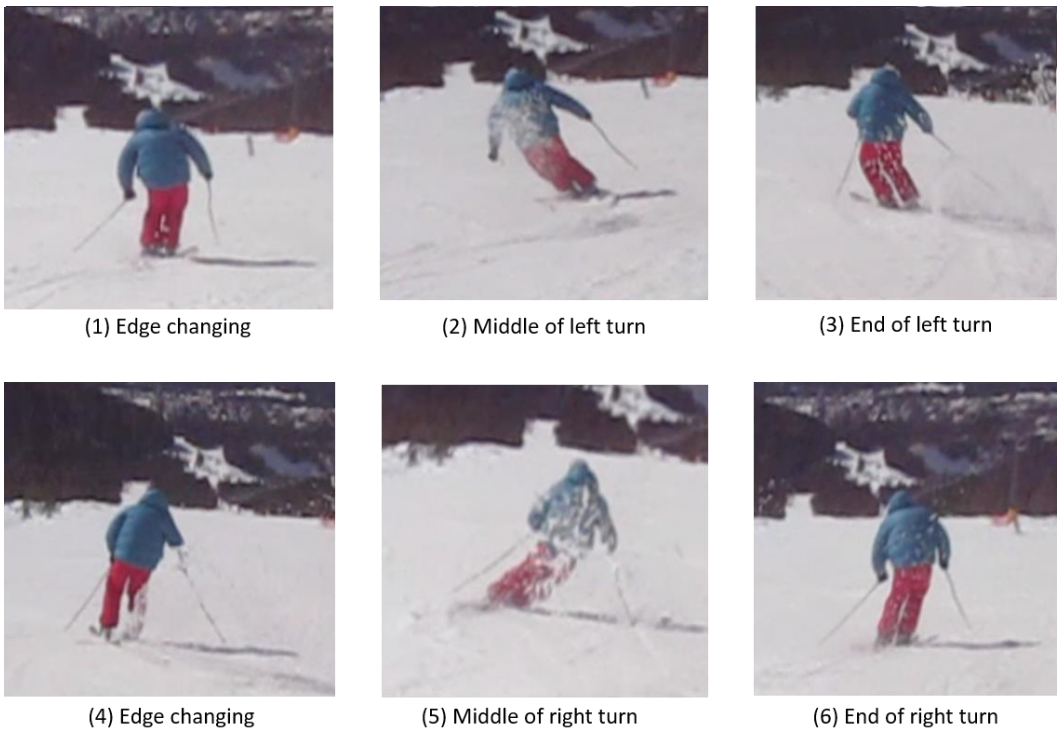

Figure 5-27: Expert skier (AS) performing short skidded turns

(b)

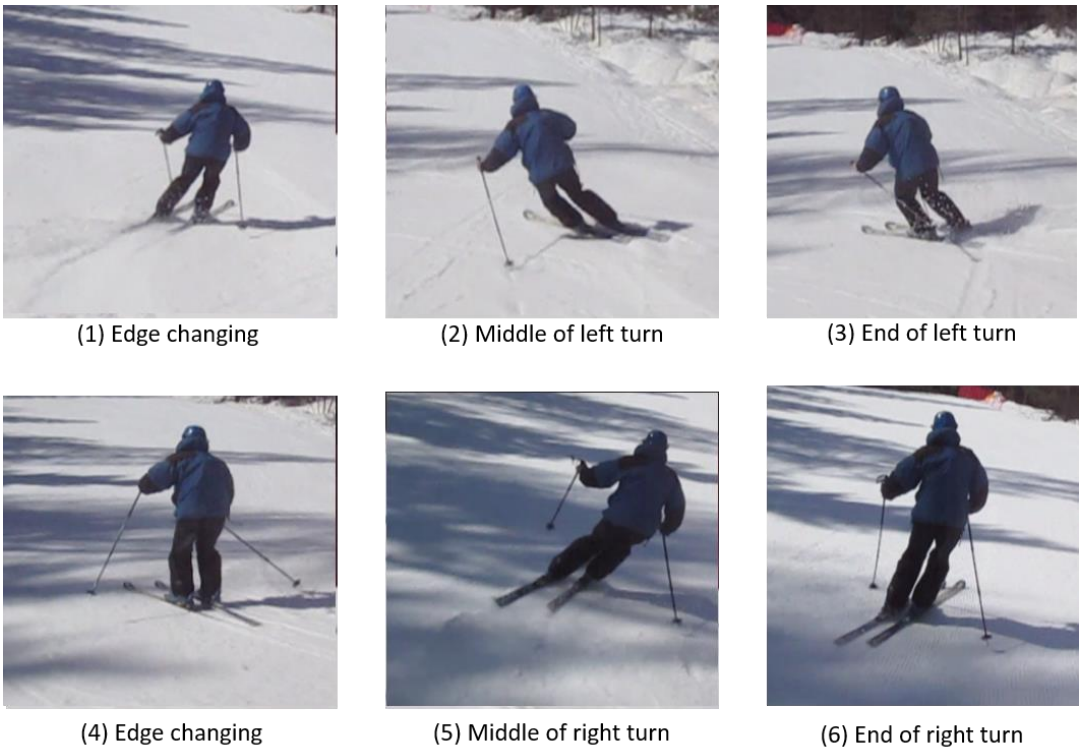

Figure 5-28: Expert skier (FC) performing short skidded turns

(c)

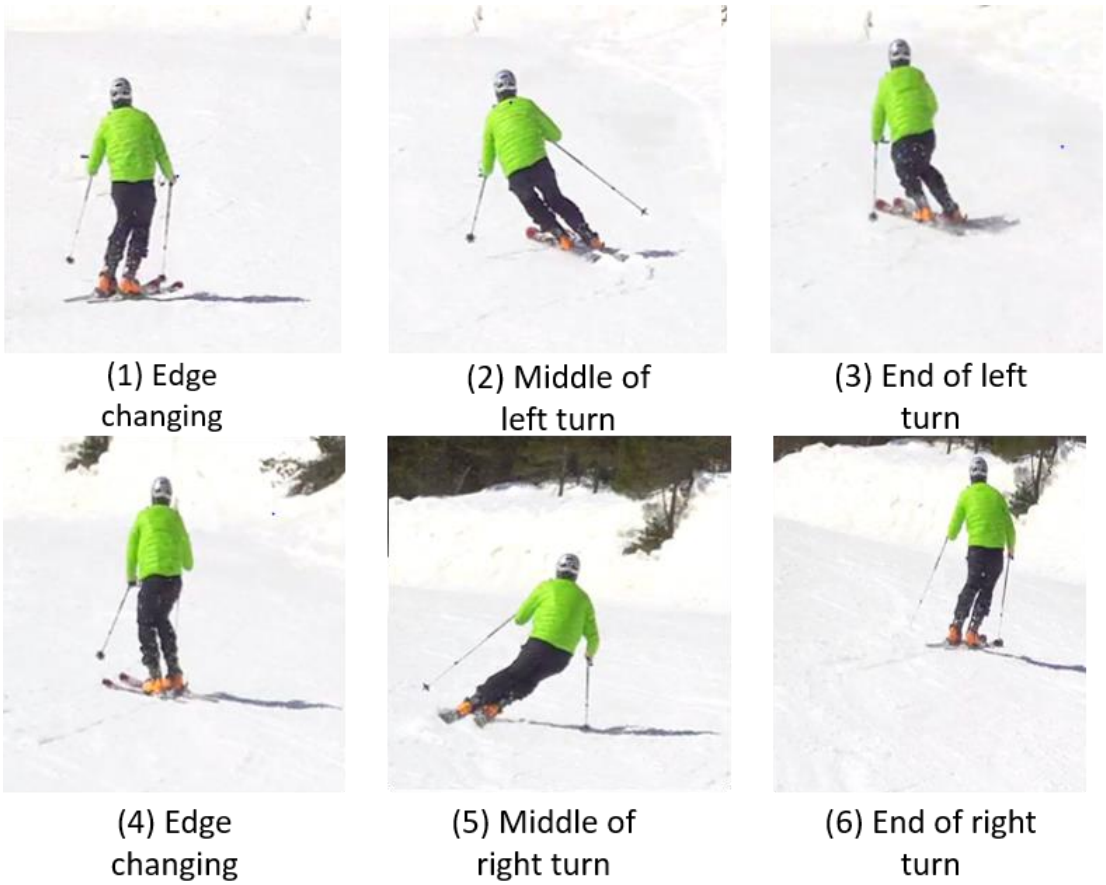

Figure 5-29: Expert skier (FF) performing short skidded turns

The three skiers in the frames above are performing short skidded turns, consisting in a rapid and continuous turning style, without using the shape of the skies to turn. The radius of turns is sensibly lower with in respect to skies sidecut radius. This results in a brushed style. It is very common in steepest slopes where high speed are dangerous. Early beginners who cannot carve the skies commonly adopt this style. In modern ski giant slalom competition, where the turn radius of the skies is sensibly higher than the track turns, racers use a brief skidded turn to enter the carved turn.

The cyclograms obtained with this type of turns is reported below. For the fourth skier (MP) it was not possible to obtain six picture of short skidded turns in good quality.

As result, the picture in next page shows cyclograms obtained by this type of turns.

It is possible to observe the differences between them: Whereas (a) has stretched cyclograms, (c) and (d) present wider cyclograms. In addition, cyclograms of tester (b) are not disposed along the bisector of first and third sector, but is disposed along the X-axis. This may be due to the tester's skiing style, in between the Intermediate and the Expert level, even if the skiers was able to control his skies, as derive from ski mountaineering framework. As it is possible to observe, those skier are expert but the cyclograms are completely different one from another, even if have some common characteristics. It

is not possible to identify a ‘more correct’ skiing technique between, but instead a personal skiing’ fingerprint, that can be analysed in time ,after training session in order to extrapolate performance gains.

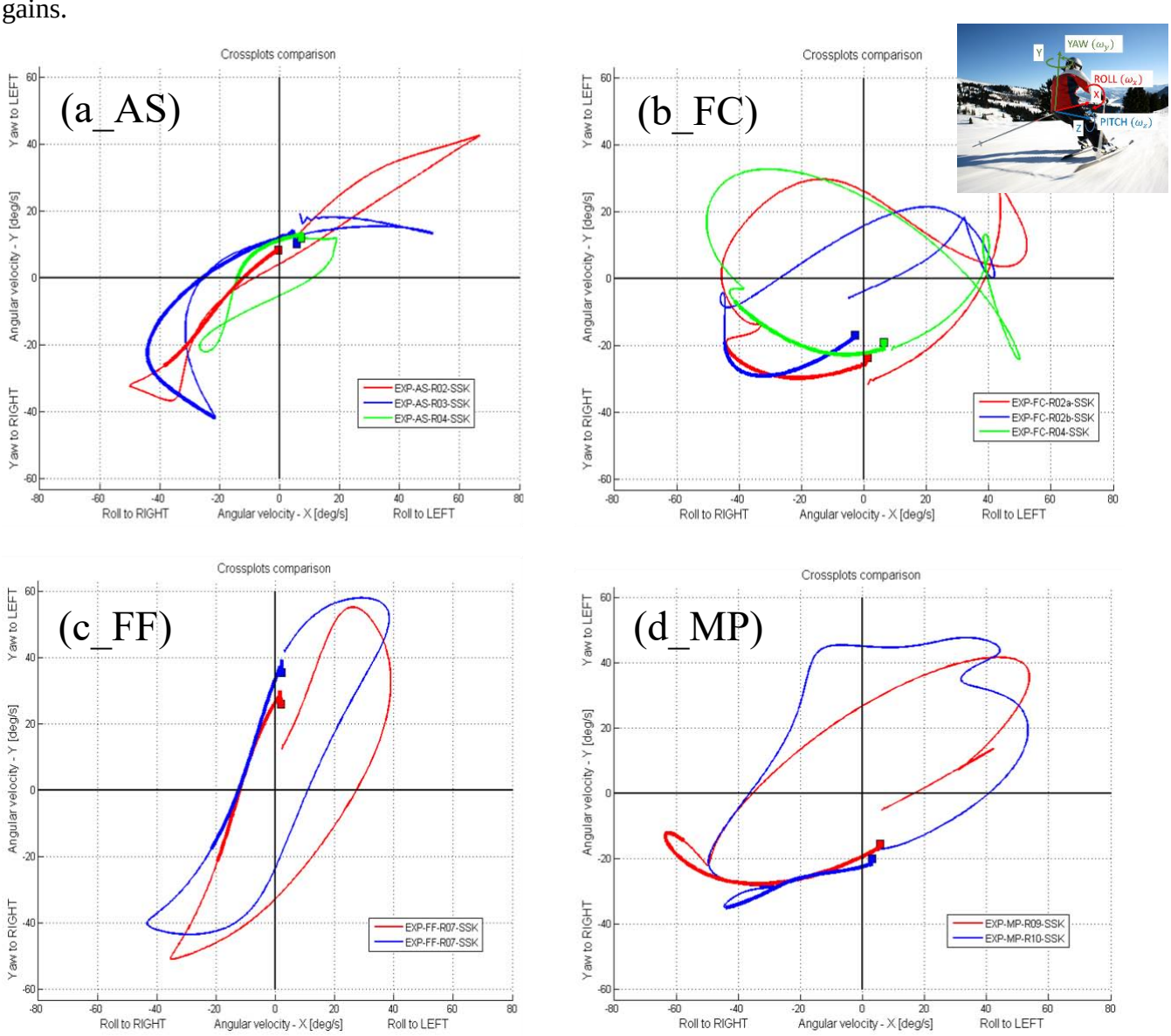

Figure 5-30: Comparison of four expert skiers performing Short Skidded Turns (SSK)

Several types of comparison can be done. In this section is reported a comparison between expert skiers performing the three different turns type.

The long carved turns are intended as high speed turns, performed using the skies’ shape to obtain a turn with a radius comparable with skies’ one. Usually, recreational skiers adopt skies with a 14-16 m turn radius.

In the following Figures 5-31, 32, 33, 34 are reported the frames obtained by the videos.

(a)

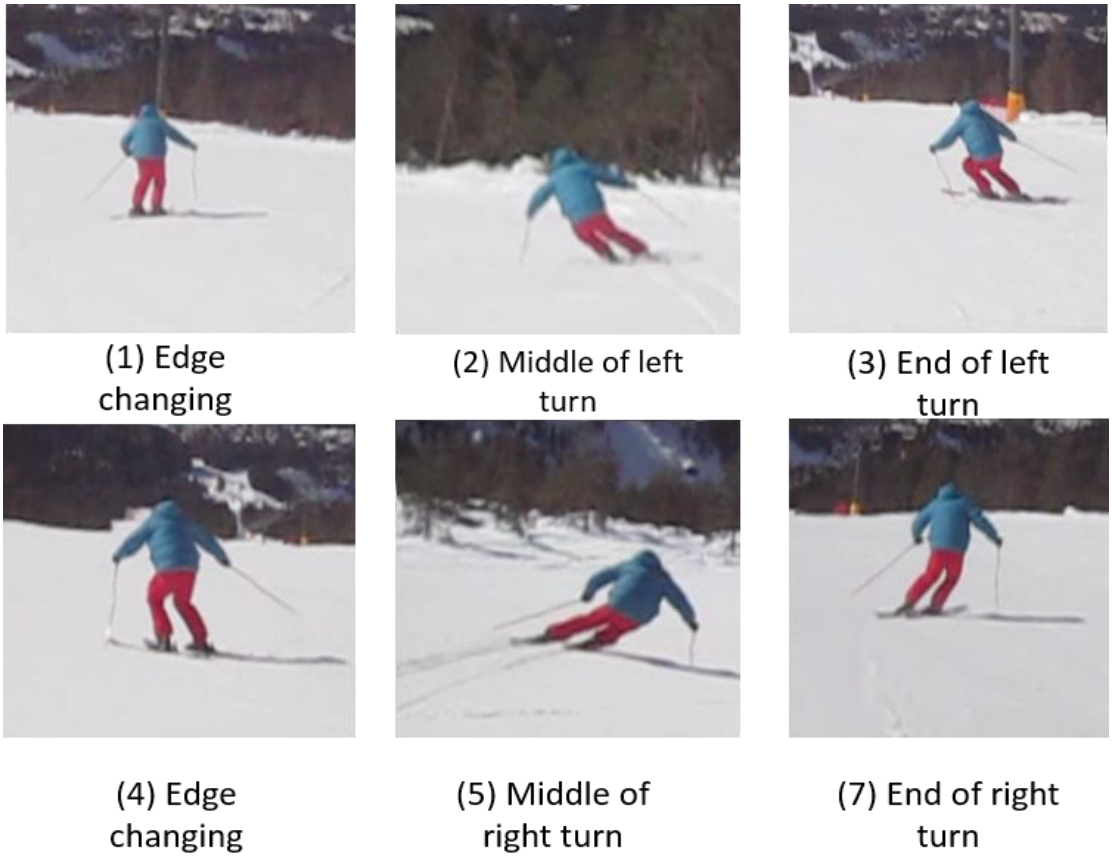

Figure 5-31: Expert skier AS performing LCV

(b)

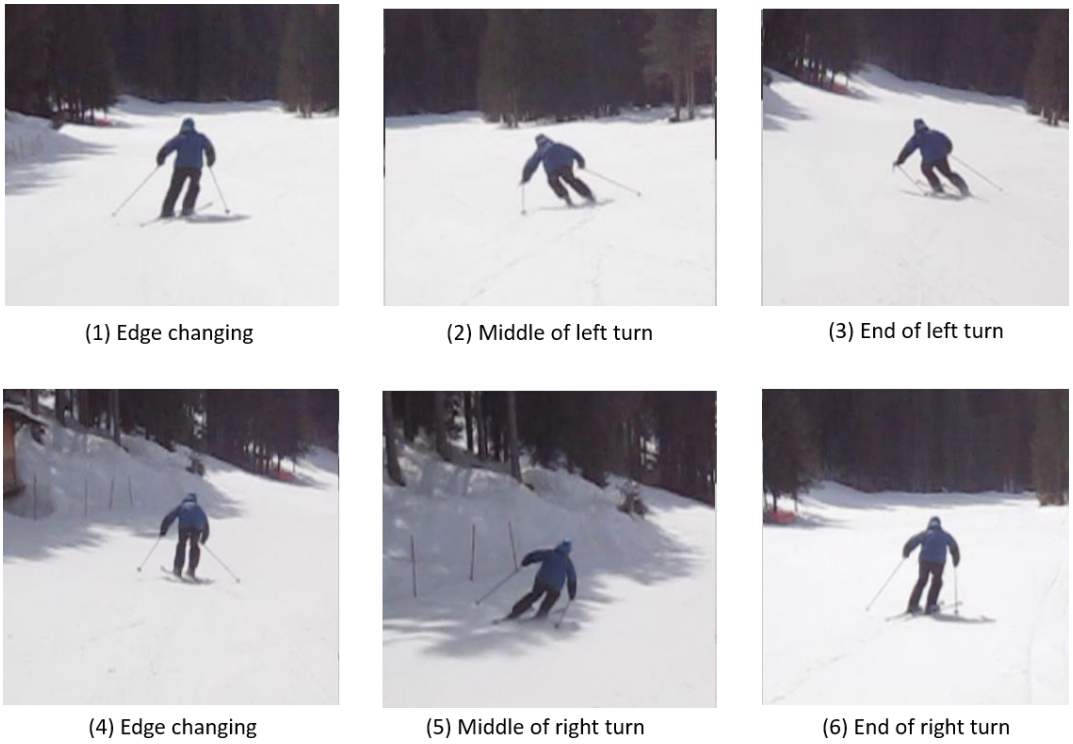

Figure 5-32: Expert skier FC performing LCV

(c)

(1) Edge changing (2) Middle of left turn (3) End of left turn

(4) Edge changing (5) Middle of right turn (6) End of right turn

Figure 5-33: Expert skier FF performing LCV

(d)

(1) Edge changing (2) Middle of left turn (3) End of left turn

(4) Edge changing (5) Middle of right turn (6) End of right turn

Figure 5-14: Expert skier MP performing LCV

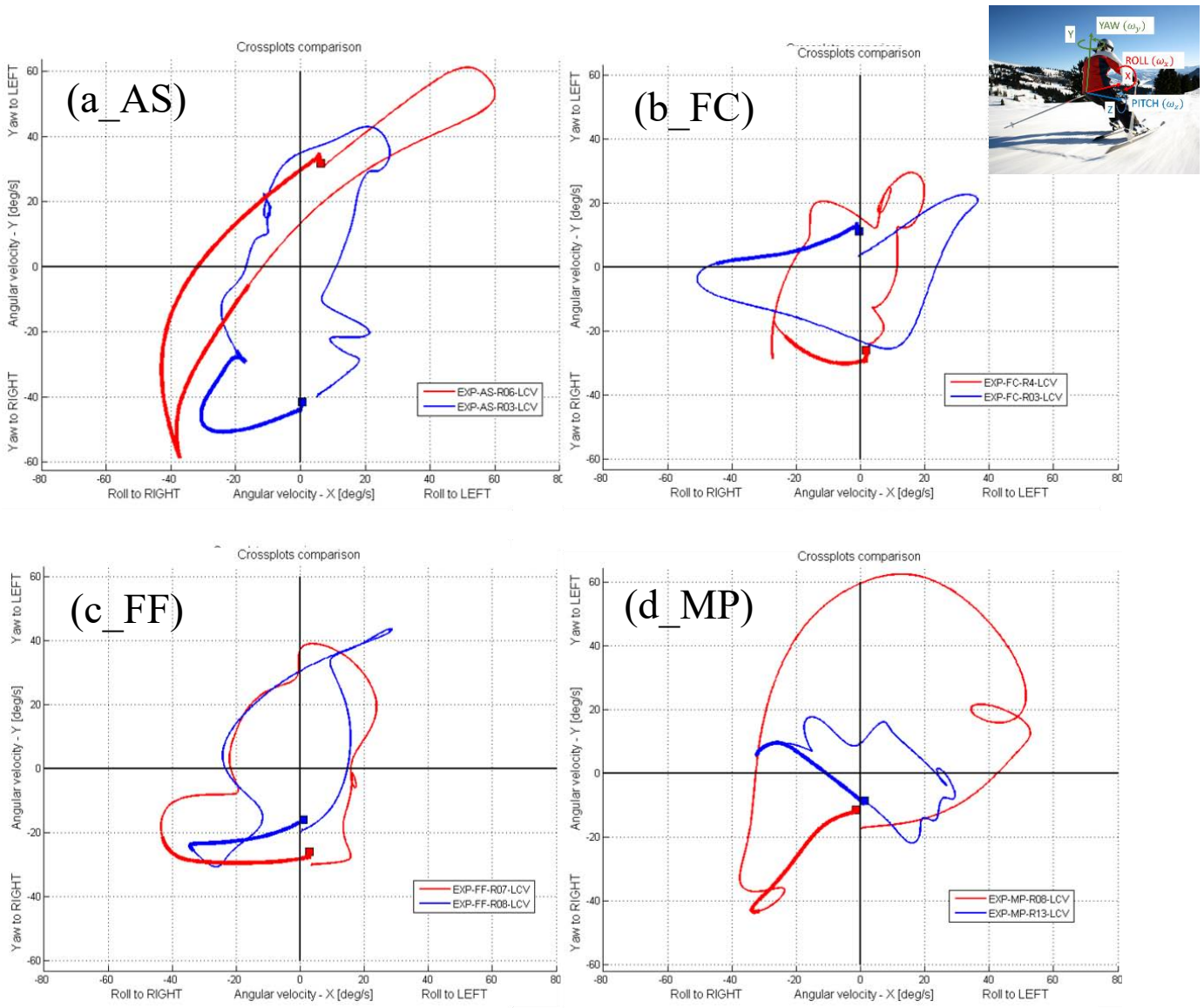

Figure 5-35: Experts skier, LCV total comparison

This style, characterised by fastest and larger-radius turns ,shows a significant difference in the cyclograms. The general trend remains the same, but the shape is different. AS has still cyclograms stretched along the bisector of the first and third sector. But his signals contains a lot of noise that results in probably corrupted cyclograms. Those do not correspond to a physical reality: the angular velocity is strongly drifted towards the second quadrant whereas in the other cases has a centre near the point (0,0). The shape of FF's cyclogram is very similar to the SSK case. Instead, MP has irregular cyclogram. This can be due to a couple of left right turns that can have altered significantly the cyclogram or to measurement noise. The FF's cyclograms shows a less regualar shape, with two rings at its ends. This shape is maintained also in short carved turns, presented below:

All the supposition will be analysed mathematically through deeper analysis, in order to confirm or dismiss hypothesis about the usefulness of cyclograms in sky performance analysis. In fact, as the aim of the thesis suggest, if distinguishing parameters able to confirm the differences between skiers will be possible to find, self-tuneable protecting devices.

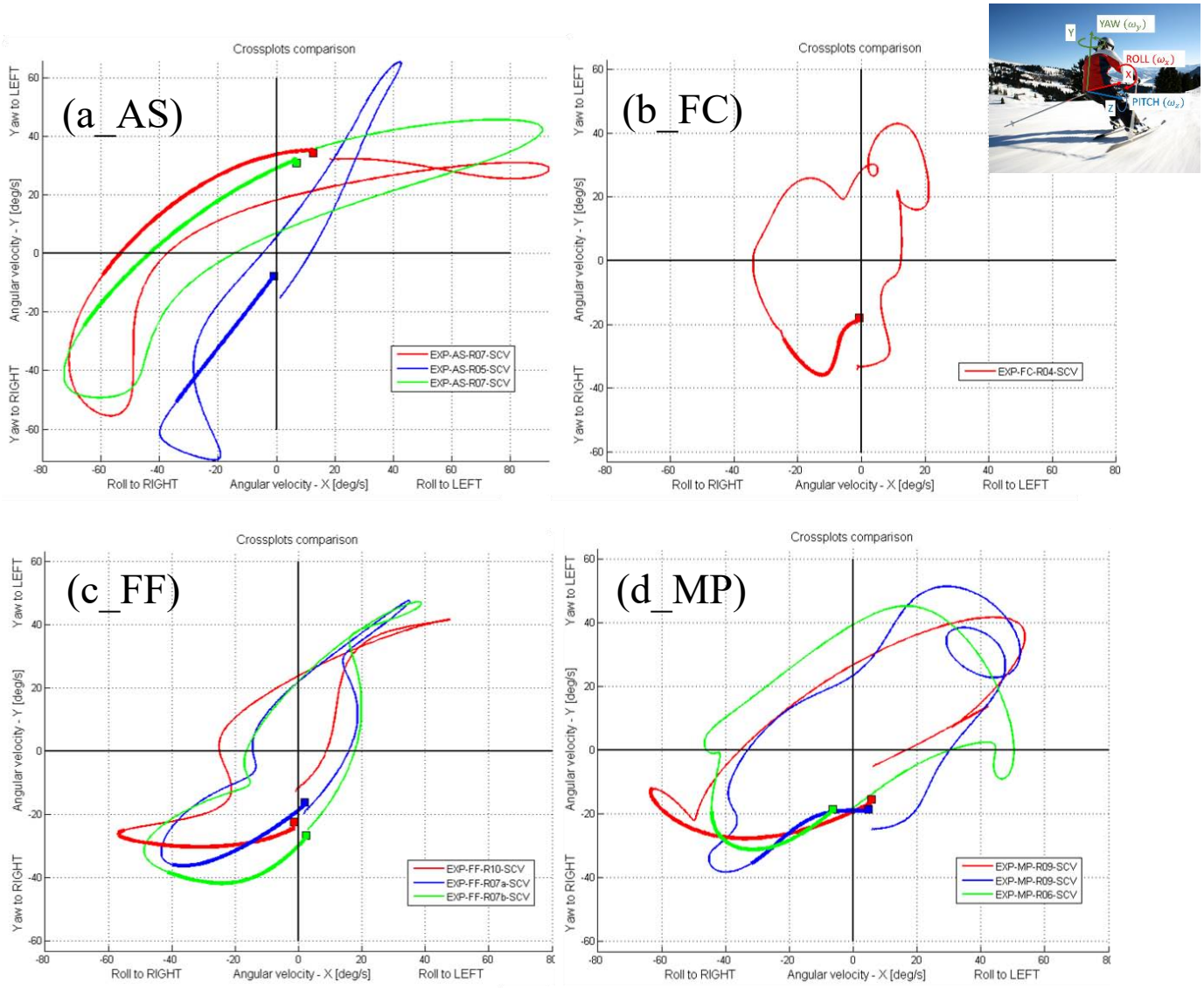

Figure 5-36: Expert skiers, SCV comparison

In those set of turns, skier maintained the cyclograms shape of LCV; with the exception of MP whose cyclograms changed completely shape. For the tester F.C. was impossible to extract another set of five short carved turns uncorrupted by noise, for the other tester were chosen the most significant cyclograms in a large group. SCV is a style that implies a good descending velocity but also a large number of turn in the same run. We can assimilate SCV with the turn made by professional skiers in special slalom competition. It is possible to observe similarities for the cyclograms with an exception: the red cyclogram of A.S. is thin, and it is due to a large noise in the signals, which has in the angular velocity about the X axis, frequent zero crossing, that made barely impossible to select the correct starting point of the turn.

In the figure below, the four expert skier in session I2, are compared in terms of different skiing technique. It is possible to observe how different are the skiing styles, but also how there is a common pattern in all expert's cyclograms. Even if the skiing styles are different, the cyclograms' pattern remains the same skier by skier. Only FC shows low repeatability in his cyclograms.

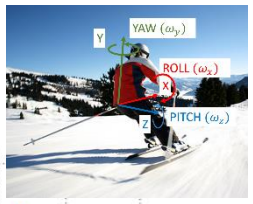

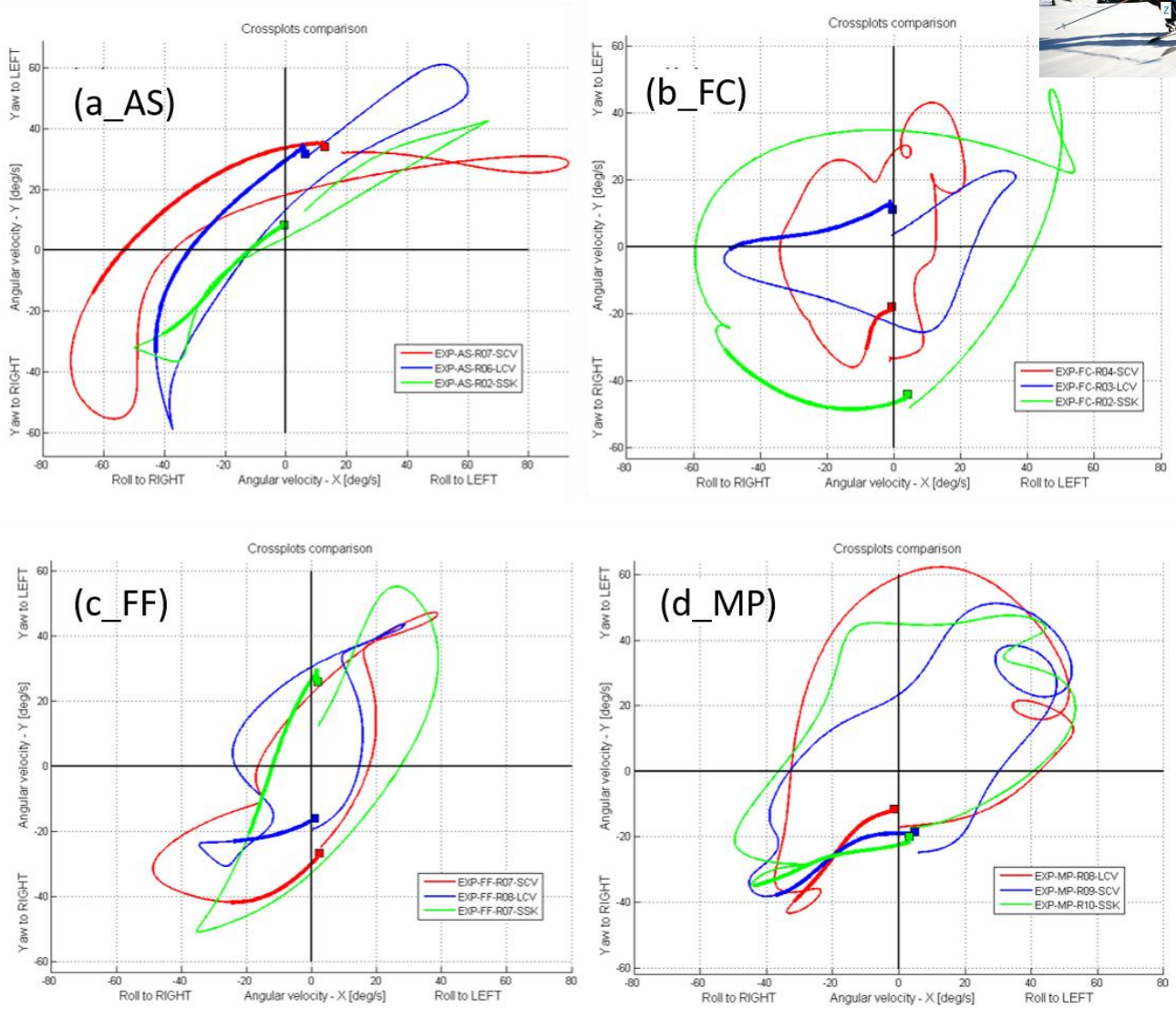

Figure 5-37: Expert skiers, comparison of the three techniques. Red line: SCV; Blue line: LCV; Green line: SSK

The red line represent the SCV, the blue line represent the LCV and the green line represent SSK. It can be possible to observe that in most cases the cyclogram is like a 'fingerprint' of the skier style of skiing. Not much difference is present visually between different skiing techniques.

But also expert skiers show unclear and different cyclograms. This analysis technique can be addressed also Intermediate and Beginner skiers. In the following, frameset of the two beginner recorded with the video cameras. Then the cyclogram obtained by analysing their data are presented.

(a)

Figure 5-38: Beginner skier AX

(b)

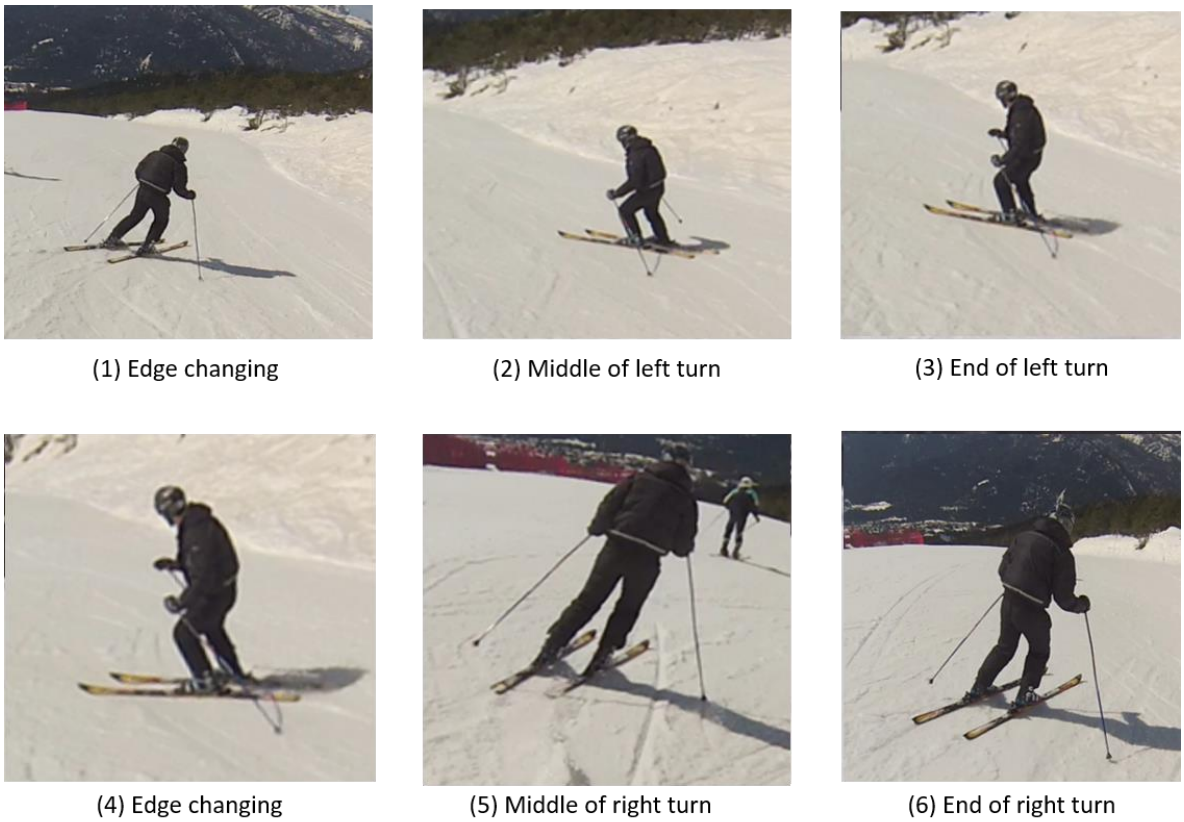

Figure 5-39: Beginner skier OQ

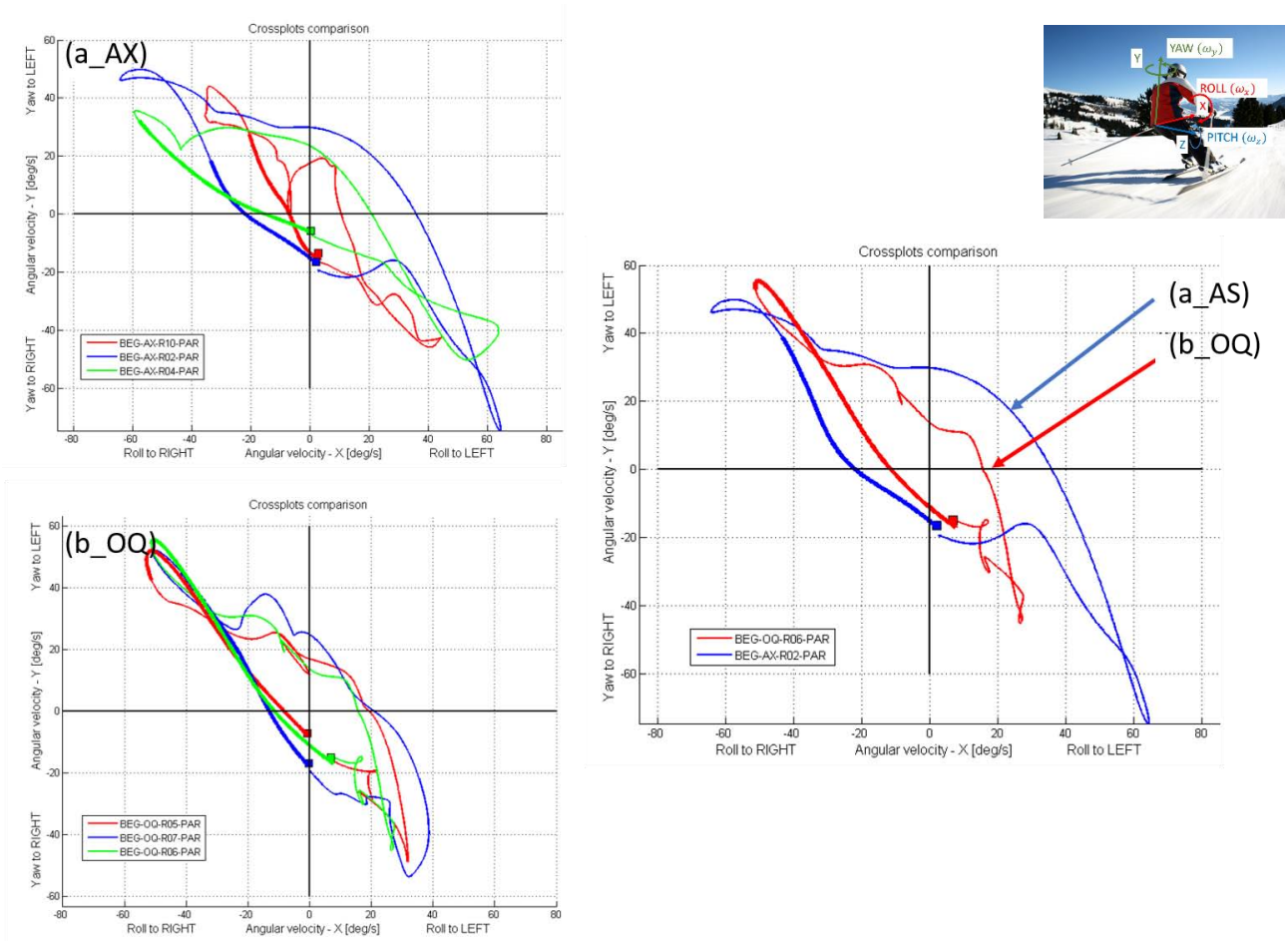

Figure 5-40: Comparison of the two beginner skiers

The analysis of beginners' cyclograms show an evident difference with those of expert skiers: it is possible to observe that both beginner skies have cyclograms that spreads on the bisector of the second and fourth sector, in contrast with expert's cyclograms. The first physical explanation for such cyclograms can be found in the tendency, in beginner skiers, to move the trunk rigidly. In addition, the positive sign of ω_y and the negative sign of ω_x in the second sector, correspond to the rigid trunk movement in the middle of the turn, pointing towards the edge changing. Assuming the case of a left turn, the roll and yaw angle are towards the interior of the turn, with a negative sign for the roll angular velocity and a positive sign of yaw angular velocity. This is repeated in the right turn, described by the part of the cyclogram that lays in the fourth sector.

.

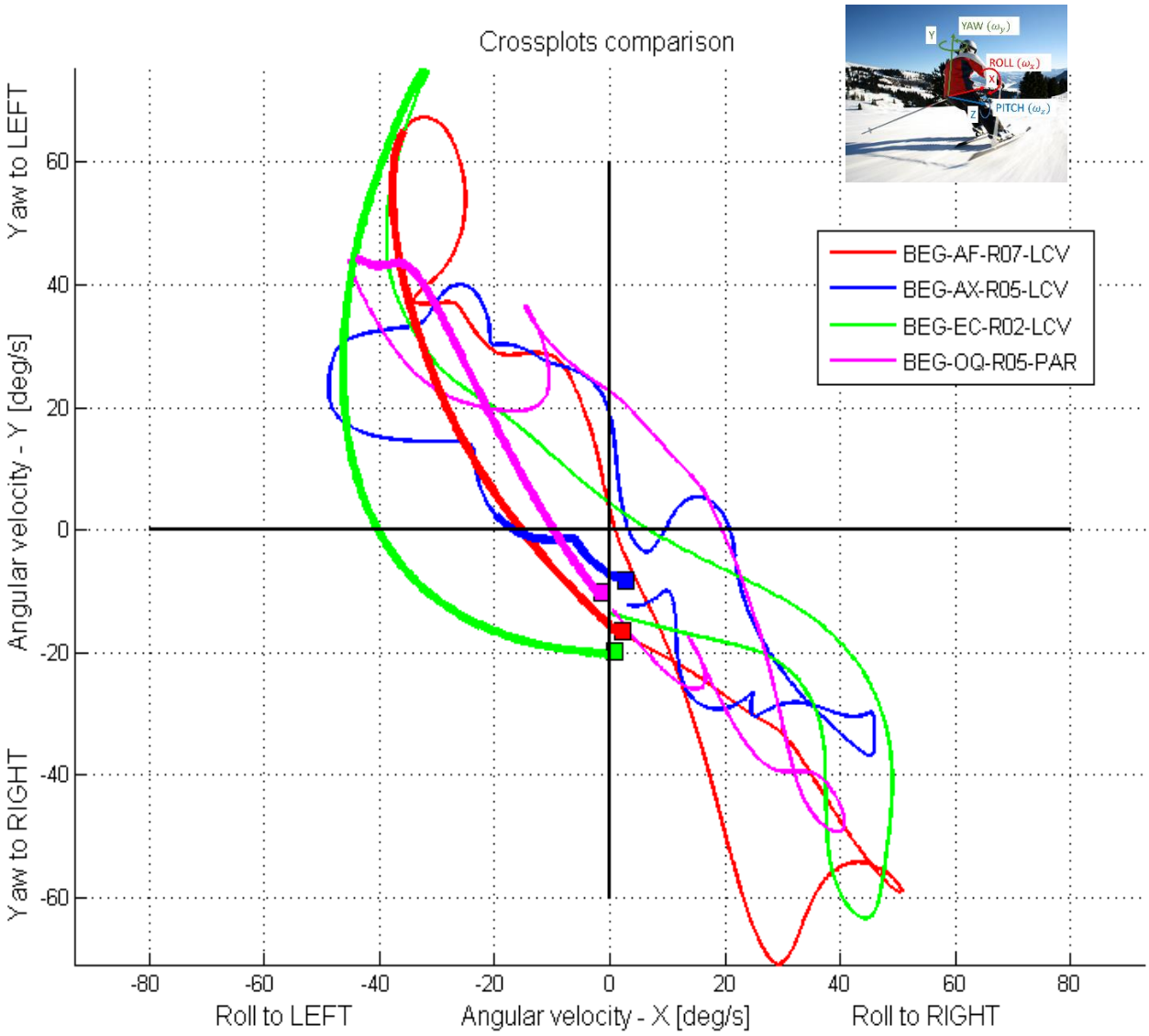

Figure 5-41: Beginner skiers' cyclograms

The figure above show a comparison between the cyclograms of all the beginner skiers in I1 and I2 test session. It is possible to observe that all the cyclograms have the same pattern, even if the extremities are different one from another.

The difference between Expert and Beginners is visually clear (Figure 5-24 vs 5-5). The difficulties came when analysing Intermediate skiers. Comparing the tester in I1 and I2 test sessions, the result shows a clear distinction between them. Some are near beginner's crossplots and some near expert's ones. In the figure below is reported a comparison between the intermediate skiers performing different techniques.

NP, an intermediate skier, performing short skidded turns. It is possible to observe that his style is far away from beginner's, but a residual upper body rigidity and a jerked movement differences his style from experts'.

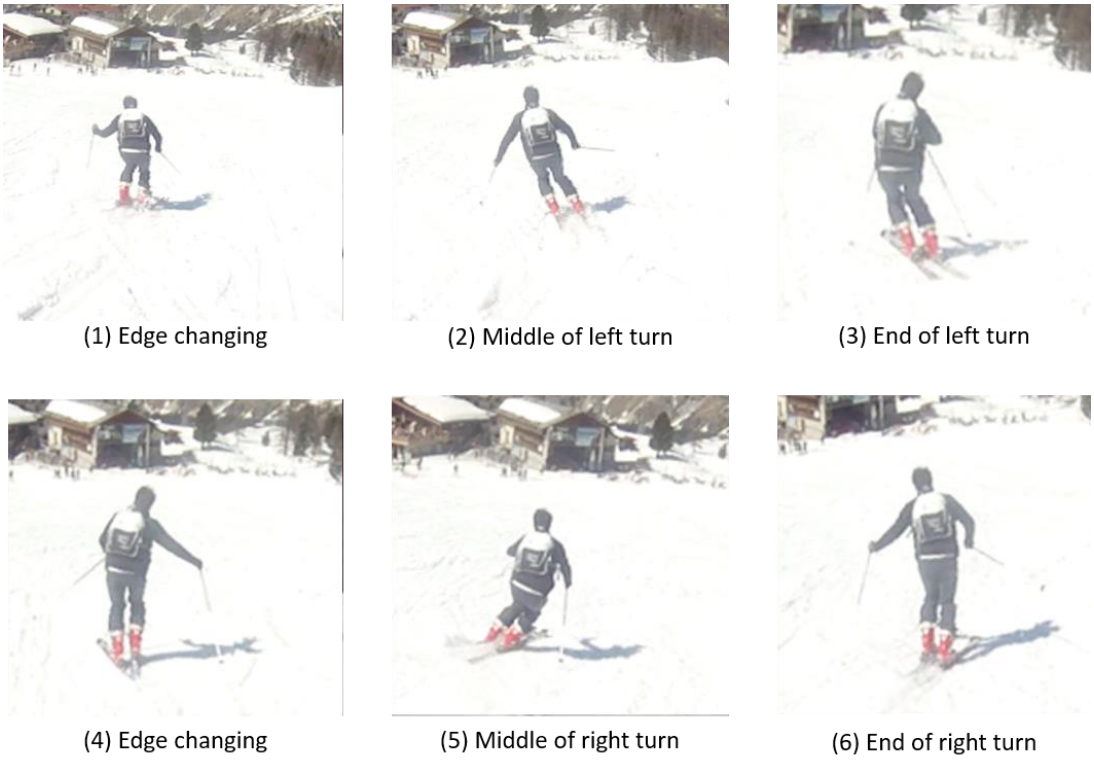

Figure 5-42: Intermediate skier NP performing SSK

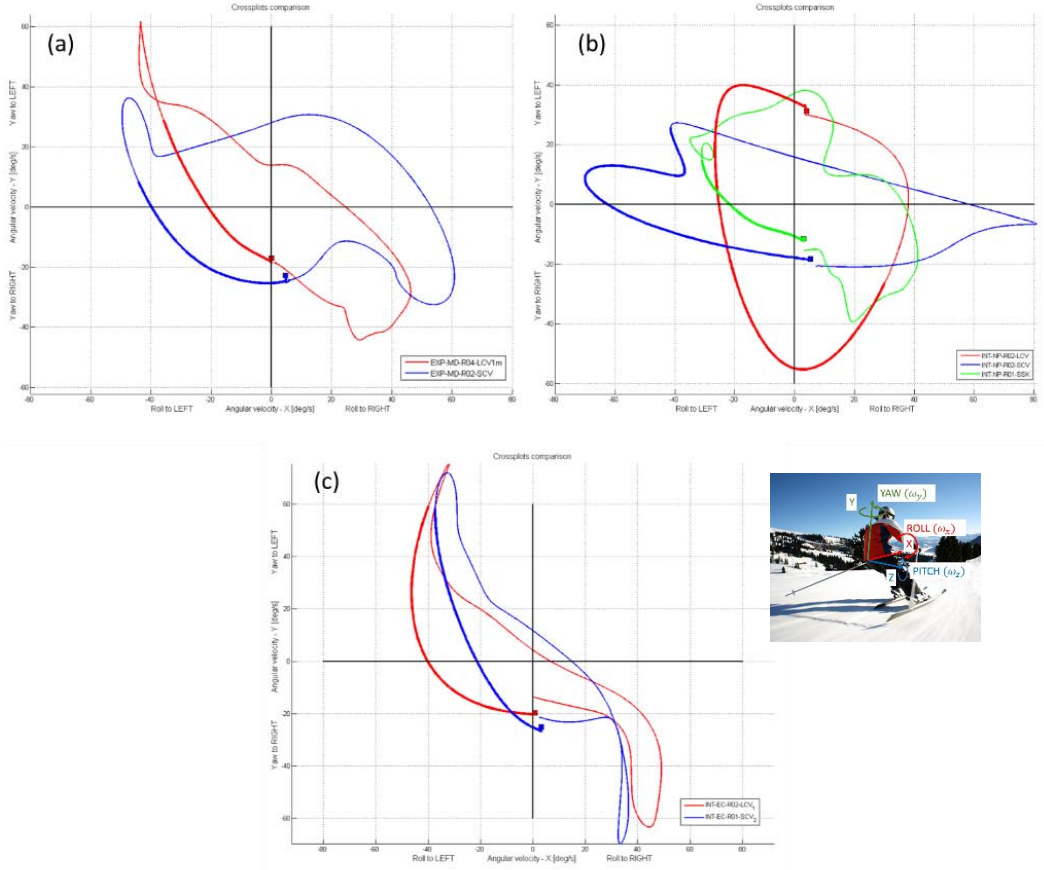

Figure 5-43: Intermediate skiers comparison; Red line: LCV; Blue line LCV; Green line: SSK

In the figure 5-26 above, a comparison of the intermediate skiers performing the different techniques is presented. Unfortunately, only few cyclograms for intermediate skier were obtained. Three intermediate (NP, EC, MD) were tested. In figure 5-27 LCV and SCV for the three testers are reported. SSK was not possible to obtain, due to the lack of this technique in EC's skills. MD was considered an intermediate in I1 session even if he is an expert skier. In that session he adopted ski mountaineering skiers that forced him a non-comfortable skiing style. In consequence, his skiing level was more near to an intermediate than an expert. It is possible to observe that cyclograms are in between experts and beginners ones. In fact EC present cyclograms stretched along the bisector of the second and fourth sector, but with a central kernel wider in respect to those of beginners. Instead NP and MD present cyclograms that lie along the abscissa axis. In SCV style, MD shows a cyclogram near to expert's.

In the figure below, a comparison between the intermediate performing the same technique is presented.

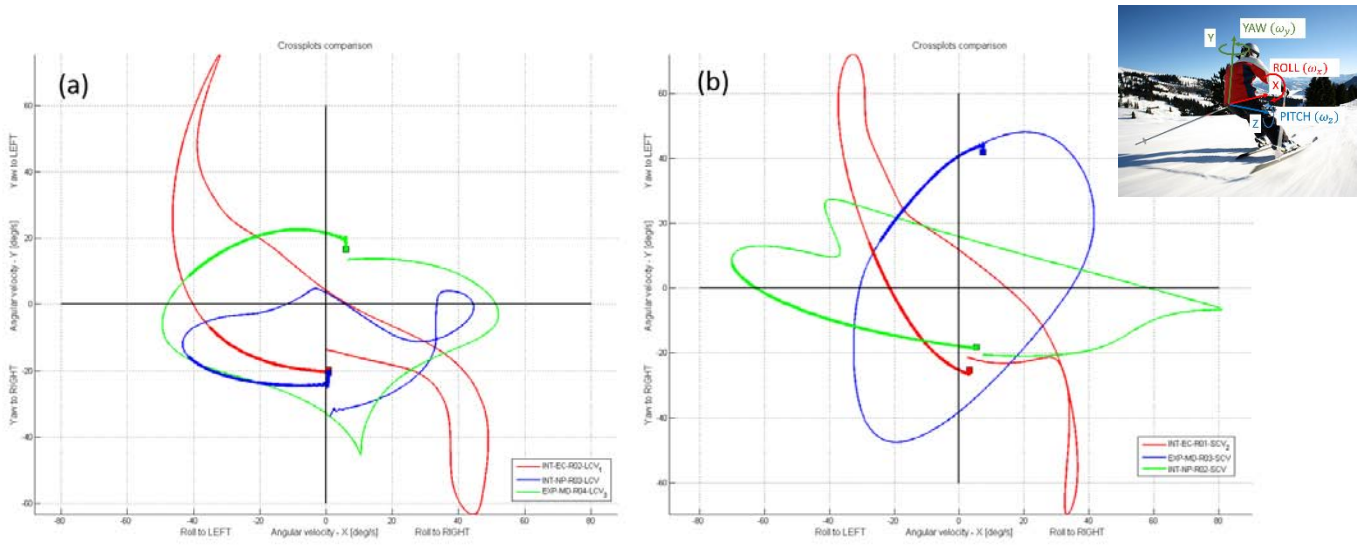

Figure 5-44: Intermediate skiers, LCV (left) and SCV (right) comparison

The last cyclogram presented is relative to a ski instructor, FG. He was the most expert tester, as he is a high-end ski instructor. In his case the cyclogram are different than the other testers as they tend to stretch along the Y-axis, with highest angular velocities if compared with the X-axis. His cyclograms are also the most repeatable. In addition, symmetries along both axes suggest a high repeatability of its turns, without variability between left and right turns.

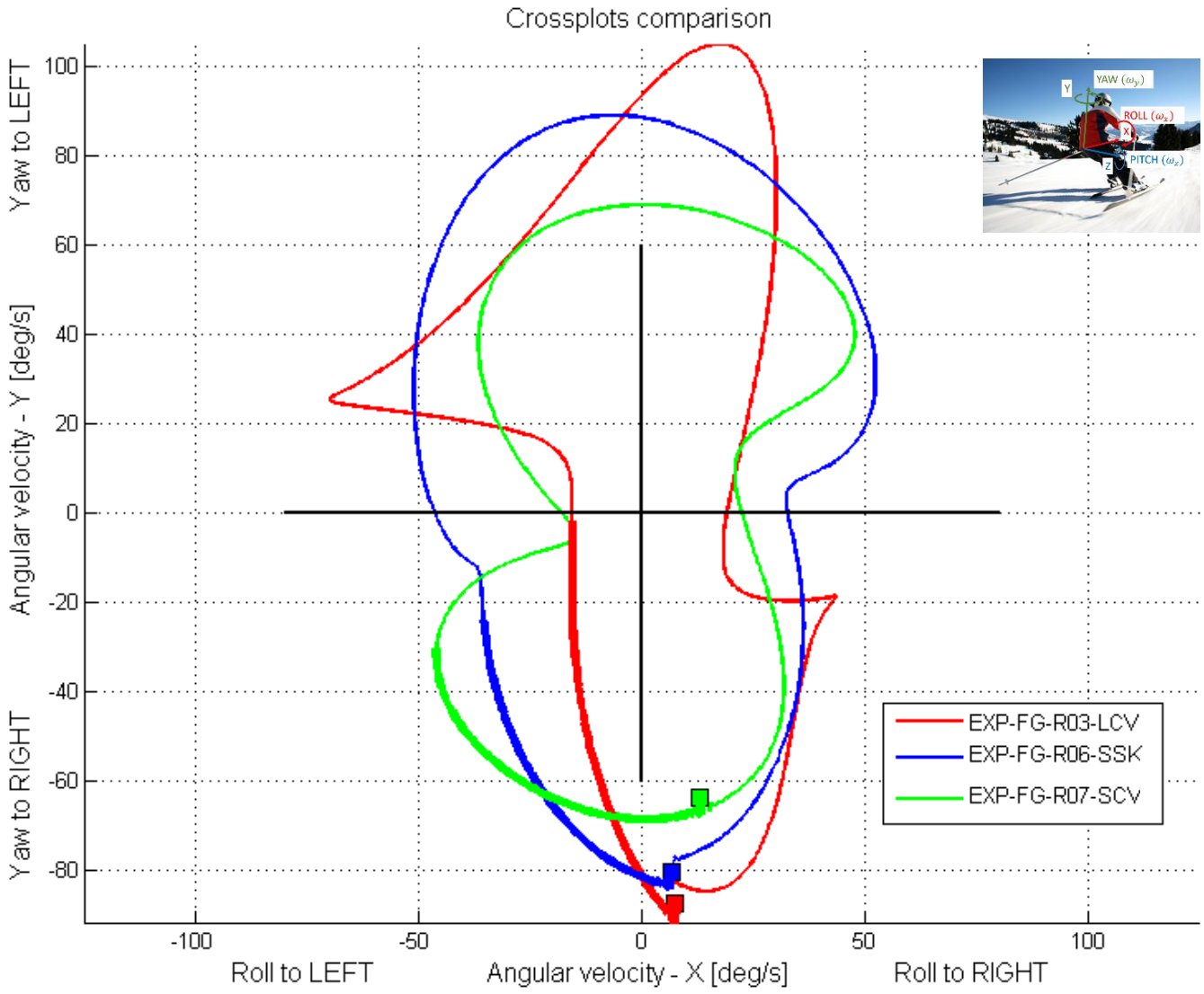

Figure 5-45: FG different skiing styles; ski instructor.

It is possible to observe that there are strong differences between the three styles, but also that the cyclograms disposition is the same for the three techniques. In addition, they are symmetric in respect both X and Y axes. Those cyclograms have to be taken as reference for future tests with this analysis method. If racer skiers will be analysed in future, a comparison between them and FG could be done, enhancing difference and similarities in order to obtain a method to compare training techniques and results.

5.2.6 **Area calculation**

As seen in the paragraph above, a mathematical method to compare the cyclograms of the different skiers, is needed. In order to do this, it is necessary to find parameters able to distinguish among the skiing levels. Having observed the difference between ski instructor cyclograms' and Beginner's

ones, the first parameter identified was the Area of the cyclograms. In addition, due to their elliptic shape, the main diagonal was considered as possible index for classification.

The area was obtained via Matlab script by using the trapezoids method, after dividing the cyclograms into an upper and a lower portion, based on the Min/Max values of ω_x. The integral was calculated in such a way that the area was positive if the cyclograms grows in a clockwise direction, negative if it grows in counter clockwise direction.

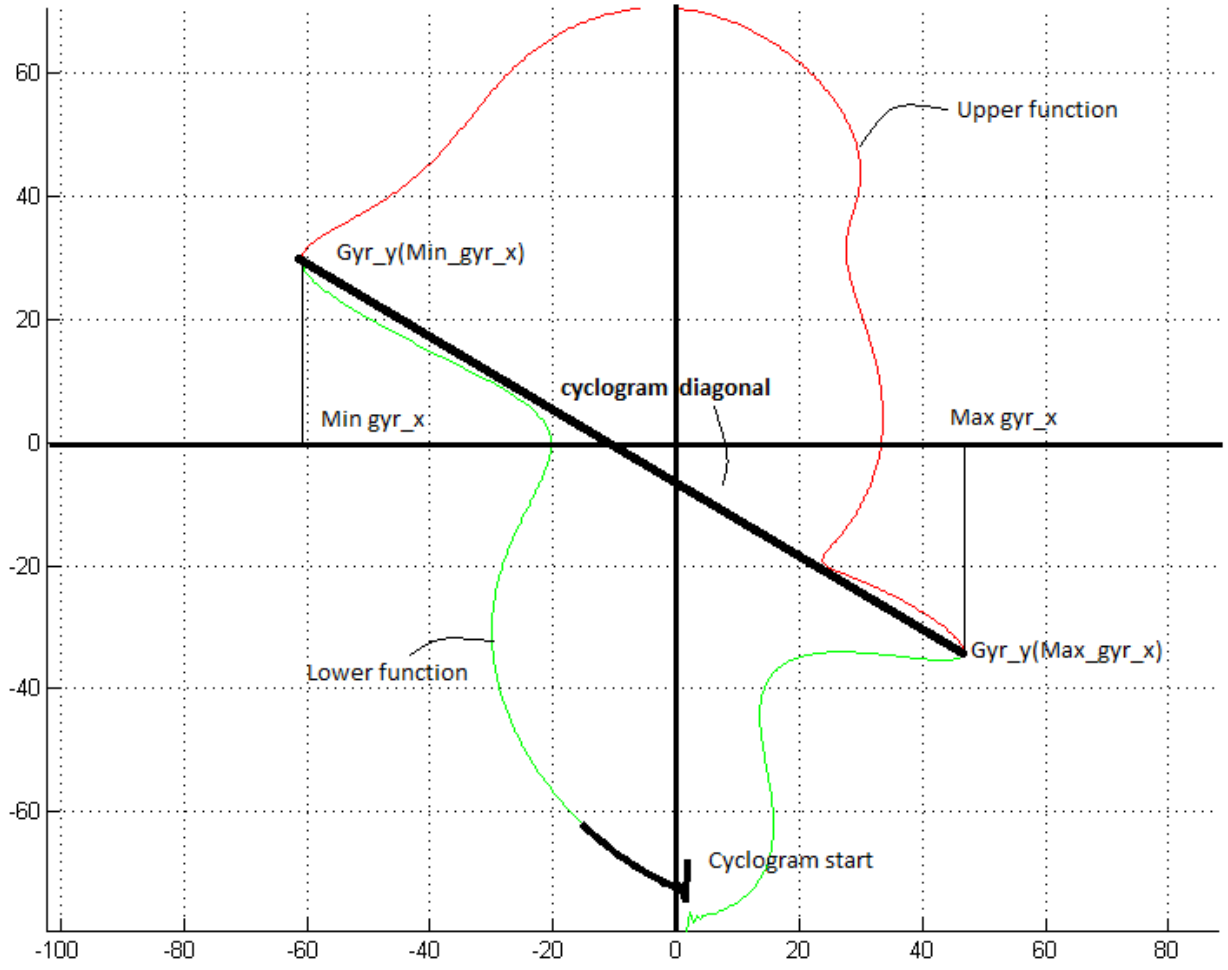

Figure 5-46: Diagonal and Area calculation scheme

The diagonal, instead, was calculate after finding the maximum and the minimum values of the X-axis ω_x angular velocity and finding the corresponding value in the ω_y angular velocity. Then the numeric index "Diag length" was calculated using Pitagora's theorem.

The "Diag" sign was associated with the sign of the slope of the diagonal segment, positive as usual in analytic geometry, when raising counter clockwise from the horizontal X-axis.

Having two indexes extracted from each cyclogram, it was possible to prepare dispersion diagrams to have a visual idea about the difference clusters corresponding to the three different skier's levels and techniques.

5.2.7 Dispersion diagrams

After the parameters selection, to better distinguish between skiing levels, it is important to setup a dispersion diagram. Selecting one parameter in abscissa and one in ordinate for each cyclogram, a point finds an unique position in the diagram. With this method, it will be possible to have a visual idea about the different clusters corresponding to different skier's levels and techniques.

The first dispersion diagram was set up using the two parameters previously identified. This resulted in a plot of the Area algebraic values against the dimension of the Diagonal.

The symbols below are to differentiate the different skiing techniques;

- '+' is adopted to identify parallel turns, performed by early beginners;
- '*' is adopted for the short skidded turns;
- 'o' is used for the long carved turns;
- 'Δ' stands for the short carved turns;

The colours are used to differentiate among the skier's levels: The black points are beginner skiers, Intermediate skiers are in red points, and expert skiers are in green points.

In the first diagram are plotted the expert skiers:

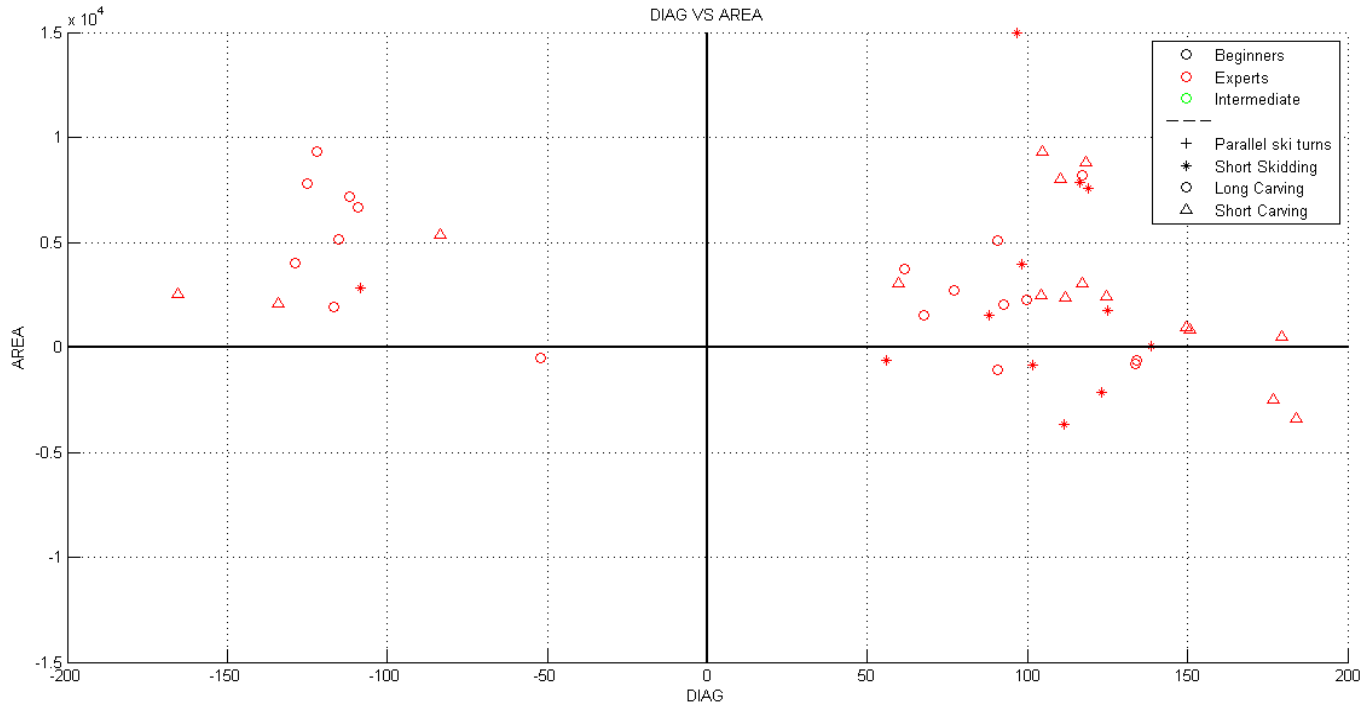

Figure 5-47: Expert skiers - dispersion diagram

It is possible to observe the high area value for most of the skiers, with some exception, due probably to A.S. deformed cyclograms.

In the picture below are reported intermediate skiers:

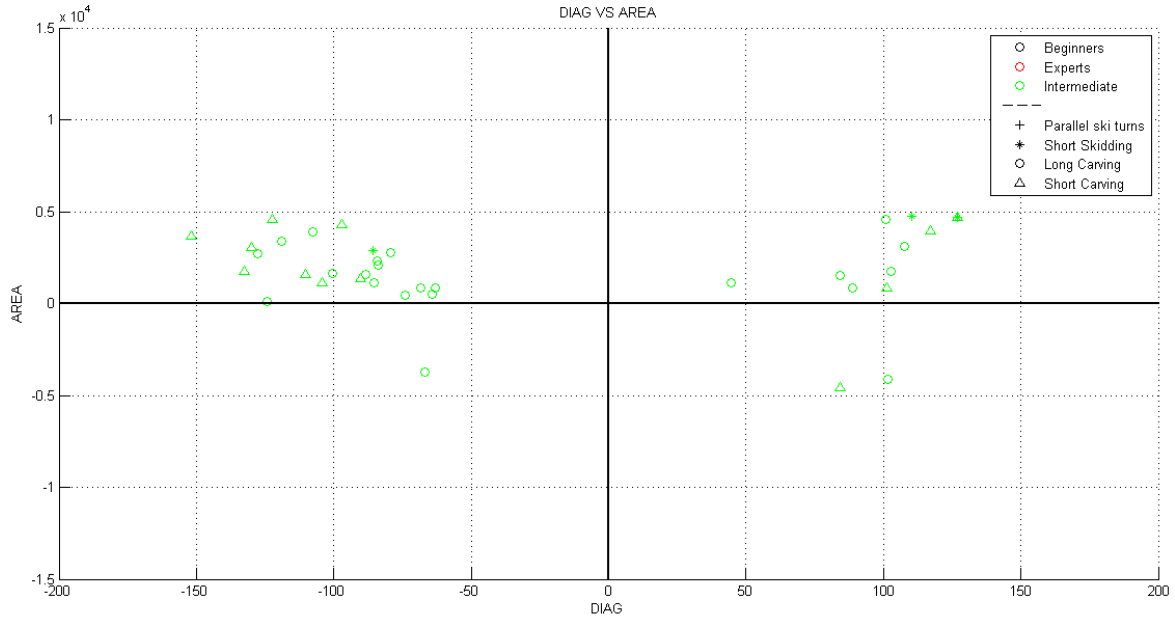

Figure 5-48: Intermediate skiers - Dispersion diagram

Those are grouped and there is less inter-individual difference. Unfortunately, this diagram overlap part of the Expert's plot. By this diagram, the difference between expert and intermediate skiers is not clear enough. We can say that expert are in large part in the positive areas part of the diagram, shifted mainly towards high Diag values, but the intermediate skiers are grouped together, both in the positive and negative area values; In the picture below are reported the cyclograms of the beginner skiers.

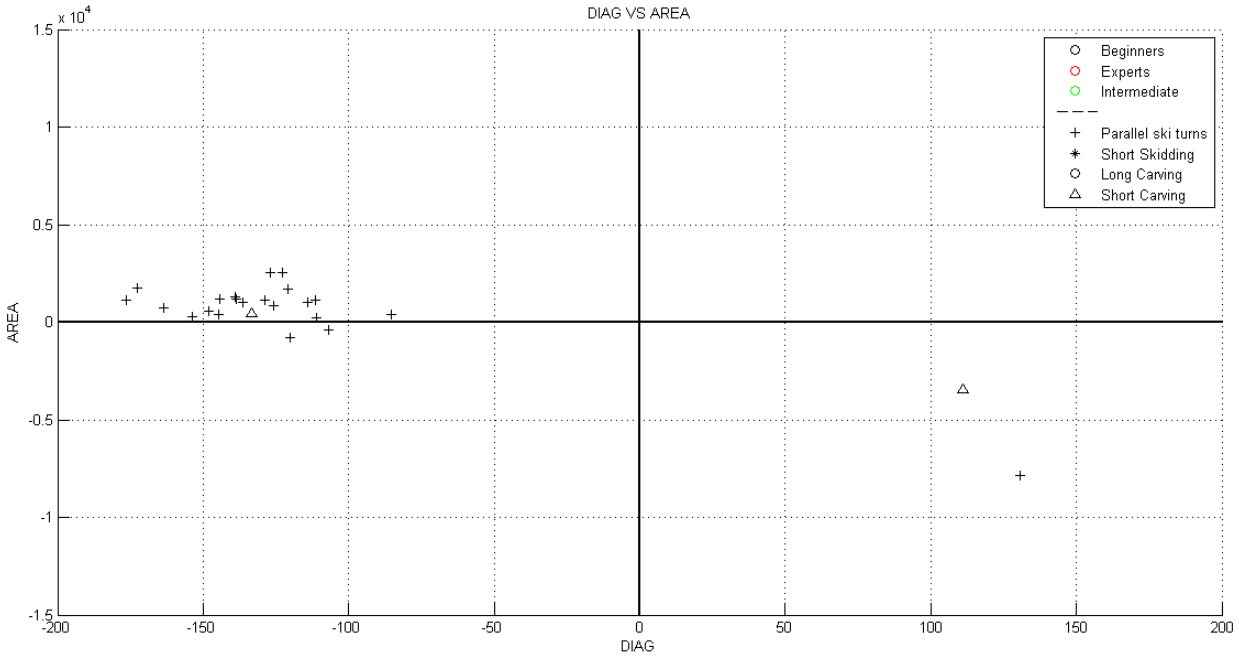

Figure 5-49: Beginner skiers - Dispersion diagram

It is possible to observe that the beginner skiers find their own collocation in the graph, having high negative Diag and low area values.

If we consider not only the single skier's group, but all the three skill levels together, we have a visual acknowledge if the information given by this classification method:

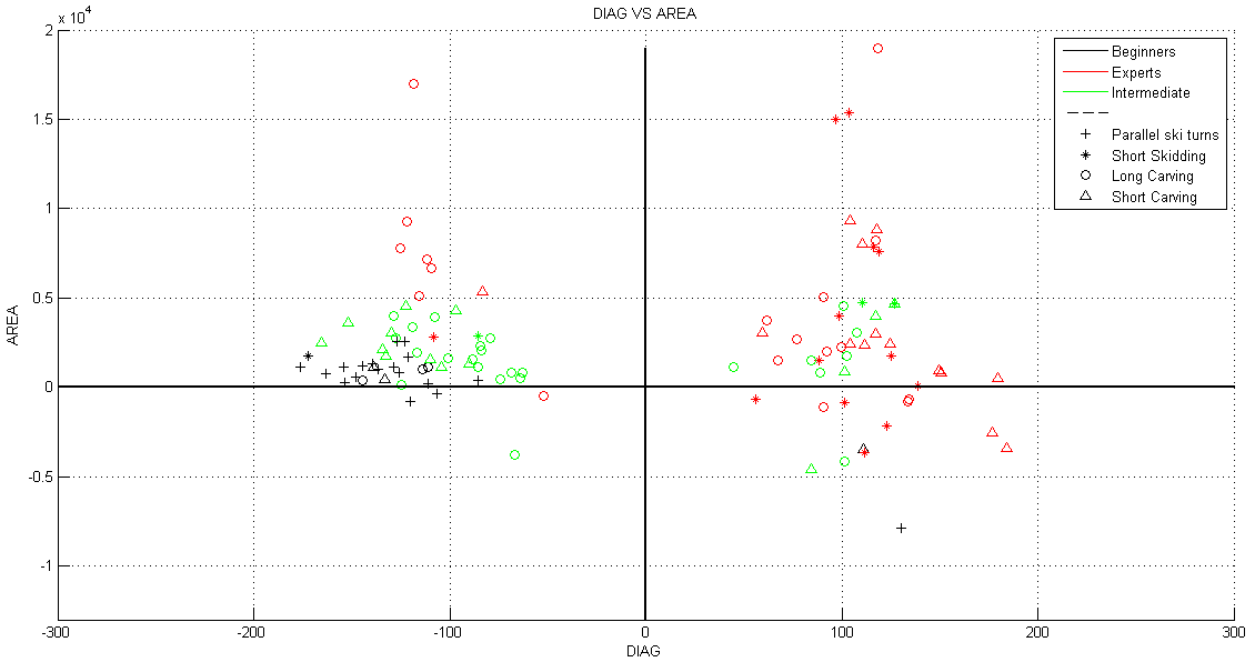

Figure 5-50: Diag vs Area - dispersion diagram

It is clear that the Intermediate group is in both in the beginners and experts region. By this method is possible to distinguish clearly between beginner and expert skiers, but the intermediate skiers class is too much in the middle way.

Because of this low differentiation, another parameter was considered. Having analysed the runs even in terms of resultant accelerations and resultant angular velocity, the parameter 'Delta acceleration' was extrapolated. We decided to use this parameters after having seen the different skiing style: an expert skiers, especially when performing short carved turns, has usually wider and faster movements resulting in higher acceleration in respect with beginners. We decided not to analyse the whole number of the couple of turns, but only the mean turns obtained by averaging the five continuous couple of left-right turns. The maximum and the minimum values of the resultant acceleration were obtained. The 'Delta acceleration' parameter was obtained by calculating the absolute value of the difference among maximum and minimum values.

This analysis was performed both for the resultant acceleration and the acceleration on the Z axis.

In the picture below, there is an example of the maximum and minimum selection, referred to the acceleration on the Z axis. The calculation of the resultant acceleration, as the square root of the square power of single channels values summed, was made directly in a Matlab script.

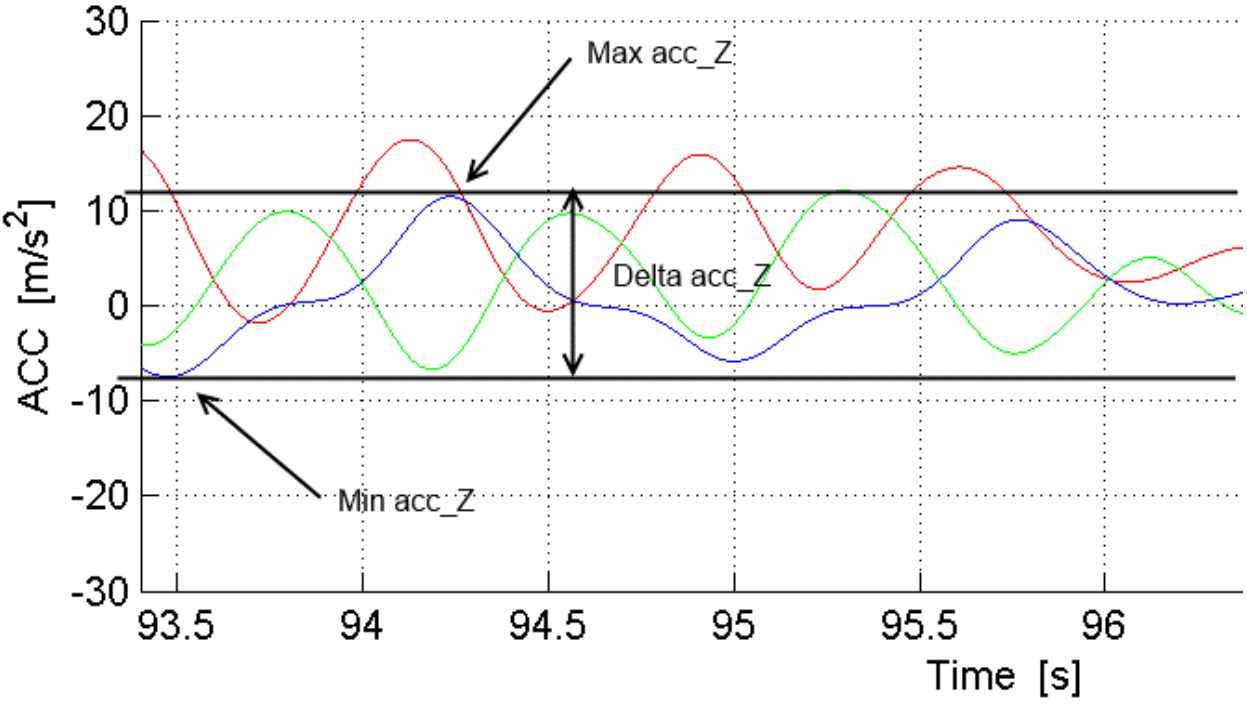

Figure 5-51: Maximum and minimum selection on Z axis acceleration (Blue line)

The Delta acceleration parameters were utilised in addition to the Area parameter to set up other dispersion diagram, with the aim of finding differences between the skiers levels and the type of turns they were doing.

Unfortunately, despite the fact that the dispersion diagram obtained by plotting the Area with its sign versus the delta acceleration resultant gave better result than the previous dispersion diagram, the three skill levels were not enough separated. Even in this case, beginners and intermediate overlapped in a portion of the diagram:

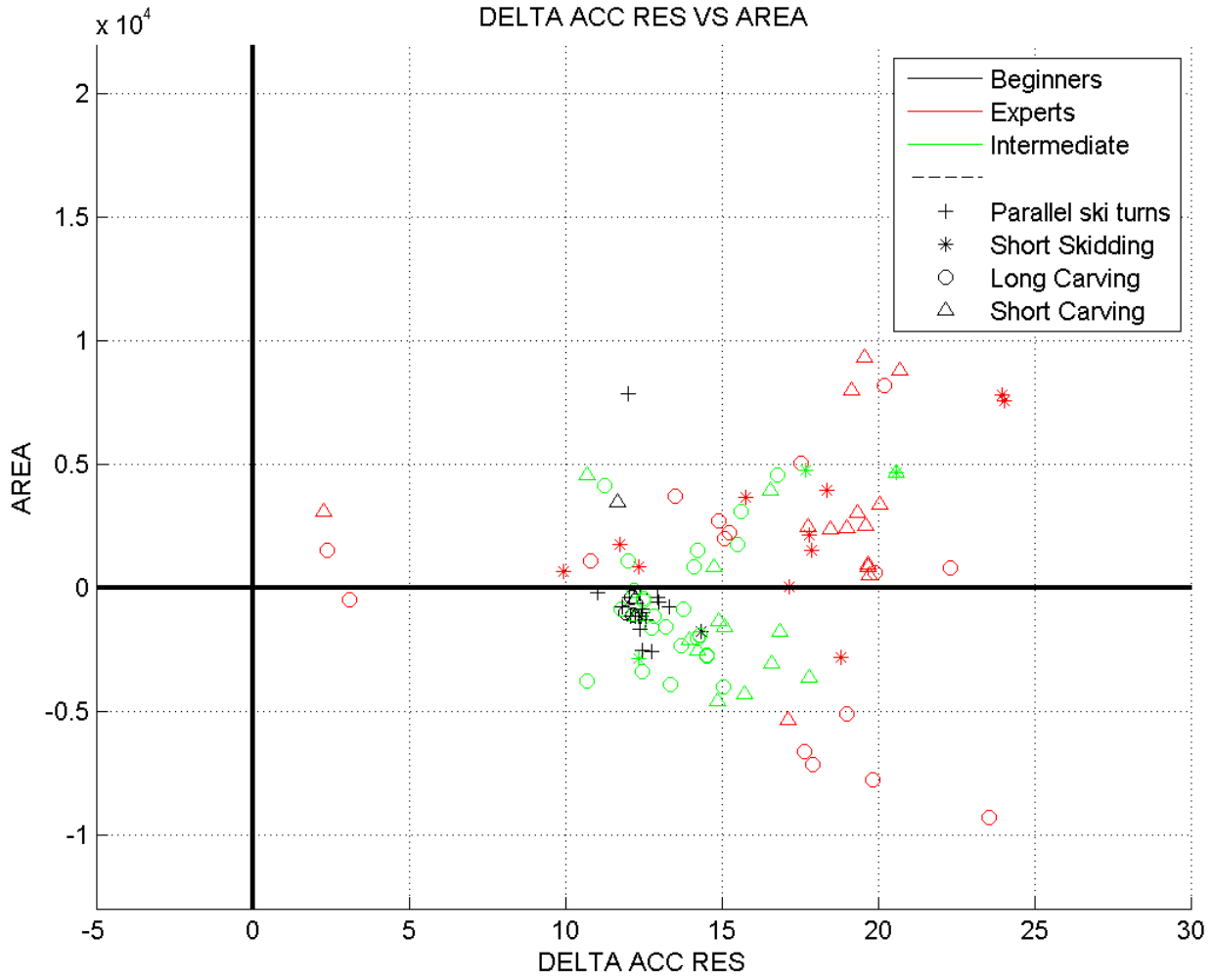

Figure 5-52: Delta acc res vs Area - Dispersion diagram

The beginners are well distinguish, with the exception of seven experts. This was due to the measurement error driven by the sensors positions. Even in this case, the single levels dispersion diagram gave useful information but, grouping the three levels together did not lead to a clear distinction.

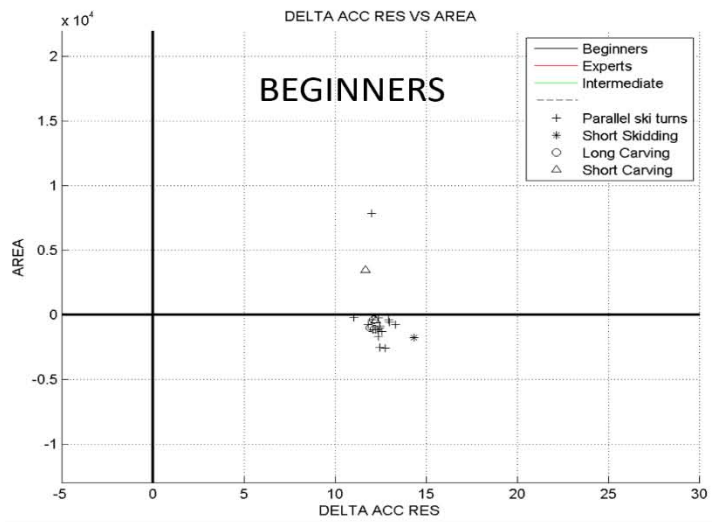

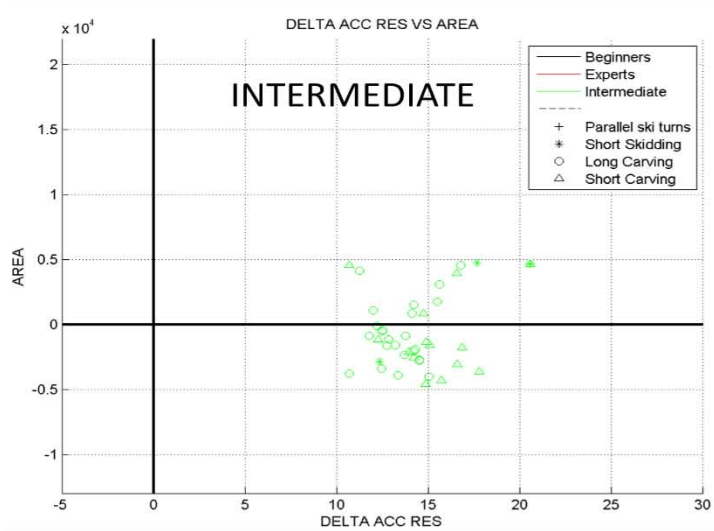

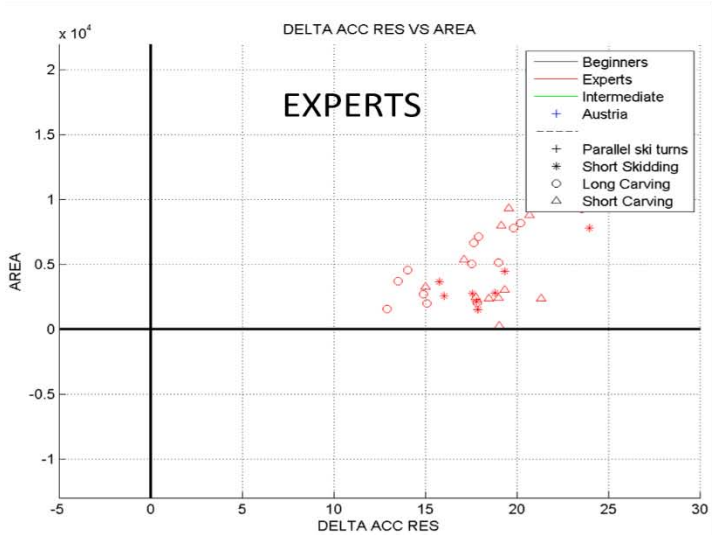

Figure 5-53: Dispersion diagram - single levels

An important factor in those parameters is the possibility to analyse the different skiing techniques. The analysis, performed only for intermediate and expert skiers, show a difference in the position of the diagram for the intermediate and expert skiers performing the three techniques: the Experts are usually in the part of the diagram with higher values of area and delta acceleration resultant, as reported in the picture below:

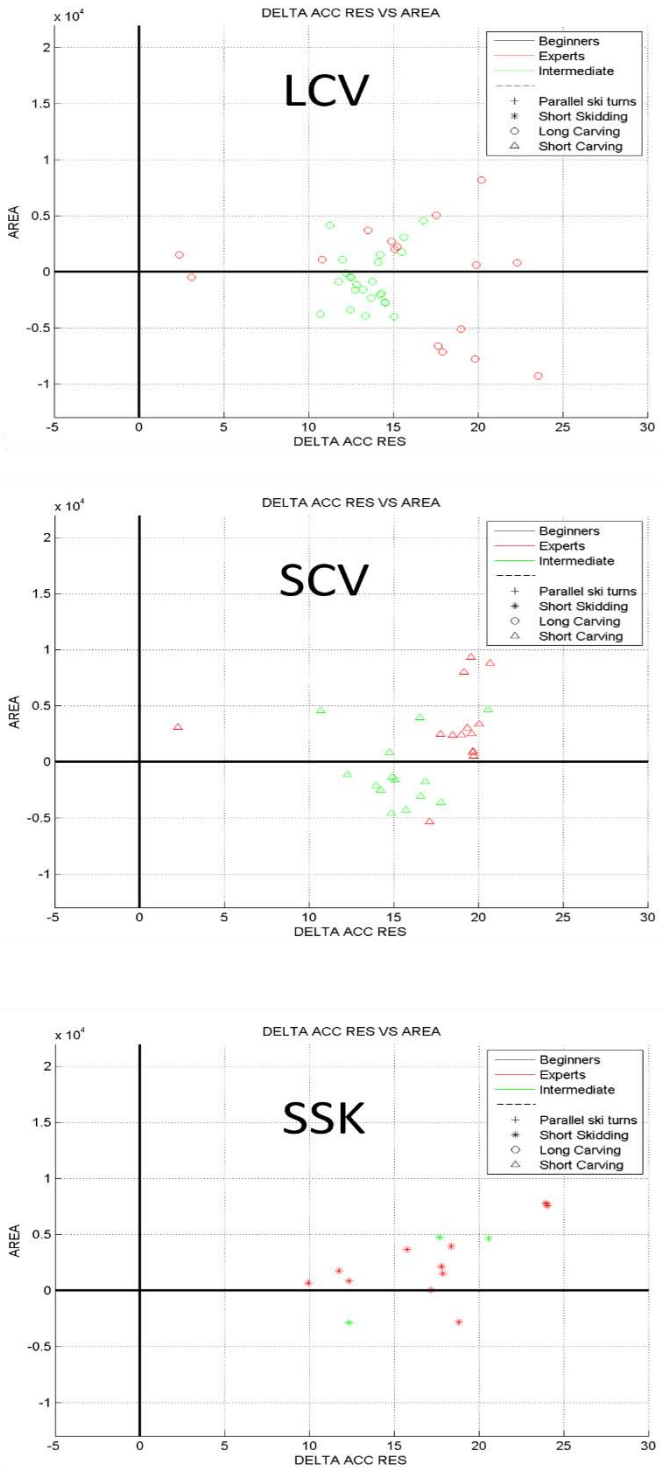

Figure 5-54: Dispersion diagram - skiing style

The dispersion diagram obtained by the Area with its sign and the Delta acceleration on the Z-axis did not gave useful results. In the picture below is reported the dispersion diagram:

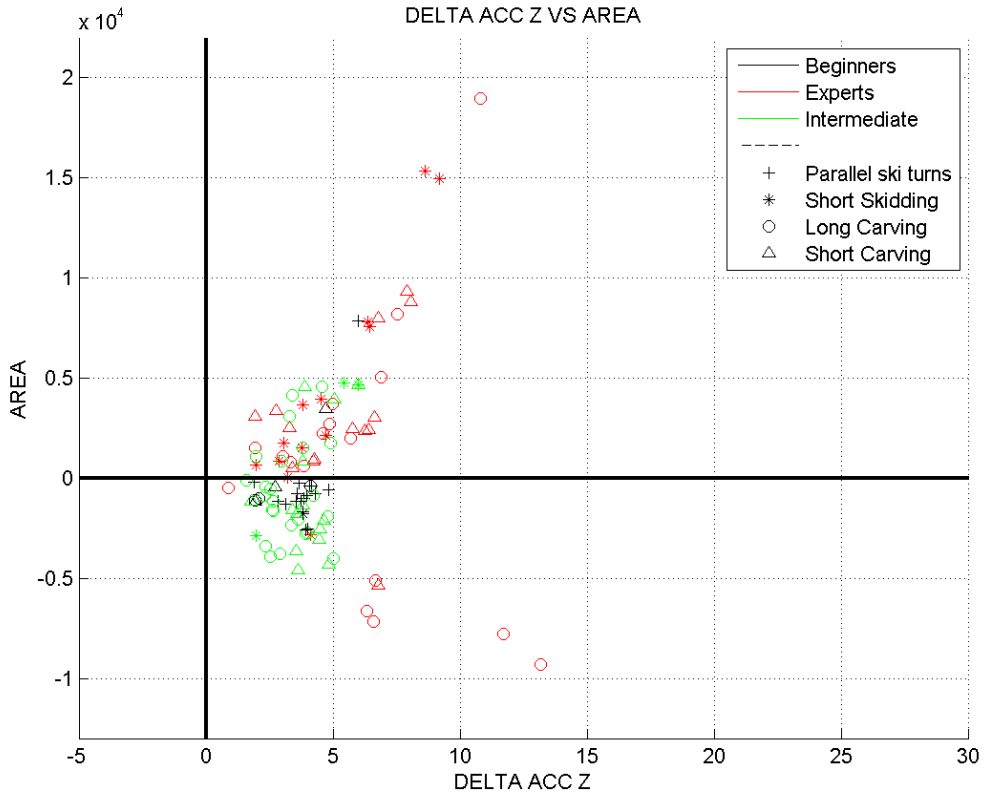

Figure 5-55: Delta acc Z vs Area - Dispersion diagram

It is possible to observe a growing trend with the level, but the portion of the diagram near the zero value for the Area is too much confused to get a clear distinction between the levels.

Having observed a high inter and intra variability for the set of turns, we decided to analyse deeply the single couples of turn for the skiers. The aim was to obtain clear information about the data reliability. Every skier was further analysed in order to find out the standard deviation of each set of five turns. The standard formula of the variance was used: $\sigma^2 = \frac{1}{N}\sum_{i=1}^{N}(x_i - x_{mean})^2$;

The standard deviation was calculated both for the ω_x and ω_y, in order to observe how much intra-individual difference was present in the skier's crossplots. In this, a selection and elimination of scattered cyclograms was possible. In the four picture below, this information is reported:

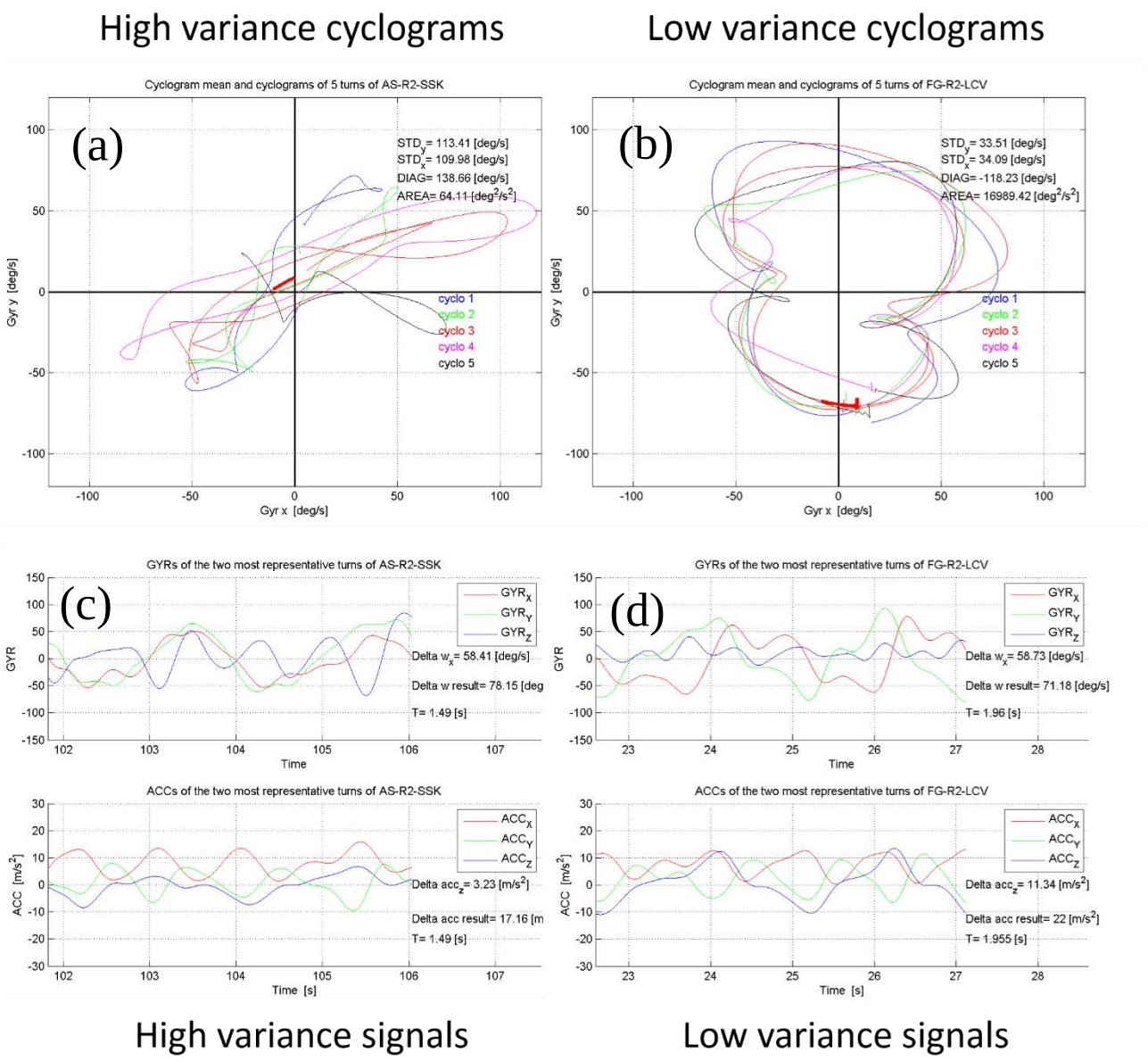

Figure 5-56: Individual turns and cyclograms: high variance cyclogram (a), low variance cyclogram (b),high variance signal (c), low variance signal (d)

It is possible to observe that the high variance signals leads to non-repeatable cyclograms. The low variance signals, instead, le ad to a clear cyclograms shape. In the case on the right, the cyclograms are considerable as a fingerprint of the skier's style. The case on the left was removed from the analysis, due to the low reliability.

5.3 Parameters Analysis

We observed that trying two parameters at time, plotting dispersion diagram and analysing them visually would take a large amount of time. It was necessary a mathematical method to extrapolate as many useful parameters as possible. Another Matlab script was developed to perform this action.

Having a large amount of data, we decided to use all the data to set up a training set. This means that, starting by known classes, such as skiing levels and techniques, with the possibility to associate each trial to a specific class (this was made possible thanks to the questionnaire given to each skier), it Is possible to adopt the training set to determine useful parameters able to classify. The training set is, in this way, adopted to extrapolate parameters. Once the parameters are identified, it is possible to adopt them to classify unknown trials.

The fastest and more robust way to perform those actions is to develop a Matlab script able to collect in field data and to understand the skier's skiing level and technique. The script divides the data into four data set:

- Beginner's data set
- Intermediate's data set
- Expert's data set
- Austria's data set

Unfortunately, the Austria's data set was not clear enough to understand both the technique adopted and the skiers' level, because of an incongruence with the Innsbruck University in the definition of the Beginner and Intermediate class. Although, the Austria's data set was adopted as reference: in fact the sensor position of Austria skiers was different in respect that of Italia testers. In this way we have a comparison of the disposition of the skiers in the dispersion diagram, both with the sensor placed at the c7 level and over the pelvis. In addition we wanted to observe if parameters identified through the Italia data set were strong enough to classify also Austria data set.

For each of the four data set mentioned above, the mean, the standard deviation were calculated. Then several parameters thanks to a Brute-Force method were analysed. For each parameter, a histogram for each category was obtained. Plotting the four histograms together, it is possible to analyse if there is a good differentiation among the levels.

In the following are reported examples of the results obtained with this method.

We analysed the following parameters:

- Δa_R (Delta resultant acceleration) versus Δ time (The time in which the turn was performed);
- Δa_xversus Δ time;
- Δa_x versus $\Delta \omega_x$;
- Δa_y versus $\Delta \omega_x$;
- Δa_y versus $\Delta \omega_y$;
- Δa_y versus Δt;
- Δa_z versus $\Delta \omega_z$;
- Δa_z versus Δt;

- $\Delta\omega_x$ versus Δt;
- $\Delta\omega_y$ versus Δt;
- $\Delta\omega_z$ versus Δt;
- Δt versus Δa_x;
- Δt versus Δa_y;
- Δt versus Δa_z;
- Δt versus ω_z;
- Δt versus ω_x;

In the following paragraphs are reported the results obtained with the most significant parameters:

[1] Δa_z versus $\Delta\omega_z$;
[2] Δa_R versus Δt;
[3] Δa_x versus $\Delta\omega_x$;
[4] Δa_y versus $\Delta\omega_x$;

All the parameters analysed with this method were implicit: this means that were obtained thanks to a ration between two physical quantities.

First examples are parameters not useful for the classification: having adopted a Brute-force method, some of the parameters identified have to be rejected. But it is important to report them to show how a parameter can be very useful to the classification aim.

5.3.1 $\mathbf{\Delta a_z}$ versus $\mathbf{\Delta\omega_z}$;

The Figure 5-40 shows the histogram obtained by analysing the implicit parameter $\Delta acc_z/\Delta\omega_z$. This was considered after having observed the nature of the signals. Both the Δacc_z and the $\Delta\omega_z$ are important signals, that correspond, in order, to the variation of the lateral acceleration, and the value of the angular velocity of the trunk bending.

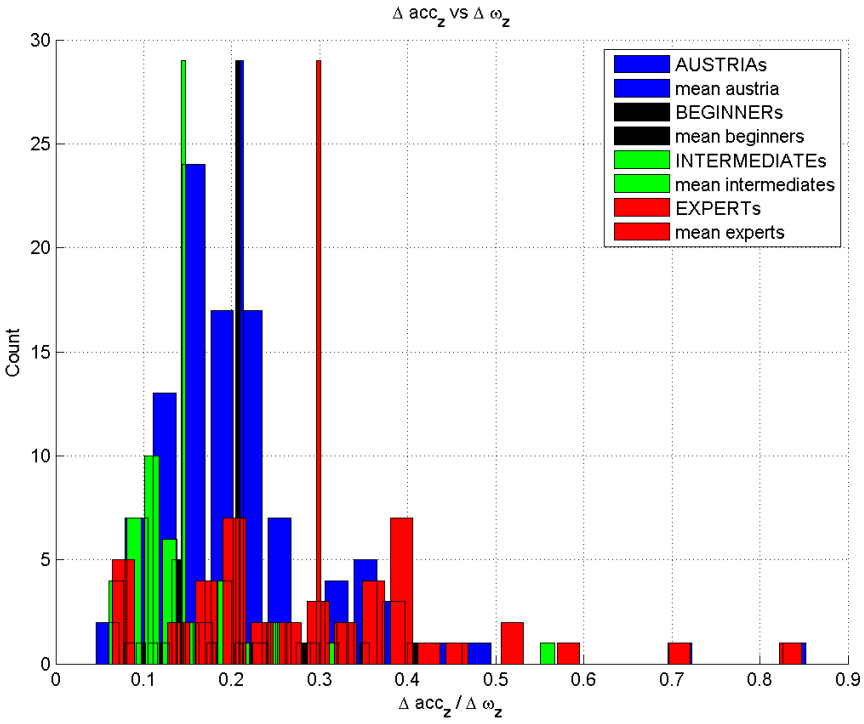

Figure 5-57: Multi level Histogram - $\Delta acc_z/\Delta\omega_z$

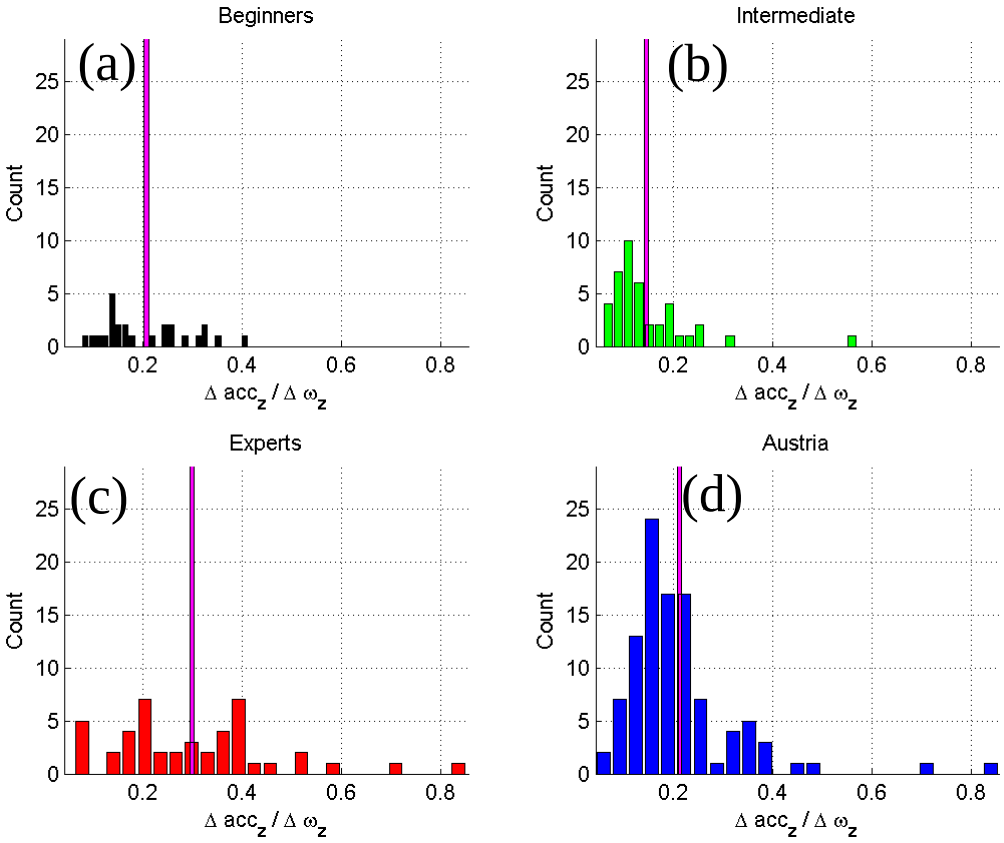

Figure 5-58: Single level Histograms - $\Delta acc_z/\Delta\omega_z$, Beginners (a), Intermediate (b), Expert (c) and Austria (d)

It is possible to observe that the mean value of the intermediate data set is lower than the beginners' one, which is middle way to Intermediate and Expert. This is in contrast to the physical evidence. In addition, the Austria's data set mean overlap perfectly Beginners' mean, which is not realistic because of the presence of both intermediate and expert skiers in Austria's data set. In addition, the expert data set is stretched along all the X axis of the histogram, without a clear disposition. This parameter has been rejected and not considered in the analysis.

5.3.2 Δa_R versus Δt;

Another parameter that has been refused after the histograms analysis, is the ratio between Δacc_{res} and the Δt, where the first parameter was consider as a summary of the turns information, and the second as an index of the time adopted to perform the left-right turns. Unfortunately also this parameter encountered the stretch of the Experts' class along the whole X axis of the histogram.

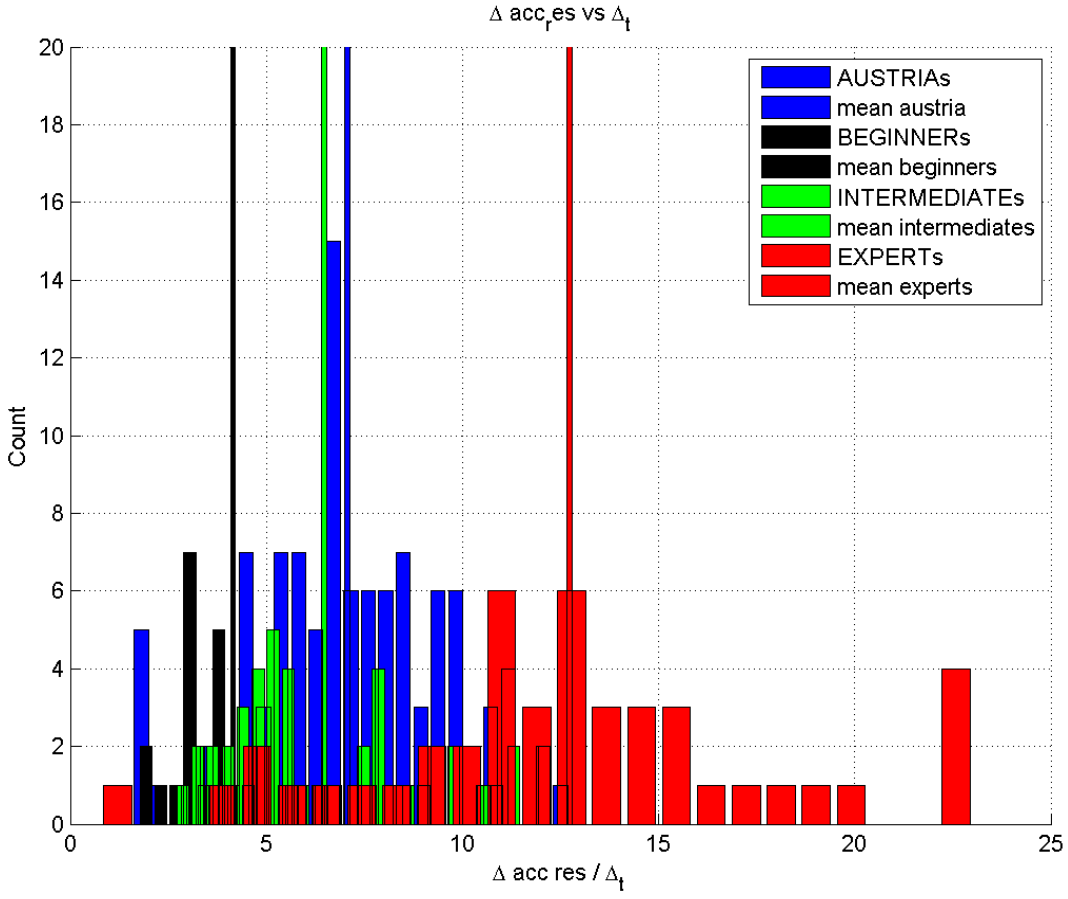

Figura 5-59: Multi level histogram - $\Delta acc_{res}/\Delta t$

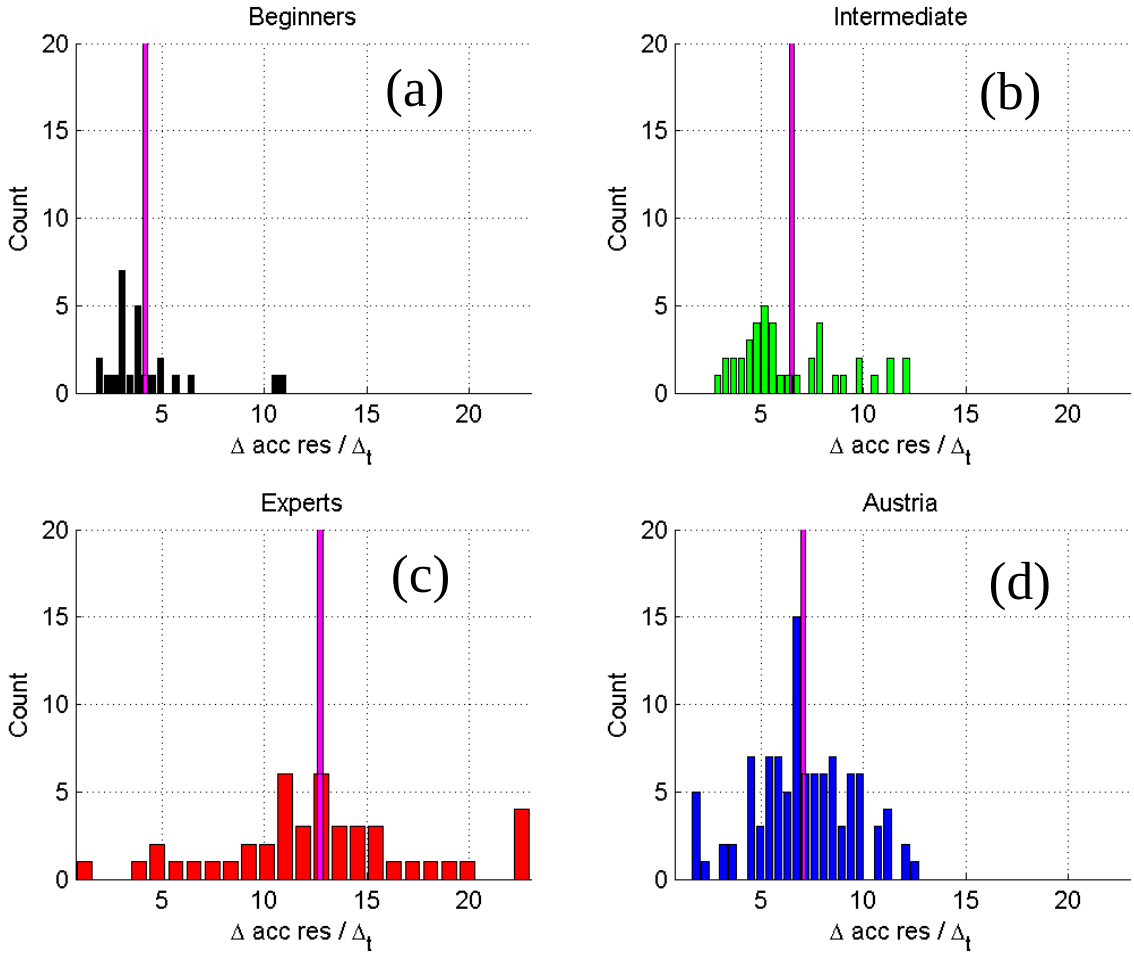

Figure 5-60: single level histograms -$\Delta acc_{res}/\Delta t$, Beginners (a), Intermediate (b), Expert (c), Austria (d).

Even if at first sight this parameter can appear useful, observing the Expert's and Intermediate's data set those parameter have to be rejected because of, once again, the stretch of the values.

5.3.3 Δa_x versus $\Delta\omega_x$;

After having analysed some parameters, the ratio between the delta acceleration along the X axis, and the delta omega about the same axis ($\Delta acc_x/\Delta\omega_x$), was considered. This is one of the parameter which better resolves the different levels. The histograms are reported in the following page, in terms of multi level histogram, where it is possible to compare the four categories together, and in terms of single level histograms.

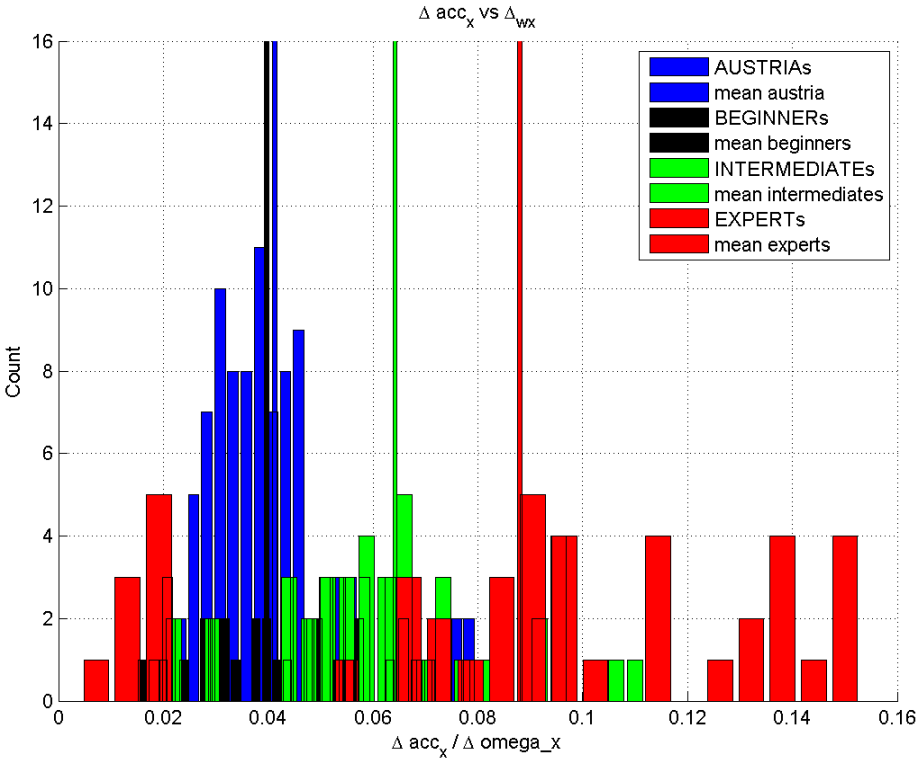

Figure 5-61: Multi level histogram - $\Delta acc_x/\Delta\omega_x$

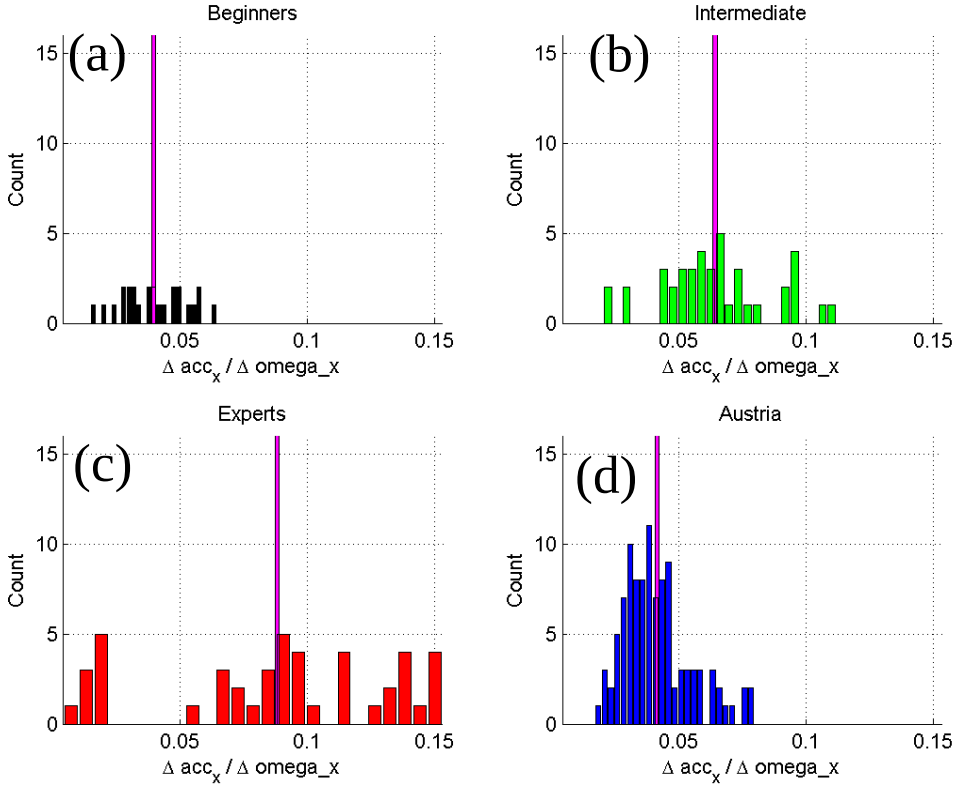

Figure 5-62: Multi level and single level histograms - $\Delta acc_x/\Delta\omega_x$, Beginners (a), Intermediate (b), Expert (c), Austria (d).

The X-axis is an important direction in skiing, because identifies the amount of acceleration in the direction of the slope and the lateral trunk bending velocity. Based on this parameter, the Austria data set should be classified as composed in large part by beginners even if the sensor is placed on the pelvis. This assumption will be confirmed in the subchapter 5.3.1 "Sensor's position comparison".

5.3.4 Δa_y versus $\Delta\omega_x$;

Only one parameter is useful to differentiate the different skiing levels but, to better set up a classifier based on dispersion diagrams, it is very useful to find another similar parameter able to resolve the different levels. This has been found analysing the ratio between the acceleration along the Y axis and the angular velocity about the X axis ($\Delta acc_y/\Delta\omega_y$). Even if this parameter shares the denominator with the previous parameter, the Y axis linear acceleration is very important in skiing and identifies the flexion-extension body movement. A higher accelerations corresponds to a faster movement, common between expert skiers but difficult to perform for beginner skiers.

This parameter is less reliable in respect to the previous one, due to a wider bound in the intermediate and expert categories, the three mean values are well resolved. The Austria data set is in between the Beginner and the Intermediate, shifted near this second one.

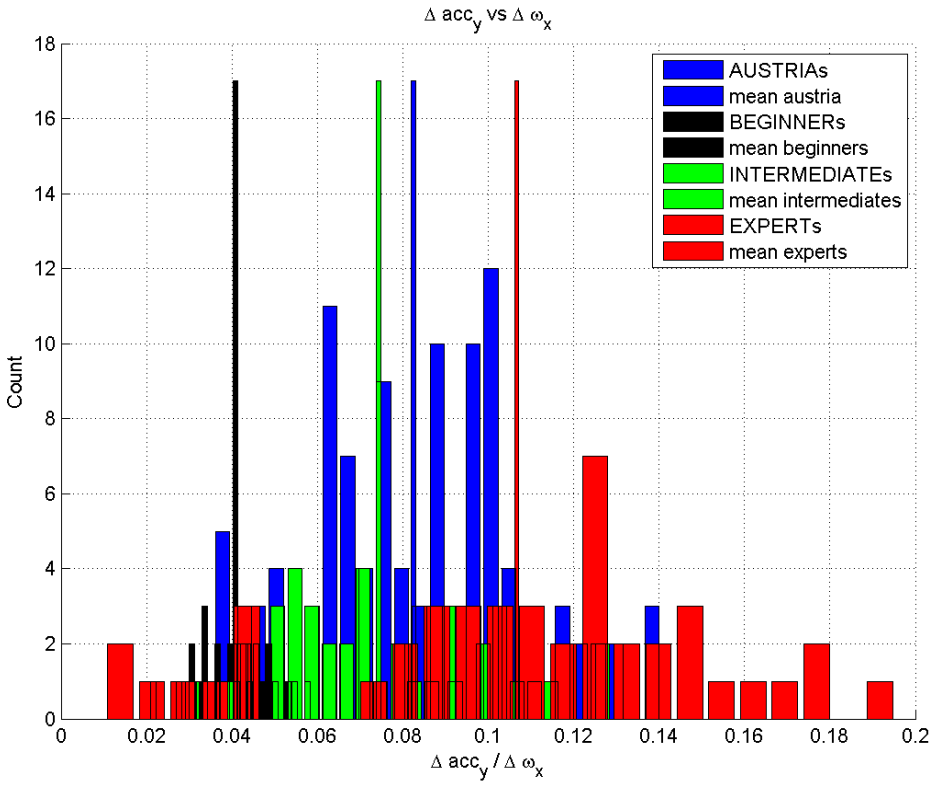

Figure 5-63: Multi level histogram - $\Delta acc_x/\Delta\omega_x$

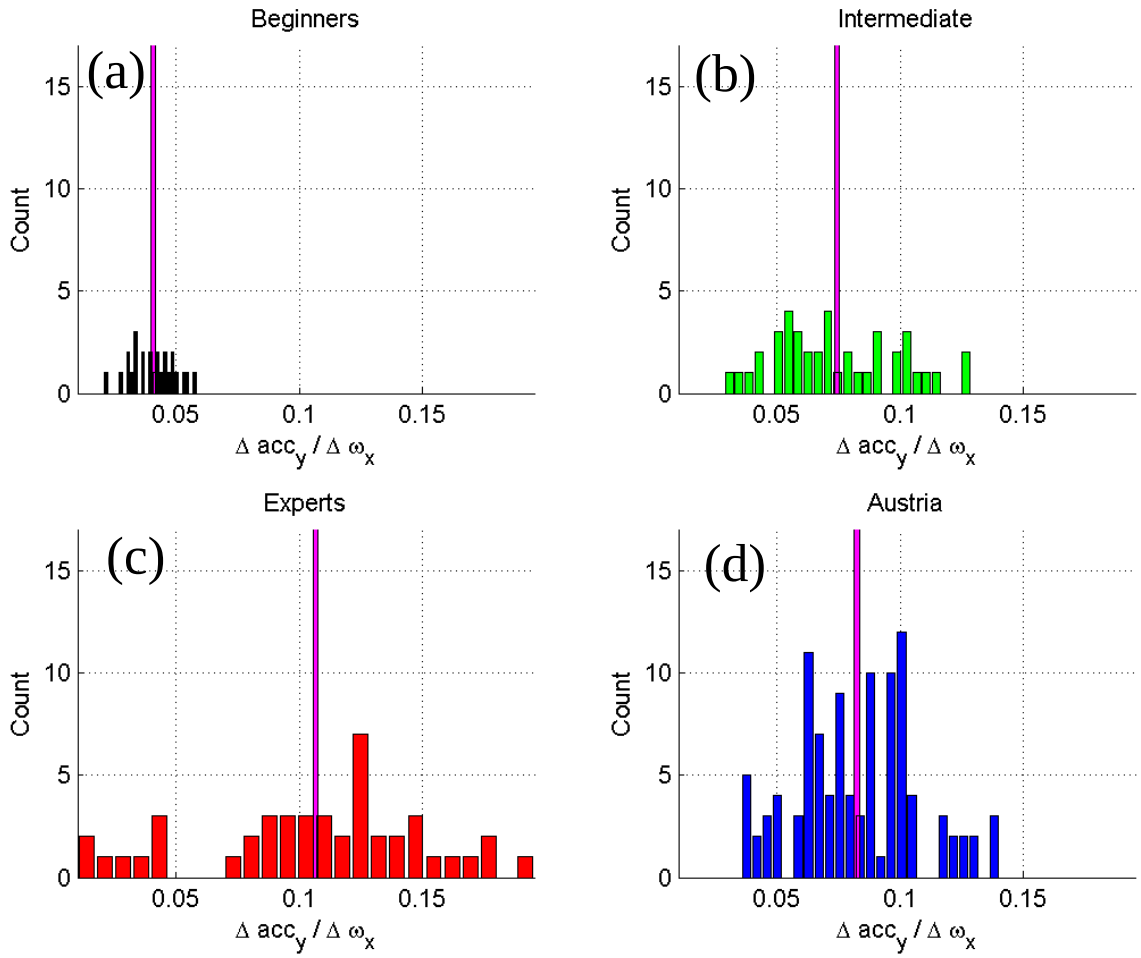

Figure 5-64: Multi level and single level histograms - $\Delta acc_y/\Delta\omega_x$, Beginners (a), Intermediate (b), Expert (c), Austria (d).

Those two parameters were selected as the most reliable and as those that better resolve the three levels in the histograms. This means that is possible now to design a dispersion diagram considering the two parameters: in the abscissa axis was located the $\Delta acc_x/\Delta\omega_x$whereas in the ordered was located $\Delta acc_y/\Delta\omega_y$.

The result is reported in the Figure 5-48 below, where take place also the Austria's data set:

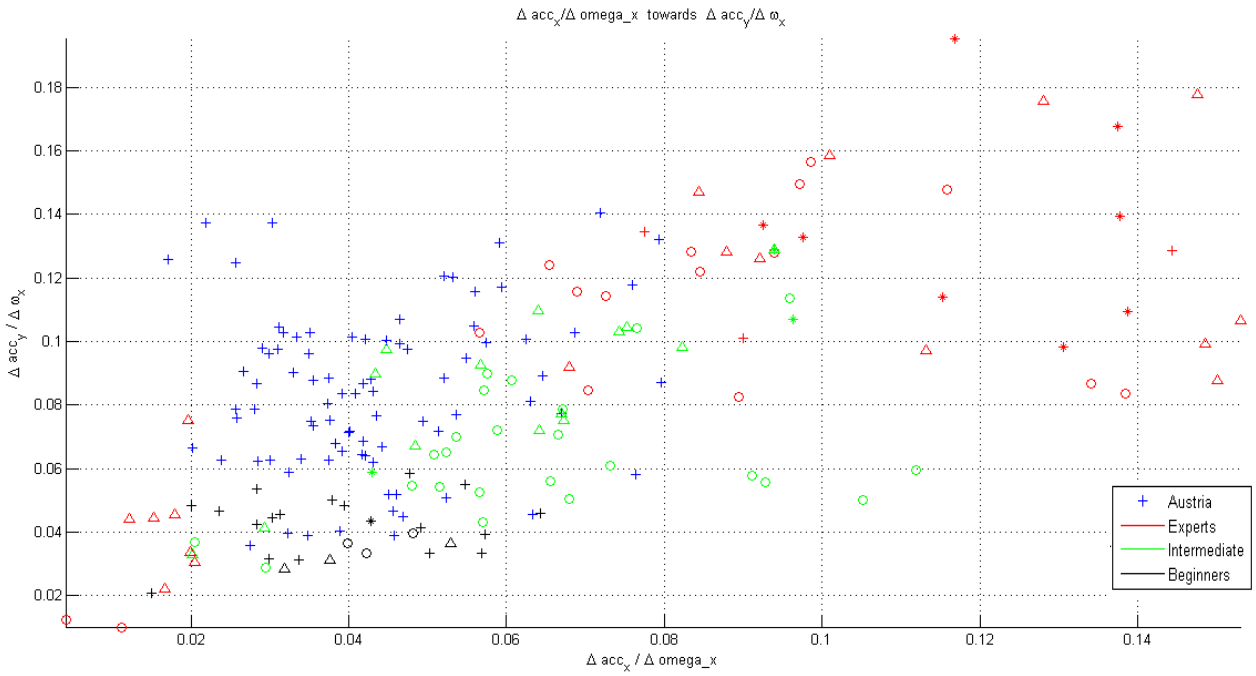

Figure 5-65: Dispersion diagram: $\Delta acc_y/\Delta\omega_x$ *towards* $\Delta acc_x/\Delta\omega_x$

Dispersion diagram in figure 5-48 is obtained by plotting the mean cyclogram obtained by the conventional averaging of the five couples of turns. The outliners in the bottom left are referred to the same skier and probably are due to a measurement error. The averaging cyclograms are useful to have a general idea but do not give a statistical value to the result. We decided instead to use the data sets in terms of single couple of turns.

Then the mean value of each data set was calculated and plotted in the dispersion diagram. Also the standard deviation was inserted, in terms of ellipsis about the mean value of the data set. This was possible thanks a Matlab script. The standard deviation was multiplied for a K factor (K=1, 2, 3).

Reminding the Chebicev's inequality, considering each point in the diagram as a realization of a random variable, we outstand that $P = (m - K * SD < x < m + K * SD) = 1 - {}^{1}/_{K^2}$;

Considering K=2, the probability that a realization of the RV is in a circle centred in the mean of the RV with a radius of two times the standard deviation is 0.75.

The figures 5-49, 5-50 show those dispersion diagram:

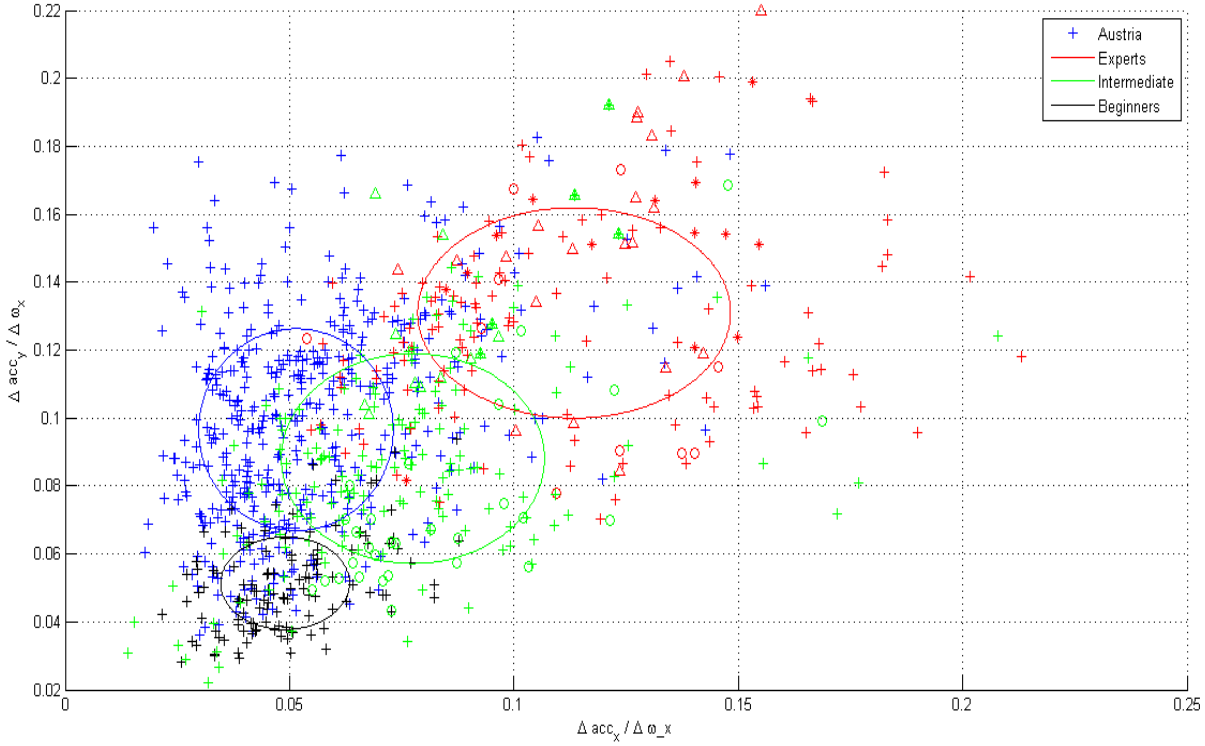

Figure 5-66: Dispersion diagram - K=1

Figure 5-49 refers to a dispersion diagram where the ellipsis are index of the standard deviation of the RV, calculated both in the abscissa and ordinate axes.

Plotting the dispersion diagram with the SD multiplied for K=2 gives the picture 5-50:

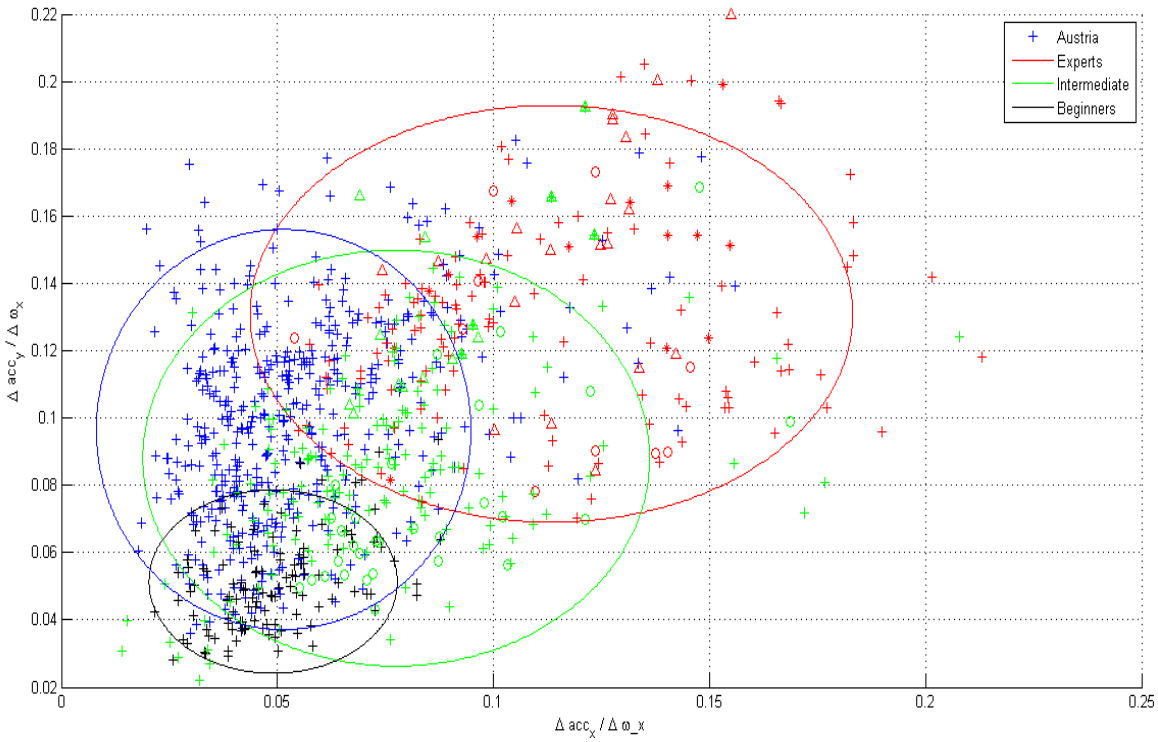

Figure 5-67: Dipersion diagram - K=2

In the dispersion diagram we can see a significant difference between the Austria's data set disposition and the other ones. Further analysis have confirmed this difference is due to the different position of the Humotion sensor. In fact, whereas in the Italians' tests it was placed over the back protector, in the upper part of the trunk, in the Austria's tests it was placed over the pelvis.

In those picture we can see an incremental trend towards the ascending X and Y axes, on the bisecting of the first dial. The beginners are in the bottom left of the dial, whereas the Expert skiers are in the opposite section of it.

To better evidence this trend, we removed Austria's data set because of the different sensor position. The Italia's data set was re-analysed in order to observe the differences between the three levels. To perform this selection, we calculated the mean value of the groups, and the standard deviation (SD) of each. The SD has been calculates both in the X and Y axes.

Then a linear interpolation within the extremes of the mean with its SD in the two axes was performed.

In the picture below are reported the results of the linear interpolation using the three means with the addition and subtraction of the SD in the X axis as passing points.

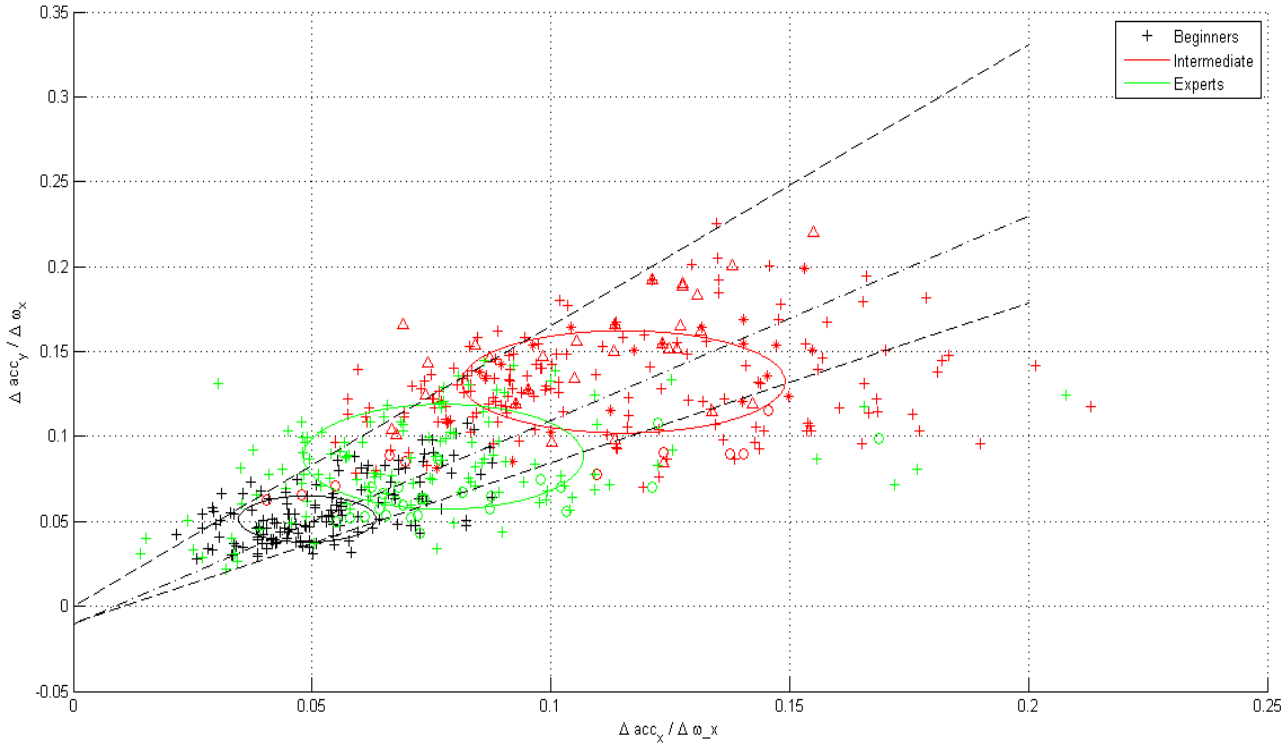

Figure 5-68: Dispersion diagrams with X-axis SD linear interpolation

In the following picture, the same process has been done for the three means and the SD in the Y axis.

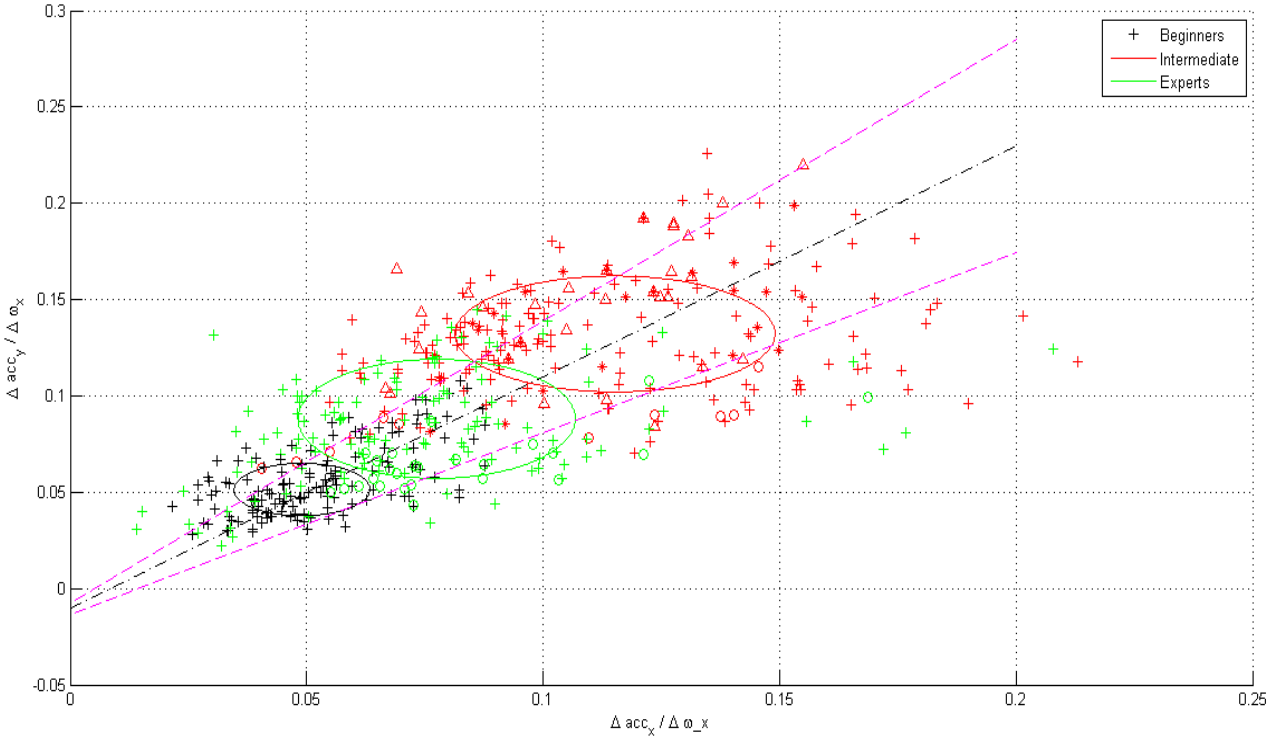

Figure 5-69: Dispersion diagram with Y-axis SD linear interpolation

5.3.5 Sensor's position comparison

A comparison between the two positions (C7 and pelvis) has been done. The Italian tester AS, an expert skier, wore an Humotion sensor over the back protector at the C7 level and another identical Humotion sensor over a belt placed in the pelvis.

The result are reported in the picture 5-37 and show clearly that the turns collected with the upper sensor are displaced in the top right part of the diagram, with high X and Y axis parameters values. Instead, the turns collected with the sensor placed over the pelvis, are located in the bottom-left part of the graph. Furthermore, a comparison between all the turns collected with the pelvis sensor (Both in Italy and Austria in field tests) has been done. The results are reported in the figure 5-53:

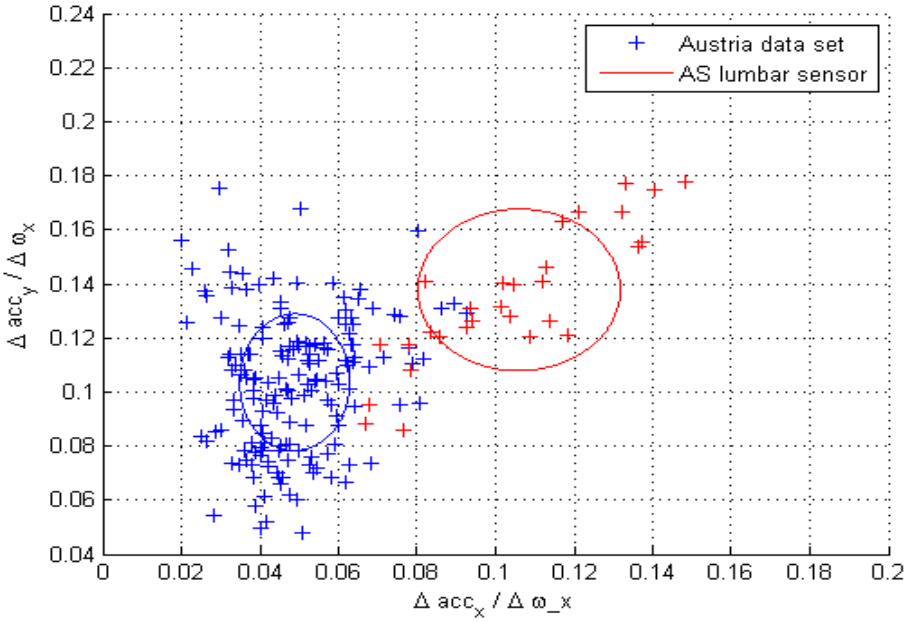

Figure 5-70: Comparison between c7 and pelvis position

As notable, the two data set have s strictly different mean and are well resolved. They also show a growing trend as noticed with the sensors placed at the C7 level. The prior classification of the Austria's data set would classify those skiers as intermediate.

In I2 test session, one skier adopted two sensors:

- Humotion over back protector, C7 level.
- Humotion over a belt, Pelvis level.

The comparison has been done considering turns in the same runs. It was not possible to analyse the same set of turns for both the sensors due to dynamic vibrations that made impossible to extrapolate the same turns.

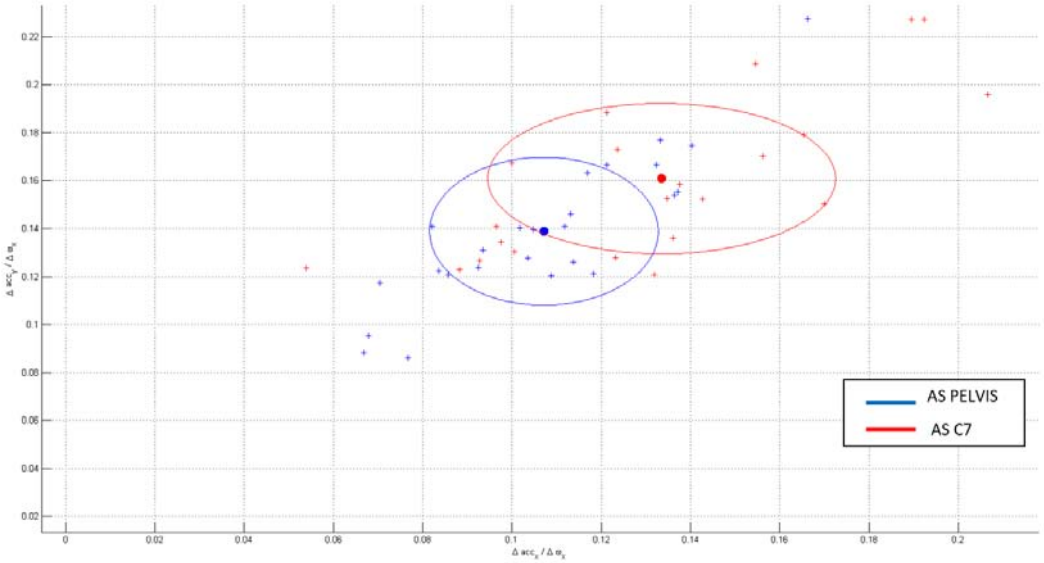

Figure 5-71: AS (Expert) Pelvis vs C7

In Figure 5-54, it is possible to observe that values obtained by pelvis sensor are shifted to the low-right part of the diagram in respect to C7 sensor. This comparison has been done on the only skier who wore two sensor. For future analysis, a largest numerosity should be considered.

A further analysis has been done, considering the Austria's experts data: seven more skiers were placed under investigation. Only six of them were considered for the dispersion diagrams analysis. In fact, a problem on the files of the Humotion nr 5, resulted in a strongly corrupted parameters. It was removed from the analysis until the problem will be solved.

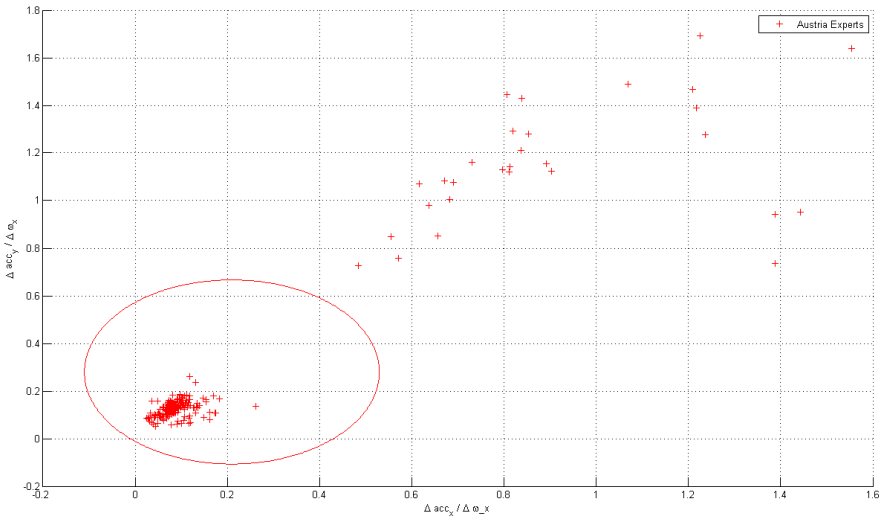

Figure 5-72: Corrupted values in the upper-right part of the diagram

Using the Matlab routine as in the previous analysis, to understand the problem source. The Austria data set was analysed and a label has been applied to each point, indicating the Humotion numbers related to the points:

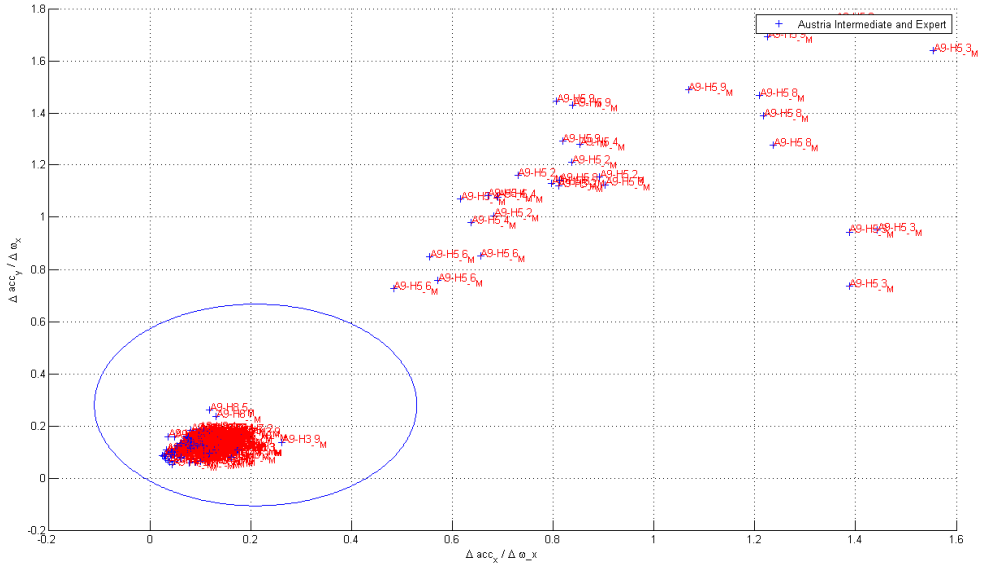

Figure 5-73: The labels applied to the points show the corruption of H5 data

Having the labels. It is clear the error is generated by only the Humotion number 5. The data collected by this sensor were removed from the analysis.

After having removed the corrupted data, the Austria data set was analysed, in order to find differences between the Experts and the Intermediates. Having some notes from the Salzburg University, it was possible to understand the skiers rated as intermediate and as expert. Unfortunately, the beginners are too much shifted towards the intermediate level, and have to be considered a single class.

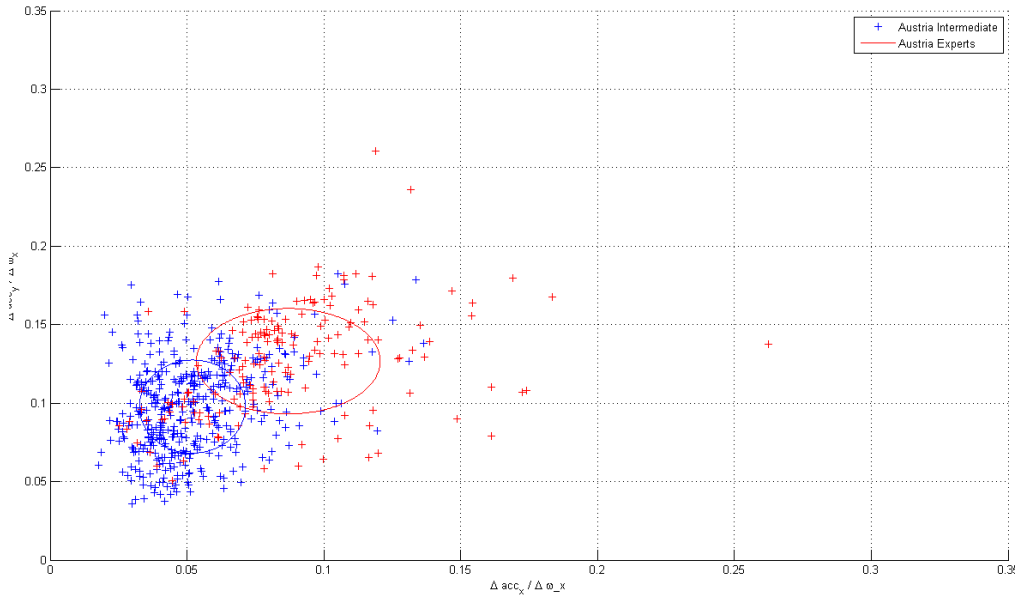

Figure 5-74: Austria data set, dispersion diagram

In the pictures5-56, the dispersion diagram of all the Austria's data has been reported.

It is possible to observe that, even with some outliners, there is a cluster between the intermediate and the experts. The experts' turns in the intermediate area, are performed by the skier with the Humotion number 4. It is possible that he is not a real expert skier or he adopted a relaxed skiing technique in those turns.

The last dispersion diagram, showed below, summarizes the observation made since now. Considering both the Austria and Italian data sets, we can set up a diagram consisting in the three levels of the Italian in field tests and the two levels of Austria in field test. Plotting those sets, with their own mean and standard deviation ellipsis, and interpolating the X-axis mean with the X-axis standard deviation to enhance the growing trend, the following diagram is obtained:

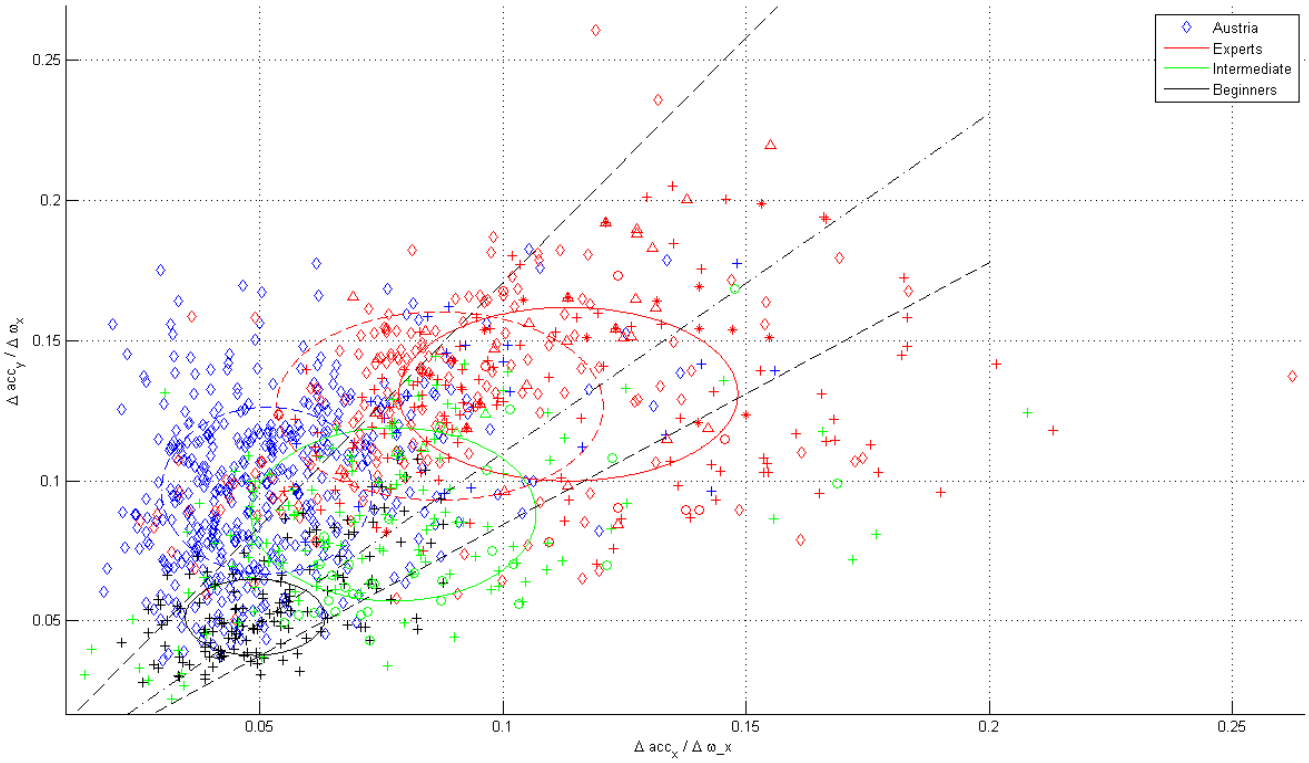

Figure 5-75: Dispersion diagrams with X-axis SD linear interpolation and Austria data set

The Austria's Intermediate and Experts ellipsis are draw with dotted lines to differentiate from Italia's. Even in the Austria's data the growing trend observed with the Italia's data is maintained.

5.4 Classification

Having collected a large set of turns for different skiing levels, it is important to elaborate a way to classify further unknown data. Different type of classifier differs by terms of shape and boundary conditions. In the following are presented some ideas behind this problem. Their feasibility will be discussed later.

5.4.1 Bounded Classifier

Using a classical approach to the classification problem, it is possible to establish ellipsis to classify skiers. Adopting ellipsis with one fulcrum in the origin of abscissa and ordered axes, levels can be assumed as build of three ellipsis with one fulcrum in the origin: it is possible to associate the levels to elliptical sectors delimitated by Cartesian axes. The result will be a classification based on quarter of ellipsis. Each ellipsis marks the superior limits for the each class. The portion of the black ellipsis is a superior limit for beginner's class. The skier are classified as intermediate if their points belongs to the area between the black and the green ellipsis. The expert are located between the green and the red ellipsis. The Austria's skiers are in this way classified in large part as intermediate, with the presence of beginner skiers and expert skiers.

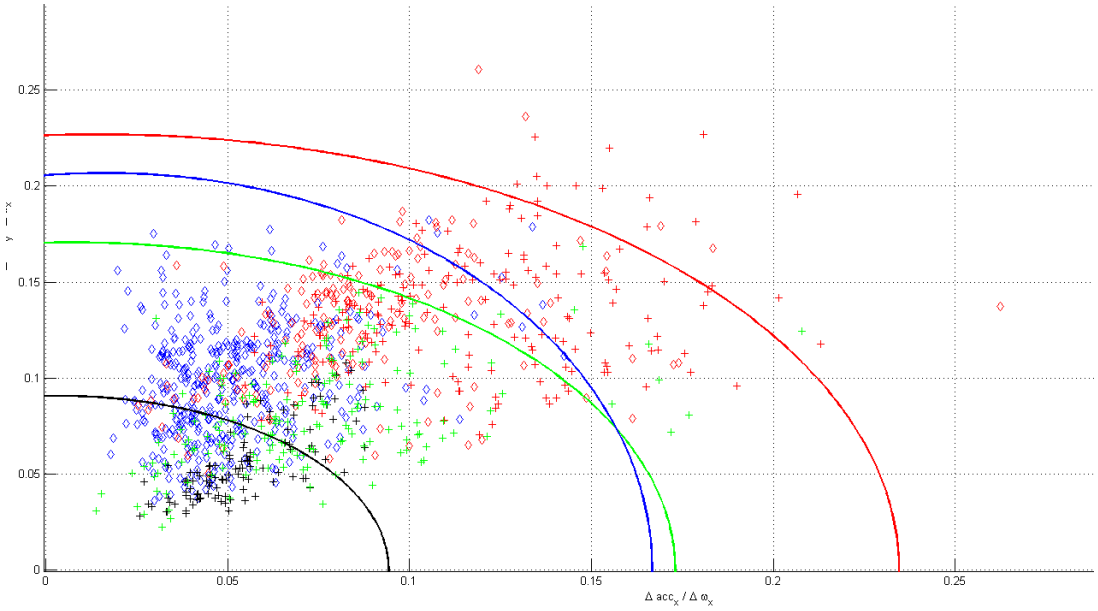

Figure 5-76: Ellipsis classifier

Ellipsis have been calculated [Figure 5-76] considering a fulcrum in the origin. (In this case, as the main semiaxis is parallel to the X-axis, the right fulcrum was bonded to origin) Then the semiaxes length have been calculated considering the mean value of each class plus three times the standard deviation, both in x and y axis.

5.4.2 **Floating Classifier**

Another way to classify the turns tries to set threshold based on the mean values and both the standard deviations for each level. Using the given SDs of each class, we can try to classify the levels observing the ellipsis in which the turns belongs.

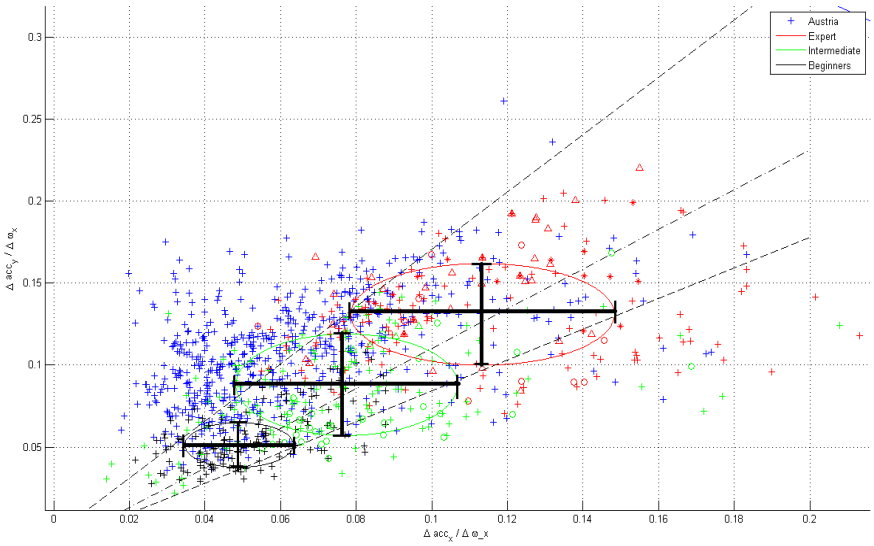

Figure 5-77: Floating classifier, considering ellipsis

This method is very useful when the levels are not dispersed, otherwise could lead easily to errors. In this case, levels are well resolved, even if some outliners are present on lateral classes' boundaries.

The performance analysis in the first part of this thesis reports methods to obtain skiers' levels using a single IMU unit placed on the back, over a back protector. Further study, with higher numerosity, would validate parameters selections. Having resolved the levels issues, it is possible to look into skiing safety. Next chapters will threat safety analysis in skiing, proposing fall's analysis-oriented methods.

Chapter 6: Safety analysis in skiing

6.1 Safety problems in skiing

Skiing is a popular sport discipline and its attraction is spreading through younger people. Safety in the slopes is becoming an important issue for disseminating the sport among beginners and ensuring a safe skiing to amateurs and athletes [Petrone et al.,2010]. Most common causes of injuries are personal falls during slalom and collisions with other skiers or snowboarders: collision with fixed obstacles are rare, but can lead to severe injuries and are important during competitions, were high speeds are sustained on icy slopes.

Even if recreational skiers usually reach low speeds in comparison to racer, falls are still dangerous. In fact, many ligament rupture and bone fractures can occur in ski falls. Falls prevention has always been a key factor in skiing, and new materials were introduced. Shorter skies (with less leverage on the knee in torsions) and carved shapes helped skier to perform turns more safely, without even reach high speeds due to the skis conformations. Longer and stable skis are fundamental to reach high speeds and are commonly used only by racers in training slopes. Recreational skiers, in addition, tend to use bindings tuned on a lower weight to get an easier release and avoid knee ligament ruptures. In competition's world things are different. High speed are reached easily. It is common to see velocities above the 100 km/h, and jumps over 40m in length. To perform turns and jumps at those speeds, strongly closed bindings are needed. The risk of falls is higher, due to very icy slopes. In the case of falls, risk of injuries is very high; even in a special slalom competition, a forked pole can be dangerous for muscles and ligaments, because of the high effort required. If muscles and ligaments injuries are hardly evitable, and can only be prevented thanks to materials, bone fracture, especially spine

fractures, can be reduced by passive protecting devices. The utilization of rigid back protectors dissipates the impact energy, distributes load on wider surfaces and prevents high damage injuries. If in addition to the rigid back protector it would be possible to apply to the skier an airbag protecting device, the risk of high injuries would be reduced.

Inspired to the motorcycles airbags, severe manufacturers developed the ski protecting device. The D-air Ski, for instance, has been created thanks to the FIS – Dainese protocol of intent on the basis of the D-air project. [A.Marega, 2015]. The hardware includes 3 gyroscopes, 3 accelerometers and a GPS. Those sensors continuously perform the algorithm on the data measured on the athlete's dynamics. Once data reach a predefined threshold level, indicating an incipient fall, the Airbag inflates in a 50ms time, protecting back trunk, shoulders and the upper front portion of the trunk. In 2014 in Kitzbuehel, during a joint press conference organised by Dainese in collaboration with FIS, the D-air Ski device was officially presented to the public. The project is a result of a cooperation agreement signed between the two parties in January 2011. "More than three years have passed since we approached Dainese regarding a possible cooperation in developing an airbag system for alpine ski racers. We have worked hard on this project. The most difficult aspects was defining the algorithm and finding the exact moment when an athlete is no longer in control and able to handle the situation", FIS chief director for the men's World Cup, Guenter Hujara explained. Dainese presented a first prototype in 2012. The first functioning D-air Ski was seen at the Val Gardena races and tested by Werner Hell (ITA), Jan Hudec (CAN), Manuel Osborne Paradis (CAN) and other skiers from the Austrian and French Ski Associations. During the press conference, Italian speed specialist Werner Hell demonstrated the inflation of the system and said: "When the protection inflates you can't feel anything, we just need to adapt the suits to the shape of the protection but this is a huge step forwards in terms of safety" [www.fis-ski.com].

Figure 6-1: Dainese's D-air Ski system

Starting from this viewpoint, in the second part of this thesis work, the focus will be on the experimental setups with the aim at inserting the ski airbag in the recreational skiers' framework. The ski airbag as it is, now suits perfectly to ski racers, but is totally unadapt for normal skiers. Velocities, accelerations and actions given in input to airbag are at the highest levels possible. To convert this technology into a lower inputs level, other algorithms are necessary. To elaborate them, several different tests have to be performed. The ski airbag is a result of over five year's project. In this thesis,

the tests performed, the results obtained thanks to data collection and analysis, and suggestion on how to continue the work in order to obtain a product at his best will be presented.

6.2 Analysis of falls

The development of an air-bag system can only be done analysing dangerous falls situation in which the device could be useful. This can't be performed easily by theoretical analysis but it should pass through I field tests. Obviously it is not acceptable to ask tester to fall at high speeds risking bone or ligament ruptures. The study must be performed adopting other equivalent and safe methodologies. To obtain valid data from safe tests, three different methodologies were analysed:

[1] Real simulated falls

[2] Rollerskating simulated falls

[3] Dummy falls

6.2.1 Real simulated falls

First method considered simulated falls performed voluntarily by an expert skier or ski instructor wearing a Humotion sensor over a back protector. This was made in low-steepness slopes, at low speed and under controlled conditions, without other skiers around. Only an expert skiers performed this type of falls, but the low speed and the controlled condition didn't gave the permission to consider this type of fall as a fully valid simulation of a real fall.

Figure 6-2: Simulated real fall

Anyway, data captured during this falls were analysed thanks to a Matlab software. Having low speeds, the accelerations were not significant, so angular velocities were mostly analysed. The Matlab software lead to the picture 6-2:

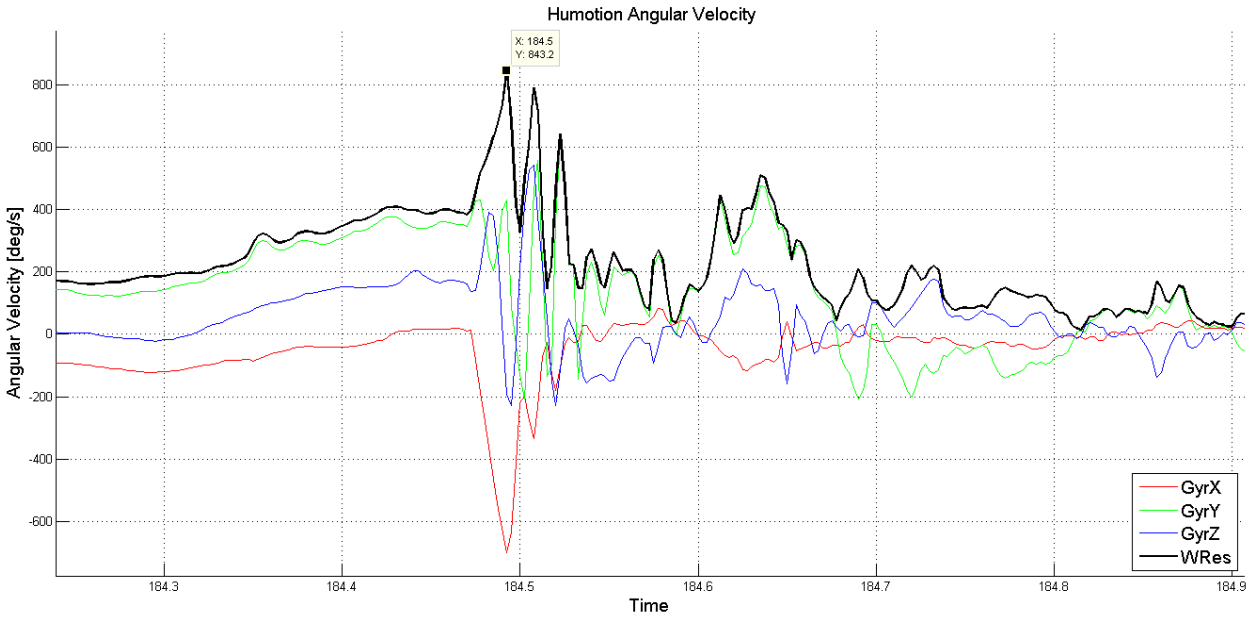

Figure 6-3: Example of Human fall's signal

By this analysis we can see an incremental trend in angular velocities Y and Z axis. The most important observation in this simulated fall is how the resultant angular velocity can be considered as a representative quantity of the fall. It is not fundamental the single channel's signal, but to understand the whole fall's dynamic, it is important to consider this parameter.

This idea was strongly considered for the subsequent methodologies. The infield tests indicated also a nomenclature for the falls' type.

According to the skiing dynamic and considering the analogies to the motorcycling world, we identified different fall's types:

- Back Side fall;
- Front Side fall
- Low Side fall;
- High Side fall;
- Unadverted Release
- Phantom Foot

The back side fall generally happens after a jump, when the skier unbalances and risks to impact the ground with its back.

Figure 6-4: Back Side fall example

The front side fall occurs when the skier impacts on an obstacle, which can be a snowdrift or another skier. Even a jump can lead to a front side fall.

Figure 6-5: Example of Front Side fall

The low side fall is the more common type of fall. Generally occurs during a turn or in steepest slopes. In high-end skiers occurs when the external boot touches with its inner part the snow or the edging angle is so high that the snow cannot sustain the pressure. It is common to see such a fall in special slalom competition. Generally it do not lead directly to injuries, but high speed and icy slopes produce a long sliding phase where the skier is not able to control himself. As consequence the skier impacts on safety nets or even other skiers, possibly supporting injuries.

Figura 6-6: Example of Low Side fall during a special slalom race

High side falls are the most dangerous in terms of leg injuries. They happen either when the external ski takes contact on the snow with the external part instead of the inner one or when the skier impacts on an obstacle blocking its legs and making the body going downwards. At highest speeds leads to long rolling and sliding phase on the slope.

Figure 6-7: Example of a high side fall during an Olympic downhill race

Phantom foot is a common type of fall that, especially in beginner skiers, leads to acl injuries. [www.pressherald.com]. It happens after a skier has fallen backward or when they are trying to get up while still moving after having fallen to the rear. The skier's hip falls below the knees and the uphill ski becomes unweight. All of the weight is transferred onto the tail of the downhill ski. Often the ACL gives way at this point.

Figure 6-8: schematic representation of a phantom foot fall

The last type of fall presented occurs when the pressure on the ski binding exceeds the imposed bind limit. The ski releases and the skiers in in an uncomfortable situation. Greatest skiers are able to face this situation by skiing on a single ski (i.e. Bode Miller during Bormio 2005 world cup combined downhill), but generally the fall is assured. In less expert skier this can lead to bone fracture.

Figure 6-9: Example of an unadverted release

6.2.2 Roller skating simulated falls

The second fall's analysis method consisted in performing simulated falls not on ski but on roller skates. The dynamics of a roller skating segment can be addressed as a simulation of skiing. This analysis was performed at Salzburg University. The tester, wearing knee and back protectors, and helmet performed a short track skating with low steepness. At the end of it a 50 cm tall mattress was placed. The tester, after having reached a good speed, impacted on a small sandbag with the rollers and felt over it. The protecting devices makes the trial completely safe, without risk of injuries. A Humotion sensor was placed over a back protector in pelvis position. In addition, other types of fall were analysed: the tester, wearing the Humotion at pelvis position, was standing on the mattress and placed its foot over a thin mat. Two people pull away the mat at an extremity and the tester felt over the mattress. The first type of falls simulates a forward-fall:

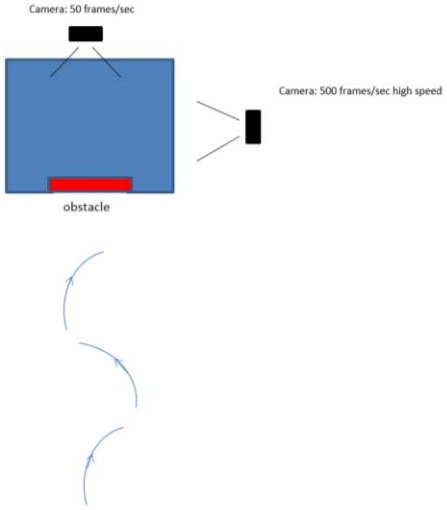

Figure 6-10: Forward fall

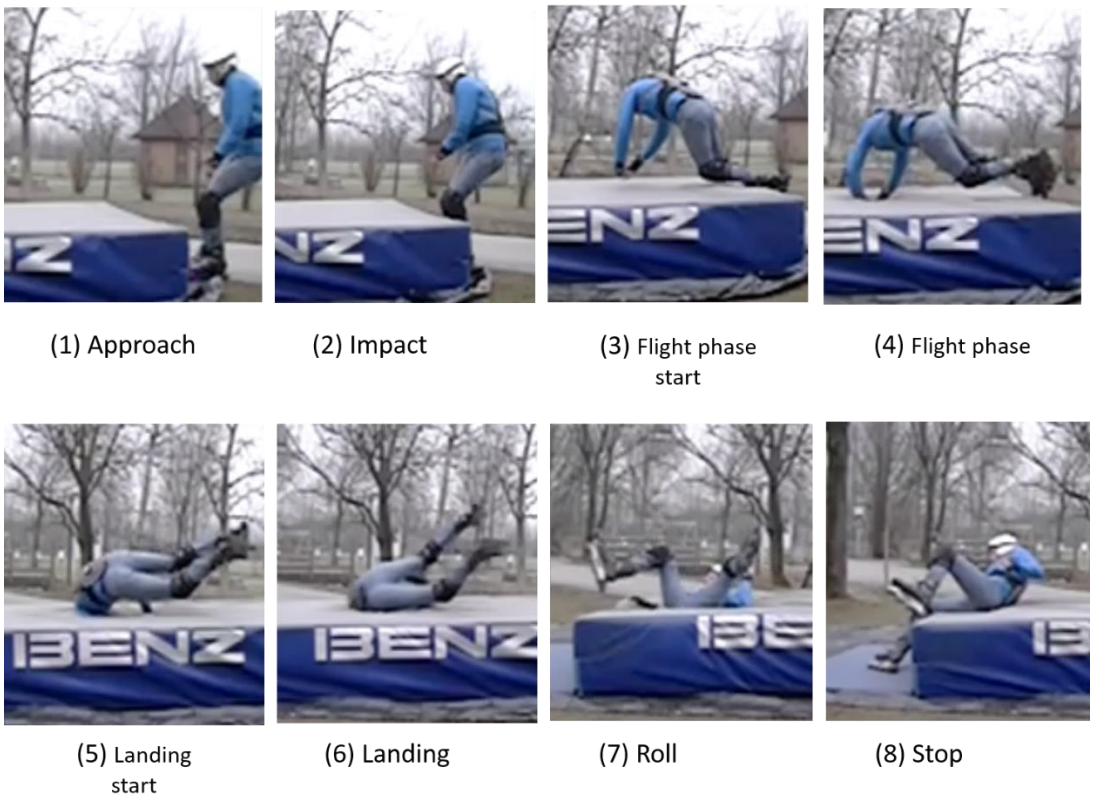

Figure 6-11: Frameset of a forward fall

The falls with the mat are to simulate backward and Lateral falls:

Figure 6-16-2: Backward fall (left) and Lateral fall (right)

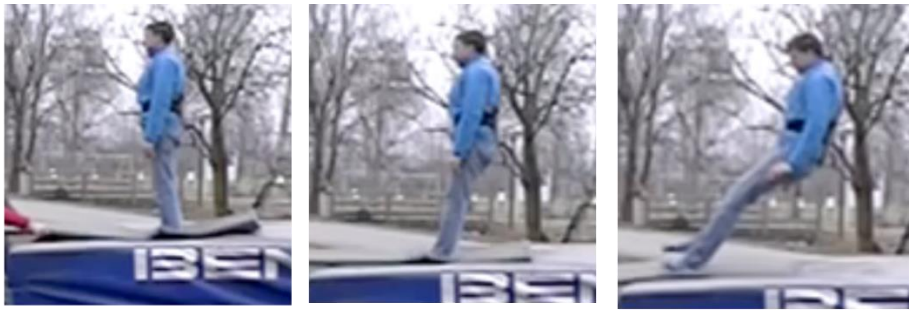

(1) Standing (2) Fall start (3) Middle fall

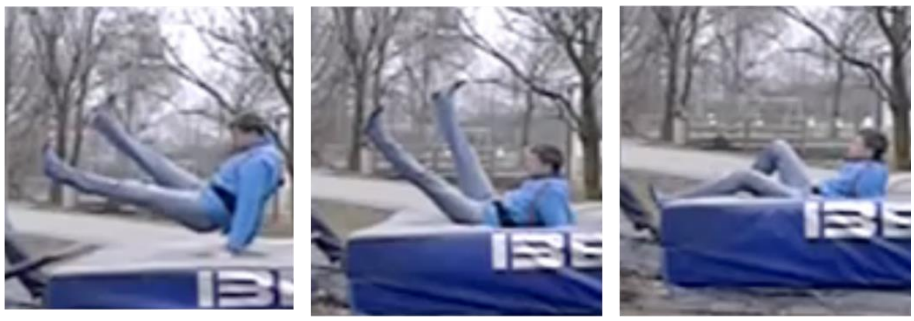

(4) Unbalancement (5) Mattress impact (6) End

Figure 6-13: Frameset of a Backward fall

(1) Standing (2) Fall start (3) Middle fall

(4) Unbalancement (5) Mattress impact (6) End

Figure 6-14: Frameset of a lateral side fall

The IMU sensor was placed over a back protector. All the three type of falls were performed with the sensor placed at the C7 level and over the pelvis.

The four tester of this session at the start off the rump had to flex their trunk (3 times) to the front, followed by stamping 3 times with one foot on the ground. This was filmed by a camera afterwards the camera was turned to the obstacle.

In the test session were performed:

- 3 forward falls during skating with IMU placed over pelvis;
- 3 forward falls during skating with IMU at C7 level;
- 2 backward falls during standing with IMU at C7 level;
- 2 lateral-falls during standing with IMU at C7 level;
- 2 backward falls during standing with IMU placed over pelvis;
- 2 lateral falls during standing with IMU placed over pelvis;

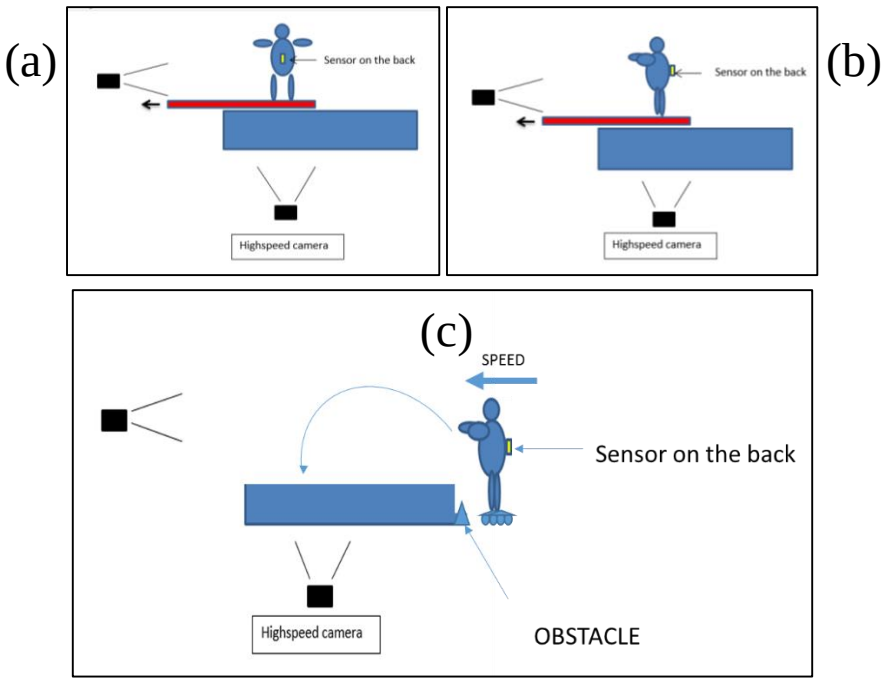

Figure 6-15: Camera positions on lateral falls (a), on backward falls (b) and on a frontal fall (c)

For each fall, the Humotion's data were analysed via Matlab, focusing on important events. For each run several point values of the resultant signals were collected.

Falls have been divided into three main phases:

- Collision: the skier impacts with an obstacle which triggers the fall;
- Flight: the skier loses ground contact
- Landing: Final phase of the fall, when the skier hit the ground.

The maximum value of the resultant angular velocity during both collision and flight phases and then during landing phases were taken, as well as the maximum value of the resultant linear acceleration. The data were stored in a database which contains:

- Run number
- Subject ID
- Fall type in Italian convention
    - HS_R: High side fall, on rollerblades
    - BW_M: Backward fall, over mattress
    - LS_M: Lateral Side fall, over mattress
- Fall type in Austria convention
    - FWF: Forward fall
    - BWF: Backward fall
    - LSF: Lateral Side fall
- Sensor position
- Significant value of $\omega_{res\_collision}$
- Significant value of $acc_{res\_collision}$
- Maximum value of ω_{res_fligth}
- Maximum value of acc_{res_fligth}
- Maximum value of $\omega_{res\_landing}$
- Maximum value of $acc_{res\_landing}$

In the picture 6-16, is reported an example of a forward fall of the subject GS with the sensor placed at C7 level.

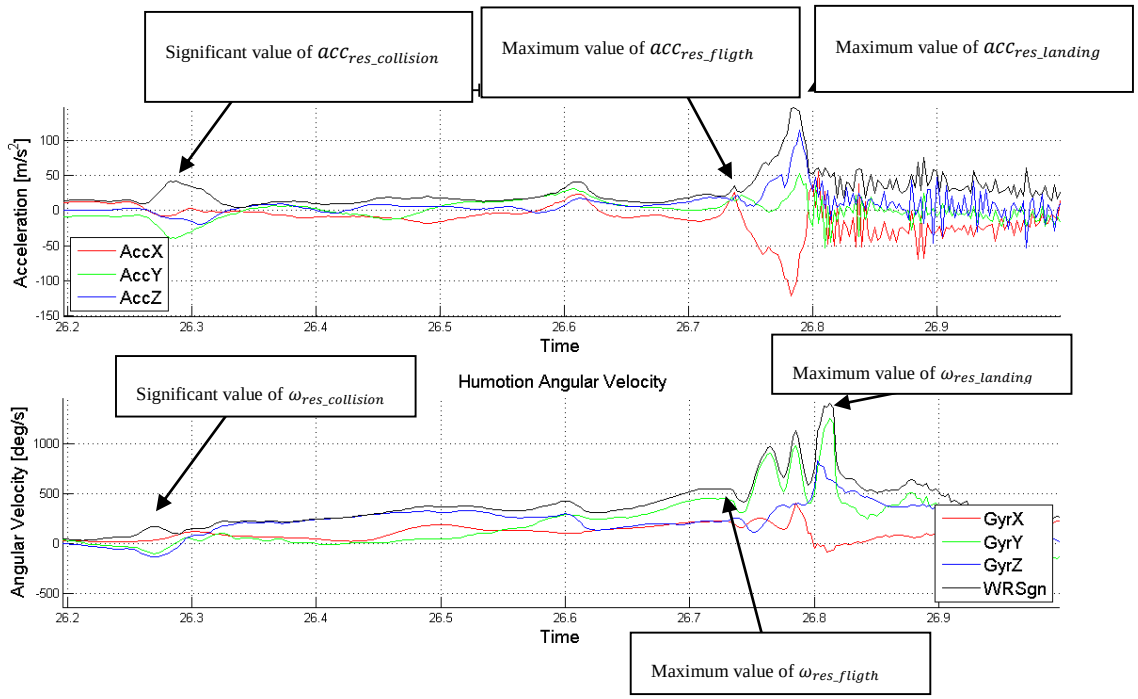

Figure 6-16: GS forward fall, sensor at C7

As the figure 6-4, the significant value of $acc_{res\_collision}$ and $\omega_{res\_collision}$ is the first notable value in the fall. It is usually due to the fall initiation trigger. Then a growing angular velocities phase starts, corresponding to almost stationary accelerations. The ω reach a maximum value of about 500 deg/s just before a small drop and an instantaneous raise due to the impact with the mattress. The accelerations during the fall reach a peak of about $150 m/s^2$, due to the X and Z axis acceleration.

The backward falls tries to simulate a trunk imbalance of the skier, which reaches the ground with its back. In the following a visual comparison between the simulated fall in controlled safety condition and the Daniel Albrecht's fall during the Kitzbuhel 2009 downhill in the final Zielschuss jump (www.hahnenkamm.com/downhill-streif.html) (29).

Figure 6-17: Simulated backward fall (left) - Real backward fall, Daniel Albrecht, Kitzbuhel 2009 (rigth)

The following picture, 6-18, shows data recorded by Humotion sensor during the backward fall:

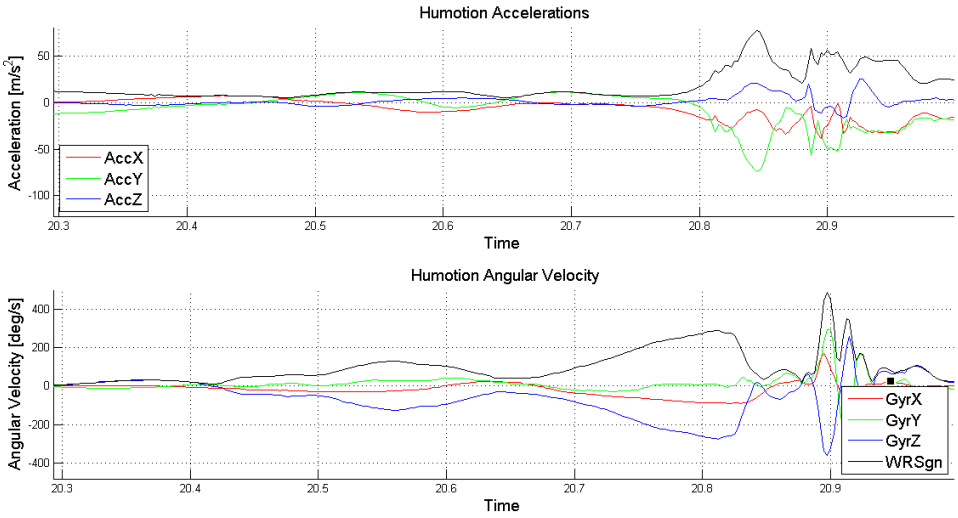

Figure 6-18: Backward fall - sensor at C7 level, Fall 7,GS

It is possible to observe that, in absence of an impact with an obstacle, the signals have a growing trend without significant peaks during the flight. The accelerations have an almost flat dynamics, even if it is noticeable an inversion of the signs in the X and Y axes, due to the trunk backward rotation. In the resultant angular velocity, the highest value is just before the landing, during which it reaches a value of 490deg/s.

The lateral fall, on the other hand, has a similar trend, with the exception of an initial maximum in the angular velocity channels. The resultant angular velocity grows up to a maximum value of almost 380 deg/s, then lowers to 200 deg/s and the in the impact instant reaches 600 deg/s [Figure 6-7].

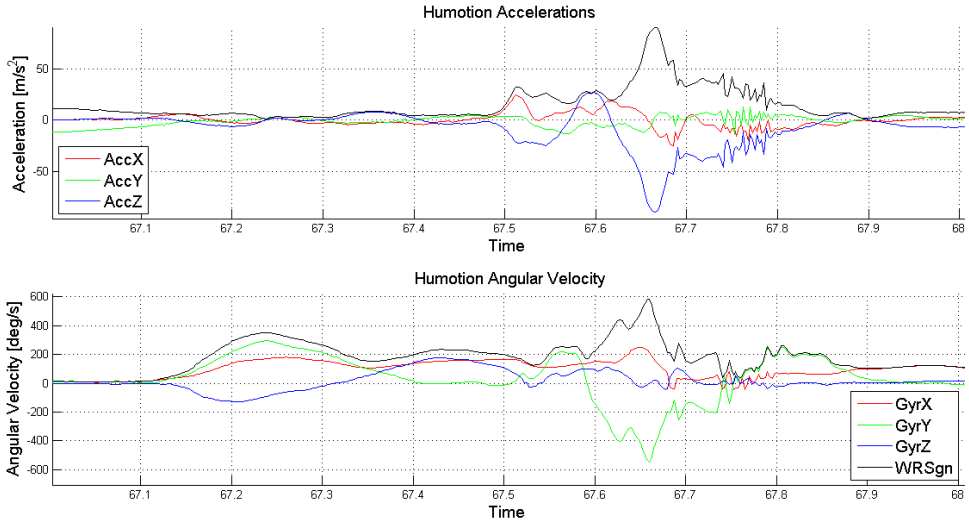

Figure 6-19: Lateral Side Fall, Fall 10, GS

6.3 Sensor's position comparison on simulated falls

Falls were performed adopting an Humotion sensor, firstly at Pelvis level and then at C7 level. A comparison between the two positions is proposed:

- Frontal falls, Pelvis versus C7 level
- Backward falls, Pelvis versus C7 level
- Lateral side falls, Pelvis versus C7 level

6.3.1 Frontal falls

Having analysed the falls with the sensor both on the pelvis and at C7 level, it is possible to observe that in the forward falls, the sensor in the pelvis [Figure 6-20], registers a rapid increase of the resultant acceleration and a decrease of the resultant angular velocity. The angular velocity about the Y-axis crosses the zero value. In the subsequent phase, acceleration values remains at low values, as in a 'free fall' situation, whereas the angular velocities grow until they reach a local maximum value. Then both accelerations and angular velocities reach a local minimum. In the successive time steps they reach the maximum value of the entire fall.

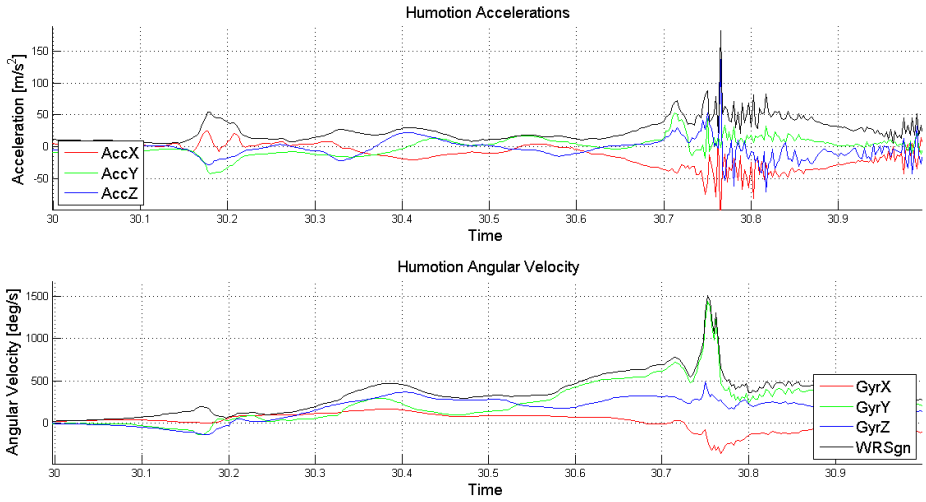

Figure 6-20: Frontal fall, Humotion at Pelvis, Fall 1, GS

If the sensor is instead placed at the C7 level [Figure 6-21], both resultant angular velocity and linear acceleration increase up to a local maximum in collision moment. The acceleration reach the maximum with a 10 ms delay. Then both rapidly decrease to a plateau zone, with low acceleration levels (Free fall situation) and relatively high angular velocities values (200-300 deg/s). Then the resultant acceleration decreases (<20 m/s^2). After a 10 ms time step, both resultant signal increase rapidly to the maximum level of the entire fall [Figure 6-9]:

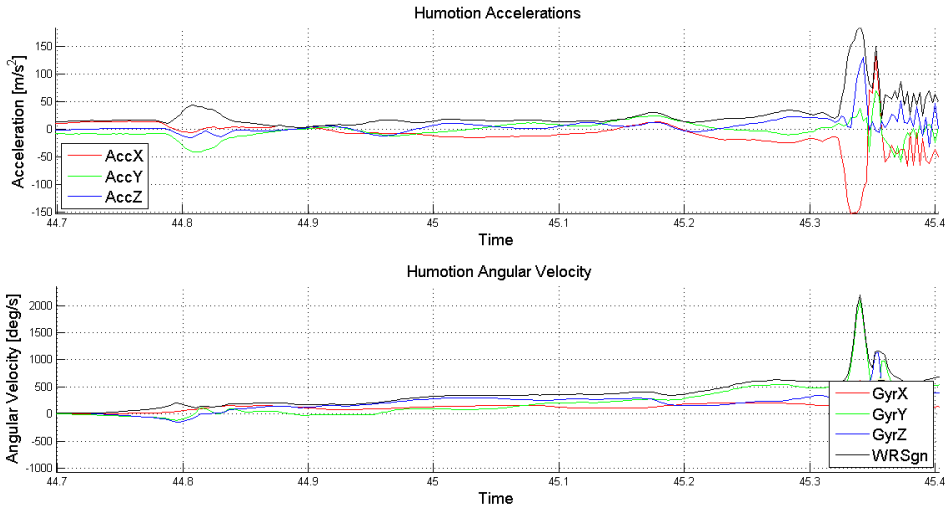

Figure 6-21: Frontal fall, sensor at C7 level, Fall 5, GS

6.3.2 **Backward falls**

In the backward falls, if the sensor is located at C7 level [Figure 6-22], the resultant angular velocity crosses two growth phases, with different duration but with the same slope. After the first growth, the angular velocity decreases to the zero value. During the first angular velocity peak, the resultant accelerations crosses a plateau zone. In the angular velocity decreasing zone, also resultant linear acceleration reach an almost zero value. Then it is possible to observe another local maximum of angular velocity and linear acceleration, followed by another decrease to the zero value. 5ms later, the impulse of the impact leads to the maximum values of the entire fall.

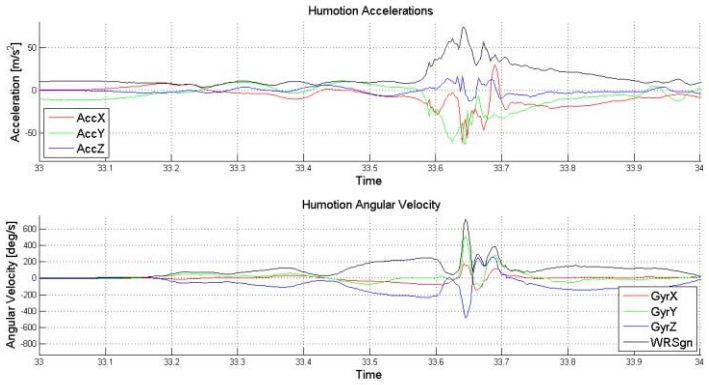

Figure 6-22: Backward fall, Humotion at pelvis level, Fall 8, GS

With the sensor placed over the pelvis [Figure 6-23], the angular velocity increases where the accelerations reach a value near the zero. The angular velocity decreases and then re-increases up to a 8ms length plateau zone. Then reaches the global maximum. In correspondence of the global maximum of the angular velocity, there is the maximum value of the resultant acceleration.

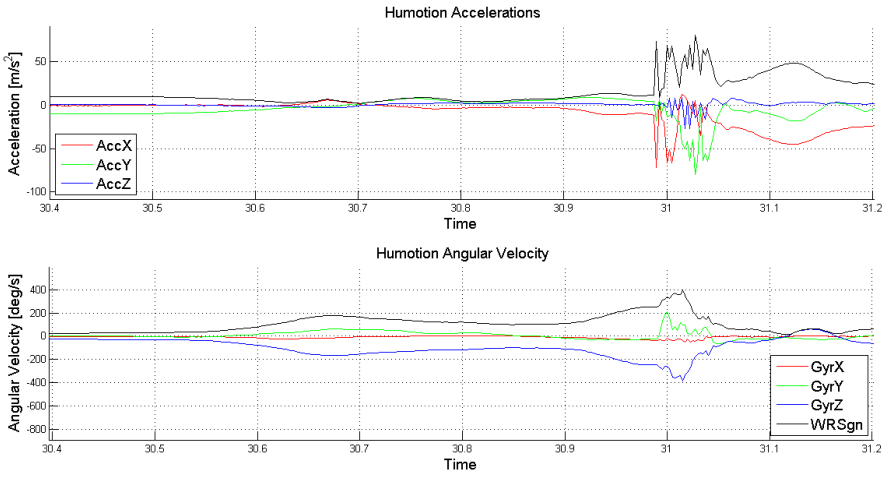

Figure 6-23: Backward fall, Humotion at C7 level, Fall 12, G

6.3.3 Lateral side falls

The Lateral side falls, with the sensor placed at C7 level [Figure 6-24], are characterised by an initial peak of the resultant angular velocity, in correspondence of an almost zero value of the liner acceleration. Then the acceleration remains stable and the angular velocity start increasing. The acceleration reach a local maximum in correspondence of a decreasing phase of the angular velocity. Shortly later, the angular velocity grows to a local maximum and the acceleration decreases to a local minimum. Then the impact leads to the global maximum of both the signals.

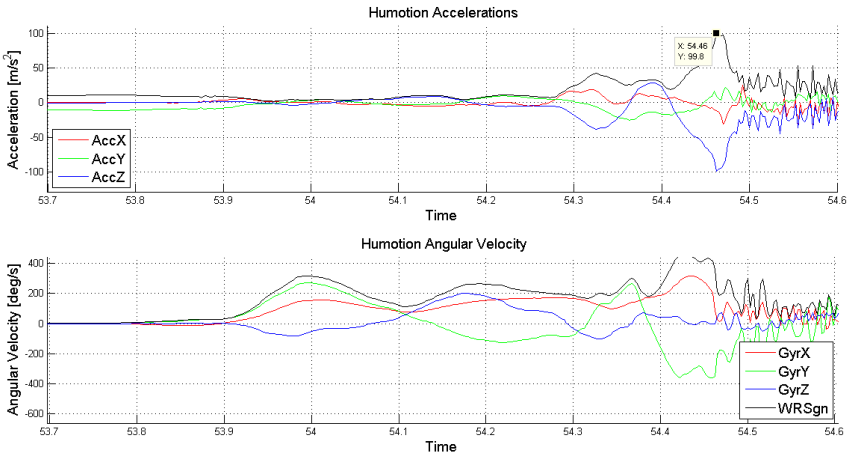

Figure 6-24: Lateral side fall, Humotion at C7 level, Fall 9, GS

With the sensor over the pelvis [Figure 6-25], the angular velocity rapidly increases, and the linear acceleration remains stable around $10 m/s^2$. Then we can find a decrease followed by an increases of the angular velocity. Then both signal reach their global maximum value.

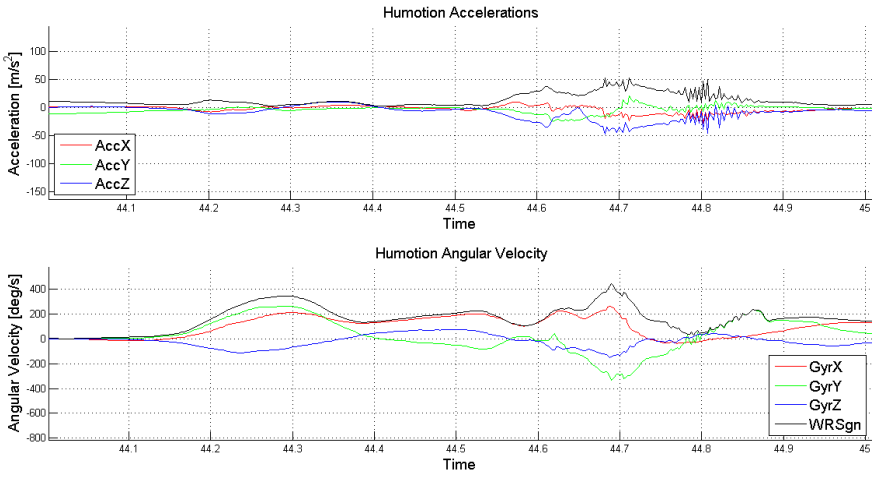

Figure 6-25: Lateral side fall, Humotion at Pelvis level, Fall 13, GS

In next page, Table 6-1 reports significant values of angular velocities and linear accelerations are reported. For each numerical column, the maximum value if highlighted with a thicker font. It is interesting to notice the difference between angular velocities, in dependence to the sensor position. In frontal falls, for example, C7 signals show higher values, due to the greater distance from sensor to body's centre of rotation at the collision moment.

Run	Subject	Fall_Type Italian	Fall_Type Austria	Sensor pos	$Max\ \omega_{res}$ COLLISION	$Max\ a_{res}$ COLLISION	$Max\ \omega_{res}$ FLIGTH	$Max\ a_{res}$ FLIGTH	$Max\ \omega_{res}$ LANDING	$Max\ a_{res}$ LANDING
					$[deg/s]$	$[m/s^2]$	$[deg/s]$	$[m/s^2]$	$[deg/s]$	$[m/s^2]$
1	GS	HS_R	FWF	PE	189.1	54.7	781.0	72.1	1506.0	182.4
2	GS	HS_R	FWF	PE	129.6	58.7	820.1	88.1	1875.0	73.3
3	GS	HS_R	FWF	PE	127.2	**62.8**	649.0	57.8	1675.0	73.6
4	GS	HS_R	FWF	C7	0.0	44.6	667.8	15.0	1422.0	202.7
5	GS	HS_R	FWF	C7	197.3	43.8	585.5	23.8	**2193.0**	186.6
6	GS	HS_R	FWF	C7	172.0	44.5	548.0	20.0	969.7	65.3
7	GS	BW_M	BWF	C7	129.9	10.5	289.0	77.2	486.0	77.2
8	GS	BW_M	BWF	C7	127.0	10.4	245.9	33.0	717.6	71.2
9	GS	LS_M	LSF	C7	318.4	4.3	169.7	42.4	461.7	99.8
10	GS	LS_M	LSF	C7	352.6	2.7	173.4	32.2	586.8	89.5
11	GS	BW_M	BWF	PE	183.2	2.9	244.3	7.6	693.1	149.0
12	GS	BW_M	BWF	PE	178.9	4.9	250.6	12.1	314.6	74.0
13	GS	LS_M	LSF	PE	347.0	5.6	225.4	37.2	443.6	52.4
14	GS	LS_M	LSF	PE	303.0	3.2	192.9	19.3	288.6	46.6
1	HPW	HS_R	FWF	PE	295.6	19.9	692.0	55.1	2081.0	111.8
2	HPW	HS_R	FWF	PE	190.9	17.1	302.9	32.0	404.6	58.4
3	HPW	HS_R	FWF	PE	489.1	43.8	518.2	54.2	1614.0	98.0
4	HPW	HS_R	FWF	C7	287.6	49.2	**909.8**	90.0	1123.0	128.2
5	HPW	HS_R	FWF	C7	339.2	30.8	727.4	80.2	1586.0	150.4
6	HPW	HS_R	FWF	C7	365.0	37.9	696.3	44.8	1595.0	159.5
7	HPW	BW_M	BWF	C7	206.0	32.4	318.2	47.0	601.0	99.4
8	HPW	BW_M	BWF	C7	195.4	22.3	504.3	**117.6**	784.0	135.8
9	HPW	LS_M	LSF	C7	226.7	2.9	263.6	33.6	225.6	31.6
10	HPW	LS_M	LSF	C7	168.6	6.4	55.2	43.8	309.8	45.3
11	HPW	BW_M	BWF	PE	68.63	10.1	209.3	67.2	520.9	110.6
12	HPW	BW_M	BWF	PE	45.62	0.8	212.9	69.6	562.4	82.6
13	HPW	LS_M	LSF	PE	106.6	3.2	143.9	1.2	207.1	37.6
14	HPW	LS_M	LSF	PE	84.2	3.3	150.0	24.7	275.2	43.8
1	RF	HS_R	FWF	PE	232.2	33.7	647.4	64.3	1209.0	125.4
2	RF	HS_R	FWF	PE	186.8	26.6	349.5	67.2	709.0	95.5
3	RF	HS_R	FWF	PE	71.2	26.3	308.3	22.2	463.5	61.6
4	RF	HS_R	FWF	C7	155.5	40.1	399.1	52.8	778.6	118.4
5	RF	HS_R	FWF	C7	136.3	28.6	213.8	32.3	552.1	76.0
6	RF	HS_R	FWF	C7	94.6	34.7	299.3	2.9	546.0	67.6
7	RF	BW_M	BWF	C7	256.2	5.1	407.8	24.9	957.2	**210.5**
8	RF	BW_M	BWF	C7	142.2	5.0	397.4	31.7	826.6	133.1
9	RF	LS_M	LSF	C7	227.1	17.9	248.4	9.4	291.8	50.3
10	RF	LS_M	LSF	C7	234.6	17.9	232.3	24.8	264.3	56.6
11	RF	BW_M	BWF	PE	140.2	19.9	304.6	11.8	660.2	135.4
12	RF	BW_M	BWF	PE	213.7	20.7	282.2	81.3	751.4	121.5
13	RF	LS_M	LSF	PE	205.0	10.9	208.4	8.2	286.8	47.2
14	RF	LS_M	LSF	PE	234.5	18.7	193.1	15.1	386.7	43.1
1	WT	HS_R	FWF	PE	471.9	2.2	751.7	58.3	1841.0	100.8
3	WT	HS_R	FWF	PE	449.5	9.8	541.5	42.9	1515.0	75.5
4	WT	HS_R	FWF	C7	355.5	13.9	594.9	48.0	1240.0	153.0
5	WT	HS_R	FWF	C7	**503.0**	30.4	546.5	34.8	984.4	133.3
6	WT	HS_R	FWF	C7	477.4	24.5	484.9	30.8	861.9	107.2
7	WT	BW_M	BWF	C7	107.8	2.3	159.7	42.2	560.2	93.8
8	WT	BW_M	BWF	C7	137.3	2.1	225.3	45.4	707.4	147.7
9	WT	LS_M	LSF	C7	169.8	4.4	216.7	39.6	397.6	96.7
10	WT	LS_M	LSF	C7	164.3	6.9	313.2	50.5	664.3	167.5
11	WT	BW_M	BWF	PE	26.4	10.3	197.3	7.9	563.6	79.5
12	WT	BW_M	BWF	PE	125.3	3.9	105.3	24.1	405.7	103.7
13	WT	LS_M	LSF	PE	185.5	5.8	249.9	27.3	441.8	83.5
14	WT	LS_M	LSF	PE	212.1	3.8	198.3	27.8	312.0	62.8

Table 6-1: Roller skating simulated falls

Registered angular velocities and linear accelerations resemble real in field simulated falls. Unfortunately, even if signal's shape is similar, dynamics events are completely different. Skiers velocities are higher, and this will be reflected in the overall fall. Even the landing phase could not be comparable to real falls, because of the snow impact instead of mattress impact. In the next subchapter, another fall testing method will be presented, with the adoption of an anthropomorphic dummy.

6.3.4 Simulated falls with anthropomorphic dummy

The last method analysed to perform an experimental fall's simulation considered the adoption of an anthropomorphic dummy. In different works, usefulness of anthropomorphic dummies on ski applications was confirmed, both in testing safety nets behaviour on impacts [Petrone et al., 2011] and in extrapolating deceleration peaks and penetration values in ski safety barriers during full scale impacts [Petrone, 2012]. Self-development of an instrumented dummy would require large economical and time effort, even with some technological limitation [Petrone et al. 2010]. In falls'analysis we decided to utilize a high-tech anthropomorphic dummy was gently borrowed by BMW which used it in motorcycle impacts tests. It was a male Hybrid III Pedestian, 50 percentile. It consist in several parts linked with joint that resembles human articular joints. The body of the crash test dummy is made of metal parts consisting in aluminium, bronze, or steel (depending on design, purpose, and body parts) as well as metal plating materials. A wide variety of plastics are also incorporated in most designs, and the plastic include Delrin (a type of long-wearing acetate resin), urethane and polyurethane foam, and vinyl. Most dummies are clothed to simulate reality. Dummy manufacturers supply little or no instrumentation. Designs provide space for instrumentation to be secured, but instrumentation is so specific to actual testing conditions that the customers of the dummy install their own. Some small potentiometers are sometimes built into the manufacturer's lines, but more sophisticated instruments like accelerometers and load measuring sensors are selected by the customer from their own instrument packages or specialized vendors. The dummy is designed with openings for instrumentation and cabling. These are in the larger parts of the body including skull, chest, abdominal cavity, and the thighs.

The design of the crash test dummies is a process limited to government agencies, dummy manufacturers, and customers like automobile manufacturers. The manufacture of crash test dummies is highly proprietary because of the complexities of design and the small number of qualified

manufacturers in the world. All design and construction meets an extremely high set of standards. There are no “B-grade” crash test dummies [www.madehow.com].

We decided to adopt such dummy to perform our in field test to better simulate a fall of a human. In our tests, the standing position with skies was a must. The initial phase of the infield test setup, was to determine if dummy could stand on his own. We tighten the screws in the thighs and knees, but those second one were too much small to permit the 76 kg dummy to stand. We decide to replace the knee joint with a stronger one, homemade by a disk of aluminium. Two disk of steel material were fixed to the lower limb, and by a strong screw were closed over the inner part of the upper leg. This permitted us to use a dynamometric wrench to tighten the screws without fear to damage the high cost dummy.

After this modification, we placed a plastic bag on both foot of the dummy to facilitate the ski boot insertion. This had to be made using a lift to support the dummy. We decided to use Dal Bello “scorpion” ski boot thanks to the high 130 flex index. Then we hooked a pair of skies.

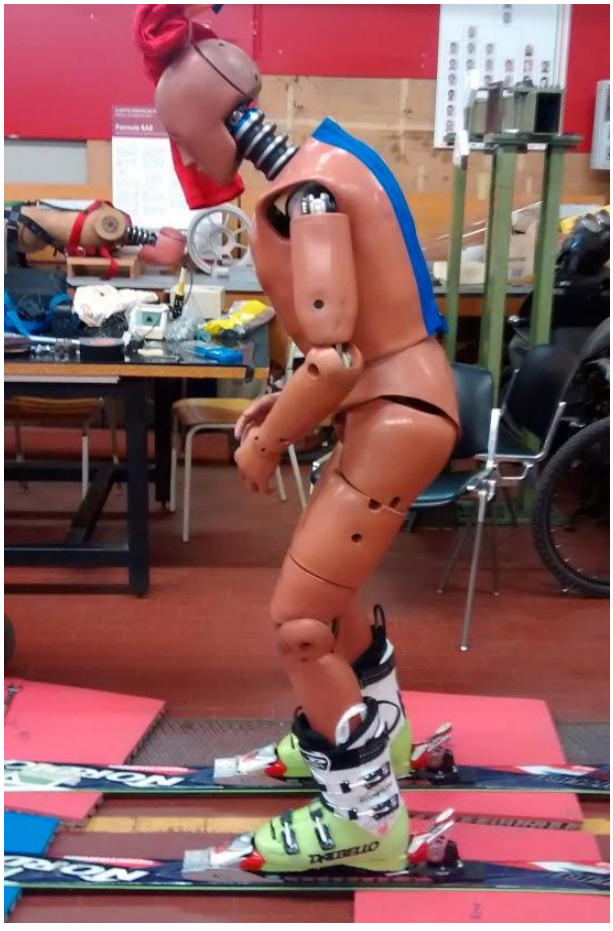

Figure 6-26: anthropomorphic dummy wearing skies

Second step was to decide which sensor to adopt and in which position. Several fall test were performed, provoking the dummy fall on mattress, from the standing position.

To get a comparison with previous tests, we decided to place a sensor in a housing inside the pelvis and two sensor in the upper trunk, in a housing at the spine. In the pelvis we used a Humotion sensor

Figure 6-27: Test dummy setup

and in the trunk a Humotion and a 2D sensors To avoid dummy damage due to the low temperature and snowing conditions of the infield test, we let the dummy wear a skiing suit, consisting both in trousers and jacket.

Tests were performed in San Vito during March 2015, at San Vito ski area. Having some collaborations with the area managers, it was possible to get a slope reservation to perform tests in safe conditions, without the risk of harming other skiers. The tests were performed with the collaboration of Dolomiticert, a certified testing laboratory located in Longarone, Belluno. Thanks to them it was possible to use a high speed camera “Motion Blitz”. After some preliminary tests without sensors, we decided to ask the snow machine manoeuvre to smooth the slope surface to get able to reach relatively high speeds. At the end of the slope, a net was placed to avoid the dummy to continue to slide. Before the net, a 500 mm snow ridge was created, to simulate the impact of the skier with snow obstacle. Thanks to snow ridge, the dummy was forced to fall, usually forward. Reference lines were tracked on the snow with spray paint. To trigger the dummy start, two fixed vertical poles and a removable transverse pole were placed in the upper part of the track. To start the test was sufficient to remove the transversal pole.

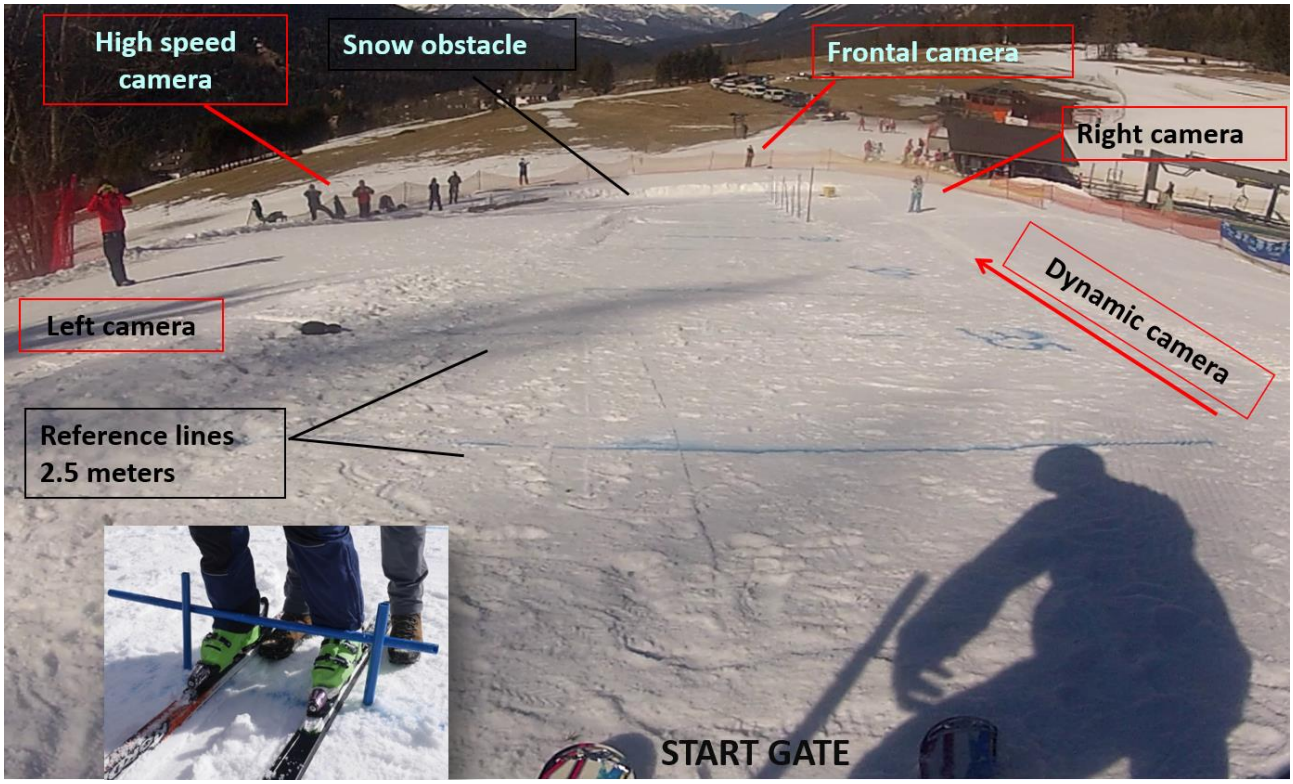

Figure 6-28: In field test setup

The picture above represent the infield test setup. It is possible to observe the slope adopted in San Vito, with the reference lines about the selected slope length. At the end of the slope, a snow ridge was built as an obstacle. In the picture on the bottom left the starting gate is represented. Six cameras were adopted. A fixed frontal camera, one fixed camera for each side of the slope, One dynamic camera on the right side, controlled by a skier, and a fixed high speed camera (courtesy of DolomitiCert). Once the dummy felt, a snowmobile was adopted to return it to the start gate.

Test were performed in 3 days, with a total of 39 impacts. 32 impacts were frontal falls. 7 impacts were side falls: Before the snow obstacle, a batten of wood was placed, inclined by 30 degrees with in respect to the speed direction. Falls were performed with different impact speeds, due to longest slope. The ski bindings were set at 2 different levels, to help the ski releasing during the impact. In the picture below, a frame show of a frontal fall recorded with the high speed camera is presented.

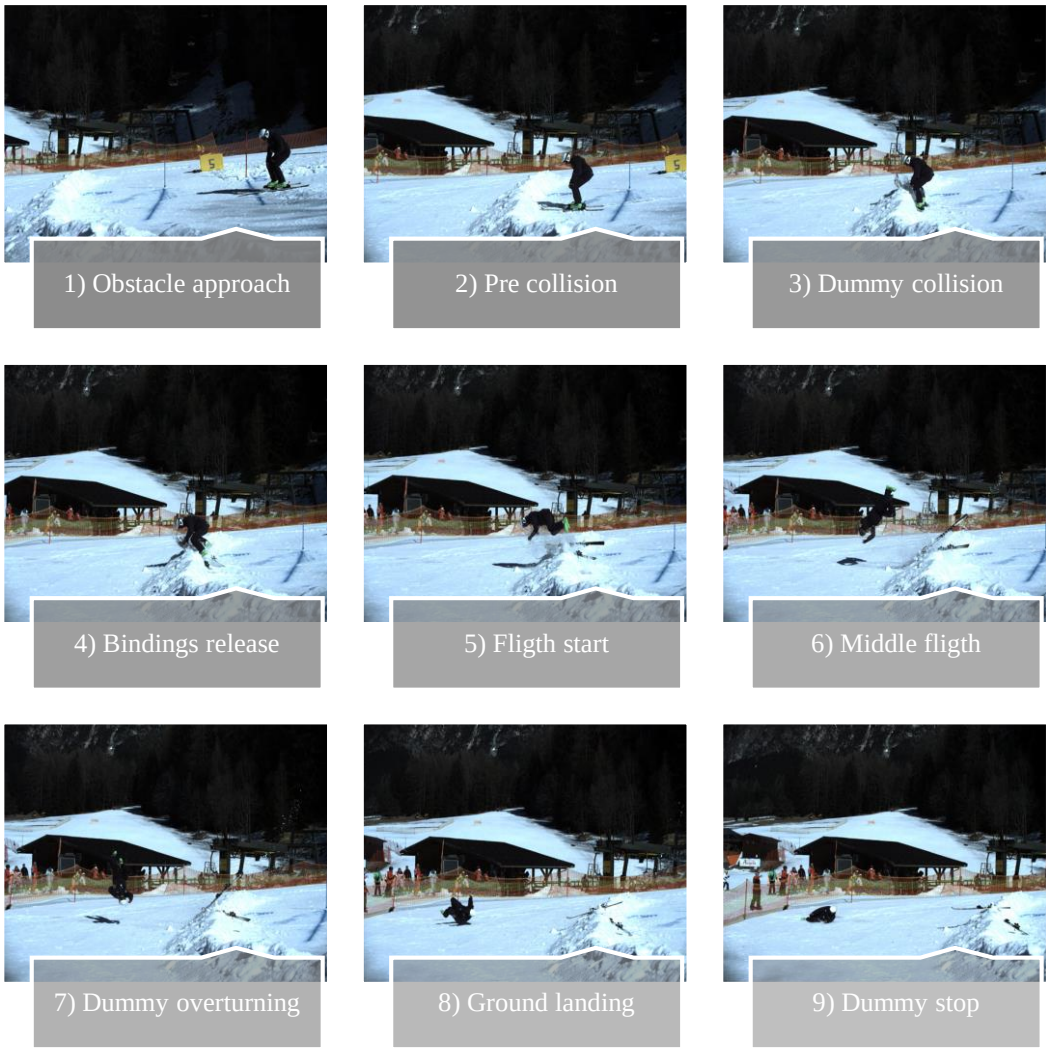

Figure 6-29: Frameset from Fall 5, day 2

From Figure 6-29, it is possible to observe the different phases of the fall. Picture 3) represent dummy's collision. Pictures 5) and 6) represent flight. In picture 8) dummy lands. In the obstacle approach, the dummy reached an estimated speed between 30 and 35 kilometres per hour (Estimated visually thanks to high speed camera and reference line). In the collision, the skis flex up to failure. This fall has been performed one time due to the high impact velocity that caused both ski failure. In the fourth picture, the bindings released the dummy which started a flight phase. In middle flight the dummy starts overturning upside-down. The eighth picture shows the landing impact with the ground, several meters far from the obstacle, and then the dummy end its run near the safety net.

The preliminary data analysis was made considering not only single channel signals, but considering the resultant signal as the square root of the single channel's signals squared and summed. The resultant angular velocity signal can be thought as a representative quantity of the whole fall. The following picture [Figure 6-30] summarized this concept.

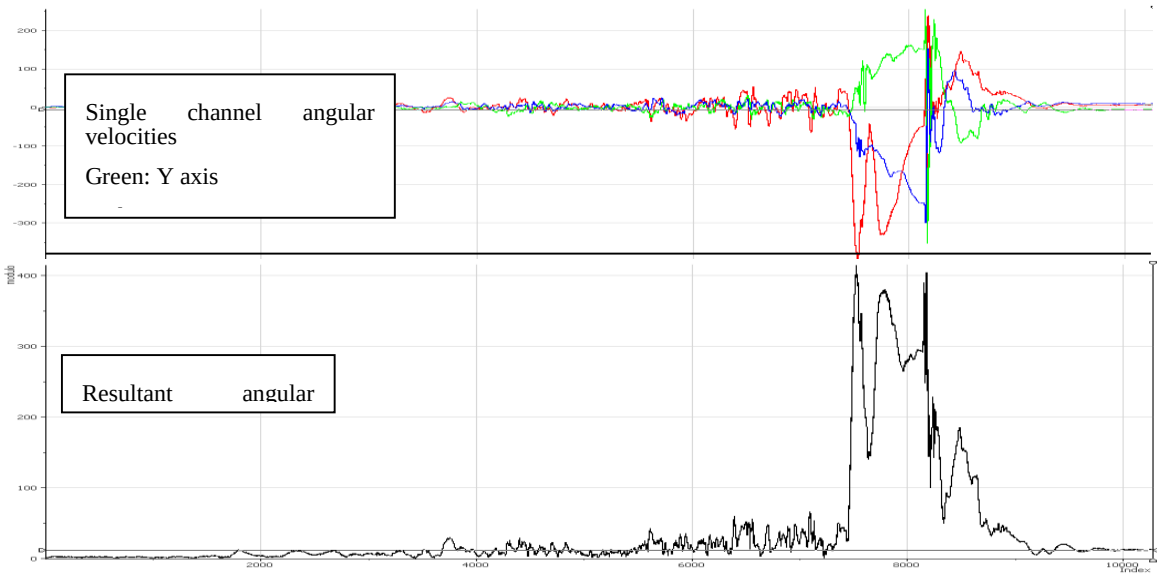

Figure 6-30: single channel and resultant angular velocity

It is possible to notice that the resultant angular velocity is influenced by the three signals, without regarding the sign of each. Another interesting method would consider the resultant signal, but with the sign of one of the single channels, basing on the most significant in the fall.

Analysing both the 2D and Humotion signals, it is possible to compare them in term of angular velocity and linear acceleration. Thanks to the students at the Vth ISEA winterschool, who worked on those infield tests, it was possible to synchronize video and data signal in order to determine the correspondence between peaks and valleys in the signal and the fall's phases.

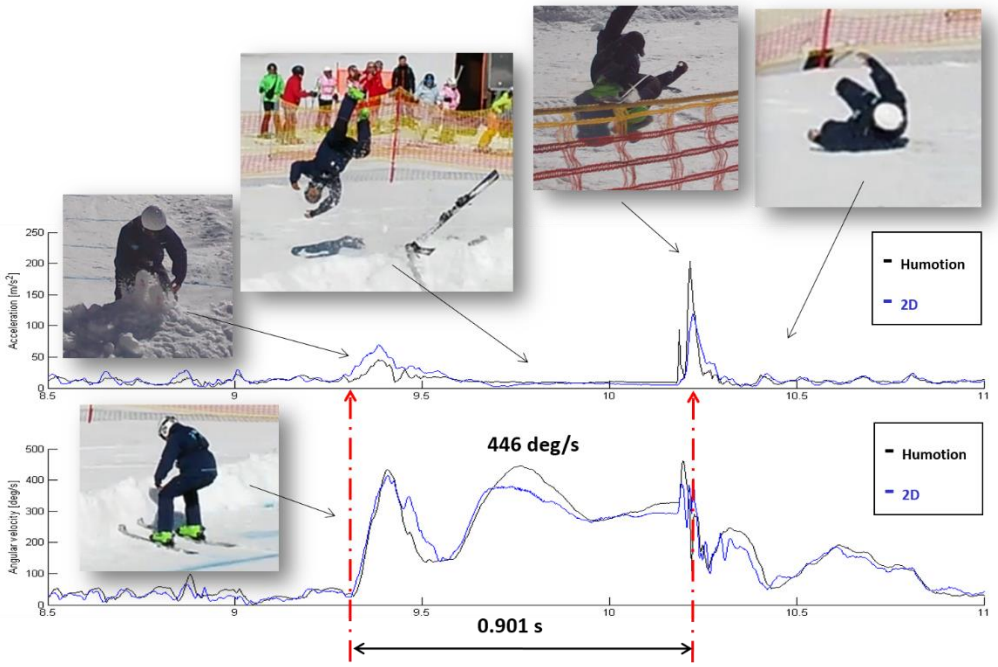

Figure 6-31: Fall's flight phases and signals

From Figure 6-31, we can see that the time between the impact and the ground impact was 0.901 seconds, with a maximum resultant angular velocity of 446 deg/s. The resultant acceleration instead reached a maximum value of about 200 m/s^2. The results were collected in a table, considering firstly the time at which the test was performed and the day. Then is reported the setup, with the column 'Start' which reports the distance of the start to the obstacle. Then the speed at which the dummy reached the obstacle or the displacement point. Then the type of skies and the sensors on the dummy. The column 'Binding' reports the strength of the skies binds closure. The column 'Knee' reports the strength of the knees screws closures. Then is reported the presence of absence of the cameras in the slope:

Day	Run N°	Time	Start [m]	Speed [m/s]	Ski	Sensors	Binding	Knee	HS	GP	RS	LS	FR
1	1	12:15	37,5	23,68	NT	1Hp,1Hc	10	16	Y	Y	Y	Y	Y
1	2	12:37	37,5	/	NT	1Hp,1Hc	10	16	N	Y	Y	Y	Y
1	3	13:00	32	21,95	NT	1Hp,1Hc	10	16	Y	Y	Y	Y	Y
1	4	13:18	30	/	NT	1Hp,1Hc	10	16	Y	Y	Y	N	Y
1	5	13:30	30	/	NT	1Hp,1Hc	10	16	Y	Y	Y	Y	Y
1	6	13:40	30	19,28	NT	1Hp,1Hc	10	16	Y	Y	Y	Y	Y
1	7	15:55	30	/	NT	1Hp,1Hc	10	18	Y	Y	Y	Y	Y
1	8	16:10	30	26,09	NT	1Hp,1Hc	10	18	Y	Y	Y	Y	Y
1	9	16:19	30	25,35	NT	1Hp,1Hc	10	18	N	Y	Y	Y	Y
1	10	16:33	30	/	NT	1Hp,1Hc	10	18	N	Y	Y	Y	Y
1	11	16:46	35	32,14	NT	1Hp,1Hc	10	18	Y	Y	Y	Y	Y
1	12	17:00	40	34,62	NT	1Hp,1Hc	10	18	Y	Y	Y	Y	Y
1	13	17:15	40	36	NT	1Hp,1Hc	10	18	Y	Y	Y	Y	Y
2	1	11:09	30	29,03	NT	1Hp, 1Hc, 2D, 1Hp, 1Hk	10	18	Y	Y	Y	Y	Y
2	2	11:35	30	21,43	NS	1Hp, 1Hc, 2D, 1Hp, 1Hk	4	18	Y	Y	Y	Y	Y
2	3	11:55	35	32,72	NS	1Hp, 1Hc, 2D, 1Hp, 1Hk	4	18	Y	Y	Y	Y	N
2	4	12:08	40	28,125	NS	1Hp, 1Hc, 2D, 1Hp, 1Hk	4	18	Y	Y	Y	Y	Y
2	5	12:25	40	36	NS	1Hp, 1Hc, 2D, 1Hp, 1Hk	4	18	Y	Y	Y	Y	Y
2	6	12:48	35	31,58	NS	1Hp, 1Hc, 2D, 1Hp, 1Hk	4	18	Y	Y	Y	Y	Y
2	7	13:16	30	26,86	NS	1Hp, 1Hc, 2D, 1Hp, 1Hk	4	18	Y	Y	Y	Y	Y
2	8	14:23	30	27,27	NS	1Hp, 1Hc, 2D, 1Hp, 1Hk, 1He	4	18	Y	Y	Y	Y	Y
2	9	14:42	35	/	NS	1Hp, 1Hc, 2D, 1Hp, 1Hk, 1He	4	18	Y	Y	Y	N	Y
2	10	14:58	35	27,27	NS	1Hp, 1Hc, 2D, 1Hp, 1Hk, 1He	9	18	Y	Y	Y	Y	Y
2	11	15:11	35	31,57	NS	1Hp, 1Hc, 2D, 1Hp, 1Hk, 1He	9	18	Y	Y	Y	Y	Y

Table 6-2: Table reporting the in field tests setup

In the analysis, the data from the Humotion on the pelvis and on the chest were considered. The speed of the dummy was deduced by the videos registered by the high speed camera, with a 5ms time resolution. It was calculated considering the distance (2,5m) between two reference lines pictured in the snow by a blue spray and dividing it by the millisecond between the passages of the ski over the lines. The speed's estimation was obtained analysing frames registered with a 5 milliseconds precision. The accuracy on the skis passage above the painted reference lines was limited due to the distance from the high speed camera to the dummy.

The following table, reports instead the values obtained by the dummy fall's analysis. The runs correspond to those reported on the table above with the setups. In the table are reported the significant values of angular velocities and linear acceleration by means of resultant signal. Are reported the maximum angular velocity and maximum linear acceleration of each fall, and the maximum values of the two signals before the impact. This analysis was performed for both the Humotion in the chest and the Humotion on the pelvis of the dummy.

			Hp - Chest				Hc - Pelvis			
Day	Run N°	Time	ω_prelmp	ω_max	a_prelmp	a_max	ω_prelmp	ω_max	a_prelmp	a_max
			[deg/s]	[deg/s]	$[m/s^2]$	$[m/s^2]$	[deg/s]	[deg/s]	$[m/s^2]$	$[m/s^2]$
1	1	12:15	802,7	484,9	44,1	102,8	577	445	108,1	55,11
1	2	12:37	328,9	1055	46,78	202,22	207,3	790,3	57,27	123,8
1	3	13:00	387,8	1386	51,3	219,3	204,7	1276	28,14	201,8
1	4	13:18	152,6	1353	33,24	215,2	276,5	1069	33,18	171
1	5	13:30	174,9	910,6	30,25	128,4	116,4	555,6	35,3	100,1
1	6	13:40	117,4	623,4	23,71	168	95,65	511,8	28,45	166,6
1	7	15:55	454,2	788,2	31,32	269,4	219,1	910,9	52,79	204,5
1	8	16:10	520,1	627,9	54,17	113,3	619,6	525	89,73	78,51
1	9	16:19	446,3	680	37,67	65,98	602,3	655,5	87,95	148
1	10	16:33	461	677,4	52,51	174,9	441,7	752,3	84,57	217
1	11	16:46	456,5	1067	43,74	95,32	507,9	910,2	102,8	139,2
1	12	17:00	466,2	764,5	31,72	80,96	615	852,6	92,6	189,6
1	13	17:15	414,4	673,7	28,51	90,82	569,3	1220	76,38	198,3
2	1	11:09	582	784,3	136,7	101,6	653,3	857,2	62,8	204,6
2	2	11:35	223,8	482,9	23,8	178,1	287,9	537,9	36,18	216,4
2	3	11:55	242,6	678,4	128,1	120,9	524,6	1132	82,75	257
2	4	12:08	158,4	501,2	60,11	165,6	270	311,1	170,7	45,96
2	5	12:25	445,8	462,1	45,95	203,2	683	1191	83,57	229,7
2	6	12:48	346,6	943,3	82,49	238,6	497,1	1076	73,84	222,1
2	7	13:16	388,8	654,9	74,59	155	555,8	803,1	67,19	198,9
2	8	14:23	273,4	375	59,36	170,3	290	381,1	34,54	109,6
2	9	14:42	329,9	393	49,84	89,01	930	370,6	228	90,36
2	10	14:58	237,5	620	21,38	136,2	512,6	242,4	38,56	87,26
2	11	15:11	345,6	640,5	135,7	246,3	389	674,4	39,62	163,1

Table 6-2: Falls' significant values analysed

The last table present some notice about the falls, in terms of notes relative to the type of fall.

Day	Run N°	Time	Fall type	Notes
1	1	12:15	FR	Front side fall on snow obstacle
1	2	12:37	FR	Front side fall on snow obstacle
1	3	13:00	FR	Front side fall on snow obstacle
1	4	13:18	SD	Small jump on snow obstacle, then side fall
1	5	13:30	SD	Side fall
1	6	13:40	BS	Back side fall, after hitting the poles
1	7	15:55	FR	Front side fall. Crosses the snow obstacle and the fall
1	8	16:10	FR	Front side fall
1	9	16:19	FL	Flipped fall; It's a front fall with a complete 180 degrees flip during flight phase
1	10	16:33	FL	Flipped fall; It's a front fall with a complete 180 degrees flip during flight phase
1	11	16:46	FR	Front fall, hit on the side part of the dummy
1	12	17:00	FL	Flipped fall; It's a front fall with a complete 180 degrees flip during flight phase
1	13	17:15	FL	Flipped fall; It's a front fall with a complete 180 degrees flip during flight phase
2	1	11:09	FL	Flipped fall; It's a front fall with a complete 180 degrees flip during flight phase
2	2	11:35	SD	Side fall
2	3	11:55	FL	Flipped fall; It's a front fall with a complete 180 degrees flip during flight phase
2	4	12:08	SD	Side fall with a long sliding phase
2	5	12:25	FL	Flipped fall; It's a front fall with a complete 180 degrees flip during flight phase
2	6	12:48	FL	Flipped fall; It's a front fall with a complete 180 degrees flip during flight phase
2	7	13:16	FL	Flipped fall; It's a front fall with a complete 180 degrees flip during flight phase
2	8	14:23	UR	Unadverted release on impact with the wooden tablet
2	9	14:42	FR	Front side fall, over skidoo
2	10	14:58	FR	Front side fall
2	11	15:11	HS	High side fall

Table 6-3: Notes on the type of each fall

The acronyms in the Tables 6-2,3,4 in the following are summarised:

Ski	NT	Nordica Trans	
	NS	Nordica Splitfire	
Sensors	Hp	Humotion on pelvis	
	Hc	Humotion on chest	
	2D	2D sensor by Dainese	
	1Hp	1 sensor on a belt placed over pelvis	
	1Hk	1 Sensor on knee	
	1He	Accelerometer on head	
Cameras	HS	High speed camera	Left side
	GP	GoPro	Follows the dummy
	RS	Normal Camera	Right side
	LS	Normal Camera	Left side
	FR	Normal Camera	Frontal
Values	ω_preImp	Max value of the angular velocity pre impact	[Deg/s]
	ω_max	Max value of the angular velocity in the fall	[Deg/s]
	a_preImp	Max value of the acceleration pre impact	[m/s]
	a_max	Max value of the acceleration in the fall	[m/s]
Units	Start	Length of the slope, from the dummy starting point to the obstacle	[m]
	Speed	Speed of the impact, estimated by videos	[Km/h]
	Binding	Closure of the ski bindings	[Nm]
	Knee	Closure of the knee screw	[Nm]
Fall type	FR	Frontal fall	
	FL	Flipped fall	
	SD	Side fall	
	HS	Hgh side fall	
	BS	Back side fall	
	UR	Unadverted release	

Table 6-4: Table summarising the acronyms used in dummy's falls analysis

The important results obtained with those tests are encouraging for a future development of them. In fact, a lot of analogies can be seen between the last two methods presented. We can recognize both a similar shape of the signals relative to the falls, and comparable maximum values both for the angular velocities and the linear accelerations. This can be address the study to one of the method, alternatively. In absence of an expensive anthropomorphic dummy, simulated falls can be a good base to develop further studies on this field, even with the possibility to set up airbag-based protecting devices not only for the back, but also for other important body joints, like knees, hips and elbows. If instead, the aim of future tests will be a simulation as more realistic as possible, the anthropomorphic dummy would be considered the best alternative, without the risk of injuring during tests. In this case it would be necessary to develop a method to move easier the dummy. Because of its weight, its handling is not easy. To stand it up after a fall, at least two people are needed. The skies are a great obstacle in those tests: They are difficult to fix to the dummy's boots and break easily. Greater speeds in respect those tested, would lead to more skies failures, with the necessity to change them after each test, resulting a consequent loss of time. A snow machine with a built-in lift would simplify manoeuvres, but would add cost to the entire experiments.

After having considered the three method for fall's analysis, the last part of this thesis will consider an infield instrumentation, still in a development stage, that could be fundamental in skiing safety.

Chapter 7: “Field Laboratory” approach for the improvement of skiing performance and safety

In this last chapters, a recently developed instrumentation setup will be presented as an attuative approach to collect infield data from large numbers of skiers, especially when conditions doesn’t permit to adopt the same equipment adopted in lab tests.

7.1 Motorialab startup

Motorialab is a spin off born by laboratories of the ICT centre group of Bruno Kessler Fondation (FBK), located in Trento, Italy. The team started in FBK by registering data on ski slopes accidents. Key words of Motorialab are safety, welfare and technologies, intended as bringing new technologies with the aim to improve sport’s quality, not only in terms of performances but also safety and welfare. Motorialab is not only addresses to ski sports, but works also in walking and cycling frameworks. The Hi-Fis project is an interesting development at this thesis’ framework. Hi-Fis is an innovative high-tech environment for ski areas and snow-parks. Hi-Fis grants access to customized systems fully supported for the high-res multimedia integration of data collected from wearable sensors and further data sharing on the social media. With Hi-Fis, the users of ski areas will be able to monitor their performance, record personal data and create their individual profiles. But the Hi-Fis infrastructure is modular and may be employed by skiing schools, athletes, individual skiers and universities.

7.1.1 Hi-Fis setup

The system developed by Motorialab best suits the work performed in both performance and safety parts of this thesis work. Thanks to a collaboration between Motorialab and the Department of

Mechanical Engineer of the University of Padua, we had the possibility to observe and collaborate to the infield setup of the instrumentation and to first experience the system.

The setup considers a good variability thanks to the modularity of the system. In its simplest configuration it consist on at least two Wi-fi antenna installed in a fixed position on the ski slope, that have to communicate each other, and have to be placed in an open field without large obstacles between them. Those antenna can communicate with an android smartphone to transmit via Wi-fi data collected by internal sensors, such as gyroscope, accelerometers and GPS. Those data are send by the antenna to a central server that can elaborate them. In addition, there is the possibility to install FullHD waterproof videocameras directly on the slope, in order to have a continuous video record of the skiers. The last add-on of the system, and the most important to our applications, is the possibility to link the smartphone via Bluetooth to wearable sensors. In the test performed we tried to recreate the setup adopted in the previous tests presented in this thesis. We adopted the Exel sensor because of its Bluetooth protocol. Thanks to an android application developed by Motorialab, it is possible to link the sensor to the smartphone and to decide via smartphone to start or stop the data collection at the beginning and at the end of each run. In addition, thanks to sensor's and video cameras' time stamps it is possible to synchronize the outputs with the video data collection.

The system is described in the picture [Figure 7-1] below:

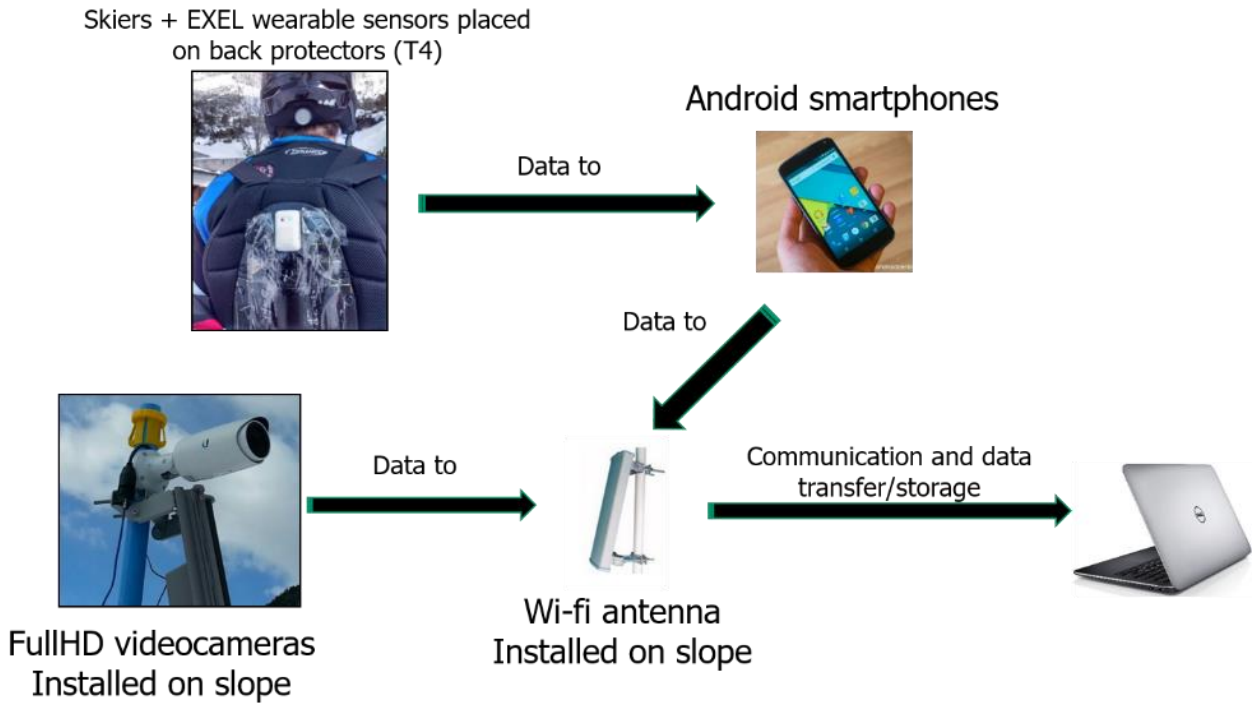

Figure 7-1: Hi-Fis system setup

Thanks to this system, it is possible to monitor a large number of skiers. In this way it would be possible to collect continuously data from skiers at different skiing levels and to increase the statistical value of the analysis presented in the first part of the thesis. In addition, a large number of skier would

also lead possibly to a significant number of falls that can be analysed visually thanks to the cameras and in terms of data analysis.

Our first infield setup was applied in San Vito di Cadore, at Seggiovie San Marco. Three videocameras were placed on the Antelao slope, a straight and wide track, adopted both by recreational skiers, but also by ski teams in giant slalom trainings. One camera, together with the receiver antenna was placed at the beginning of the slope. The second camera was placed at the middle of the slope, in the left part (if the reference is the start of the slope, pointing downhill) of it, pointing to the main camera. The last one was placed in the intersection between the Antelao and Serpentina slopes.

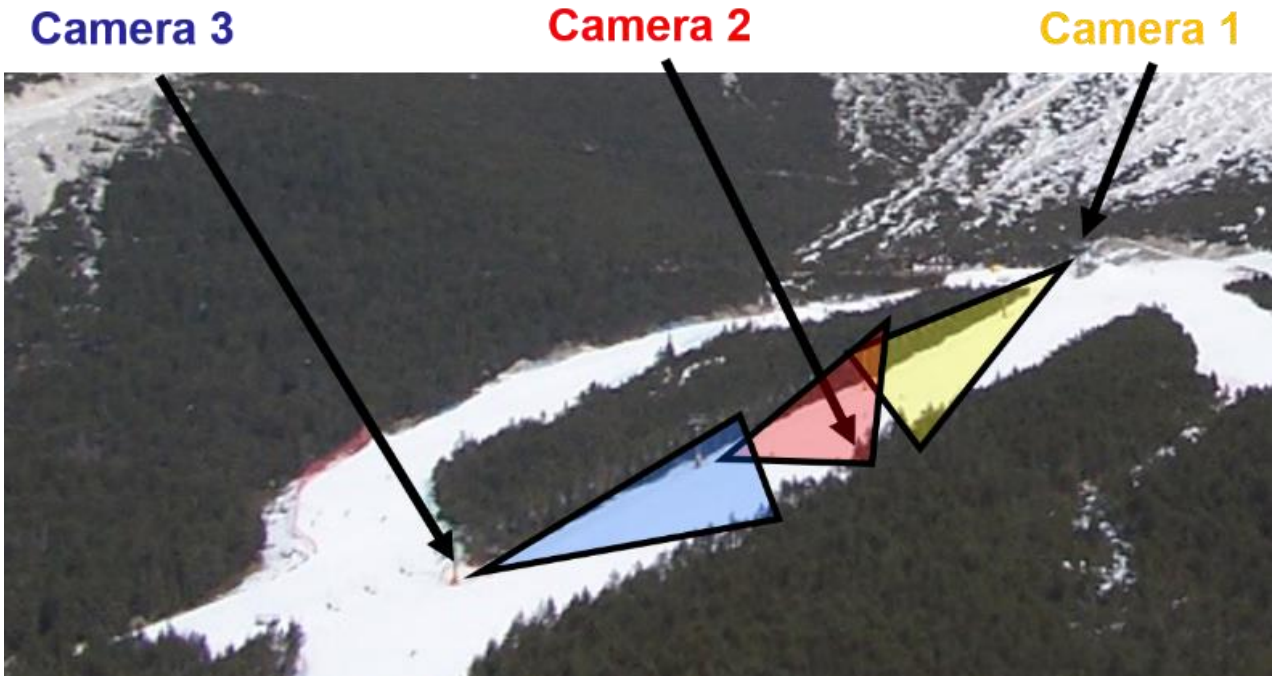

Figure 7-2: Cameras disposition on Antelao slope

Thanks to this cameras disposition it was possible to monitor the entire run from different points of view: tests performed during the Vth ISEA winterschool demonstrated the validity of this setup:

The cameras recorded the skier's runs; a sensor was placed on each skier, over a back protector at the C7 level. The GPS signal of the smartphone was also collected. Unfortunately, the synchronization between videos and signals was not possible yet due to a lack of communication between the server, located at Motorialab offices and the technicians on field, but a signals visualization on Matlab showed the potential of such a system. With the adoption of a third part software like Diadem, such a synchronization would have been possible, but in those preliminary tests software's experts were still needed. The picture below shows the cameras' points of view:

Figure 7-3: Cameras point of view

Key factors of this technological approach to data collection is the simplicity of the setup needed for tests: once the system is settled and fixed, users can perform as many tests as needed, without the difficulties linked to high weight or long-setup instrumentations. To communicate with antenna and cameras only a wearable sensor and a smartphone are needed. Thanks to the current spread of smartphones, those requirements are fully affordable. In addition, the presence, in the application developed, the possibility to start and stop the runs is not the only option available. Also small portion of text or comments can be added to a data collection, avoiding the need to submit questionnaires to tester in order to understand the slope, the technique or other significant points about the run performed.

Future development of this technology can point to lower power consumption, real against factor of this technology. Having both Bluetooth and GPS active with also Wi-Fi data transmission would ran the battery out in short time. With an average Android smartphone, with a 2000mA battery this would bring the battery to low levels in about three hours of test. Considering, for example, voice commands to trigger starts and stops of the runs avoiding turning on the screen would lower battery consumption. In addition, if wearable devices such as smartwatches or activity trackers would take place in the market, moving to those platform would lower such problems.

Chapter 8: Conclusions

This thesis work is the result of a 18 month study, started first as course project and later on developed during my Master Thesis work, within the framework of the Interreg IV 'AirSki' project. The collaboration with DolomitiCert and University of Salzuburg permitted to extend the thesis' objectives towards different analysis methods focused both on research for performance and safety.

Summarizing, the work started with data collection at San Vito ski area's slopes and continued with the data analysis during the subsequent months. Having collected data with Humotion sensor from different skiers of different skiing levels, it was possible to set up analysis methods oriented to classify the different levels. First difficulties encountered during data analysis were related to data handling. Having collected sensor's data during a whole day test session, files obtained by the sensor had large dimension. A big effort was put in the direction of a standardized data storage in order to facilitate future re-analysis. With this aim, the first studies took a great amount of time in obtaining clear data, in terms of skied turns. Later, great effort was set in understanding meaningful events during skiing.

The successive analysis regarded cyclograms. Having observed in first sessions encouraging results from cyclograms analysis, we decided to analyse the testers in terms of crossplots. The result was a clear distinction in Experts' and Beginners' cyclograms. The distinction between Intermediate and Experts, instead, was not satisfactory. Further analysis considered the testing of different parameters, as cyclograms' area, diagonal or diagonal slope. We eventually decided to extrapolate parameters directly from the signals, and we stated that best differentiation between levels was obtained considering $\Delta acc_x/\Delta\omega_x$ and $\Delta acc_y/\Delta\omega_x$ .Thanks to those synthetic parameters the results in chapter

5 were obtained: a good differentiation between the three different levels was obtained and it can be considered as a basis for future further analysis on those parameters.

After this result we decided to move on the safety analysis framework, as planned by the INTERREG Project. The results in the performance analysis gave the possibility to analyse safety, in terms of falls protection.

The possibility to analyse real falls is limited due to testers' safety requirements. Firstly, thanks to the collaboration with University of Salzurg, we got the opportunity to analyse simulated falls on mattresses, in order to obtain peak values of angular velocities and linear accelerations during fall events. Then, the collaboration with DolomitiCert gave the possibility to perform in field tests with an anthropomorphic dummy. In the framework of Vth ISEA Winterschool, several dummy's falls were performed.

Humotion sensors were placed on pelvis and on chest. Falls were filmed with several HD videocameras and with a HighSpeed video camera. Thanks to the video, we were able to reconstruct the falls dynamics and to analyse the falls under different aspects. Thanks to the High speed video camera, impact velocity was estimated. Angular velocity and linear acceleration values were obtained, both terms of single-axis value (X, Y, Z) and resultant signals.

In addition, it was necessary to analyse real falls in order to compare not only the maximum or significant values of falls, but also general dynamics, risk factors and fall's injuries. Obviously, this was not possible to obtain easily with real testers. Falls have to be collected in real slopes, with real skiers in normal skiing conditions. Motorialab, targeted this objective and developed the Hi-Fis system, a fixed in field setup based on video cameras, wifi antennas and sensors. In the near future, after a beta testing phase, it will be possible to obtain a large amount of data from recreational skiers.

Thanks to those analysis, future works could take effort on selecting limit values in order to trigger an Airbag based protecting device targeted to recreational skiers.

Bibliography

[1] [A. Marega,2015] A. Marega "*Market research on the functional, ergonomic and performance characteristics of the airbags present on the market*", project "AirSki" San Vito 2015

[2] [Brodie et al., 2007] M. Brodie, A. Walmsley, W. Page "*Fusion motion capture: the biomechanics of alpine skiing*", Journal of Biomechanics 40 (S2), 2007.

[3] [Dadashi et al., 2013] F.Dadashi, G.P. Millet, K. Aminian, "*A Bayesian approach for pervasive estimation of breaststroke velocity using wearable IMU*", Pervasive and Mobile computing, 2013.

[4] [Dadashi et al., 2014] F. Dadashi, G.P. Millet, K. Aminian, "*Gaussian process framework for pervasive estimation of swimming velocity with a body-worn IMU*" (IEE Electron. Lett 49 (2013) 44-46, 2014).

[5] [Kooij et al., 1999] Kooij, H.v.d., et al., *A multisensory integration model of human stance control.* Biological Cybernetics, 1999. **80**: p. 299-308.

[6] [Larsson et al., 2005] Larsson P, Henriksson-Larse´n K. "*Combined metabolic gas analyser and dGPS analysis of performance in cross-country skiing*". J Sports Science 2005; 23(8): 861–870.

[7] [Petrone et al., 2008] Petrone N., Pollazon C., Morandin T., "*Structural behaviour of ski safety barriers during impactsof an instrumented dummy*", Proceedings of 7th Internatonal Conference on the Engineering of Sport, Bierritz, 2-6 June 2008. ISBN 978-2-287-09412-5.

[8] [Petrone et al., 2009] Petrone N., Ceolin F., "*Methods for full scale impact testing of ski safety barriers*" Abstract. 18th International Conference on Ski Trauma and Safety, May 2009, Garmish

[9] [Petrone et al., 2009] Petrone N., "*Sviluppo di metodi di prova full scale per la caratterizzazione ad impatto di barriere di protezione per applicazioni sportive*", XXXVIII Convegno Nazionale AIAS, 9-11 September 2009, Turin polytechnic.

[10] [Petrone et al., 2010] Petrone N., Ceolin F., Morandin T., "*Full scale impact testing of ski safety barriers using an instrumented anthropomorphic dummy*". Procedia Engineering, Volume 2, Issue 2, June 2010. Pages 2587-2592.

[11] [Petrone et al.,2010] Petrone N., Tamburlin L., Panizzolo F., Atzori B., "*Development of an instrumented anthropomorphic dummy for the study of impacts and falls in skiing*". Procedia Engineering, Volume 2, Issue 2, June 2010. Pages 2593-2598.

[12] [Petrone et al., 2011] Petrone N.,Morandin T., "*Behaviour of ski safety barriers during full scale impact testing*". Abstract. 19th International Conference on Ski Trauma ans Safety, May 2011, Keystone, Colorado.

[13] [Petrone et al., 2011] Petrone N., Marcolin G., Panizzolo F., "*Behaviour of an instrumented anthropomorphic dummy during full scale drop tests*". 5th Asia Pacific Congress on Sports Technology. Procedia Engineering, vol 13, p. 304-306, ISSN: 1877-7058, Melbourne, Aug 2011.

[14] [Petrone, 2012] Petrone N., "*The effects of impact speed, construction, and layout of different ski safety barriers on peak decelerations and penetration values of a solid dummy during full scale impacts*" (2012) ASTM Special Technical Publicaiton, 1553 STP, pp. 153-170

[15] [Petrone et al., 2013] Petrone N., Marcolin G., Cognolato M., Conte D., Jahnel R., Jurgen P., Rieder F., Muller E., "*Identification of skiing techniques with a single inertial sensor on the back: preliminary methodological approaches*". VI International Conference on Science and Skiing, St. Anton am Arlberg, Austria, December 2013. *Poster*.

[16] [Supej, 2010] M. Supej, " *3D measurement of alpine skiing with an inertial sensor motion capture and GNSS RTK system*" Journal of sports sciences, May 2010, 28(7): 759-769.

[17] [Zacharopoulos et al., 2015] Zacharopoulos A., Smyrnis A, Champipis A., "*The risk of injury for children in alpine sports. A 7 years case-control study*", 21th ISSS, San Vito, Italy

[18] U.S. Patent No. 4711125 issued to Morrison

[19] U.S. Patent No. 3823990 issued to P.J. Gilinson Jr. on July 16, 1974

Webgraphy

[1] https://aerospace.honeywell.com/~/media/Brochures/GG1320AN%20Digital%20Laser%20Gyro.ashx

[2] http://alpine.usskiteam.com/alpine

[3] http://www.crlsensors.com/pdf/ForceBalanceTechInfo.pdf

[4] http://cortina.dolomiti.org/index.cfm/Ski-Area/Ski-Area-Faloria-Cristallo-Mietres/

[5] http://electroiq.com/blog/2010/11/introduction-to-mems-gyroscopes/

[6] http://www.emcore.com/wp-content/uploads/EMP-1.2K.pdf

[7] https://www.endevco.com/7264b-500/

[8] https://en.wikipedia.org/wiki/Alpine_skiing_at_the_2014_ Winter_Olympics

[9] www.exelmicroel.com
[10] http://www.fisski.com/data/document/icr2008.pdf
[11] www.fis-ski.com/news-multimedia/news/article=air-ski-the-airbag-made-for-skiing-becomes-reality.com
[12] http://www.folgariaski.com/it/neve/ski-area-folgaria-fiorentini
[13] https://law.resource.org/pub/us/cfr/ibr/005/sae.j211-1.1995.pdf
[14] www.hahnenkamm.com/downhill-streif.html.
[15] http://www.hintertuxergletscher.at/en/skiing/hintertux-glacier.html
[16] https://www.inghams.co.uk/ski-holidays/ski-resorts/austria/arlberg-ski-area/st-christoph
[17] http://www.kvh.com
[18] http://www.madehow.com/Volume-5/Crash-Test-Dummy.html
[19] http://www.newworldencyclopedia.org/entry/Gyroscope
[20] www.skiareasanvito.com
[21] http://standards.sae.org/j2570_200109/
[22] http://www.tedligety.com/blog/fis-should-relinquish-regulations-to-the-ski-companies
[23] http://teledyne-cdl.com/img/MINIPOS-3.pdf-1390333353.pdf
[24] http://www.tf.uni-kiel.de/matwis/amat/semitech_en/kap_7/backbone/r7_1_1.html
[25] https://www.xsens.com/products/mtw-development-kit-lite/